

# **Investigating the use of gold nanoparticles in vaccine delivery**

Submitted by Anthony Edward Gregory, to the University of Exeter  
as a thesis for the degree of  
Doctor of Philosophy in Biological Sciences  
December 2013

This thesis is available for Library use on the understanding that it is copyright material and that no quotation from the thesis may be published without proper acknowledgement.

I certify that all material in this thesis which is not my own work has been identified and that no material has previously been submitted and approved for the award of a degree by this or any other University.

Signature: .....



## **Acknowledgements**

I would like to thank the many people who have helped and supported me throughout this Ph.D. Firstly, I would like to give a special thanks to my supervisors Professor Richard Titball and Dr Andrew Shaw for giving me the opportunity to work on this project and for the continuous support they have given me over the last 3-4 years. I would like to thank the National Institutes for Health (NIH) for funding this project and the University of Exeter for their academic support. Thank you to my collaborators at UTMB, particularly Professor Alfredo Torres, Dr Barbara Judy and Carla Blumentritt for their input on animal study design and helpful discussions. A big thank you to all my lab members in the BPRG research group and colleagues in the School of Biosciences, past and present, for their help and advice. Thanks to Tom Read who has shared this journey with me since undergraduate studies, through the highs and the lows. A special mention must go to Dr Monika Bokori-Brown for training me in cell culture technique, Dr Chris Thornton for helpful immunology discussions and Pete Splatt for support with confocal microscopy.

Most of all I would like to thank my family, particularly my parents for their unconditional love and support throughout my education. I could not have done any of this without them. Finally, I would like to thank Maddie for her unwavering belief in me and her patience over the last 12 months.

## Abstract

Vaccination is one of the most effective public health interventions in the world, saving millions of lives and preventing the onset of debilitating diseases. With widespread emergence of multi-drug resistant pathogens, the importance of preventative medicine has become even more apparent. However, one of the limiting factors in developing novel vaccines that are both safe and highly immunogenic is the availability of adjuvant delivery systems licensed for human use. The purpose of this study was to investigate the role gold nanoparticles could play as an effective vaccine delivery system. A variety of coupling chemistries were explored for their ability to conjugate protein and polysaccharide antigens onto the surface of gold nanoparticles for the development of vaccines against a number of biologically important human pathogens including *Y. pestis*, *B. mallei* and *S. pneumoniae*. Retention of antigenicity and coupling efficiency of conjugated molecules was measured using characterisation techniques such as localised surface plasmon resonance and immunoblotting. Gold nanoparticle coupled antigens were then used to immunise mice and to measure the protective efficacy and the immunological response induced. The findings indicate antigen-specific immune responses are elevated when an antigen is coupled onto gold nanoparticles. Moreover, immunological data from nanoparticle coupled glycoconjugate vaccines against *B. mallei* and *S. pneumoniae* indicate the likely presence of a strong T cell immune response which is essential for providing immunological memory. Finally, an intracellular trafficking assay was carried out to identify some of the mechanisms that might be involved in uptake of gold nanoparticles into professional phagocytes. Confocal imaging of receptors associated with endosomal compartments revealed that gold nanoparticles may enter cells through multiple pathways. The findings reported in this study suggest that gold nanoparticles may be an excellent candidate for further investigation as a novel vaccine delivery system.

## List of contents

Acknowledgements		i
Abstract		ii
List of contents		iii
List of figures		vii
List of tables		x
Abbreviations		xi
<b>Chapter 1</b>	<b>Nanoparticles in vaccine delivery</b>	<b>1</b>
1.1	Introduction	1
1.2	Vaccine-induced immunity	3
1.3	Adjuvants	8
1.4	Nanoparticle vaccines	10
1.4.1	Virus-like particles	11
1.4.2	Liposomes	14
1.4.3	ISCOMs	14
1.4.4	Polymeric nanoparticles	15
1.4.5	Non-degradable nanoparticles	16
1.5	Nanoparticle uptake and immunity	19
1.5	Limitations and ongoing questions	21
1.6	Objectives	23
<b>Chapter 2</b>	<b>Materials and methods</b>	<b>24</b>
2.1	Gold nanoparticles synthesis	24
2.2	Nanoparticle characterisation	24
2.3	Bacterial culture	25
2.4	Protein expression and purification	25
2.5	Glycoconjugate quantification	27

2.6	Immunisation/protection studies	28
2.7	Immunoanalysis	29
2.8	Flow cytometric analysis	31
2.9	Live <i>in vivo</i> analysis	32
2.10	Transmission electron microscopy	32
2.11	Fluorescent particles	33
2.12	Phagosomal staining	33
2.13	Statistical analysis	34
<b>Chapter 3</b>	<b>Peptide Antigens Coupled to Nanoparticles</b>	<b>35</b>
3.1	Introduction	35
3.1.1	Gold nanoparticles	35
3.1.2	Nanoparticle characterisation	35
3.1.3	Protein-based vaccines	39
3.1.4	Objectives	40
3.2	Materials and methods	41
3.2.1	Protein coupling onto gold nanoparticles	41
3.2.2	Purifying protein conjugated nanoparticles	41
3.2.3	Protein quantification	41
3.3	Results	42
3.3.1	Nanoparticle synthesis and characterisation	42
3.3.2	Peptide coupling and purification of nano-conjugates	49
3.3.3	Nanoconjugate quantification	56
3.3.4	Immunisation assay	62
3.3.5	Flow cytometric analysis	66
3.4	Discussion	68
3.4.1	Gold nanoparticle synthesis	68

3.4.2	Peptide coupling to gold nanoparticles	69
3.4.3	Immunisation study	71
3.4.4	Conclusions	74
<b>Chapter 4</b>	<b>A Glycoconjugate Vaccine against Glanders</b>	<b>75</b>
4.1	Introduction	75
4.1.1	<i>Burkholderia</i>	75
4.1.2	Glanders and melioidosis	76
4.1.3	Virulence factors	77
4.1.4	Objectives	81
4.2	Materials and methods	82
4.2.1	LPS purification	82
4.2.2	LPS coupling onto gold nanoparticles	82
4.3	Results	84
4.3.1	LPS extraction	84
4.3.2	Nano-glycoconjugate synthesis	86
4.3.3	Serum antibody responses 1	95
4.3.4	Protection study	102
4.3.5	Serum antibody responses 2	107
4.4	Discussion	115
4.4.1	LPS extraction	115
4.4.2	LPS coupling	115
4.4.3	Immunoglobulin G response	117
4.4.4	Immunoglobulin class switching	118
4.4.5	Survival and tissue colonisation	120
4.4.6	Conclusions	121
<b>Chapter 5</b>	<b>A Glycoconjugate Vaccine against Pneumococcus</b>	<b>122</b>

5.1	Introduction	122
5.1.1	Pneumococcus	122
5.1.2	Pneumococcal vaccines	125
5.1.3	Objectives	126
5.2	Materials and methods	127
5.2.1	CPS coupling onto gold nanoparticles	127
5.3	Results	129
5.3.1	CPS conjugation	129
5.3.2	Glycoconjugate characterisation	133
5.3.3	Immunoglobulin response	137
5.3.4	Protection study	144
5.4	Discussion	147
5.4.1	CPS conjugation	147
5.4.2	Immunoglobulin response	148
5.4.3	Protection study	148
5.4.4	Conclusions	149
<b>Chapter 6</b>	<b>Discussion and Future Work</b>	<b>150</b>
6.1	Discussion	150
6.2	Future work	162
<b>Appendix A</b>	<b><i>Burkholderia</i> virulence factors</b>	<b>165</b>
<b>Appendix B</b>	<b><i>S. pneumoniae</i> Xen10 infected MF1 mice</b>	<b>168</b>
<b>Publication</b>	<b>Gregory A.E. <i>et al.</i>, Conjugation of <i>Y. pestis</i> F1-antigen to gold nanoparticles improves immunogenicity. <i>Vaccine</i> 2012; 30(48) 6777-82</b>	<b>172</b>
<b>Publication</b>	<b>Gregory A.E. <i>et al.</i>, Vaccine delivery using nanoparticles. <i>Frontiers in Cellular and Infection Microbiology</i> 2013; 3</b>	<b>178</b>
<b>References</b>		<b>192</b>

## List of figures

<b>Chapter 1</b>	<b>Nanoparticles in vaccine delivery</b>	<b>1</b>
Figure 1.1	Dendritic cell activation	7
Figure 1.2	Nanoparticle vaccine delivery systems	18
<b>Chapter 3</b>	<b>Protein Antigens Coupled to Nanoparticles</b>	<b>35</b>
Figure 3.1	Spectral properties of LSPR	38
Figure 3.2	TEM of 5 nm gold nanoparticles	44
Figure 3.3	TEM of 15 nm gold nanoparticles	44
Figure 3.4	TEM of 50 nm gold nanoparticles	44
Figure 3.5	Plasmon spectra for gold nanoparticles	46
Figure 3.6	Plasmon spectra time-course	47
Figure 3.7	Gold nanoparticle extinction time course	48
Figure 3.8	Reaction scheme for carbodiimide chemistry	51
Figure 3.9	Gel filtration chromatography of AuNP-F1	52
Figure 3.10	Gel filtration chromatography of AuNPs-TetHc	53
Figure 3.11	Calibration curve of colloidal dilution	54
Figure 3.12	Plasmon spectra for protein coupled AuNPs	55
Figure 3.13	NaCl aggregation assay	57
Figure 3.14	Band densitometry quantification for F1	58
Figure 3.15	Densitometry quantification for proteins	59
Figure 3.16	MALDI-TOF spectra for AuNP-F1	61
Figure 3.17	F1 specific IgG concentration	63
Figure 3.18	Competitive ELISA for binding to F1	65
Figure 3.19	F1 specific IgG concentration over time	73
<b>Chapter 4</b>	<b>A Glycoconjugate Vaccine against Glanders</b>	<b>75</b>
Figure 4.1	Silver stain gel and western blot of LPS	85

Figure 4.2	Plasmon spectra for reductive amination and oxime coupling	87
Figure 4.3	Reaction scheme of thiol maleimide coupling	89
Figure 4.4	Skeletal structure of <i>B. thailandensis</i> LPS	90
Figure 4.5	Plasmon spectra for thiol maleimide coupling	92
Figure 4.6	Two-colour western blot of AuNP-TetHc-LPS	93
Figure 4.7	Calibration curve for phenol-sulphuric acid assay	94
Figure 4.8	Calibration curve for antibody ELISA	97
Figure 4.9	IgG concentration, study 1	98
Figure 4.10	LPS specific IgG concentration, study 1	99
Figure 4.11	LPS specific IgG subclass concentration, study 1	100
Figure 4.12	IgM concentration, study 1	101
Figure 4.13	<i>B. mallei</i> challenge survival curve	103
Figure 4.14	<i>B. mallei</i> colony counts spleen	104
Figure 4.15	<i>B. mallei</i> colony counts lungs	105
Figure 4.16	IgG concentration, study 2	109
Figure 4.17	LPS specific IgG concentration, study 2	110
Figure 4.18	LPS specific IgG subclass concentration, study 2	111
Figure 4.19	LPS-IgG isotypes	112
Figure 4.20	IgM concentration, study 2	113
<b>Chapter 5</b>	<b>A Glycoconjugate Vaccine against Pneumococcus</b>	<b>122</b>
Figure 5.1	Disease associated serotypes of pneumococcus	123
Figure 5.2	Plasmon spectra for CDAP coupling	130
Figure 5.3	Skeletal structure of <i>S. pneumoniae</i> serotype 3 CPS	131
Figure 5.4	Reaction scheme for reductive amination	132
Figure 5.5	Progressive plasmon spectra for CPS coupling	134
Figure 5.6	Plasmon spectra for reductive amination coupling	135

Figure 5.7	Western blot for CPS glycoconjugate	136
Figure 5.8	IgG concentration	138
Figure 5.9	CPS specific IgG concentration	139
Figure 5.10	IgM concentration	140
Figure 5.11	IgG subclass concentration	142
Figure 5.12	IgG subclass ratio	143
Figure 5.13	<i>In vivo</i> imaging of <i>S. pneumoniae</i> challenged mice	145
Figure 5.14	<i>S. pneumoniae</i> challenge survival curve	146
<b>Chapter 6</b>	<b>Cellular Uptake of Gold Nanoparticles</b>	<b>150</b>
Figure 6.1	TEM of J774A.1 macrophage and gold nanoparticles	154
Figure 6.2	TEM of J774A.1 macrophage and gold nanoparticles	155
Figure 6.3	Confocal microscopy image of J774A.1 macrophage and GFP conjugated gold nanoparticles	157
Figure 6.4	Confocal microscopy image of J774A.1 macrophage and GFP conjugated gold nanoparticles	158
Figure 6.5	LAMP-1 stained J774A.1 macrophage and GFP conjugated gold nanoparticles	159
Figure 6.6	4.54 $\mu\text{m}$ z-cross section of J774A.1 macrophage and GFP conjugated gold nanoparticles	160
Figure 6.7	9.08 $\mu\text{m}$ z-cross section of J774A.1 macrophage and GFP conjugated gold nanoparticles	161

## List of tables

<b>Chapter 1</b>	<b>Nanoparticles in vaccine delivery</b>	<b>1</b>
Table 1.1	Toll-like receptor agonists	4
Table 1.2	Nanoparticle vaccine delivery systems	13
<b>Chapter 3</b>	<b>Peptide Antigens Coupled to Nanoparticles</b>	<b>35</b>
Table 3.1	Conjugated protein measurements	60
Table 3.2	F1-specific IgG1 and IgG2a isotypes	64
Table 3.3	Percentage of splenocytes with CD45	67
<b>Chapter 4</b>	<b>A Glycoconjugate Vaccine against Glanders</b>	<b>75</b>
Table 4.1	Summary of results from “immunisation study 1”	106
Table 4.2	Summary of results from “immunisation study 2”	114
<b>Chapter 5</b>	<b>A Glycoconjugate Vaccine against Pneumococcus</b>	<b>122</b>
Table 5.1	Structural diversity of <i>S. pneumoniae</i> CPS serotypes	124

## Abbreviations

Alhy	Alhydrogel
APC	Antigen-presenting cell
AuNP	Gold nanoparticle
BCA	Bicinchoninic assay
Bsa	<i>Burkholderia</i> secretion apparatus
BSL	Bio-safety level
CDAP	1-cyano-4-dimethylaminopyridine tetrafluoroborate
CFU	Colony Forming Units
CpG	Cytosine-guanine dinucleotides (unmethylated)
CPS	Capsular polysaccharide
CRM <sub>197</sub>	Cross-reactive material 197
DNA	Deoxyribonucleic acid
EDC	<i>N</i> -(3-dimethylaminopropyl)- <i>N'</i> -ethylcarbodiimide hydrochloride
EDTA	Ethylenediaminetetraacetic acid
ELISA	Enzyme-linked immunosorbent assay
EMCH	6-maleimidocaproic acid hydrazide
ER	Endoplasmic reticulum
Hcp	Haemolysin-coregulatory protein
HBV	Hepatitis B virus
Hib	<i>Haemophilus influenzae</i> type b
HPV	Human papillomavirus
IFN	Interferon
Ig	Immunoglobulin
IL	Interleukin
IM	Intramuscular
IN	Intranasal

IP	Intraperitoneal
IR	Infrared
ISCOMs	Immune stimulating complexes
KWC	Killed whole cell
LA	Luria agar
LB	Luria broth
LD <sub>50</sub>	Median lethal dose
LPS	Lipopolysaccharide
LSPR	Localised surface plasmon resonance
mAb	monoclonal antibody
MALDI-ToF	Matrix-assisted laser desorption/ionisation time-of-flight
MES	2-(N-morpholino)ethanesulfonic acid
MHC	Major histocompatibility complex
MHDA	16-mercaptohexadecanoic acid
MMR	Measles, mumps and rubella
MPLA	Monophosphoryl lipid A
MS	Mass spectrometry
NF- $\kappa$ B	Nuclear factor kappa-light-chain-enhancer of activated B cells
NHS	<i>N</i> -hydroxysuccinimide
NP	Nanoparticle
OMV	Outer membrane vesicles
pAb	Polyclonal antibody
PBS	Phosphate buffered saline
$\gamma$ -PGA	Poly( $\gamma$ -glutamic acid)
PLA	Poly(lactic acid)
PLGA	Poly(lactic-co-glycolic acid)
PPV23	Pneumococcal polysaccharide vaccine (23 CPS serotypes)
SATA	S-acetylthioglycolic acid <i>N</i> -hydroxysuccinimide ester

SC	Subcutaneous
SDS-PAGE	Sodium dodecyl sulphate polyacrylamide gel electrophoresis
D-Sug	2-acetamido-2,6-dideoxy-D-xylo-hexos-4-ulose
TetHc	Tetanus toxoid Hc fragment
TEM	Transmission electron microscopy
TGF	Transforming growth factor
Th	T helper cell
Tc	Cytotoxic T cell
Tfh	Follicular helper T cell
TLR	Toll-like receptor
Tm	Memory T cells
TNF- $\alpha$	Tumour necrosis factor - alpha
Treg	Regulatory T cell
T3SS	Type III Secretion System
T5SS	Type V Secretion System
T6SS	Type VI Secretion System
UTMB	University of Texas Medical Branch
UV/Vis	Ultraviolet/visible
VgrG	Valine-glycine repeat protein G
VLP	Virus-like particle

## Chapter 1: Nanoparticles in Vaccine Delivery

---

### 1.1 Introduction

The discovery of vaccines is arguably one of the greatest achievements in medical science of the 20<sup>th</sup> century. Vaccination was pioneered by Edward Jenner who in 1796 showed that people were no longer susceptible to smallpox infection once they had been inoculated with cowpox, a far less severe disease [1]. Since then, global immunisation programmes have led to the eradication of smallpox and have almost completely eliminated many other infectious diseases including diphtheria, tetanus, poliomyelitis, measles, mumps, rubella and *Haemophilus influenza* type b [2]. Vaccination not only prevents many from suffering debilitating diseases but saves approximately 2 to 3 million lives globally every year [3].

Whilst varied in their composition and application, the mechanism by which all vaccines work is essentially the same. Consisting of a biological substance (antigen), which can be either a whole microbe (killed or attenuated) or microbial components, a vaccine stimulates an immune response. The antigen is then remembered by the immune system so that it can mount a more effective response should it encounter the corresponding microbe in the future. This is best achieved by inducing long-term protection in individuals, a hallmark of adaptive immunity rather than innate immunity which provides immediate yet short-lived protection.

One approach for inducing an adaptive immune response is to immunise an individual with a live attenuated strain of a pathogen which has a significantly reduced virulence. These vaccines provide the immune system with the entire make-up of a microbe, enabling it to produce antibodies against conserved structures for future recognition. There are several approaches to attenuating microbes for use as a vaccine. One involves growing the microbe in artificial growth medium at a temperature lower than the human body. Over time this can be used to select for a mutant that grows well at lower temperatures but has reduced growth in humans. This allows the immune system to mount a response and eliminate the microbe before it causes infection. The cold-

adapted influenza vaccine is an example of this approach [4]. A combinational vaccine against measles, mumps and rubella (MMR) was developed using another method, by growing the viruses in a foreign host. Both measles and mumps viruses are grown in chick egg fibroblasts to select for mutants with an enhanced virulence for the host. Subsequently, these mutants show a significant attenuation in humans and are selected as vaccine strains [5, 6]. Both of these methods of attenuation are particularly well suited to RNA viruses, which have a high mutation rate, but are rarely applied to bacterial pathogens. Recombinant DNA techniques to create attenuated mutants is used instead, such as the *Vibrio cholerae* CVD 103-HgR strain that does not express the enzymatically activate subunit of cholera toxin [7]. By priming the immune system with a living microbe the resulting response is similar to that of a natural infection. Live attenuated vaccines are therefore often able to elicit strong cellular and humoral responses that confer lifelong immunity after just one or two doses in childhood [8]. However, one of the major concerns with live attenuated vaccines is their potential for reversion to virulence [9]. There are also safety concerns with the use of some live vaccines in immunocompromised individuals [10]. Whilst some live vaccines can be lyophilised, they often have to be kept refrigerated to remain effective. This can be particularly problematic for vaccinating in developing countries which may lack widespread refrigeration.

Another type of vaccine involves immunising with the whole microbe once it was been inactivated using heat, chemicals or radiation. These vaccines are termed killed whole cell (KWC) vaccines and consist of the microbe in its native wild-type form. Unlike live attenuated vaccines, KWC are unable to cause disease and do not require refrigeration. However the method used to kill the bacteria may affect its immunogenicity, with some studies suggesting that radiation treatment retains some of the antigenic structures destroyed by heat treatment [11]. One of the first KWC vaccines produced was against typhoid in 1896, although its efficacy was not established until 1960 [12]. A two dose vaccination with KWC typhoid resulted in 73% efficacy over three years (95% confidence interval) [13]. However, adverse side-effects were reported in 17% of vaccine recipients and is therefore not available for use as a public health vaccine, despite being licensed [14]. Local reactions at the site of vaccination are a common feature of KWC vaccines but are often caused by an adjuvant which is added to boost the weak adaptive immune responses induced by

KWC. This is due to the fact that they are unable to replicate in the host, meaning periodic boosters must be given to maintain immunity. This can be a problem for people who do not have regular access to health care. Another disadvantage of a non-living vaccine is that they are unable to elicit CD8<sup>+</sup> T cell responses which are important for protection against intracellular pathogens. A problem that is common to both types of vaccines, that are using the whole microbe as an immunogen, is the unspecificity of the immune response induced because some antibodies are raised against proteins that are not involved in virulence. There may also be some microbial proteins in the vaccine strain that down-regulate the adaptive immune response.

Instead of using the whole microbe for immunisation, recent vaccine design strategies have focused on identifying microbial components (subunits) that best stimulate the immune system. These vaccines are much better characterised than whole microbial vaccines, making them safer for human use. Once identified, microbial components can be isolated in one of two ways: either by purifying directly from the microbe, or using recombinant DNA techniques to express the antigen in a foreign host and then purifying. An example of a recombinant subunit vaccine is the hepatitis B vaccine which uses *Saccharomyces cerevisiae* to express one of the viral envelope proteins, hepatitis B surface antigen (HBsAg) [15]. This vaccine induces a protective antibody response in over 90% of individuals, in whom protection is life-long [16]. However, like KWC vaccines, microbial components are often weak immunogens that require adjuvants to boost their efficacy. Adjuvants may be either organic or inorganic and function by delivering the antigen to antigen-presenting cells (APCs) or by acting as an immunostimulant. There are currently very few adjuvants licensed for human use and those which are licensed can induce local reactions and may fail to generate strong cell-mediated immunity [17-19]. Whilst the use of microbial components for vaccines remains appealing, there remains a great need for discovering novel adjuvants and delivery systems in order to develop safe and effective vaccines in the future.

### 1.2 Vaccine-induced immunity

The objective of any vaccine formulation is to activate an antigen-specific B and/or T cell immune response to induce an immunologically mediated

resistance to a disease [20]. The predominant interface between these two immune responses is APCs, particularly dendritic cells, which are widely distributed throughout the body as immature cells. APCs recognise a number of conserved structures in pathogens, termed pathogen-associated molecular patterns (PAMPs), by pattern recognition receptors such as toll-like receptors (TLR), which initiate an innate immune response, Table 1.1 [21-23]. APCs also undergo maturation upon antigen recognition which results in a redistribution of major histocompatibility complex (MHC) molecules from intracellular compartments to the cell surface, cytoskeleton reorganisation and the secretion of cytokines and chemokines to recruit other APCs [24-27].

**Table 1.1.** Pattern recognition receptors and their corresponding major ligand.

<b>Receptor</b>	<b>Major Ligand (PAMPS)</b>
TLR 1	Triacyl lipoproteins
TLR 2	Peptidoglycan and lipoproteins of Gram-negative bacteria
TLR 3	Double-stranded RNA
TLR 4	Lipopolysaccharide
TLR 5	Flagellin from Gram-positive and Gram-negative bacteria
TLR 6	Diacyl lipoproteins
TLR 7	Single-stranded RNA
TLR 8	Oligosaccharides
TLR 9	Unmethylated CpG sequences in DNA
TLR 10	Single-stranded RNA
TLR 11	Profilin
TLR 12	Profilin

Dendritic cells are capable of using a variety of endocytic mechanisms to engulf foreign antigens. Generally, but not exclusively, this process is receptor-mediated whereby surface receptors capture microbes by binding to specific ligands [23, 28]. Endocytosis of bacteria and larger particles ( $> 0.5 \mu\text{m}$ ) mostly occurs by either phagocytosis or macropinocytosis that form cell-surface extensions which engulf the pathogen [23, 29]. Phagosomes or macropinosomes then fuse with early and late endosomes as well as lysosomes to form phagolysosomes. These compartments contain proteolytic enzymes and reactive oxygen species that degrade bacterial peptides [30]. Degraded peptides are then displayed on MHC class II molecules for recognition by  $\text{CD4}^+$  T-helper (Th) cells which are able to stimulate both humoral and cellular arms of the adaptive immune response [31]. Once activated by APCs,  $\text{CD4}^+$  Th cells differentiate into one of two major subtypes of effector T cells; Th1 or Th2. This is regulated by the cytokine environment generated by APCs and other cells that form part of the innate immune response including natural killer cells, basophils and mast cells [32-34]. Interleukin (IL)-12 is believed to play a key role in the generation of Th1 cells, whereas IL-10 suppresses this development [35, 36].

Th1 cells play a pivotal role in cellular immunity against intracellular pathogens by inducing a predominantly pro-inflammatory response with the secretion of IL-2, interferon (IFN)- $\gamma$  and tumour necrosis factor (TNF)- $\alpha$  [37, 38]. Moreover, a fraction of these Th1 cells will also persist as memory  $\text{CD4}^+$  T cells (Tm), providing a quantitatively enhanced response upon secondary infection [39]. IL-4 is responsible for stimulating the development of Th2 cells which are critical during infection by extracellular pathogens and secrete the anti-inflammatory cytokines IL-4, IL-5 and IL-13 [40-42]. Th cells may also activate B cells in germinal centres (GC) leading to differentiation of GC B cells into memory B cells (Bm) or plasma cells [43]. Whilst naive B cells produce low affinity immunoglobulin (Ig)-M and IgD, Th activated B cells undergo Ig class switching to generate IgG, IgA or IgE depending on the cytokine environment [44]. Follicular helper T (Tfh) cells also play a key role in supporting B cell differentiation and Ig class switching. Tfh cells induce clonal proliferation and affinity maturation of B cells through a series of co-stimulatory markers, including IL-10 and IL-21, to generate antibodies of a higher binding capacity [45, 46]. The generation of effector Th cells is controlled by regulatory T cells

(Treg) which maintain immune homeostasis by secreting IL-10 and transforming growth factor (TGF)- $\beta$  [47]. Tregs are also essential in preventing autoimmune diseases as well as allergic reactions by suppressing immune responses to self and non-self antigens [48-50].

In some cases antigens may be present in the cytosol of APCs as a result of infection from viruses, intracellular bacteria or non-phagocytic uptake. When this occurs, antigens are degraded by the proteasome before being transported to the endoplasmic reticulum (ER) by transporters associated with antigen presentation (TAP-1 and -2) and loaded onto MHC class I molecules [51]. MHC class I-peptide complexes that are translocated to the cell surface are recognised by CD8<sup>+</sup> T cells which are subsequently activated in the presence of IL-2 from CD4<sup>+</sup> Th1 cells and undergo clonal expansion as cytotoxic T cells (Tc) [25]. Tc cells are then able to induce cytolysis of infected cells using one of two mechanisms; granzyme-mediated or Fas-mediated apoptosis. In the first of these two pathways perforin and granzyme are released from Tc cells which form a pore in the plasma membrane of the target cell through which granzyme enters [52]. These molecules then stimulate the caspase cascade in the target cell, leading to apoptosis. The other mechanism of cytolysis employed by Tc cells is by the upregulation of FasL (CD95L) which binds with Fas (CD95) on target cells to initiate apoptosis [53]. Following infection, the majority (90-95%) of activated Tc cells will also undergo programmed cell death whilst the remaining antigen-specific CD8<sup>+</sup> T cells will generate a pool of long-lived memory T cells, Figure 1.1 [54, 55].

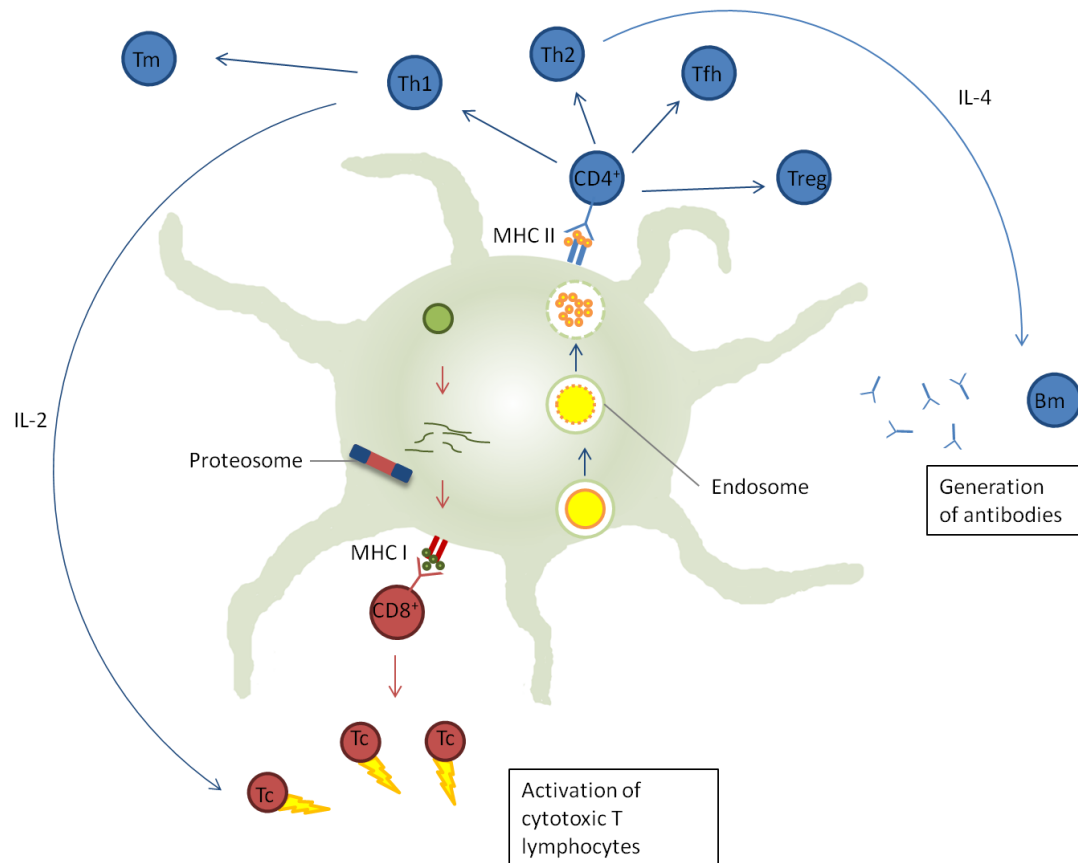


**Figure 1.1.** Activation of dendritic cells in response to different antigen stimuli. Antigens larger than 200 nm (e.g. bacteria) typically enter antigen-presenting cells via endosomal pathways (blue arrows). They are then degraded within a vesicle before the contents are displayed on the cellular surface by MHC II receptors and recognised by CD4<sup>+</sup> T cells. Antigens smaller than 200 nm (e.g. viruses, nanoparticles) present in the cytosol (red arrows) are broken down and presented on MHC I receptors, which are recognised by CD8<sup>+</sup> T cells.

Presentation of antigenic peptides to either MHC class I or class II molecules was originally believed to be dependent on whether proteins were produced endogenously or captured via endocytosis. However, it is now known that in some cases dendritic cells are able to load exogenous peptides onto MHC class I molecules in a process known as cross-presentation [56]. The precise mechanisms underlining this process are yet to be elucidated but involve fusion of phagosomes with the ER before being loaded onto MHC class I molecules [57]. Cross-presentation is critical for priming a CD8<sup>+</sup> T cell response to intracellular pathogens without APCs becoming infected and avoids intracellular immune evasion strategies. Consequently, attempts have been made to develop vaccines against intracellular pathogens using cross-presentation and this has been achieved using a variety of NP delivery systems [58-60].

Whilst an infection is likely to induce a mixed response of both B and T (CD4<sup>+</sup> and CD8<sup>+</sup>) cells, the composition and delivery of vaccines has a direct influence on the type of immune response elicited. It stands to reason that tailoring a vaccine-induced immune response to a specific pathogen may be a useful strategy when designing a vaccine. Bacterial polysaccharide vaccines, for example, generally elicit B cell responses in a T-independent manner (lacking CD4<sup>+</sup>/CD8<sup>+</sup> activation), although some studies have identified zwitterionic polysaccharides as stimulating CD4<sup>+</sup> T cells [61]. Polysaccharide antigens are typically characterised by inducing an immune response which is isotype restricted and lacking T cell memory [62, 63]. However, by conjugating polysaccharides to a protein carrier (glycoconjugate) peptide antigens are recognised by CD4<sup>+</sup> or CD8<sup>+</sup> T cells and elicit a B cell response in a T-dependent manner [64].

For vaccines against intracellular pathogens, inducing a CD8<sup>+</sup> Th1 and/or CD8<sup>+</sup> Tc cell response might be advantageous. Whereas this was previously limited to live attenuated vaccines, this type of immunity can now be achieved using novel adjuvants and delivery systems.

### *1.3 Adjuvants*

For more than 70 years adjuvants have been added to vaccine formulations to either enhance or manipulate a vaccine induced immune response. Whilst the precise mechanism of how many adjuvants work is only poorly understood,

adjuvants can mediate their effect by extending the duration of an immune response, stimulating cell-mediated immunity or by modulating the antibody avidity and subclass distribution [65]. Stimulatory adjuvants such as unmethylated cytosine-guanine dinucleotides (CpG) found in bacterial DNA and monophosphoryl lipid A (MPLA) are characterised by their ability to activate co-stimulatory signals or intracellular signalling pathways. For MPLA, its major receptor in humans has been identified as TLR 2 [66]. This triggers the release of pro-inflammatory cytokines via nuclear factor kappa-light-chain-enhancer of activated B cells (NF- $\kappa$ B), an important feature of the innate immune response [67]. CpG however has been identified as binding to TLR 9 which, through the expression of co-stimulatory molecules, releases TNF- $\alpha$  and IL-12 to induce a potent Th1 response [68, 69]. Alternatively, cytokines can be used directly as an adjuvant, the most extensively studied being IL-2, IL-12 and IFN $\gamma$ . However, problems with stability and a relatively high manufacturing cost means that the use of cytokines for routine vaccination is unlikely [70, 71].

Aluminium-based compounds (principally aluminium phosphate or hydroxide) remain the most widely used adjuvants incorporated into licensed human vaccines. However, the mechanism by which alum potentiates the immune response is poorly understood. It was initially believed to be due to a depot effect at the site of injection, prolonging exposure of the antigen to the immune system for a better response [72, 73]. This theory was later challenged by Holt who showed that excision of the injection site from guinea pigs did not interfere with the development of a humoral response [74]. Recent studies have also documented the rapid release of antigens from alum adjuvants; approximately 80% of aluminium phosphate adsorbed tetanus toxoid had disappeared from the site of injection within 4 hours [75, 76]. It is now believed that alum plays a more active role based on observations of its electrostatic interaction with lipopolysaccharide [77]; and its demanding effect on some protein antigens [78] leading to corrugated layers of aluminium oxyhydroxide held together with hydrogen bonds. Aluminium gel particles are generally no more than 10  $\mu$ m in diameter, and antigens adsorbed to these particles may be phagocytosed more readily than those without alum [79]. The generation of particulate molecules *in vivo* may create an inflammasome response which in turn may activate the Nlrp3 (NOD-like receptor family, pyrin domain containing 3) [80, 81] causing an influx of eosinophils and an upregulation of MHCII

expression and antigen-presentation cell activity [82]. Once activated, this cytoplasmic Nlrp3 protein promotes the production of pro-inflammatory cytokines such as interleukin 1beta and interleukin 18 (IL-1 $\beta$  and IL-18) [80, 83]. Of these cytokines, IL-1 $\beta$  has been shown to be a potent stimulus for T-cell dependent antibody production *in vivo* [84]. Alternatively, prostaglandins or other moieties may mediate the inflammatory response to the alum [85]. Although alum is renowned for its ability to produce antibody responses, it induces strong CD4<sup>+</sup> mediated cellular responses (predominantly Th2 but also Th1) and can also induce CD8<sup>+</sup> T cell activation [82]. Stimulation of these cellular responses induces cellular memory which is important for protection against many pathogens as well as generating long-term protective immunity [86-88].

Whilst alum-based adjuvants are generally well tolerated, there may be some associated toxicity problems such as the formation of granulomas when subcutaneous or intradermal injection is preferred over intramuscular. Weak renal function can result in allergenicity and accumulation of aluminium which is not only toxic but has also been associated with amyotrophic lateral sclerosis and Alzheimer's disease [76, 89-91]. Consequently, there is an urgent need to develop safe adjuvants which are able to stimulate both Th1 and Th2 immune responses.

#### 1.4 Nanoparticle vaccines

Nanotechnology is an emerging field which focuses on manipulating matter on a nanometer scale. The International Organisation for Standardisation (ISO) defines a nanostructure as 'an object that has at least one dimension within the nano-scale'; 1-1000 nm (1 nm = 10<sup>-9</sup> m) [92]. The application of these nanostructures, including nanoparticles (NPs), holds great promise for the development of a new generation of vaccines and adjuvants [93-100]. NP vaccines allow antigens to be either encapsulated within or decorated onto the surface of the NP. By encapsulating antigenic material, NPs provide a method for delivering antigens which may otherwise degrade rapidly upon injection or induce a short-lived, localised immune response. The large surface area of NPs also means that molecules decorated on the surface are at a high concentration and are presented to the immune systems in much the same way that it would be presented by the pathogen, thereby provoking a similar or even enhanced

response. Moreover, NPs made from some composites enable not only site directed delivery of antigens but also prolong the release of antigens to maximise exposure to the immune system.

Whilst nanoparticles vary significantly in their composition, size and shape they can be broadly grouped into the following categories: Virus-like particles, liposomes, non-degradable and polymeric nanoparticles. A summary of nanoparticles studied as vaccine delivery systems is shown in Table 1.2.

#### 1.4.1 Virus-like particles

Amongst some of the first studied NP delivery systems were virus-like particles (VLPs), attracting interest because of their ease of production and ability to stimulate strong immune responses [101-103]. Typically in the size range of 20-150 nm, VLPs consist of a self-assembled viral envelope, generated from a single protein to form a multimeric complex displaying a high density of epitopes [102, 104]. Unlike viruses, VLPs assemble without encapsulating any viral RNA meaning they are non-replicating and non-infectious. Genes coding for viral integrase are also deleted prior to expression to prevent integration of the packed genome into the host cell and/or prevent recombination with live or defective virus in an infected individual [105]. VLPs can be engineered to express additional proteins either by fusing these proteins to the particle or by expressing multiple antigens [101, 106]. Using this approach, VLPs can be generated to provide protection not only against the virus of origin but also against heterologous antigens. Moreover, non-protein antigens such as polysaccharides or small organic molecules can be chemically coupled onto the viral surface to produce bioconjugate VLPs [107, 108].

The baculovirus expression system is most commonly used for the generation of VLPs, and has a good safety profile since baculoviruses do not naturally infect humans. The *Autographa californica* multiple nuclear polyhedrosis virus (AcMNPV) is the most extensively studied VLP component [109]. In this system, a non-essential gene coding for the protein(s) forming the viral occlusion body (polyhedrin) is replaced with a gene of interest [104]. The vector encoding the modified VLP can then be used to infect insect cells (Sf9 or Sf21 derived from *Spodoptera frugiperda*, or BTI-TN-5B1-4 derived from *Trichoplusia ni*) to generate sufficient quantities of the viral protein which can then self assemble into multimeric complexes. The advantage of using such a

system is that not only does AcMNPV have a large genome (130 kb), allowing the insertion of multiple/large genes, but there is typically a high protein yield driven by the strong polyhedrin promoter [109]. Despite its versatility, the main disadvantage to the baculovirus/insect expression system is its inability to produce authentic recombinant mammalian glycoproteins due to differences in post-translational modification patterns between insect and mammalian cell lines [110]. One way to overcome this has been the development of “humanised” insect cell lines to constitutively express mammalian genes such as  $\beta$ 1, 4-galactosyltransferase and  $\alpha$ 2,6-sialyltransferase to enable the expression of terminally galactosylated and sialylated glycoproteins [111-115]. Another problem associated with the baculovirus expression system is the resulting cell death and lysis of insect cells within a few days after infection with baculovirus. This can be problematic for proteins which are selected for secretion or are vulnerable to degradation. Subsequent efforts to alleviate this problem have been in the form of a non-lytic baculovirus developed by random mutagenesis resulting in almost a 10-fold decrease in cell lysis and a reduction in degradation of expressed protein [116].

**Table 1.2.** Examples of nanoparticle vaccine delivery systems

	Matrix/ expression system	Size	Antigen	Route of immunisation	References
<b>Virus like particles</b>	Baculovirus (Sf9, Sf21, Hi5); <i>E. coli</i> ; Mammalian cells; <i>S. cerevisiae</i>	55-60 nm (HPV) 100-200 nm (HIV) 80 -120 nm (H1N1)	Major capsid protein, L1 (HPV); fms-like tyrosine kinase receptor ligand, FL, gag precursor protein, pr45, HIV env cDNA (HIV); Haemagglutinin, nicotinamide, matrix protein M1 (H1N1)	Intramuscular, Subcutaneous, Intraperitoneal, Oral, Intranasal	[97, 117-124]
<b>Liposomes</b>	Outer membrane vesicles (OMV) Phospholipid S100 and cholesterol; Phosphatidylcholine and cholesterol	20-200 nm 50-500 nm 193 nm	R32NS1 ( <i>Plasmodium falciparum</i> ); Cholera toxin; Circumsporozoite ( <i>P. falciparum</i> ); CtUBE fusion peptide ( <i>Helicobacter pylori</i> ); KWC <i>Y. pestis</i>	Intramuscular, Intravenous, Subcutaneous, Oral, Intranasal	[93, 125-129]
<b>Non-degradable</b>	Gold; Silica; Carbon	2-470 nm	Plasmid DNA expressing haemagglutinin 1 (Influenza); Hepatitis B	Intradermal, Intramuscular, Subcutaneous,	[100, 130-134]
<b>Polymeric</b>	Poly(lactic-co-glycolic acid) (PLGA); Poly(lactic acid) (PLA); Poly(glycolic acid) (PGA); Chitosan;	100-200 nm 800 nm 1-5 $\mu$ m 248 nm	Docetaxel, TetHc ( <i>C. tetani</i> ), Hepatitis B, Dtxd ( <i>Corynebacterium diphtheriae</i> ) SBm7462 ( <i>Boophilus microplus</i> ); Rv1733c ( <i>Mycobacterium tuberculosis</i> ); SPf66 ( <i>P. falciparum</i> )	Intramuscular, Intravenous,	[93, 94, 135]

### 1.4.2 Liposomes

Like VLPs, liposomes are self-assembling but consist of a phospholipid bilayer shell with an aqueous core [136, 137]. They can be produced naturally from the outer membrane of Gram negative bacteria as outer membrane vesicles (OMVs) or generated synthetically. There are two main types of synthetic liposome, either unilamellar vesicles which consist of a single phospholipid bilayer, or multilamellar vesicles that are made of several concentric phospholipid shells separated by layers of water. As a consequence, liposomes can be tailored to incorporate either hydrophilic molecules into the aqueous core or hydrophobic molecules within the phospholipid bilayer. There are a large number of methods published for preparing liposomes [138-140]; however, they typically involve a reverse phase evaporation process by dissolving phospholipids (such as MPLA or phosphatidylcholine) in an organic solvent (e.g. chloroform, methanol). Water is then added, along with the antigen, and the solvent is evaporated resulting in the vesicles [141, 142]. Cholesterol can also be added to provide additional stability to the phospholipid bilayer [143]. Other approaches to encapsulate antigens in liposomes include using repeated freeze thaw cycles [141], a pH gradient [144] or an ammonium sulphate method [145] with antigen encapsulation rates varying between 25-72% [128, 129, 146].

### 1.4.3 ISCOMs

Colloidal saponin-containing micelles of around 40 nm can be used as self-adjuvanting vaccine delivery systems and are collectively known as immune stimulating complexes (ISCOMs) [147]. Two types of ISCOMs have been described, both of which consist of cholesterol, phospholipid (typically either phosphatidylethanolamine or phosphatidylcholine) and saponin (most often Quil A from the tree *Quillaia saponaria*) [148-150]. Classically, ISCOMs have been used to entrap viral envelope proteins such as those from herpes simplex virus type 1, hepatitis B and influenza [65]. However, proteins from a range of bacteria and parasites including *Escherichia coli*, *Brucella abortus* and *Plasmodium falciparum* have also been used to assemble ISCOMs [151-153]. Complexes without viral proteins are also used and are often referred to as ISCOM matrices [148]. ISCOMs are self-assembling at an optimal ratio of 1:1:5 (cholesterol:phospholipid:saponin) for matrices or 1:1:5:0.1/1 for classical

ISCOM forming in the presence of a non-ionic detergent, which is then removed using dialysis or ultracentrifugation [150, 154]. The resulting complex is a pentagonal dodecahedron arrangement of micelles containing saponin and lipid held together by hydrophobic interactions and stabilised through its negative surface charge [154, 155].

#### 1.4.4 Polymeric nanoparticles

Polymeric NPs have attracted attention for their ability to deliver drugs as well as for being biodegradable [156]. Moreover, the release kinetics of loaded drugs from polymeric NPs can be controlled by compositional changes to the copolymer [156]. This class of NP can be prepared from a range of polymers including poly( $\alpha$ -hydroxy acids), poly(amino acids) or polysaccharides to create a vesicle which can either accommodate or display antigens. The most commonly used poly( $\alpha$ -hydroxy acids) for preparing polymeric NPs are either poly(lactic-co-glycolic acid) (PLGA) or poly(lactic acid) (PLA) which are often synthesised using a double emulsion-solvent evaporation technique [157-159]. Firstly, a polymer of choice is dissolved in an organic solvent like ethyl acetate or methylene chloride followed by the addition of the antigen which is then vortexed to get a primary emulsion. A water-in-oil-in-water emulsion is then formed with the addition of an emulsifying agent (e.g. polyvinyl alcohol or polyvinyl pyrrolidone). This results in the polymer precipitating around the antigen. The solution is then left to allow solvent evaporation and then dried to prevent degradation of the polymer due to water-catalysed ester hydrolysis [160-164]. The use of this method is limited since antigen entrapment efficiency is low and there is a possibility of protein denaturation at the oil-water interface [165]. The addition of stabilizers such as surfactants or sugars, including trehalose and sucrose, provide stability against denaturation by keeping the protein hydrated in its native form.

An alternative method for retaining encapsulated protein stability uses poly(amino acids) such as poly( $\gamma$ -glutamic acid) ( $\gamma$ -PGA), poly( $\epsilon$ -lysine), poly(L-arginine) or poly(L-histidine) which do not require an emulsion step in their synthesis [166-169]. These amphiphilic copolymers self-assemble via hydrophobic interactions to form polymeric structures consisting of a hydrophobic core and a hydrophilic outer shell [158, 170]. Moreover,  $\gamma$ -linked

glutamic acids in  $\gamma$ -PGA are not easily recognised by common proteases resulting in added stability [171, 172].

Hydrophilic polysaccharide polymers are also good candidates for vaccine delivery with both dextran and chitosan being chosen for preparing NPs [173-175]. Much attention has focused on chitosan NPs because of the biocompatibility of chitosan, its biodegradability into non toxic products *in vivo* and its ability to open up tight junctions between epithelial cells [176]. Chitosan NPs can be prepared in a number of ways. One method is a self-assembly technique through chemical modification, producing particles with a mean diameter of 160 nm [177]. Similarly, a complex coacervation process is sometimes used whereby particles form spontaneously when two hydrophilic colloids are mixed together, with chitosan precipitating around plasmid DNA [175]. These particles are 100-250 nm in diameter and protect the DNA from nuclease degradation. The emulsion-droplet coalescence technique pioneered by Tokumitsu and colleagues was developed for intra-tumoral injection [178]. It is based upon the emulsion crosslinking of chitosan and precipitation around the drug (gadopentetic acid). The particles formed were 450 nm in diameter and were appraised for their slow release and long-term retention within the tumour, making them an excellent delivery vehicle. An ionic gelation process based on the positively charged amino groups in chitosan and the negative charge of tripolyphosphate has also been used to prepare chitosan NPs in the size range of 20-400 nm [173, 179]. Sometimes these colloids will be further modified by the addition of an adjuvant on the surface, such as polyethylene glycol in order to aid absorption or to slow down release.

#### 1.4.5 Non-degradable nanoparticles

In contrast to the above NPs that consist of biological or biodegradable materials, non-degradable NPs are also being investigated for vaccine delivery [132, 180-182]. Among those commonly studied for vaccine delivery include gold, platinum, carbon and silica, which are used to generate a shell in which to encapsulate antigens or to provide a surface for covalent attachment. Gold NPs in particular are considered favourable for biomedical use due to their biocompatibility, non-toxicity and pre-existing license for human use [183-186]. Furthermore, the size of NPs made from gold, ranging from 1-100 nm, can be easily controlled by reducing a gold salt ( $\text{H}(\text{AuCl}_4)$ ) with various reducing

agents. The gold surface readily forms covalent bonds with thiol groups, allowing surface functionalisation with thiol containing compounds. Gold NPs synthesised using a gold salt reduction are typically monodisperse and uniform in shape, which is essential for maintaining antigen loading consistency between batches [187]. The smaller particles, formed from using a strong reducing agent, can then be grown to form larger particles with a desired aspect ratio using a “seeding” method with cetyltrimethylammonium bromide and silver acetate [133, 188-190]. Carbon NPs have also been investigated for their use in vaccine delivery including oral delivery [134]. Using silica NPs as a template, the particles are then carbonized at high temperatures under nitrogen gas and using sucrose as a carbon source. The resulting particle is over 450 nm in size with 50 nm mesopores embedded within the particle surface. Within these pockets a protein antigen can be protected from the harsh environment of the gastrointestinal tract, allowing oral administration to promote mucosal immunity [134]. An illustration of the various nanoparticle composites is shown in Figure 1.2.

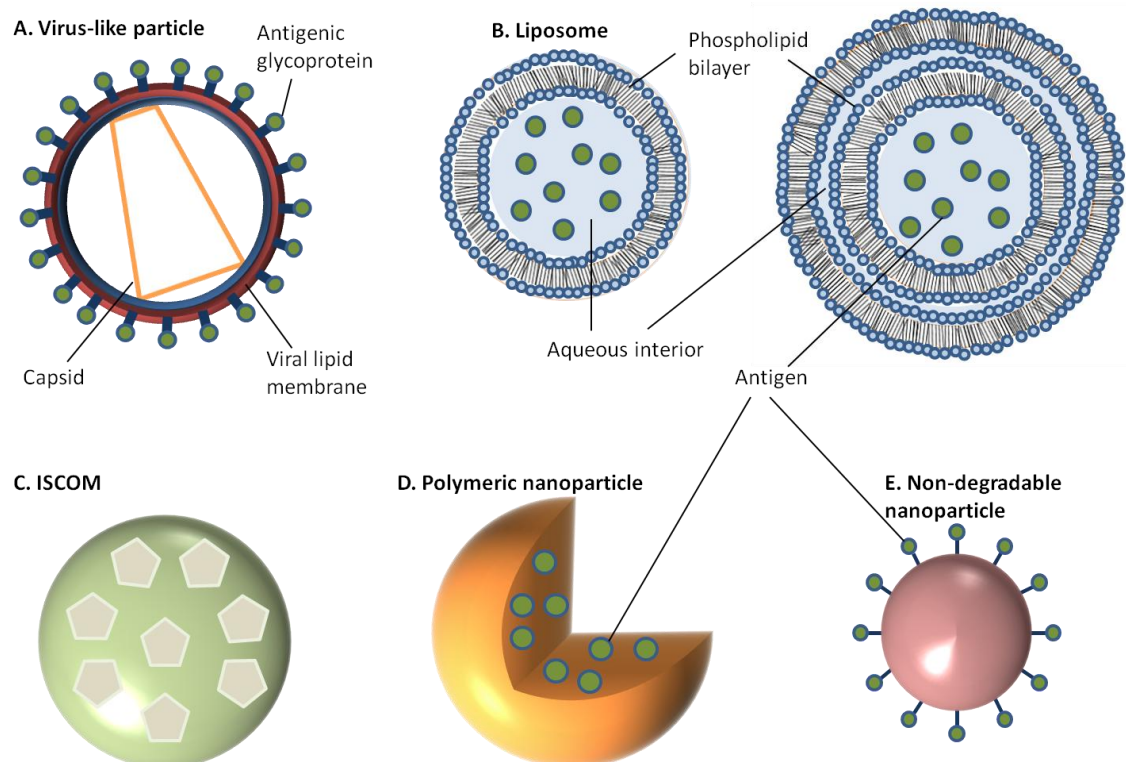


**Figure 1.2.** Schematic representation of different nanoparticle vaccine delivery systems. (A) Virus-like particle, (B) Liposome, (C) ISCOM, (D) Polymeric nanoparticle, (E) Non-degradable nanoparticle.

### 1.5 Nanoparticle uptake and immunity

The delivery of antigens to APCs is essential for developing antigen-specific B and T cell responses. This means that vaccine delivery systems are often targeted to these cells and modified to induce the desired immune response. By using NPs to deliver antigens, the efficiency of uptake into dendritic cells is significantly increased compared with soluble antigen alone; in some instances a 30-fold increase in uptake can be achieved [191, 192]. Similarly, studies comparing differences in uptake between micro- and nano- PLA particles have found that uptake by APCs is significantly increased for NPs. Chithrani *et al.* investigated the dependency of gold NPs size on uptake into HeLa cells by incubating cells with a range of NP sizes (14-100 nm) and then measuring their gold content using inductively coupled plasma atomic emission spectroscopy. The results showed that the optimal size for uptake was 50 nm and uptake increased significantly for the first 2 hours before it plateaued at between 4 and 7 hours post exposure [193]. Particle shape and surface charge are also important physicochemical factors playing crucial roles in the interaction between particles and APCs. In general, cationic particles are taken up into cells much more readily than those with an overall negative surface charge due to the anionic nature of cell membranes, whilst spherical compared to rod-shaped particles are also more readily endocytosed [194-196].

As well as the degree of uptake, the mechanisms by which NPs enter cells will have a direct impact on the type of immune response induced. This too is dependent on NP size, composition, shape and charge [29, 197-199]. Whilst PLGA microparticles typically enter macrophages through phagocytosis, there are a variety of mechanisms by which NPs may be internalised. It has been suggested that 43 nm polymeric NPs are taken up by HeLa cells via clathrin-dependent endocytosis, whilst 24 nm particles enter a cholesterol-independent, non-clathrin and non-caveolar dependent pathway [200]. NP shape can have a significant effect on the ability of macrophages to internalise particles via actin-driven movement of the macrophage membrane. Subsequently the phagocytosis of rod-shaped particles is often negligible when compared to spherical NPs [197, 201]. Both polymer and gold cationic NPs have been shown to enter various mammalian cell lines via non-endosomal pathways using a range of pharmacological inhibitors or cell lines with endogenous proteins considered essential for a transport mechanism knocked-out [202-207].

When poly(amino acid) NPs with encapsulated ovalbumin were used to immunise mice, significantly higher levels of total IgG, IgG1 and IgG2a were induced compared with the response to soluble ovalbumin, suggesting the particles have the ability to prime humoral and cellular immune responses since CD4<sup>+</sup> and CD8<sup>+</sup> T cell activation produces IFN $\gamma$  which induce Ig class switching to IgG2a [98, 99, 208]. Similarly, the loading of Hepatitis B core antigen into PLGA NPs (300 nm) induced a stronger cellular immune response in a murine model compared to Hepatitis B core antigen administered alone. Particle size also plays an important role in directing the immune response. Immunization with PLA NPs (200–600 nm) was associated with higher levels of IFN $\gamma$  production related to a Th1 response. In contrast, immunization with PLA microparticles (2–8  $\mu$ m) promoted IL-4 secretion related to a Th2 response [209]. Both PLGA NPs and liposomes are efficiently phagocytosed by dendritic cells in culture, resulting in their intracellular localization [210-212].

VLP's have been shown to produce strong humoral immune responses that are able to protect against human papillomavirus (HPV) infection in both animal models and human clinical trials using the HPV L1 protein [118, 213-216]. Through mimicking the native viral structure, VLP based vaccines (including those against influenza A and HIV) are able to enhance the production of neutralising antibodies by presenting antigens in their natural state as membrane-bound proteins rather than soluble ectodomains [217, 218]. However, this is mostly type-specific and may not protect against infection with heterologous types. Furthermore, cell mediated immune responses were also achieved with HPV VLPs, including T cell proliferation (CD4<sup>+</sup> and CD8<sup>+</sup>) [96, 219]. There is also an association of increases in Th1 and Th2 type cytokines (IFN $\gamma$  and IL-5, IL-10 respectively) stimulated with VLP immunisation [219, 220]. Once *in vivo*, particulate vaccine formulations of all types constitute an antigen depot, the effect of which is to allow a gradual release of antigens, prolonging exposure of the immune system to the antigen and essentially providing a booster dose. The pharmacokinetics/pharmacodynamics of each formulation will determine how slowly or otherwise antigen is released from the depot. In general though, particulate formulations confer benefits in terms of a reduced need for the administration of booster doses and a self-adjuvanting effect due to the enhanced uptake of particulates by APCs.

### *1.6 Limitations and ongoing questions*

The limitations of using NPs for the delivery of vaccines range from concerns over the toxicity of the particles, to difficulties in producing the materials and presenting antigens in their native form. The production of suitable NPs can also present some technical challenges. For other systems there are concerns over the stability or potential to scale up production. One of the greatest obstacles with liposome delivery systems is their instability [221, 222]. One of the ways in which this has been overcome is by modifying the surface with a hydrophilic polymer, such as glycol (e.g. polyethylene glycol, glycol chitosan). This serves as a barrier to reticuloendothelial system cells to extend its circulatory lifetime [223, 224]. The scale-up of production of sterile polymeric particles has also been problematic, though this has to some extent been overcome by the introduction of scaled-up spray-drying techniques. This allows polymer and payload, together with a stabiliser such as trehalose, to be sprayed at high temperature (80-100°C) through an orifice in clean room conditions [174, 225]. This is a batch process, typically yielding hundreds of milligrams of product (depending on equipment size and operating conditions), but care needs to be taken that a protein payload will not be damaged by either the heat or shear force. One way around this is to spray-dry the polymer and subsequently surface-absorb the protein antigen(s). Additionally, in order to overcome the risk of traces of unacceptable solvents in the final NP product, super-critical fluid technology is being applied to the generation of NP [226, 227]. In this approach, the PLGA polymer is solubilised in super-critical fluid solvent (freon/propanol) and the solution is compressed under pressure prior to introduction of the aqueous phase containing, for example, the recombinant protein. Polymeric particles then form of typical size range 300 nm-3 µm.

An ongoing concern with the introduction of NPs into biomedical applications has been their potential toxicity, not least because some materials which would otherwise be considered safe take on different characteristics in a nanoparticulate form and can sometimes become harmful [228]., In its naturally occurring mineral state titanium dioxide, for example, is biologically inert however, when administered as a NP smaller than 20 nm in diameter it causes an inflammatory reaction in animals and humans [229, 230]. Similarly, gold is generally regarded as a safe, inert material and is used routinely for medical implants. However, gold NPs with a diameter of 1.4 nm behave very differently

and have been shown to permeate cells and nuclear membranes and bind irreversibly in the major grooves of DNA causing instability [231]. The same is not true of all gold NPs and those of a slightly larger diameter (15 nm) are considered non-toxic at up to 60-fold higher concentrations [184, 232-234].

Other toxicity concerns associated with NP is the accumulation within cells, particularly with continuous exposure or long-term use. Indeed, fluorescent quantum dots have been observed in mice 2 years after injection [235]. As previously mentioned, the methods used to characterise cellular trafficking of NPs are often carried out using pharmacological inhibitors or mutant cell lines. The problem with these experiments is the specificity of the methods for one mechanism of trafficking, so the data can often be difficult to interpret or sometimes contradictory to other literature. For example, whilst Rejman *et al.* show that treating B16 cells with chlorpromazine strongly inhibits the uptake of negatively charged 50 nm polystyrene NPS compared with 200 nm particles, Santos *et al.* report an opposite result [198, 205]. In many cases it is perhaps best to use a combination of various inhibitors and mutated cell lines with carefully selected controls. Another problem associated with pharmacological inhibitors is their cell line specific efficacy, meaning that care must be taken when interpreting results from such studies and perhaps highlights the need for using several different cell lines to draw conclusions applicable to an *in vivo* model.

There are also some more specific concerns about components used in NPs. Despite the number of veterinary vaccines which utilise ISCOMs, there are uncertainties over the toxicity of some saponin-based adjuvants and this has to date prevented their licensure for use in humans. The toxicity of Quil A for example, has been identified in murines at an LD<sub>50</sub> of 0.67 mg/kg [236]. Similar results have also been documented with subcutaneous and intraperitoneal administration of Quil A [237, 238] where it is believed to cause degeneration of the liver [149]. However, this has so far only been documented in rodents, with little toxicity reported in larger terrestrial animals including rhesus monkeys, chickens, dogs and cattle [239-242].

***1.7 Objectives***

This study has been carried out to explore the use of gold nanoparticles as a vaccine delivery system. A variety of different size nanoparticles are considered and characterised according to their physicochemical properties to select an optimal size for antigen loading. The objective is then to explore methods for the chemical conjugation of peptides and polysaccharides (lipopolysaccharide and capsular polysaccharide) onto gold nanoparticles and identify an appropriate strategy. It is then the intention to evaluate the immunogenicity and protective capacity of these vaccines through a series of immunological assays and animal studies. Finally, this study aims to identify some of the underlying mechanisms involved in macrophage uptake of gold nanoparticles.

## Chapter 2: Materials and Methods

---

### 2.1 Gold nanoparticle synthesis

Unless otherwise stated, all reagents were purchased from Sigma-Aldrich Co. Ltd. (Gillingham, UK) and all solutions were prepared in ultrapure water (18 M $\Omega$ -cm at 25 °C, MilliQ, Millipore).

All nanoparticle synthesis reactions were performed in glass beakers cleaned with *Aqua Regia* (1 volume of HNO<sub>3</sub> and 3 volumes of HCl) and thoroughly rinsed with de-ionised water.

Citrate reduced gold nanoparticles were synthesised using the method of Turkevich [189, 243]. In a glass beaker, 90 mL 1 mM gold(III) chloride trihydrate (HAuCl<sub>4</sub>·3H<sub>2</sub>O, 99.9%) was heated to 90 °C. The solution was stirred vigorously with a Teflon® coated magnetic bar as 10 mL 90 mM sodium citrate dihydrate (Na<sub>3</sub>C<sub>6</sub>H<sub>5</sub>O<sub>7</sub>·2H<sub>2</sub>O, 99%) was added rapidly from a plastic syringe. The reaction underwent a colour change of gold to black, to colourless, to ruby red. Once the solution had reached this point it was allowed to cool to room temperature and then stored in the dark until needed.

Borohydride-reduced gold nanoparticles were also synthesised based on several previously published methods [244-247]. To 94 mL 1 mM gold(III) chloride trihydrate, 3 mL ice-cold sodium borohydride (NaBH<sub>4</sub>, ≥99%) was added rapidly at either 100 mM or 400 mM (final concentration 5 mM and 20 mM, respectively) followed by continuous stirring for 2 hours. These colloidal solutions were stored at room temperature in the dark.

### 2.2 Nanoparticle characterisation

Transmission electron microscopy was performed on the resulting borohydride and Turkevich colloid samples to image the resulting particles and assess their size distribution. A 2-4  $\mu$ L drop of nanoparticle colloid was placed directly onto a copper/palladium mesh grid with a formvar/carbon support film. After drying under a hot lamp, the nanoparticles were viewed at 80,000 x magnification in a Jeol JEM-1400 TEM and image capture was carried out using Digital Micrograph software (Gatan). Nanoparticle sizes were measured using the particle size

analysis function of the software. This method is based on a high contrast between the image background and the nanoparticles. The algorithm detects dark pixels, which are assigned as nanoparticles based on their large scattering cross section from their metallic composition, their shape and the measured diameter. The nanoparticle diameter is equivalent to the greatest dimension of each patch of dark pixels, thus, nanoparticle sizes determined in this way are given as 'equivalent spherical diameter'.

UV-visible absorbance spectra were recorded for nanoparticle colloids using 1 cm optical path length plastic cuvettes and a UV-visible spectrometer (Jenway 6705 UV/Vis spectrophotometer).

Nanoparticle tracking analysis were performed with a NanoSight LM20 (NanoSight, Amesbury, United Kingdom), equipped with a sample chamber with a 640-nm laser and a Viton fluoroelastomer O-ring. The samples were injected in the sample chamber with sterile syringes (BD Discardit II, New Jersey, USA). All measurements were performed at room temperature. The software used for capturing and analyzing the data was the NTA 2.0 Build 127.

### 2.3 Bacterial culture

Bacterial cultures were carried out in Luria Broth (LB) containing 10 g/L Tryptone, 5 g/L yeast extract, 10 g/L NaCl and pH 7.5. The solid medium, Luria Agar (LA), contained 1.5 % (w/v) standard microbiological agar; both were sterilised by autoclaving at 121°C for 15 minutes. All liquid cultures were incubated at 37°C, aerobically on a rotary shaker at 200 rpm.

Optical density (OD) was preferentially used to monitor bacterial growth and replication. The OD of bacterial cultures at 600 nm ( $OD_{600}$ ) was measured in 1 cm optical path length cuvettes with a UV-Visible Spectrophotometer (Jenway). Alternatively, bacterial viable cell numbers were measured as colony forming units (CFU). For this, a sample of culture was 10-fold serially diluted in ¼-strength Ringer's solution (7.2 g/L NaCl, 170 mg/L  $CaCl_2$  and 370 mg/L KCl in ultrapure water, pH 7.2) and a known volume of each dilution was spread onto LA medium in a petri dish. Colonies were counted after an overnight incubation at 37°C.

### 2.4 Protein expression and purification

Untagged recombinant F1-antigen was produced in *E. coli* JM101 containing plasmid pAH34L encoding the *caf* operon from *Y. pestis* strain GB and cultured in LB containing 50 µg/mL kanamycin [248]. The cultures were centrifuged at 14,000 × *g* for 45 minutes at 4 °C and the cell pellet and flocculant layer resuspended in 200 mL phosphate-buffered saline (PBS), pH 7.2 and incubated with gentle rolling at room temperature for 30 minutes. The resuspension was centrifuged at 14,000 × *g* for 30 minutes and the supernatant was adjusted to 50% ammonium sulphate saturation. After stirring for 1 hour, the fractionate was centrifuged at 14,000 × *g* for 30 minutes at 4 °C. The ammonium sulphate pellet was resuspended in PBS and dialysed against 4 × 2 L of the same buffer, overnight. The dialysed crude extract was centrifuged at 27 000 × *g* to remove insoluble material, followed by filter sterilisation using a 0.22-µm disposable filter (Amicon, Stonehouse, UK). Aliquots of 200 µL of the dialysed extract were applied to an FPLC Superose 12 HR 10/30 column that had been previously equilibrated with PBS. The rF1 was eluted with the same buffer at a flow rate of 0.5 mL/minutes. Peak fractions were collected and analysed for F1 by SDS-PAGE, Native PAGE and Western blotting (using a monoclonal antibody raised to F1). An enzyme-linked immunosorbent assay was performed to determine the concentration of F1 antigen produced, using purified F1 antigen from *Y. pestis* as a standard [249].

His-tagged recombinant TetHc was produced in *E. coli* BL21 containing plasmid pKS1 encoding the Hc fragment of TeNT from *Clostridium tetani* strain and cultured in LB containing 50 µg/mL kanamycin [250]. The cultures were grown to early log phase before the plasmid was induced with 1 mM IPTG for 4 hours at 37 °C. The cultures were centrifuged at 14 000 × *g* for 20 minutes at 4 °C and the cell pellet and flocculant layer resuspended in 100 mL BugBuster® (mixture of non-ionic detergents) solution, 30 Ku/µL lysozyme, 25 u/µL benzonuclease and 1 EDTA-free protease inhibitor tablet before incubating with gentle rolling at room temperature for 30 minutes. Insoluble cell debris was removed by centrifuging at 16,000 × *g* for 20 minutes at 4 °C and supernatant was added to HisBind column. The TetHc peptide was desalted in a PD10 buffer exchange column before concentrating in a vivaspin 6 column at 4,000 × *g* for 20 minutes at 4 °C. The resulting solution was collected and analysed for TetHc by SDS-PAGE, and Western blotting (using a monoclonal antibody

raised to TetHc). A bicinchoninic assay (BCA) assay was performed to determine the concentration of TetHc antigen produced, using purified BSA as a standard.

His-tagged recombinant Hcp1 (BMA\_A0742; residues 1-169) from *B. mallei* was expressed in *E.coli* ( $\lambda$ DE3) Rosetta containing pET28a (+) expression vector (Novagen) and cultured in Overnight Express instant TB medium (Novagen) for 18-20 hours [251]. The culture was lysed using 10 x CellLytic B (Sigma) and purified by Ni<sup>2+</sup> affinity chromatography. The Hcp1 peptide was dialysed against two changes of 10 mM Hepes/150 mM NaCl pH 7.4 and run on an SDS-PAGE to check for purity before being aliquoted and stored at -80 °C [251]. A bicinchoninic assay (BCA; Pierce) assay was performed to determine the concentration of the antigen produced, using purified BSA as a standard.

His-tagged recombinant FliC (BPSL3319) from *B. pseudomallei* was expressed in *E. coli* ( $\lambda$ DE3) Rosetta containing pET28a (+) expression vector (Novagen) and cultured in Overnight Express instant TB medium (Novagen) for 18-20 hours [251]. The cultures were lysed using 10 x CellLytic B (Sigma) and purified by Ni<sup>2+</sup> affinity chromatography. The FliC peptide was dialysed against two changes of 10 mM Hepes/300 mM NaCl pH 7.4 and run on an SDS-PAGE to check for purity before being aliquoted and stored at -80 °C [251]. A bicinchoninic assay (BCA) assay was performed to determine the concentration of the antigen produced, using purified bovine serum albumin (BSA) as a standard.

Purification of *B. mallei* and *B. pseudomallei* proteins was carried out by collaborators at the University of Texas, Austin, USA.

### 2.5 Glycoconjugate quantification

Confirmation of nano-glycoconjugate formation was done by measuring the absorbance spectra using a UV-visible spectrometer (Bio-Rad 680 microplate reader) where a red-shift in  $\lambda_{\text{max}}$  of AuNPs was indicative of coupling to the surface. A two-colour Western blot was also performed, where possible, using a rabbit polyclonal antibody (pAb) raised against TetHc and either a mouse mAb against LPS or rabbit sera against CPS (Statens Serum Institut; Denmark) before incubating with a goat secondary antibody raised against either rabbit or mouse, tagged with an infrared dye at 680 nm or 800 nm (LI-COR®),

respectively. The two infrared channels could then be viewed simultaneously on an Odyssey® CLx. Protein concentrations were measured using a BCA assay.

A modified version of a phenol-sulphuric acid assay was performed to determine the concentration of LPS conjugated onto AuNPs [262, 263]. As previously described, the MHDA linker attached to the AuNP surface was displaced using 11-mercapto-1-undecanol and the gold colloid removed by centrifugation. Next, 50  $\mu\text{L}$  of cleaved LPS or CPS was added in triplicates to a 96-well micro-titre plate alongside a known concentration of LPS or CPS. To each sample, 150  $\mu\text{L}$  concentrated  $\text{H}_2\text{SO}_4$  was added followed by the rapid addition of 30  $\mu\text{L}$  5% (w/v) phenol. The plate was covered and carefully floated on a static water bath for 5 minutes at 90 °C before cooling to room temperature and reading on a micro-titre plate reader (Bio-Rad 680 microplate reader) at 490 nm. In addition to using an LPS standard, a monosaccharide mixture of  $\beta\text{-D}$  glucose and  $\beta\text{-D}$  galactose (a C2 epimer of talose) in a 0.8:1 molar ratio was chosen to reflect the  $\beta\text{-D}$  glucopyranose and  $\alpha\text{-L}$  talopyranose composition of *B. thailandensis* LPS [264].

Since the centrifugation method of purifying AuNP conjugates was not completely efficient, a dilution of AuNPs matching the absorbance of cleaved polysaccharide at  $\lambda_{\text{max}}$  was added to the standards to control for the effects AuNPs have on colorimetric assays.

### 2.6 Immunisation/protection studies

**Chapter 3** Groups of 5 female 6-8 week old BALB/c mice were immunized once with 0.1 mL per mouse by the intra-muscular (IM) route: group 1 received 0.93  $\mu\text{g}$  F1-antigen conjugated NPs formulated in 0.26% (w/v) alhydrogel (AuNP-F1/alhy); group 2 received 0.93  $\mu\text{g}$  rF1-antigen conjugated NPs in PBS (AuNP-F1/PBS); group 3 received empty NPs in PBS (NP/PBS); group 4 received 0.93  $\mu\text{g}$  F1 formulated in 0.26% (w/v) alhydrogel (F1/alhy); and group 5 received 0.93  $\mu\text{g}$  F1 in PBS (F1/PBS). Mice were bled from the lateral tail vein each week to obtain blood for antibody analysis. Mice were euthanized after six weeks with terminal blood sampling and splenectomy. Animal handling and immunisations were carried out by collaborators at the defence, science and technology laboratory (DSTL).

**Chapter 4** Groups of 9 female 6-8 week old BALB/c mice which were immunised three times at two-weekly intervals, receiving 0.1 mL per mouse by

the intra-peritoneal (IP) route. One week after the final boost, mice were bled from the lateral tail vein to obtain blood for antibody analysis. Three weeks after the final boost, the mice were challenged by the intranasal (IN) route with  $2.27 \times 10^5$  CFU  $50 \mu\text{L}^{-1}$  ( $3 \times \text{LD}_{50}$ ) *B. mallei* strain ATTCC 23344 (China 7).

The groups of mice were as follows: group 1 received AuNPs conjugated with  $0.93 \mu\text{g}$  F1-antigen (NP-F1); group 2 received AuNPs conjugated with  $0.93 \mu\text{g}$  F1-antigen and  $0.93 \mu\text{g}$  LPS (NP-F1-LPS); group 3 received AuNPs conjugated with  $0.93 \mu\text{g}$  TetHc (NP-TetHc); group 4 received AuNPs conjugated with  $0.93 \mu\text{g}$  TetHc and  $0.93 \mu\text{g}$  LPS (NP-TetHc-LPS); group 5 received AuNPs conjugated with  $0.93 \mu\text{g}$  LPS (NP-LPS); group 6 received  $0.93 \mu\text{g}$  LPS (LPS) and group 7 received PBS (PBS). All of the vaccine materials were formulated in PBS with 0.26% (*w/v*) alhydrogel.

Mice were euthanized after three weeks when terminal blood sampling, a splenectomy and a lobectomy were performed at the end of the experiment. The protection study and organ removal were performed by collaborators at the University of Texas Medical Branch, Galveston, USA.

**Chapter 5** Groups of 6 female 6-8 week old MF1 mice were immunised by the subcutaneously (SC) route, three times bi-weekly receiving;  $0.5 \mu\text{g}$  CPS conjugated to AuNPs (AuNP-CPS),  $1 \mu\text{g}$  TetHc conjugated to AuNPs (AuNP-TetHc),  $0.5 \mu\text{g}$  CPS conjugated to  $1 \mu\text{g}$  TetHc on AuNPs (AuNP-TetHc-CPS), or Pevnar 13® (Pfizer). Pevnar 13 contains  $0.44 \mu\text{g}$  CPS serotype 3 in a  $100 \mu\text{L}$  dose. One week after the final boost, mice were bled from the lateral tail vein to obtain blood for antibody analysis. Four weeks after the final boost, the mice were challenged by the intranasal route with  $2.5 \times 10^5$  CFU  $50 \mu\text{L}^{-1}$  *S. pneumoniae* strain Xen10. All of the vaccine materials were formulated in PBS with 0.26% (*w/v*) alhydrogel. Mice were euthanized after 10 days or at an earlier time point if clinical symptoms deemed it appropriate.

### 2.7 Immunoanalysis

**Chapter 3** Serum from individual animals were assayed for F1-specific IgG titre using an enzyme-linked immunoassay (ELISA) [265]. Briefly, sera were aliquoted into microtitre wells pre-coated with  $5 \mu\text{g/mL}$  F1 (in PBS). Binding of serum was detected using an HRP-conjugated goat anti-mouse IgG, anti-mouse IgG1 or anti-mouse IgG2a (Abcam; 1:5000 in 1% skimmed milk in TBS) followed by incubation ( $37^\circ\text{C}$ , 1 hour). ABTS substrate was added (Pierce) and

the absorbance measured at 415 nm using a Multiskan plate reader. Titres were determined by comparison with a standard curve using Ascent software. Geometric mean titres were determined  $\pm$  standard error of the mean for each treatment, allowing a statistical comparison of mean titres between groups, using the Student's t-test.

A method for detecting antibody binding competition to F1-antigen with a protective polyclonal macaque serum was based on Williamson *et al.*, 2005 [266]. F1-antigen was coated (5  $\mu\text{g}/\text{mL}$ ) onto microtitre plate wells followed by the addition binding of reference serum at a 1:10 dilution. Individual sera were added in duplicate in a 2-fold dilution series in 1% (*w/v*) skimmed milk powder in TBS. Naive macaque serum was used as a negative control. HRP-conjugated goat anti-mouse IgG (Abcam; 1:5000 in 1% skimmed milk in TBS) was added followed by incubation (37 °C, 1 hour). Plates were washed prior to the addition of ABTS substrate (Pierce) with subsequent reading of the absorbance at 415 nm.

**Chapter 4** Sera was collected from animals 5 weeks post immunisation and assayed for antibody isotypes and IgG subclasses using an ELISA [265]. Microtitre plate wells were incubated with 50  $\mu\text{L}$  5  $\mu\text{g}/\text{mL}$  LPS and an anti-mouse Fab-specific antibody (both in PBS) overnight at 4 °C. The following day the plate was washed with 0.05% (*v/v*) Tween 20 in PBS and the wells blocked with 200  $\mu\text{L}$  3% (*w/v*) skimmed milk powder in PBS for 1 hour at 37 °C before washing again with Tween/PBS. Serum samples were diluted to 1:100 in 1% (*w/v*) skimmed milk powder in PBS before doing a 2-fold serial dilution on the plate. The appropriate antibody isotype or IgG subclass was diluted across the wells coated with anti-mouse antibody to construct a standard curve. Serum from mice given PBS was used as a negative control. The plate was incubated at 37 °C for 1 hour before it was washed three times with Tween/PBS. An appropriate isotype or IgG subclass specific goat anti-mouse horseradish peroxidase conjugate was added to the wells at a dilution specified by the manufacturer (Abcam) followed by incubation at 37 °C for 1 hour. The plate was washed a further three times with Tween/PBS before adding an ABTS substrate (Pierce). The absorbance from the wells was measured at 415 nm using a Multiskan plate reader. Titres were determined by comparison with a standard curve using Ascent software. Geometric mean titres were determined  $\pm$

standard error of the mean for each treatment with a 95 % confidence limit, allowing a statistical comparison of mean titres between groups.

Spleen and lungs were removed at the end of the experiment where they were then homogenised in Dulbecco's Modified Eagles Medium before plating out onto media selective for *B. mallei*. Colony counts were performed and compared with relative tissue mass before they were plotted on a histogram and comparative statistics were carried out.

**Chapter 5** Serum was collected from animals 5 weeks post immunisation and assayed for antibody subclasses and IgG isotypes using an ELISA [265]. Briefly, microtitre plate wells were incubated with 5 µg/mL CPS and an anti-mouse Fab-specific antibody (both in PBS) overnight at 4 °C. The following day the plate was washed with 0.05% (v/v) Tween 20 in PBS and the wells blocked with 200 µl 3% (w/v) skimmed milk powder in PBS for 1 hour at 37 °C before washing again with Tween/PBS. Serum samples were diluted to 1:100 in 1% (w/v) skimmed milk powder in PBS and diluted 2-fold down the plate. The appropriate antibody isotype or IgG subclass was diluted across the wells coated with anti-mouse antibody to construct a standard curve. Serum from mice given PBS was used as a negative control. The plate was incubated at 37 °C for 1 hour before it was washed three times with Tween/PBS. An appropriate isotype or IgG subclass specific goat anti-mouse horseradish peroxidase conjugate was added to the wells at a dilution specified by the manufacturer (Abam) followed by incubation at 37 °C for 1 hour. The plate was washed a further three times with Tween/PBS before adding an ABTS substrate (Pierce). The absorbance from the wells was measured at 415 nm using a Multiskan plate reader. Titres were determined by comparison with a standard curve using Ascent software. Geometric mean titres were determined ± standard error of the mean for each treatment, allowing a statistical comparison of mean titres between groups.

### 2.8 Flow cytometric analysis

Spleens from individual mice were homogenised in Dulbecco's Modified Eagles Medium supplemented with L-glutamine, penicillin and streptomycin and the suspension splenocytes washed by centrifugation (10,000 rpm; 5 minutes) prior to collecting the cell pellet and re-suspending the cells in DMEM supplemented as described above, with additional 10% (v/v) foetal calf serum. Live

splenocytes were enumerated and 200  $\mu$ L of each was aliquoted in duplicate to the wells of a 96-well plate, and F1-antigen was added to each well at a final concentration of 25  $\mu$ g/mL. Plates were incubated overnight (37 °C/5% CO<sub>2</sub>). The following day, plates were centrifuged and cell culture supernatants were collected and frozen (-80°C) pending analysis of cytokines by cytometric bead assay (Becton Dickinson, UK). Non-adherent splenocytes were removed after centrifugation, collected and stained with a mastermix of antibodies specific for surface markers CD3, CD4, CD8 and CD45, and each labelled with a different chromophore (Becton Dickinson, UK). Antibody-bound cells were analysed by fluorescence activated cells sorting (Cantifluor, Becton Dickinson, UK) and the percentage and activation status of cells in the mixed splenocyte suspension was determined. Splenectomy and flow cytometry was carried out by collaborators at DSTL.

### 2.9 *Live in vivo imaging*

The use of *S. pneumoniae* bioluminescence strain Xen10 enabled *in vivo* imaging of bacteria to track the progression of the disease. This was done by anaesthetising mice with nitrous oxide at given time points and imaging using an FxPro imaging system.

### 2.10 *Transmission electron microscopy*

The procedures used to prepare J774A.1 murine macrophages for electron microscopy imaging have been previously described [267-269]. Cells were grown on 3 cm glass bottom Mattek Petri sides (Mattek Co., USA) at a density of  $2 \times 10^5$  and incubated overnight (37 °C/5% CO<sub>2</sub>). The following day, plates were incubated with 15 nm AuNPs for one hour before they were fixed with 4% paraformaldehyde (EM grade) and 1% glutaraldehyde (EM grade, TAAB, England) in 0.1 M cacodylic buffer pH 7.2 for 10 minutes, then for a further 30 minutes in 4% paraformaldehyde (EM grade) in 0.1 M cacodylic buffer pH 7.2. Cells were then washed in PBS for 10 minutes and then in distilled water for 10 minutes, two times. The cells were incubated in 1% osmium tetroxide (TAAB) in water for 1 hour in the dark (to counter-fix the membranes). The cells were then washed in distilled water 3 times, 10 minutes each. Uranyl Acetate (SIGMA, England) 1% in water was added for 1 hour. After washing with distilled water 3 times, 5 minutes each, the cells were

dehydrated in water/ethanol series 10 minutes each 50, 70, 90, and 100% (100% was repeated 3 times). After that the cells were incubated in ethanol/Epon812 (EMS, England) 1/1 for 1 h, and then in pure resin Epon812 for a further 1 h. The cells with fresh resin were incubated in an oven at 65°C for 24 hours. Once the cells were incorporated into the resin block, thin (70 nm) sections cut with UltraCut-UCT (Leica, Netherlands) microtome were collected onto Formvar-coated copper slot grids and post-stained [with aqueous uranyl acetate or Reynold's lead citrate (EMS)] to enhance contrast/visualization. Thin sections were surveyed using a JEOL 1014 electron microscope (JEOL, Japan) operated at 80 kV to assess the quality of ultrastructural preservation, collect sets of 2D images.

### *2.11 Fluorescent particles*

Enhanced green fluorescent protein (eGFP; BioVision) was coupled onto AuNPs using the previously described carbodiimide coupling chemistry and characterised using previously described methods of UV/Vis spectrophotometry and band densitometry.

### *2.12 Phagosomal staining*

The procedures used to prepare J774A.1 murine macrophages for confocal microscopy imaging were as follows. Cells were grown on 35 mm glass bottom, uncoated,  $\mu$ -dish (Thistle scientific) at a density of  $2 \times 10^5$  and incubated overnight (37 °C/5% CO<sub>2</sub>). The following day, plates were washed with PBS for 10 minutes, three times before they were incubated with eGFP conjugated AuNPs for 2 hours and then fixed with 4% paraformaldehyde. The cells were washed with PBS for 10 minutes, three times, before adding a blocking/permeabilisation solution containing 0.2% saponin and 5% foetal bovine serum (FBS) in PBS for 10 minutes at room temperature. Following this, the cells were washed thoroughly with PBS for 10 minutes, three times. The presence of endosomal vesicles was detected using a rabbit anti-LAMP1 polyclonal (Abcam; 1:1000 in 0.2% saponin and 5% FBS in TBS) followed by incubation (4 °C, 2 hours). The cells were washed with PBS for 10 minutes, three times before adding a Cy5 conjugated goat anti-rabbit polyclonal antibody (Abcam; 1:5000 in 0.2% saponin and 5% FBS in TBS) followed by incubation in the dark (4 °C, 2 hours). The cells were washed with PBS for 10 minutes, three

times before adding 1 drop of DAPI containing vectashield (Vector laboratories) to stain the cell nuclei. Cells were surveyed using a Zeiss LSM510 Meta confocal-laser scanning microscope (Zeiss, USA) to assess the localisation of AuNPs with endosomal compartments.

### *2.13 Statistical analysis*

Statistical differences between mean values were calculated using an unpaired, two-tailed Student's t-test or a one-way ANOVA with orthogonal contrast. A Mantel-Haenszel test was used to compare survival curve data. A  $p$  value of  $\leq 0.05$  was considered significant.

## Chapter 3: Protein Antigens Coupled to Gold Nanoparticles

---

### 3.1 Introduction

#### *3.1.1 Gold nanoparticles*

The use of nanomaterials for biomedical purposes has increased significantly over the last 50 years with composites varying in size, shape and material. Gold, in particular, has attracted much interest due to its unique optical properties for imaging and site-directed release of drugs or antigens as well as being non-toxic and biocompatible [231, 270-274]. There are also established techniques for the fabrication of gold nanofibres (nanorods or nanotubes) and nanoparticles of various sizes with limited size dispersity [275]. The versatility and structural diversity of gold nanomaterials allows for a variety of approaches towards their application in therapy, biosensing and diagnostics. In this study, colloids were chosen over nanofibres based on their uniform presentation of antigens and uptake into APCs.

#### *3.1.2 Nanoparticle characterisation*

With a variety of methods available for synthesising nanoparticles of different shapes, sizes and compositions, it is important to be able to characterise accurately their physicochemical properties. Characterisation can be done using a variety of techniques; those which are relevant to this study are detailed below.

Electron microscopy is one of the most commonly used techniques for determining the size and shape of nanoparticles. Unlike optical microscopes which have a limited resolution of approximately 0.2  $\mu\text{m}$ , electron microscopes are able to achieve better than 50 pm resolution. This is because electron microscopes utilise the electro-magnetic wave properties of electrons rather than visible light. Whereas the minimum wavelength for visible light is approximately 400 nm, for electrons operating at an accelerating potential of 100 kV the minimum wavelength is approximately 1.2 pm, Equation 3.1. In this

study, transmission electron microscopy (TEM) was used to image gold nanoparticles in which a beam of electrons are accelerated through a vacuum and interact with the specimen. The resulting image is based on the diffraction of electrons as they pass through the specimen, although for gold nanoparticles this appears as an electron shadow as the electrons are unable to pass directly through. As well as providing a visual representation of nanoparticles, the mean size and distribution of particle size can also be measured using analytical software.

$$\lambda = \frac{h}{\sqrt{2m_0eU}}$$

**Equation 3.1.** The de Broglie equation, considering rest mass, where  $\lambda$  = wavelength,  $h$  = Planck's constant,  $m_0$  = rest mass of an electron,  $e$  = elementary charge and  $U$  = electric potential.

Optical spectroscopy is a useful technique for determining the structure and composition of gold nanoparticles, where the extinction (absorbance and scattering) spectrum is dominated by a localised surface plasmon resonance (LSPR). This is also the property which gives colloidal gold its vibrant colours [276, 277]. In the presence of an incidence light, the surface plasmon is made up of oscillating free electrons on the metal surface which have a resonant frequency dependent on the size, shape and material of nanoparticles [278]. Consequently, the plasmon is sensitive to changes at the NP surface and is limited by the penetration depth of LSPR which is approximately 90 nm [279]. An association between plasmonic shifts and NP surface functionalisation means that this property can be exploited for determining the association of biomaterials and is exclusive of the surrounding media [274, 280, 281]. The result is a change in the wave propagation and therefore the position and intensity of the wavelength of maximum extinction ( $\lambda_{\max}$ ) [282, 283]. The ability to characterise the NP surface using LSPR has been demonstrated both

theoretically and experimentally where  $\lambda_{\max}$  for coupled nanoparticles is significantly red-shifted from that of individual particles [278]. This also makes optical spectroscopy a useful method for measuring the stability of nanoparticles in suspension. The stability of nanoparticles is dependent on the electrostatic repulsion between particles due to surface ions or ligands. This can also be defined by the Hamaker constant, characterised by the polarisability of nanoparticles and the surrounding medium, which for metal nanoparticles is relatively large [284-286]. For spherical nanoparticles, the LSPR signal displays as a single peak due to a uniform surface polarization. However, for other nanomaterials with less symmetry, the LSPR signal intensity reduces,  $\lambda_{\max}$  red-shifts and multiple peaks appear due to an increase in charge separation, Figure 3.1 [287, 288].

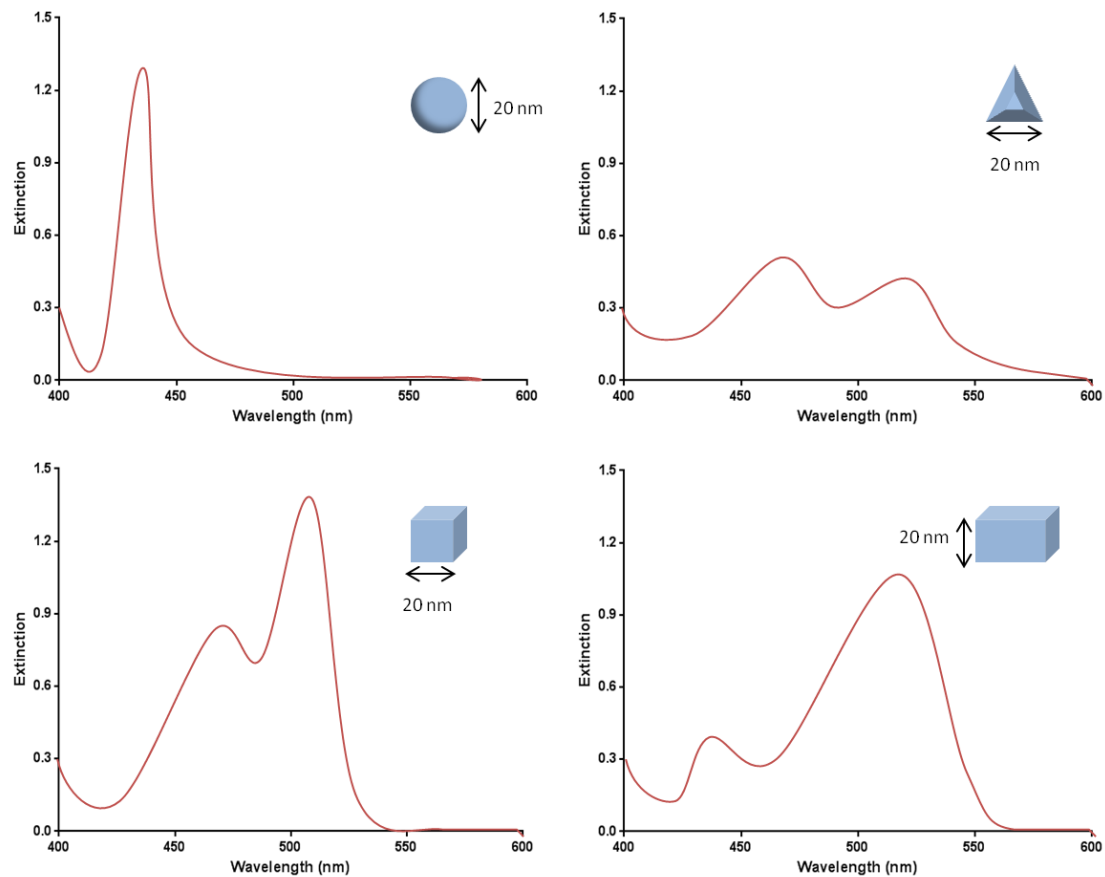


**Figure 3.1.** The spectral properties of LSPR are dependent on size and shape of nanomaterials. The number of modes in which a nanomaterial can be polarised determines the number of LSPR peaks. Therefore spherical particles exist as a single peak whereas non-spherical particles exhibited multiple red-shifted peaks. Image adapted from Hong *et al.* [289].

### 3.1.3 Protein-based vaccines

Protein-based vaccines (including toxins) have an advantage over other microbial component-based vaccines, such as polysaccharides and nucleic acids, in that they are recognised by T cells; an essential part of developing immunological memory. This is a result of peptide presentation on MHC I or MHC II molecules on the surface of APCs which activate CD8<sup>+</sup> and CD4<sup>+</sup> T cells respectively. Protective protein antigens are commonly membrane-bound to the pathogen and identified using a combination of genetic and immunoproteomic techniques such as two-dimensional electrophoresis and mass spectrometry. Whilst the first protein-based vaccines relied on purifying antigens from the hepatitis B virus (HBV) infected blood of human carriers, recent applications utilise recombinant DNA technology [290]. A diverse range of prokaryotic and eukaryotic cell lines have since been employed to express antigens which are then isolated to a high level of purity. The HBV vaccine later became the first licensed recombinant subunit vaccine in 1987 after its successful expression and purification in *Saccharomyces cerevisiae* [291, 292]. However, as previous discussed, protein-based vaccines often require an adjuvant to boost their immunogenicity. For the HBV vaccine, an alum-based adjuvant is commonly administered alongside immunisation.

Other subunit vaccines benefit from particulate vaccine delivery systems which adjuvant the immune response, such as VLPs. A vaccine against the human papillomavirus (HPV) consists of a surface protein, L1, from either two or four strains of the virus [293, 294]. The protein is then recombinantly expressed in *S. cerevisiae*, a well characterised eukaryotic cell line, after which it spontaneously self-assembles into an empty capsid, or VLP. In some instances proteins themselves can have an adjuvant effect and are covalently coupled or fused to antigens. Commonly referred to as 'protein carriers', these are often bacterial toxoids such as diphtheria and tetanus toxoid which are truncated, non-toxic forms of the original exotoxins. Diphtheria and tetanus toxoid are described as having universal Th epitopes, capable of eliciting both Th1 and Th2 responses [295-298]. As well being used in prophylactic formulations, tetanus toxoid has been studied as an immunotherapeutic vaccine against chronic HBV infection. By coupling tetanus toxoid to the HBV core protein, the vaccine was shown to elicit higher levels of HBV-specific Tc cells which play a key role in clearing infection [299]. A major structural protein of

Gram-negative flagella, FliC (flagellin), has also been studied for its adjuvant role in vaccine formulations [300-303]. This has been attributed to its high affinity binding to TLR5, which plays a fundamental role in activating innate immunity [304, 305]. Through the induction of cytokines and chemokines, flagellin increases the recruitment of B and T lymphocytes to draining lymph nodes resulting in enhanced activation of B cells and the generation of plasma and memory cells [306, 307].

#### *3.1.4 Objectives*

Whilst there are a wide variety of NP types to choose from, gold NPs are the subject of this study due to their excellent biocompatibility and low cytotoxicity [308]. The aim of this chapter will be to identify a gold nanoparticle composite suitable for vaccine delivery by comparing the physicochemical properties of different size gold colloids. A method of conjugating gold nanoparticles with previously identified antigenic peptides will then be explored with an aim to characterise the amount loaded and optimise the chemistry. The immunogenicity of a gold nanoparticle-antigen construct will then be assessed using a variety of immunological assays on sera derived from immunising BALB/c mice.

### 3.2 Materials and Methods

#### *3.2.1 Coupling chemistry for proteins onto gold nanoparticles*

Recombinant peptides were immobilised onto AuNPs using carbodiimide coupling chemistry. This was done by adding 0.1 mM 16-mercaptohexadecanoic acid (MHDA) followed by 0.1% (v/v) Triton® X-100 to a gold nanoparticle solution and incubated for 4 hours at room temperature. The mixture was centrifuged at 13,000 x g for 10 minutes, the supernatant removed and the pellet re-suspended in 50 mM 2-(*N*-morpholino)ethanesulfonic acid (MES) buffer pH 5.5, *N*-(3-dimethylaminopropyl)-*N*'-ethylcarbodiimide hydrochloride (EDC) and *N*-hydroxysuccinimide (NHS, 98%), 0.6 mM and 0.15 mM respectively were added before further adding the recombinant protein at the optimal concentration. The solution was incubated at room temperature for 18 hours.

Protein was added to the functionalised nanoparticles at a range of concentrations (10-100 µg/mL). The optimal concentration required to coat the gold nanoparticles was determined by those that did not undergo a colour change from burgundy to blue when 10% (w/v) NaCl was added to the solution. The appropriate concentration of protein was then used for conjugating to nanoparticles in further studies.

#### *3.2.2 Purifying protein conjugated nanoparticles*

Attempts at removing free protein from conjugates were first made using gel filtration chromatography. Solutions of F1- and TetHc-AuNP were added to Sepharose® 4B-cross linked chromatographic resin (GE Healthcare) in a 1.5 X 30 cm<sup>2</sup> column (flow rate of 1.3 ml minute<sup>-1</sup>). Eluted fractions of 0.5 mL were collected and their UV/Vis absorbance was measured at 280 and 520 nm.

Centrifugation was also used to separate unbound protein by adding 1.76 mM Triton X-100<sup>TM</sup> and spinning at 14,500 rpm for 10 minutes. AuNP conjugated proteins were resuspended in PBS with or without 0.26% (w/v) alhydrogel.

#### *3.2.3 Protein quantification*

Conjugated protein was released from AuNPs by displacing the MHDA linker from the gold using 0.1 mM 11-mercapto-1-undecanol (99%, Sigma-Aldrich)

and incubating at room temperature for 4 hours. The sample was separated through a NuPAGE® 4-12% Bis-Tris gel alongside known amounts of protein, before staining with Coomassie blue. Band densitometry, relative to a known standard, was used to determine the mass of protein released from the AuNPs. A BCA assay was used to support band densitometry data.

Coupling of proteins to AuNPs was confirmed by measuring shifts to the refractive index (RI) of AuNPs derived from the UV-visible absorbance spectra over the wavelength recorded.

Matrix assisted laser desorption/ionisation (MALDI) time-of-flight (ToF) mass spectrometer (Applied Biosystems, Framingham, USA) was employed to measure the mass of gold nanoparticles with and without conjugated protein. Mass analysis was performed using a 355 nm Nb:YAG laser in positive reflector mode with a 20 kV acceleration voltage [252].

### 3.3 Results

#### *3.3.1 Gold nanoparticle synthesis and characterisation*

Citrate reduction of gold (III) cations was shown to form spherical nanoparticles in a thermally induced reaction where the diameter of the particles was controlled by the concentration of citrate. The particles remain stable due to an electrostatic repulsion of the citrate coated anionic surface of the gold nanoparticles [309]. NP size was measured using the particle size analysis function from TEM software (Gatan). This identified that those particles synthesised via strong borohydride reduction (20 mM) were spherical in appearance and had a broad distribution of particles sizes. They had a mean diameter of  $5.3 \pm 4.3$  nm and a modal diameter of 2-3 nm, Figure 3.2. Gold NPs reduced using sodium citrate were also spherical but had a much narrower size distribution. The mean diameter of these particles was  $15.6 \pm 2.3$  nm with a modal diameter of 14 nm, Figure 3.3. Weak borohydride (5mM) reduction of gold (III) formed NPs with a truncated icosahedral shape and large size distribution. The mean diameter of these particles was  $45.6 \pm 17.4$  nm with a modal diameter of 35-39 nm, Figure 3.4. To determine the dispersity of NP size distribution, the coefficient of variation (that is,  $CV = \sigma/d$  where  $\sigma$  and  $d$  are the standard deviation and the mean size, respectively) was calculated whereby a CV of <5% is considered monodisperse and <15% indicates near

monodispersity [310]. Of the three NPs synthesised in solution, the two borohydride reduced NPs had a CV of 82% and 38% for 20 mM and 5 mM, respectively. Citrate reduced NPs had a CV of 14% meaning they were near monodisperse, whilst the other two solutions were polydisperse.

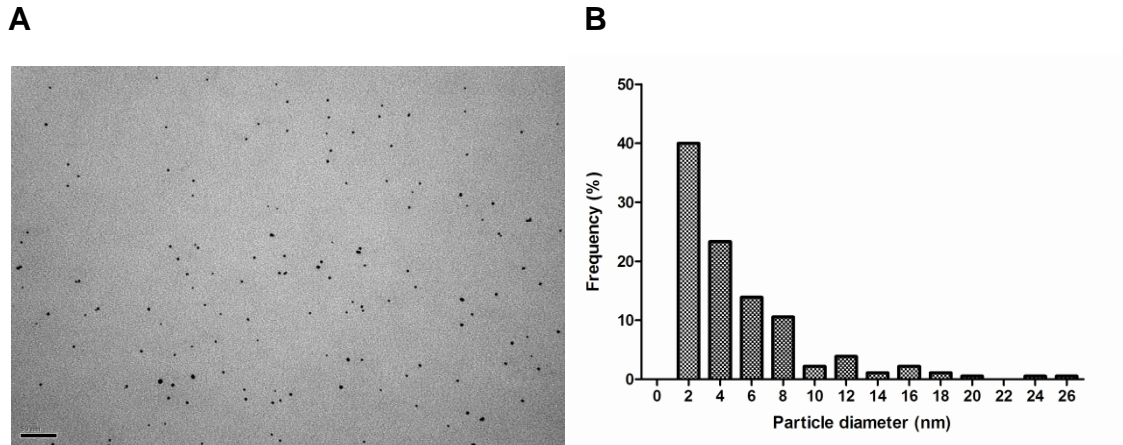


**Figure 3.2.** Transmission electron micrograph of gold nanoparticles formed by strong (20 mM)  $\text{NaBH}_4$  reduction (A) and histogram showing size distribution of particles (B). Bar is 50 nm

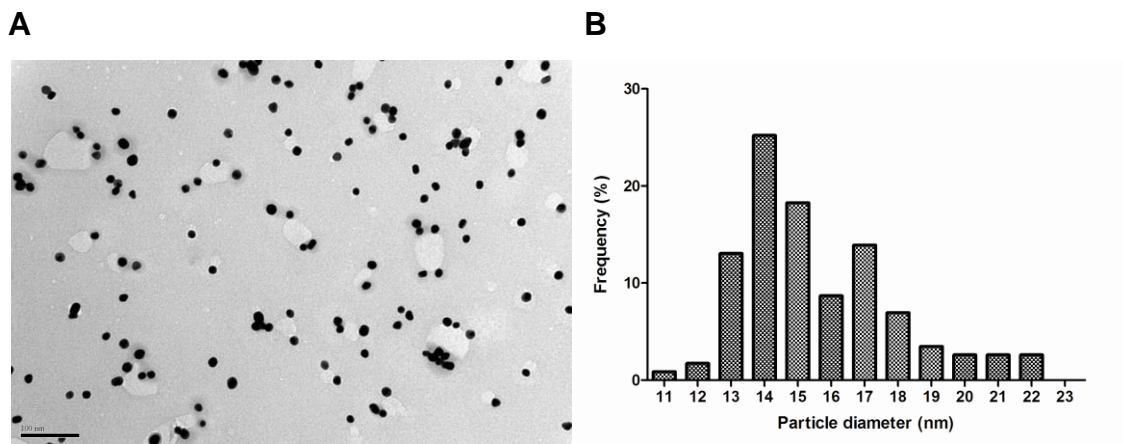


**Figure 3.3.** Transmission electron micrograph of gold nanoparticles formed by sodium citrate (9 mM) reduction (A) and histogram showing size distribution of particles (B). Bar is 100 nm

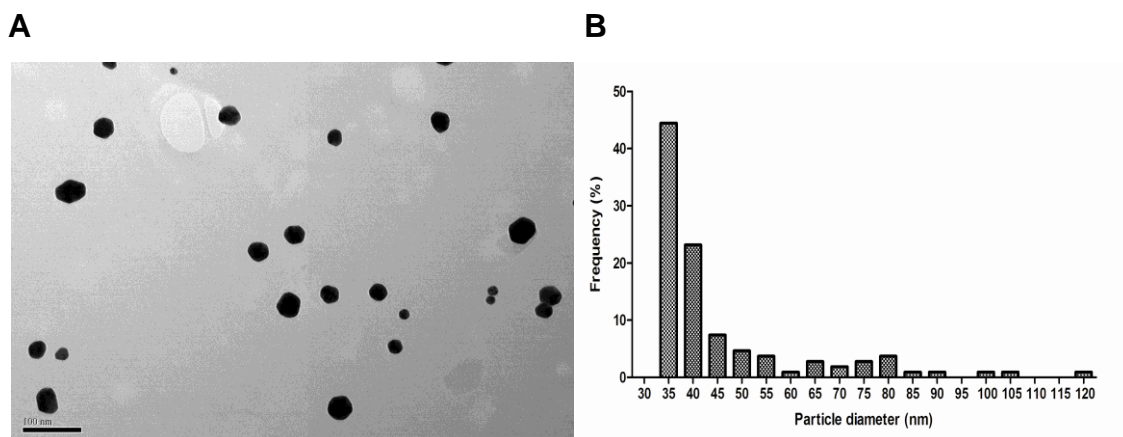


**Figure 3.4.** Transmission electron micrograph of gold nanoparticles formed by weak (5 mM)  $\text{NaBH}_4$  reduction (A) and histogram showing size distribution of particles (B). Bar is 100 nm

Further characterisation of gold NPs was carried out by measuring their extinction spectra in a spectrophotometer and recording the wavelength at maximum extinction (absorbed/scattered ( $\lambda_{\max}$ )). The position and shape of the extinction profile is dependent on the size, shape and composition of NPs. As expected from the TEM data, colloids synthesised using borohydride reduction had broad extinction peaks with  $\lambda_{\max}$  at 505 and 555 nm for strong and weak  $\text{NaBH}_4$  reduction respectively. Citrate reduced gold NPs gave a single, narrow extinction peak with  $\lambda_{\max}$  at 519 nm, Figure 3.5. As citrate reduced NPs consistently demonstrated a spherical shape and narrow size distribution it was therefore decided that only citrate reduced NPs would be used for further study, which are herein referred to as AuNPs.

The stability of AuNPs was measured over 300 days by recording the extinction spectra, Figure 3.6. Whilst  $\lambda_{\max}$  of 519 nm remained fairly constant ( $\pm 0.94$  nm) for the time period chosen, overall absorption fell by over 50% after 180 days. This could be due to small changes in pH over time, causing some of the particles to aggregate and sediment which would reduce the concentration of particles in solution and subsequently the overall absorption. The maximum extinction for AuNPs over time was recorded to demonstrate the half-life of particles, which was approximately 200 days, Figure 3.7. As a result, a fresh batch of AuNPs was prepared every 6 months. Using NP tracking analysis by NanoSight NS500, which relates the rate of Brownian motion to particle size, the concentration of AuNPs was measured to be  $1.37 \times 10^{12}$  particles  $\text{mL}^{-1}$ .

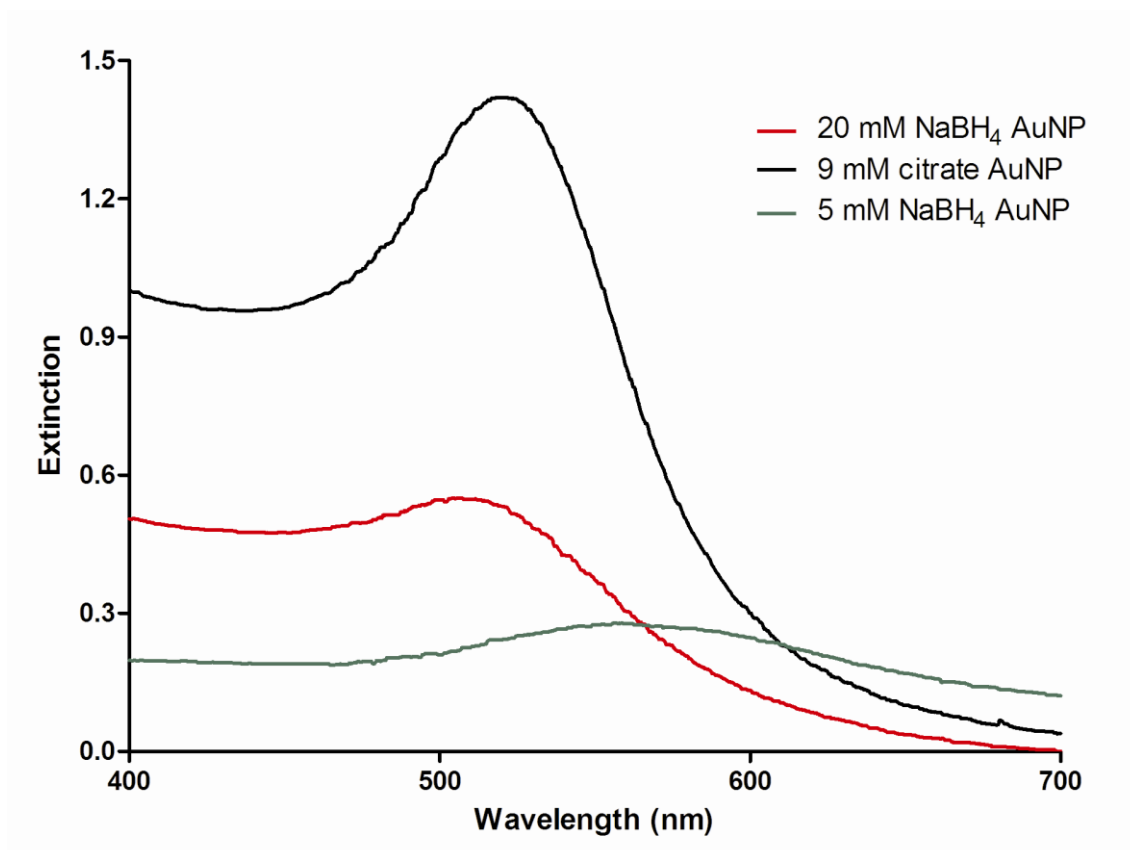


**Figure 3.5.** UV-visible extinction spectra for gold nanoparticles formed by reduction of gold (III) cations using either sodium borohydride (NaBH<sub>4</sub>) or sodium citrate.

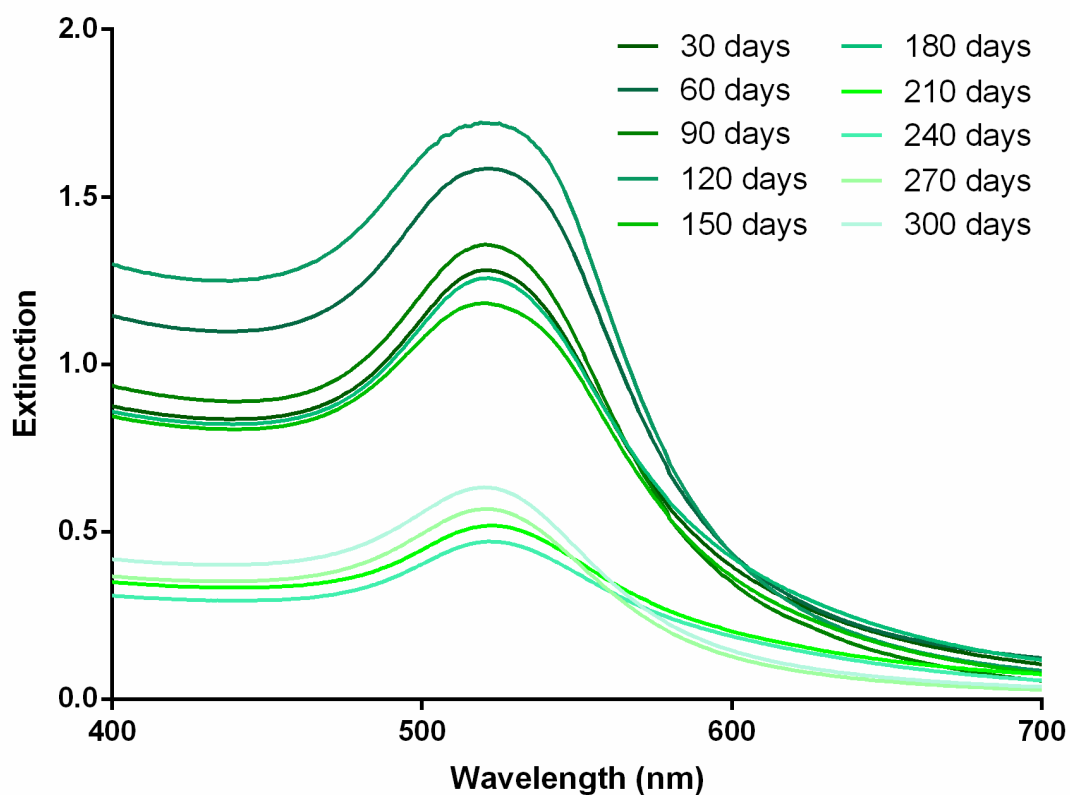


**Figure 3.6.** UV-visible extinction spectra for citrate reduced gold nanoparticles over a 300 day period.

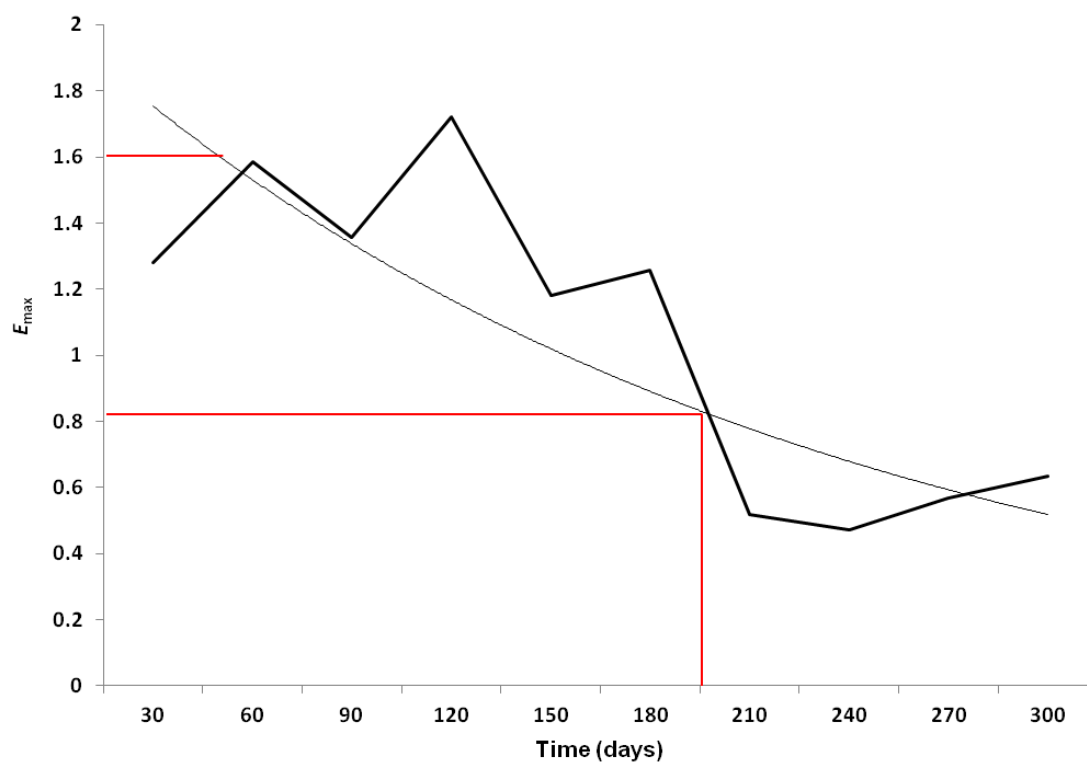


**Figure 3.7.** Maximum extinction of AuNPs over time, demonstrating the half-life

### 3.3.2 Peptide coupling and purification of nano-conjugates

To prepare the AuNPs for conjugation to a protein carrier, 16-mercaptohexadecanoic acid (MHDA), consisting of a thiol group at one end and a carboxyl group at the other, was added to the AuNP solution. The thiol groups in this molecule readily bind to gold resulting in a self assembled monolayer with projecting carboxyl groups. Carbodiimide chemistry was employed to carry out protein conjugation onto an MHDA linker attached to the surface of AuNPs. In this reaction, the terminal carboxyl group from MHDA reacts with EDC to form a mixture of unstable O-acylisourea intermediate isomers. These are susceptible to nucleophilic attack from primary amino groups which come from  $\epsilon$ -lysine residues in the protein chosen for conjugation. Four proteins were individually coupled onto functionalised AuNPs; *Y. pestis* capsular F1 antigen (F1), tetanus toxoid (TetHc), *B. mallei* T6SS protein (Hcp1) and *B. pseudomallei* flagellin (FlIC). The addition of NHS activates the MHDA linker by forming an NHS ester on the MHDA linker, with isourea acting as a leaving-group. This also prevents the formation of an undesirable N-acylisourea by rearrangement chemistry. The nucleophilic primary amine from the protein then replaces NHS in a  $S_N2$  type reaction and an amide bond between the protein and MHDA linker is formed, Figure 3.8. The reaction must be carried out in buffers which do not contain any carboxyl groups or amines to avoid any unwanted crosslinking, and at an acidic pH for greatest efficiency. For these reasons, MES buffer at pH 4.5 was used.

Separation of unbound protein from AuNP conjugated protein was first attempted by gel filtration chromatography. Samples containing F1 and TetHc conjugated AuNPs were loaded onto a 1.5 X 30 cm<sup>2</sup> column containing Sepharose® 4B chromatographic resin and 0.5 mL fractions were collected before being measured using UV-visible absorption at 280 and 520 nm to identify protein and AuNPs, respectively. Unfortunately, the resin used was unable to separate sufficiently the unbound protein from AuNP-conjugated protein and were both eluted in the same fractions, Figures 3.9 and 3.10. Centrifugation at a range of speeds for various lengths of time was then used to separate bound/unbound protein but this resulted in aggregation of AuNPs. However, further optimisation showed that the addition of a non-ionic surfactant, Triton X-100™ at a concentration above its critical micelle concentration (CMC = 0.24 mM) was able to overcome this problem. Using Triton X-100 at a

concentration below the CMC was unsuccessful at preventing NP aggregation. Centrifugation at 14,500 rpm for 10 minutes was sufficient for pelleting 95% of colloidal gold from the solution. A calibration curve of colloidal dilutions was used to determine the separation efficacy using the centrifugation method, Figure 3.11.

Functionalisation of AuNPs with MHDA, followed by protein coupling was confirmed by measuring the extinction spectra and observing a red-shift in the plasmon, Figure 3.12. When measured,  $\lambda_{\text{max}}$  increased by 8 nm from 519 nm for bare AuNPs to 527 nm with MHDA attached and a further 5 nm to 532 nm with a protein conjugated.

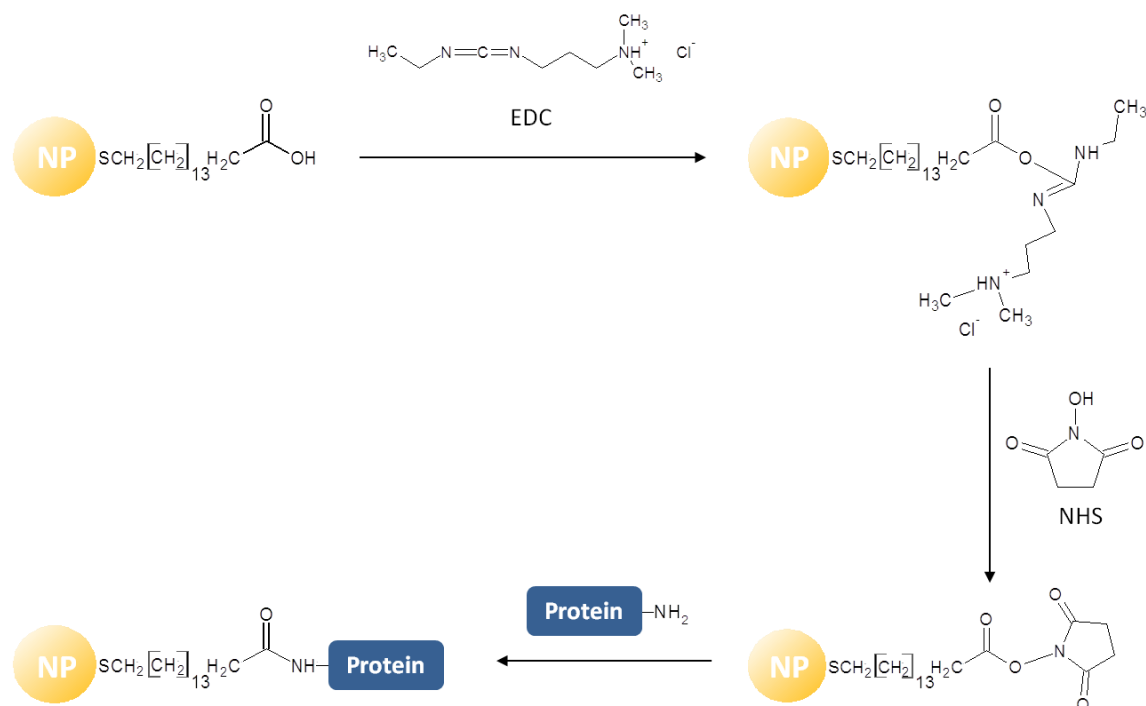


**Figure 3.8.** Reaction scheme between MHDA linker and protein using EDC/NHS carbodiimide coupling chemistry

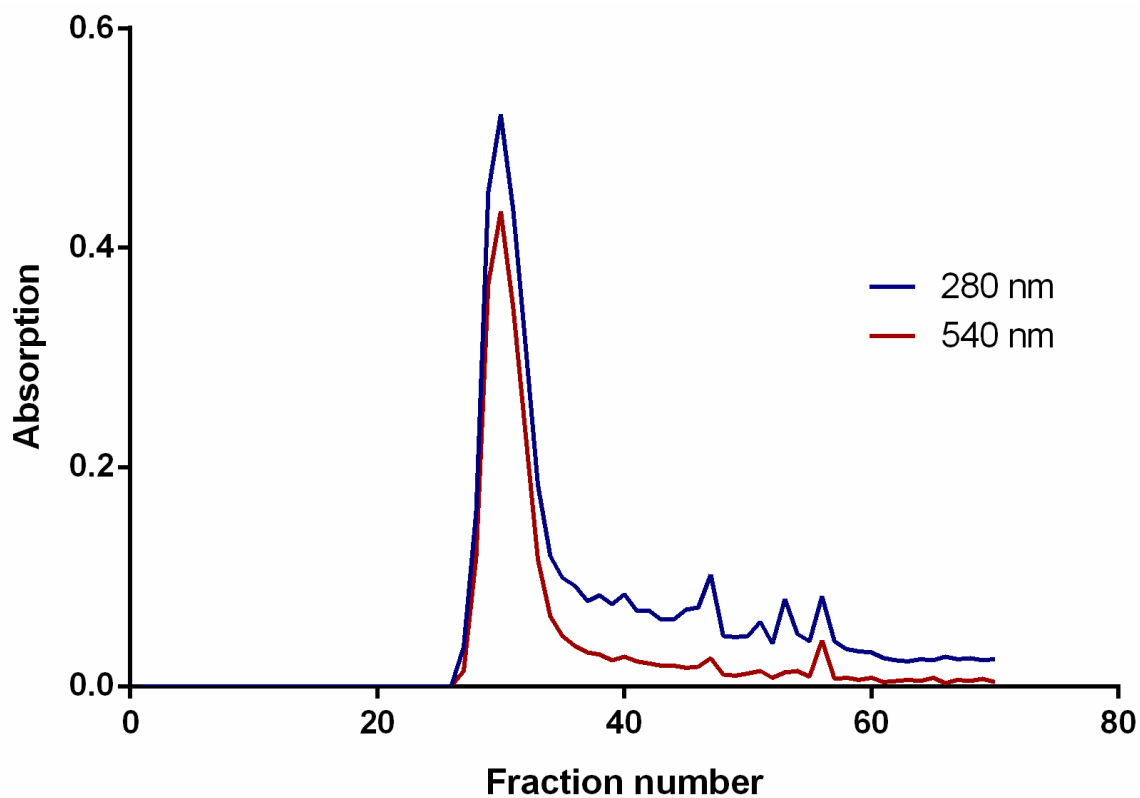


**Figure 3.9.** Gel filtration chromatography profile for F1 conjugated AuNPs. Fractions of 0.5 mL were collected from a 1.5 X 30 cm<sup>2</sup> column containing Sepharose® 4B-cross linked chromatographic resin and the absorption measured at 280 and 520 nm. The resin was unsuccessful at separating the unbound protein from AuNP conjugated protein.

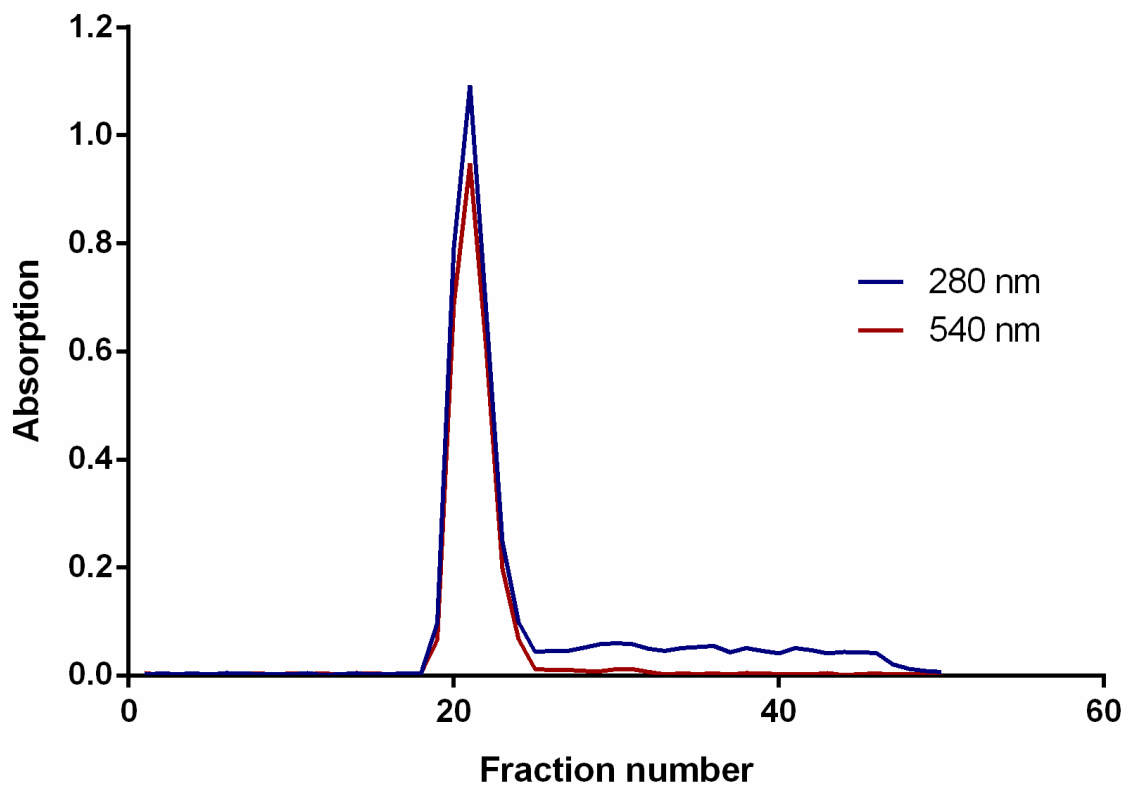


**Figure 3.10.** Gel filtration chromatography profile for TetHc conjugated AuNPs. Fractions of 0.5 mL were collected from a 1.5 X 30 cm<sup>2</sup> column containing Sepharose® 4B-cross linked chromatographic resin and the absorption measured at 280 and 520 nm. The resin was unsuccessful at separating the unbound protein from AuNP conjugated protein.

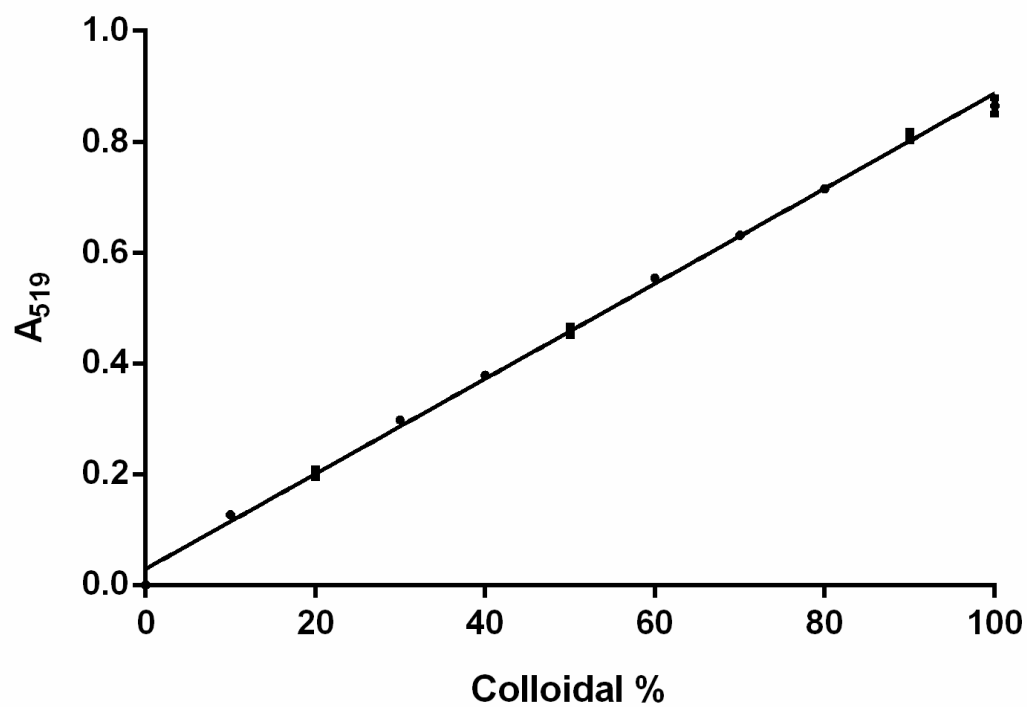


**Figure 3.11.** Calibration curve of colloidal dilution. This was used to determine the efficacy of removing AuNPs by centrifugation. Each point represents the mean of three values and error bars represent the standard error of the mean.  $R^2=0.9989$

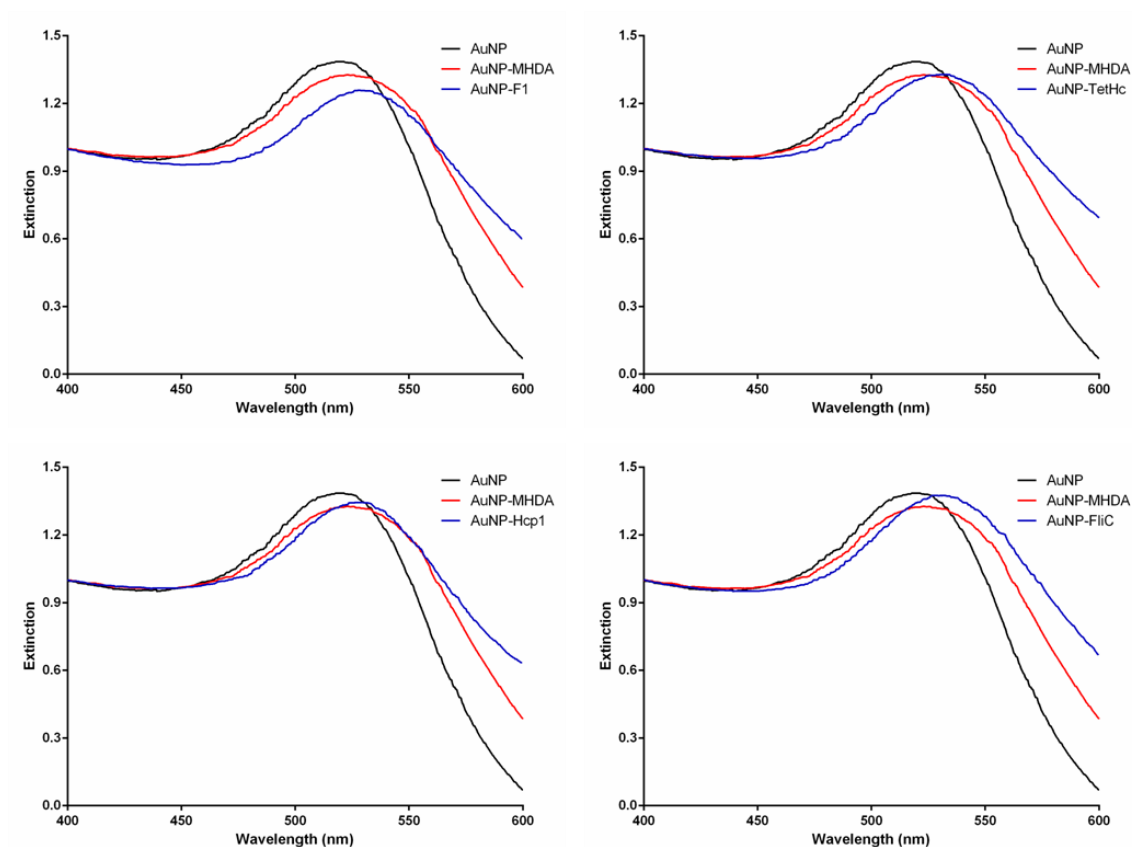


**Figure 3.12.** UV-visible absorption spectra for AuNPs, AuNPs functionalised with MHDA and AuNPs functionalised with MHDA coupled with either F1, TetHc, Hcp1 or FliC

### 3.3.3 Nanoconjugate quantification

The optimal concentration of protein required for saturating the gold surface was determined by adding 10% (w/v) NaCl to AuNPs conjugated to a range of protein concentrations, Figure 3.13. Since the Na<sup>+</sup> ions in the salt neutralise the anionic surface of AuNPs, those which are not fully decorated with protein aggregate and fall out of suspension. For F1, this was determined to be 30 µg/mL. For TetHc it was 35 µg/mL, Hcp1 was 25 µg/mL and FliC was 30 µg/mL.

Quantification of protein loaded onto the NP surface was done using a combination of methods. The first involved displacement of the MHDA linker from the gold surface by adding 11-mercapto-1-undecanol. The solution was then run on an SDS-PAGE gel alongside a range of known protein concentrations to generate a calibration curve, Figures 3.14 and 3.15. Whilst AuNPs remain at the top of the well, the protein runs freely through the gel and the relative intensity of the protein band could be quantified against a standard curve of known concentrations. Using this technique, the amount of F1, TetHc, Hcp1 and FliC conjugated to AuNPs was 20 µg/mL, 28 µg/mL, 25 µg/mL and 20 µg/mL respectively.

A BCA assay was also used to quantify the amount of protein coupled to AuNPs. As before, the protein coupled linker was displaced with 11-mercapto-1-undecanol but then the released protein was separated from the AuNPs by centrifugation. This method of purifying the released protein was effective at removing over 95% of AuNPs determined by comparing absorption at  $\lambda_{\max}$ . However, since the colourimetric Cu<sup>2+</sup> reduction of the BCA assay absorbs light at 562 nm, the remaining 5% colloid was enough to affect the results of the assay. To overcome this, the absorption spectra for the supernatant were recorded and bare nanoparticles were diluted to this value and added to the known concentration of protein to be used for the standard curve. Using this technique, the amount of F1, TetHc, Hcp1 and FliC conjugated to the AuNPs was 18 µg/mL, 30 µg/mL, 16 µg/mL and 12 µg/mL respectively. A summary of the measured protein concentrations is shown in Table 3.1

MALDI-ToF was used for direct quantification of total protein load. It was hoped that by comparing the m/z of bare AuNPs to protein coupled AuNPs, the amount of protein coupled could be calculated using a known concentration of the protein as a standard, Figure 3.16. Unfortunately this was unsuccessful and the resultant spectrum shows peaks of approximately 197 m/z apart, the atomic

mass of gold, suggesting that gold is being ablated from AuNPs atom by atom but that the conjugates are too heavy to allow desorption from the matrix surface.

Information regarding NP concentration, protein concentration and protein molecular weight was then used to determine the number of protein molecules per NP. The number of F1 proteins conjugated to each NP is approximately 72, for TetHc its 38, Hcp1 is 77.6 and FliC is 50.4 protein molecules  $\text{NP}^{-1}$ . These numbers fit comfortably within the theoretical estimate of coupling capacity on AuNPs which is between 10 and 100 molecules  $\text{NP}^{-1}$ . This is based on the surface area of AuNPs, which is approximately  $640 \text{ nm}^2$  (16 nm diameter) and assuming the protein molecules have a footprint of approximately  $25 \text{ nm}^2$ .

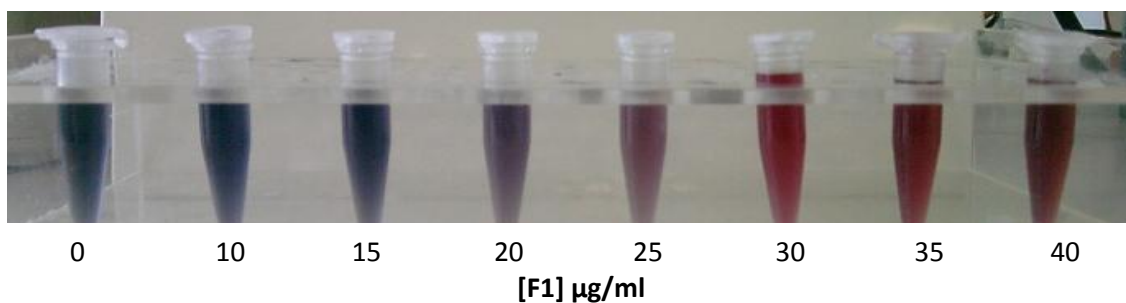


**Figure 3.13.** Aggregation assay to determine the minimum concentration of protein required to saturate AuNPs. Proteins at a range of concentrations were conjugated onto AuNPs and the minimum concentration required to saturate the surface was identified as the ones which did not undergo a colour change from burgundy to blue upon addition of 10% (w/v) NaCl.

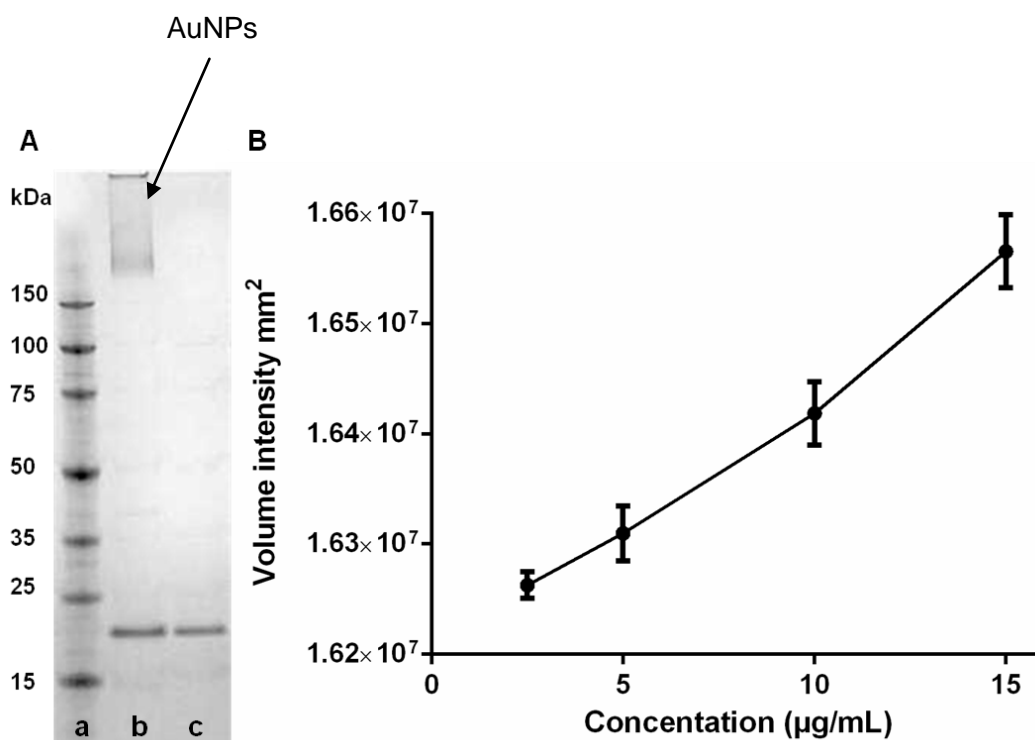


**Figure 3.14.** Quantification of F1 conjugated onto AuNPs. Coomassie blue stained NuPAGE 4-12% Bis-Tris gel showing protein displacement from AuNPs (A); Perfect Protein™ marker (a), 0.3 µg F1 conjugated onto AuNPs and treated with 11-mercapto-1-undecanol (AuNP at top of lane) (b), 0.2 µg F1 (c). Standard curve used to calculate protein concentration released from nanoconjugates based on protein band intensity from known concentrations of the same protein (B).

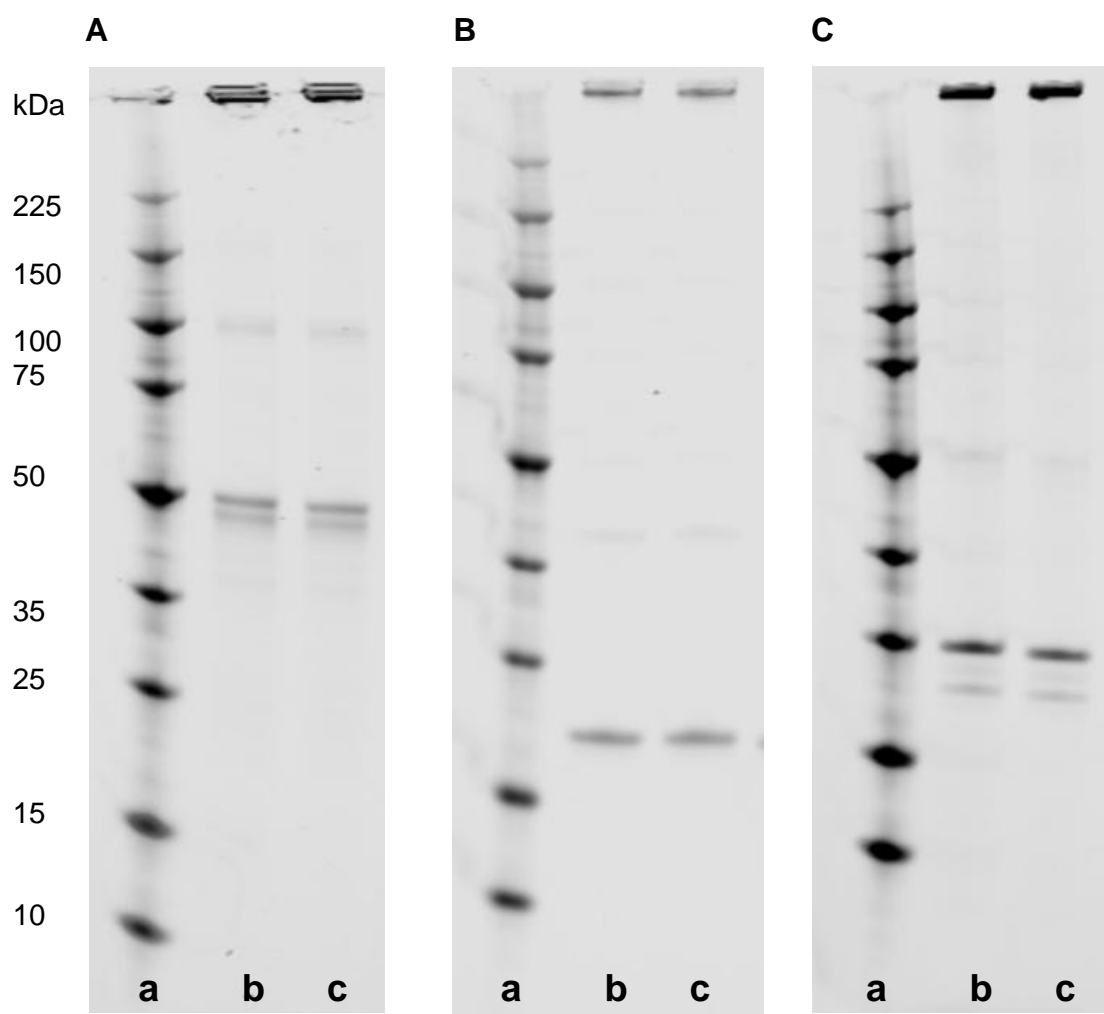


**Figure 3.15.** Coomassie blue stained NuPAGE 4-12% Bis-Tris gel showing AuNP displacement from 0.3  $\mu\text{g}$  TetHc (A), 0.3  $\mu\text{g}$  Hcp1 (B) and 0.3  $\mu\text{g}$  FliC (C); Perfect Protein™ marker (a), AuNP-protein treated with 11-mercapto-1-undecanol (AuNP at top of lane) (b and c)

**Table 3.1.** Summary of measured protein concentrations conjugated to AuNPs

<b>Technique</b>	<b>F1 conc. (<math>\mu\text{g/mL}</math>)</b>	<b>TetHc conc. (<math>\mu\text{g/mL}</math>)</b>	<b>Hcp1 conc. (<math>\mu\text{g/mL}</math>)</b>	<b>FliC conc. (<math>\mu\text{g/mL}</math>)</b>
NaCl assay	30	35	25	30
SDS-PAGE	20	28	25	20
BCA assay	18	30	16	12
<b>Average</b>	<b><math>23 \pm 4</math></b>	<b><math>31 \pm 2</math></b>	<b><math>22 \pm 3</math></b>	<b><math>21 \pm 5</math></b>

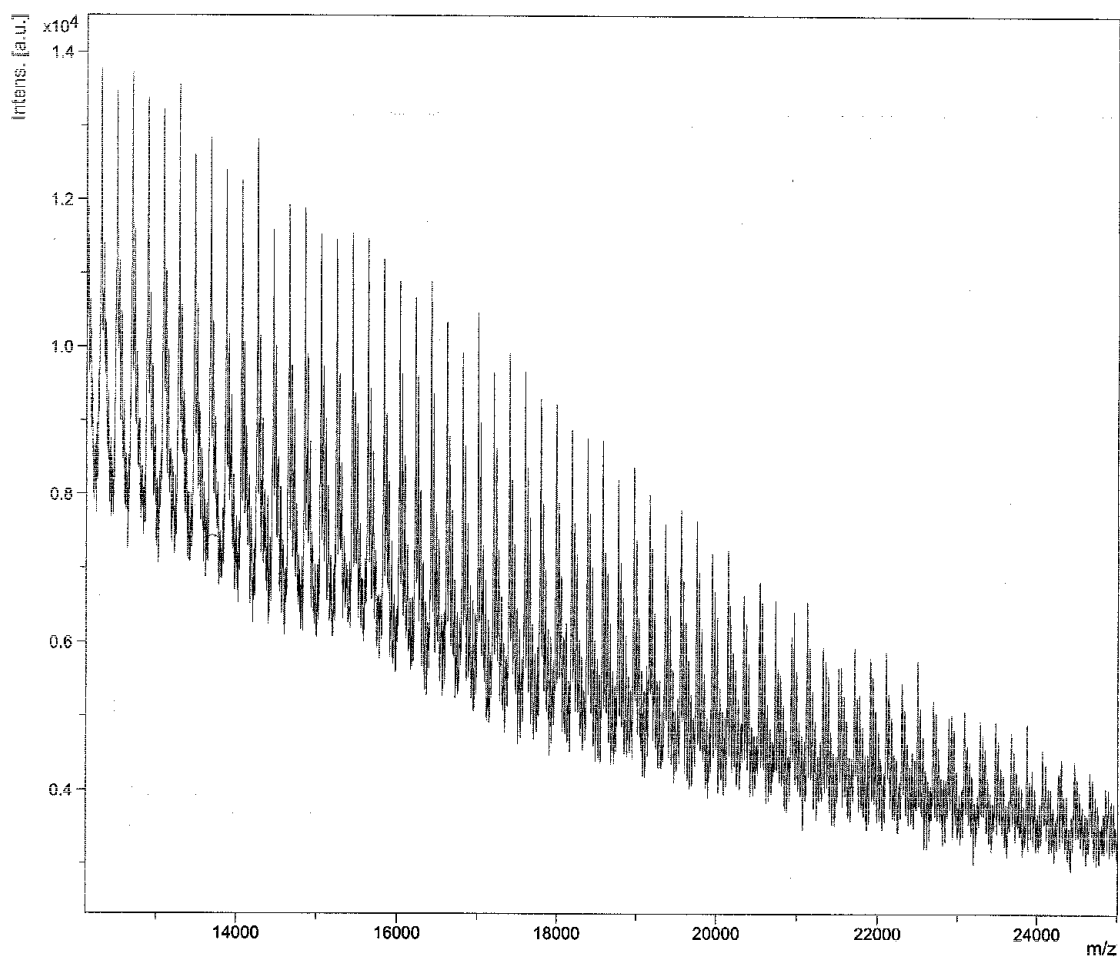


**Figure 3.16.** MALDI-ToF spectra for AuNP-F1 showing desorption of atomic gold from the matrix surface. Measurements were taken using a 355 nm Nb:YAG laser in positive reflector mode with a 20 kV acceleration voltage

### 3.3.4 Immunisation study

To evaluate the immunogenicity of an antigen coupled to AuNPs, BALB/c mice were immunised IM with a single dose of F1 conjugated AuNPs with or without an aluminium hydroxide adjuvant (alhydrogel). The experiment ran for six weeks and the development of antibody to F1-antigen in sera was measured using an ELISA, Figure 3.17. Control mice received F1-antigen in either alhydrogel or PBS, or AuNPs alone. After 14 days, mice given AuNP-F1/alhy had the highest level of F1-antigen-specific antibody when compared with mice immunised with AuNP-F1/PBS ( $p < 0.01$ ). Mice immunised with F1/alhy generated a greater IgG titre than those in the groups with PBS instead of alhydrogel ( $p < 0.01$ ). There was a significant decline in IgG titres in mice immunised with unconjugated F1-antigen with or without alhydrogel from days 35 or 21 days respectively, post immunisation ( $p < 0.01$ ). Mice given AuNP-F1/alhy showed no decline in IgG titre at 42 days post-immunisation. Mice immunised with empty AuNPs alone did not develop antibody against F1-antigen (data not shown). IgG subclasses were also measured and showed the concentration of F1-specific IgG2a in mice immunised with AuNP-F1/PBS was significantly increased compared with mice administered unconjugated F1/PBS ( $p < 0.05$ ). Formulation of AuNP-F1/alhy significantly increased both IgG1 and IgG2a responses, ( $p < 0.01$  and  $p < 0.05$ , respectively), compared with AuNP-F1/PBS. However, in all of the immunised groups the concentration of F1-specific IgG1 exceeded IgG2a, Table 3.2.

Sera collected from mice in individual treatment groups was assessed for the ability to compete with sera from macaques previously immunised with F1-antigen. This serum has been shown to provide passive protection to mice from a *Y. pestis* challenge [311]. The sera from mice immunised with F1-antigen formulations was able to displace the macaque sera, Figure 3.18. Sera from animals immunised with AuNP-F1/alhy competed most successfully with the macaque antibody, with a significantly greater percentage binding than any other group for the initial two dilutions ( $p < 0.01$ ). Sera from mice immunised with AuNP-F1 or unconjugated F1-antigen competed similarly with the macaque sera.

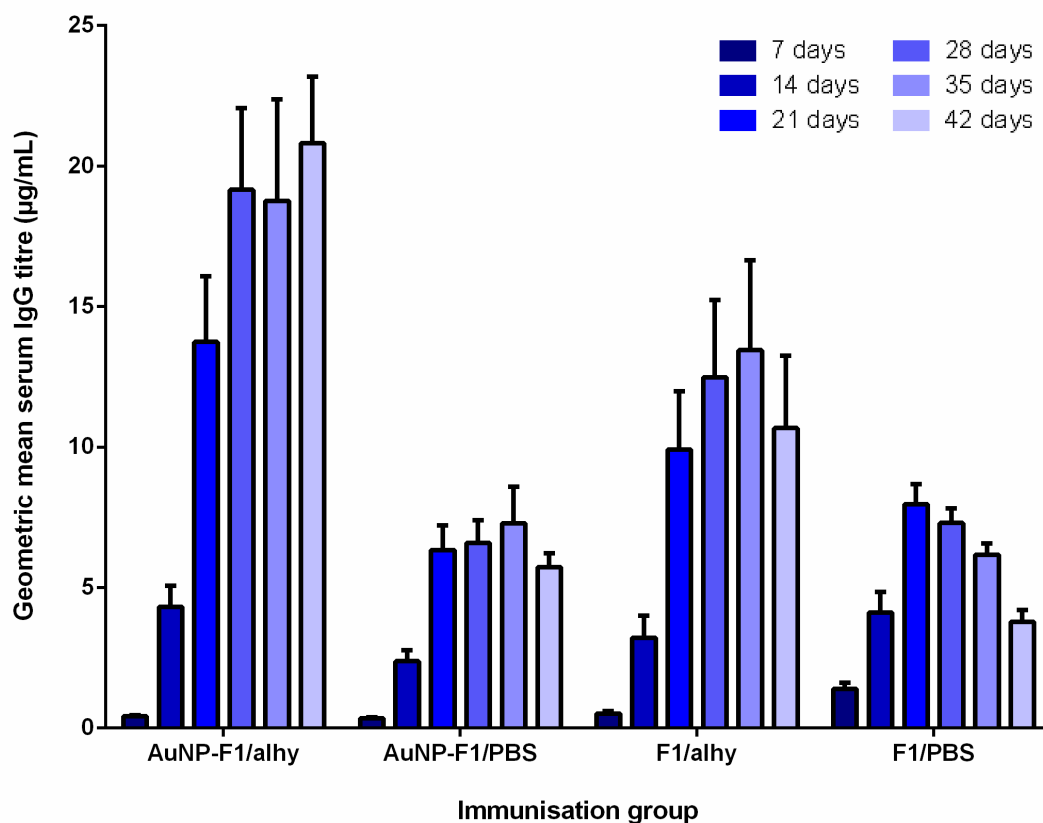


**Figure 3.17.** Concentrations of F1-specific total IgG in sera from BALB/c mice at different times after giving a single dose of the immunogens indicated. After 14 days, mice immunised with gold AuNP-F1/alhy generated a significantly higher IgG titre compared with AuNP-F1/PBS or unconjugated F1-antigen in PBS ( $p < 0.01$ ). AuNP-F1/alhy immunised mice did not show a decline in IgG at 42 days post-immunisation. Each point is the mean of values from five mice.

**Table 3.2.** Measurements of F1-specific IgG1 and IgG2a isotypes in sera taken from six immunised mice.

<b>Group</b>	<b>IgG1 (<math>\mu\text{g/mL}</math>)</b>	<b>IgG2a (<math>\mu\text{g/mL}</math>)</b>	<b>Ratio IgG1:IgG2a</b>
<b>AuNP-F1/alhy</b>	$23 \pm 4$	$1.7 \pm 0.1$	13.75
<b>AuNP-F1/PBS</b>	$6.6 \pm 0.9$	$0.9 \pm 0.1$	6.72
<b>F1/alhy</b>	$13 \pm 3$	$0.9 \pm 0.2$	14.57
<b>F1/PBS</b>	$6.4 \pm 0.4$	$0.5 \pm 0.1$	14.04

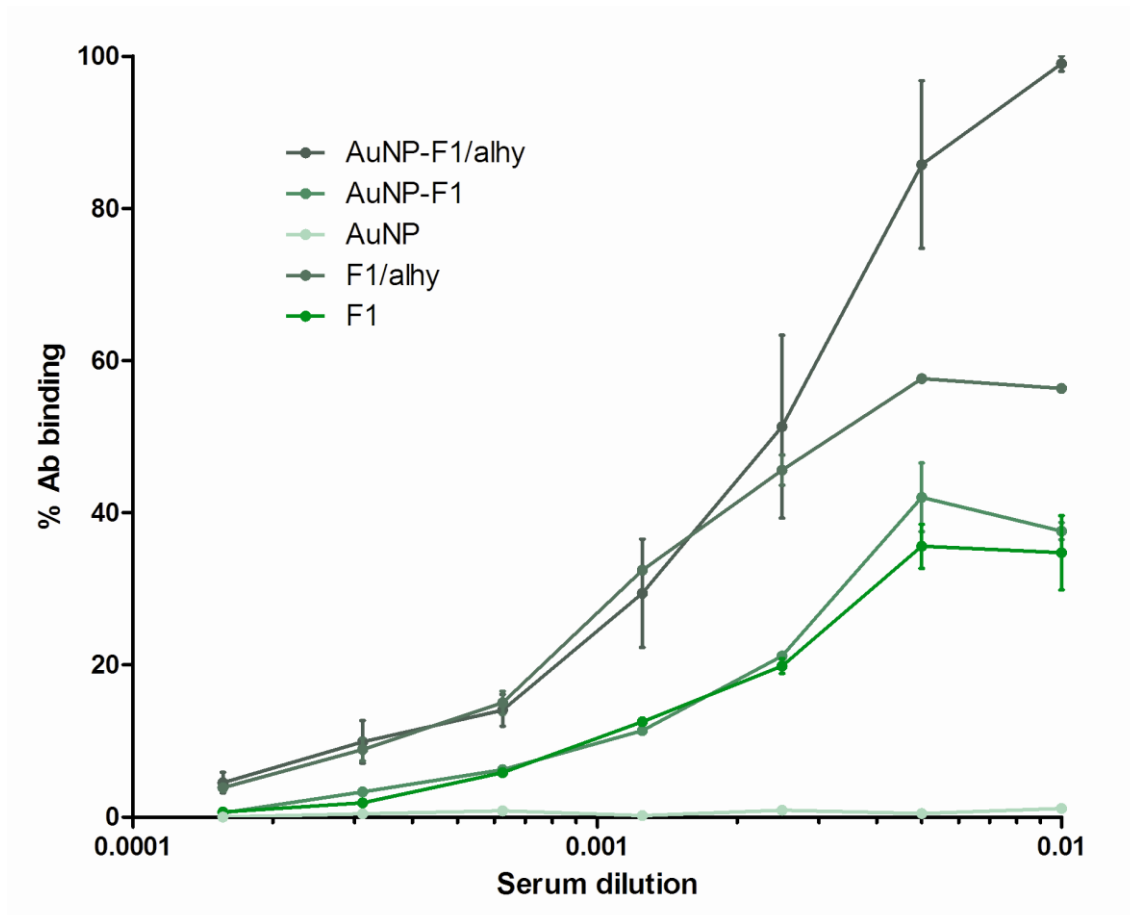


**Figure 3.18.** Competitive ELISA for binding to F1-antigen. After 14 days, mice immunised with AuNP-F1/alhy generated significantly higher IgG titre compared with AuNP-F1/PBS and unconjugated F1-antigen in PBS ( $p < 0.01$ ). Mice dosed with AuNP-F1/alhy did not show a decline in total IgG at 42 days post-immunisation. Each point is the mean of values from five mice.

### 3.3.5 Flow cytometric analysis

Flow cytometry of splenocytes showed that a high percentage of cells positive for the activation/maturation marker CD45 existed in all treatment groups (Table 3.3). CD4<sup>+</sup> cells as a percentage of cells bearing the pan T-cell marker (CD3) exceeded CD8<sup>+</sup> cells as a percentage of the CD3<sup>+</sup> population by approximately 2:1 for all treatment groups, with no significant differences between groups. Analysis of IFN $\gamma$  in culture supernatants of splenocytes re-stimulated *ex vivo* with F1-antigen, revealed a significantly reduced level from cells obtained from mice immunised with AuNP-F1/alhy, compared with those from mice administered F1/PBS ( $p < 0.05$ ), indicating the anti-inflammatory influence of alhydrogel in the vaccine formulation.

**Table 3.3.** Percentage of CD3<sup>+</sup> splenocytes displaying the activation marker CD45 *on ex vivo* re-stimulation with F1-antigen.

<b>Group</b>	<b>CD45<sup>+</sup> (% of CD3<sup>+</sup> cells ± s.e.m.) specifically activated by F1 <i>ex vivo</i></b>	<b>IFN<math>\gamma</math> output (ng/mL ± s.e.m.) in recall response specific for F1</b>
<b>AuNP-F1/alhy</b>	90 ± 2	327 ± 24
<b>AuNP-F1/PBS</b>	86 ± 5	704 ± 187
<b>F1/alhy</b>	82 ± 10	542 ± 121
<b>F1/PBS</b>	75 ± 14	775 ± 113

### 3.4 Discussion

#### *3.4.1 Gold nanoparticle synthesis*

AuNPs synthesised in this study were characterised using TEM, where the shapes of particles can be visualised and their sizes measured. Using this technique, we determined that reduction of gold (III) with a weak borohydride solution resulted in particles smaller than those generated with a higher molar borohydride solution. In both cases there was a wide distribution of sizes suggesting  $\text{NaBH}_4$  might not be suitable for producing a monodisperse population of nanoparticles, likely to be due to the strength of borohydride as a reducing agent. Whilst  $\text{NaBH}_4$  is added quickly to gold (III), the gold is likely to reduce at varying degrees as the concentration of  $\text{NaBH}_4$  equilibrates through the solution resulting in nanoparticles of different sizes. The solutions were stirred vigorously upon addition of a reducing agent, and for 2 hours afterwards, but the presence of irregular shapes when using  $\text{NaBH}_4$  at a lower concentration suggests the solution has not been stirred fast enough despite this being done at a maximum speed of 500 rpm. AuNPs formed using sodium citrate as a reducing agent produced spherical colloids with a mean diameter of  $16 \pm 2$  nm. These were much more uniform in shape, as calculated using the coefficient of variation, and had a narrower size-distribution. This is significant because the ability to produce spherical nanoparticles of a consistent size and shape is important for maintaining consistency of antigen loading between nanoparticle batches.

UV-visible spectrophotometry was also used to characterise the nanoparticles, which typically have a distinctive absorption and scattering pattern in the visible range of the electromagnetic spectra. From this we can ascertain that decreasing the concentration of  $\text{NaBH}_4$  increases the mean diameter of the nanoparticles in solution based on the  $\lambda_{\text{max}}$  red-shift. Also, reduction using sodium citrate forms nanoparticles which are slightly larger than those produced using 20 mM  $\text{NaBH}_4$  but much smaller than those using 5 mM  $\text{NaBH}_4$ . The shape of the extinction spectra indicates dispersity of nanoparticles within the solution since a broadening of the extinction peak is indicative of a broad size and shape distribution [312, 313]. Whilst a narrow peak is present for sodium citrate reduced AuNPs, there is a much broader peak for those reduced using  $\text{NaBH}_4$ . Since the end use of these nanoparticles is to conjugate antigenic

material for use as a vaccine, it is favourable to have a uniform population of nanoparticle shape and size within a solution and between batches. This is to ensure a consistent mass of immunogen is coupled to the gold surfaces and they are similarly presented to the immune system. For this reason, only citrate reduced AuNPs were chosen for further study.

The stability of AuNPs was measured over a 300 day time period by recording the absorption spectra. Whilst  $\lambda_{\max}$  of 519 nm remained fairly constant ( $\pm 0.94$  nm) for the time period chosen, overall absorption fell by more than 50% after 180 days. This is likely to be the result of small changes to pH within the solution over time which would affect the surface charge on the nanoparticles and cause some of the particles to aggregate and sediment. This would reduce the concentration of particles in solution and subsequently total absorption. This data helped us to ascertain that AuNPs are stable enough to be used for vaccine production and determine the maximum time for which these particles can be stored before use. As a result of these studies, a fresh batch of AuNPs was prepared every 6 months for the duration of the work described here.

#### *3.4.2 Peptide coupling to gold nanoparticles*

Under physiological conditions, proteins readily bind to the surface of nanoparticles using hydrophobic and electrostatic interactions to form a protein corona [314-317]. Whilst this simple method for coupling proteins is effective under controlled conditions, in a biological fluid there is a rapid dynamical exchange between the adsorbed proteins and those in sera, resulting in loss of protein carrier [318, 319]. There is also some evidence of reduced activity and protein denaturation when adsorbed to a nanoparticle surface [320]. It was therefore decided that a covalent coupling approach for attaching proteins to AuNPs would be best suited for vaccine delivery of antigens. The advantages of using gold for bioconjugation is that it readily reacts with both thiol and amide groups, allowing for direct conjugation of molecules, including proteins, onto the surface [321-323]. Although nanoparticles have a much larger surface to volume ratio compared to macromolecules, direct coupling to the nanoparticle surface is only really suitable for DNA vaccines or small drug molecules. For larger molecules, such as proteins, a spacer is often used to tether the molecule to the nanoparticle surface to maximise the surface area and prevent steric hindrance. Quite often the spacer used for conjugating onto gold will consist of

an aliphatic carbon chain with a thiol group at one end, which binds to the gold, and a carbonyl group at the other which is used to conjugate the molecule of interest [132, 324, 325]. In this study 16-mercaptohexadecanoic acid was chosen as a spacer, which forms a self-assembled monolayer on the gold surface and projects carboxyl groups. Carbodiimide chemistry was used to conjugate proteins to the spacer due to the mild reaction conditions required so as to not alter the conformation of antigenic epitopes.

Once the minimal protein concentration required for AuNP saturation was determined, a combination of several methods was used to quantify the amount of protein conjugated. The main difficulty with this was the complete separation of nanoparticles and coupled protein once they had been covalently linked. Once initial efforts of acid hydrolysis, enzymatic degradation (chymotrypsin) and pH changes failed to isolate the protein without first degrading it, I began to look into small molecules which may be able to displace the MHDA linker. Three molecules were investigated for their ability to competitively bind to the gold surface; 11-mercapto-1-undecanol, 11-mercaptoundecanoic acid and mercaptoethanol. Of which 11-mercapto-1-undecanol proved the most successful after incubating at room temperature for 4 hours. Moreover, a novel method was devised to purify the nanoparticles via simple centrifugation. Prior to this study, purification of functionalised nanoparticles involved specialised diafiltration or chromatography techniques which are not only time-consuming but can affect the stability of the colloid [326, 327]. However, it was determined that by supplementing the solution with a non-ionic surfactant at concentrations above the known critical micelle concentration the particles could be easily purified without aggregation, making it possible to produce and batches of AuNPs much more efficiently. However, there were some problems with this purification method since there would still be traces of AuNPs in the protein supernatant which would interfere with colorimetric assay results due AuNP characteristic scattering patterns of light in the red end of the spectrum. This was overcome by reading the absorbance at  $\lambda_{\max}$  of the released protein, diluting some bare AuNPs to this value and adding this to the standard curve to be used in a BCA assay. One of the problems with this method is the adsorption of proteins onto the added AuNPs and the changes this can have on the activity of the protein (mentioned above). In conjunction with this method protein was removed from AuNPs, again using 11-mercapto-1-

undecanol, and run through an SDS-PAGE gel alongside a range of known protein concentrations to generate a calibration curve. The density of these bands were then measured and calibrated to the standard curve. Whilst this method also has its limitations and may not release 100% of the bound protein, the results from this assay were the most replicable. A combination of band densitometry and BCA assay were used to calibrate the amount of protein conjugated onto AuNPs.

### 3.4.3 Immunisation study

The immunogenicity of an antigen coupled to AuNPs was evaluated in BALB/c mice using F1 as the model antigen since previous studies have shown that IM immunisation with recombinant F1-antigen induces a protective immune response against *Y. pestis* [265, 328, 329]. Previously, this was delivered by encapsulating the antigen, alongside recombinant V antigen (a secreted *Y. pestis* protein), within polylactide microspheres [265, 330]. Although promising, the immune response to this vaccine was slow to develop and was attributed to the slow release of antigen from the microparticles; something which is true of many encapsulation strategies [331-333].

When immunised IM into mice, F1 conjugated to AuNP induced IgG responses which were superior to the responses induced by F1-antigen alone. The immune response seen in AuNP-F1/alhy immunised mice is also more prolonged, when compared to other immunisation groups, Figure 3.19. The elevated and sustained response to F1 when coupled onto AuNPs suggests there was a depot effect created by the combination of AuNPs and alhydrogel enabling the recruitment of APCs to the site of immunisation for increased antigen processing by immune cells. NP conjugated F1 also generated higher IgG2a titres suggesting activation of Th1 cells. However, IFN $\gamma$  levels from splenocytes taken from mice immunised with AuNP-F1/alhy were lower than from mice immunised with F1/PBS or with AuNP-F1/PBS. This is likely to be due to the effect alum adjuvants have on activating a Th2 immune response. As a consequence, cytokines associated with a Th2 response suppress Th1 production and result in lower levels of IFN $\gamma$  [334, 335]. Unlike other studies using microspheres to deliver antigens, our data show no delay in inducing an antigen-specific antibody response. This is likely to be attributed to the presentation of F1-antigen on the NP surface. Similarly an attenuated strain of

*Salmonella* Typhimurium expressing F1-antigen on its surface was a potent immunogen and protected mice against challenge with *Y. pestis* [248].

Other studies have reported AuNPs enhancing the ability of antigen to evoke antibody responses compared with antigen given alone [133, 336, 337]. In the case of merozoite surface protein 1 or Nogo-66 receptor, coupling to AuNPs resulted in antibody responses exceeding those elicited by the antigen given with Freund's adjuvant [336, 337]. Some studies have also reported that the use of alum as an adjuvant further enhanced the responses elicited by antigen bound to AuNPs [336] but others have used antigen bound to AuNPs without an additional adjuvant [133, 337]. In this study, the use of alum as an adjuvant enhanced the antibody response to F1-antigen linked to AuNPs.

Whilst mice were not challenged on this study, the ability of sera from mice immunised with AuNP-F1 to compete with a protective macaque antiserum for binding to F1-antigen indicates that AuNP-F1 has induced a protective antibody response [338-340]. This suggests that the conjugation of F1-antigen to AuNPs has been successfully achieved without interference of protective B-cell epitopes in F1-antigen.

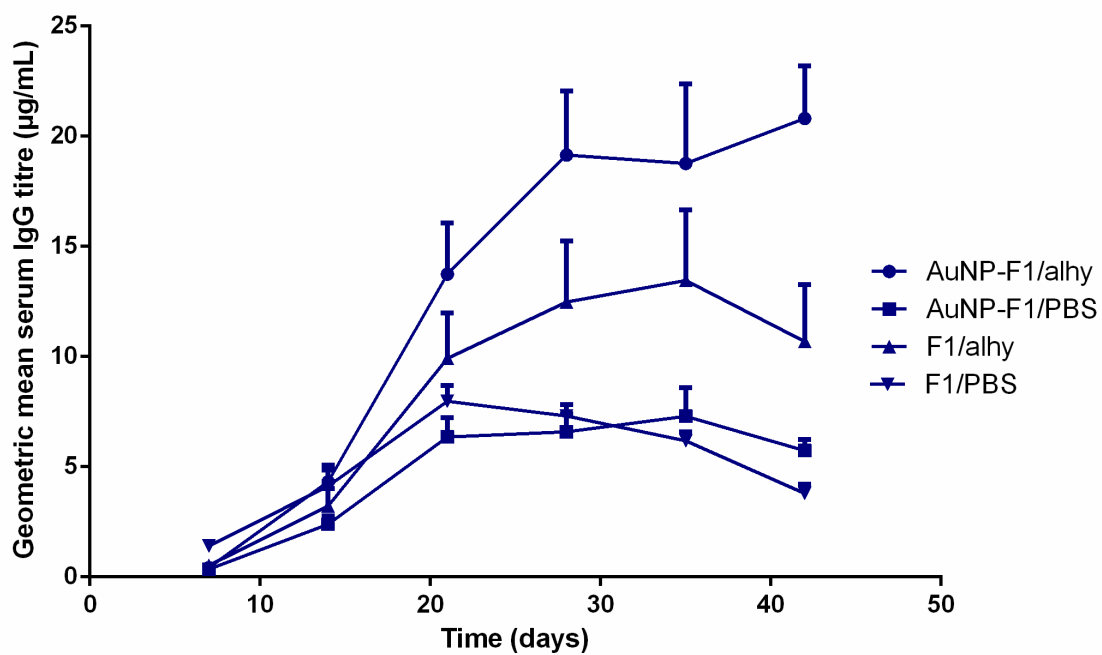


**Figure 3.19.** Development of F1-specific IgG concentrations from BALB/c mice over time.

#### 3.4.4 Conclusions

Through the experiments described in this chapter, we have determined a production method which results in nanoparticles that are optimized for vaccine delivery in terms of size, shape, and monodispersity. We have characterised these nanoparticles through a variety of methods to demonstrate their suitability for use in vaccine production and identified the maximum time for which they can be safely stored without losing viability. This provides us with an ideal baseline from which nanoparticle vaccines can be developed and tested. We have also demonstrated the ability to successfully couple four different protein antigens (Hcp1, FliC, F1 and TetHc) onto the AuNPs using carbodiimide chemistry and proven that the proteins were bound to the AuNPs, showing the ability to reproducibly produce and quantify subunit vaccine candidates. We have shown that immunising mice with AuNP-F1 resulted in a greater total antigen-specific antibody response than F1 alone and higher levels of IgG2a titres, which suggests Th1 activation which is ideal for producing a vaccine capable of long term protective immunity. Further, competitive displacement of protective macaque antiserum suggests that the same epitopes are important for protection but the immunogenicity of the antigen is improved.

## Chapter 4: A Glycoconjugate Vaccine against Glanders

---

### 4.1 Introduction

#### 4.1.1 *Burkholderia*

The *Burkholderia* genus currently includes over 40 species, including some environmental and clinically important pathogens [341]. The genus was proposed in 1992 based on 16S rRNA sequences, DNA-DNA homology values and phenotypic characteristics. The genus includes seven species, which were previously classed under the genus *Pseudomonas* [342]. Within this genus is the aerobic, Gram-negative, bacterium *Burkholderia mallei* which is the causative agent of glanders in humans. However, the pathogen mostly affects equines and humans are considered accidental hosts. *B. mallei* is unable to survive in the environment alone, so instead infected animals serve as a natural reservoir for this obligate parasite. A whole genome shotgun approach was used to sequence the genome of *B. mallei* ATCC 23344 which identified two circular chromosomes of 3.5 megabase pairs and 2.3 megabase pairs in size, with a G+C content of 68% and a total of 5535 predicted coding sequences [343].

A clonal relative of *B. mallei* is *B. pseudomallei* which causes a severe and potentially fatal human disease known as melioidosis. It too is an aerobic, Gram-negative bacterium but unlike *B. mallei* is motile and able to survive in the environment without a host. Subsequently, *B. pseudomallei* is cultured easily from the environment and is commonly found in wet soil and surface water in the tropics. Isolated in 1996 from a 34-year old female diagnosed with acute melioidosis in Thailand, the genome for *B. pseudomallei* strain K96243 was sequenced and shown to be composed of two chromosomes (4.07 and 3.17 megabase pairs) [344]. With 5855 predicted coding sequences between the two chromosomes it is one of the most complex bacterial genomes sequenced to date. Genome analysis identified the large chromosome as carrying genes mainly associated with core functions necessary for metabolism and cell growth, whilst the smaller chromosome encodes for accessory functions such

as adaptation and survival in different environments. An interesting feature of the genome is the presence of 16 genomic islands, making up 6.1 % of the total genome. The absence of these islands from other closely related *Burkholderia* species, suggest horizontal gene acquisition by *B. pseudomallei* has played a pivotal role in the genetic evolution of this species [344].

Genome wide comparisons between *B. mallei* and *B. pseudomallei* reveal 99% homology and suggests *B. mallei* has evolved from a single clone of *B. pseudomallei* and undergone 'genomic downsizing' [345]. Consequently, it is believed that this has resulted in a loss of ability to survive in the environment.

Also within the *Burkholderia* genus is *B. thailandensis*, a close relative of *B. pseudomallei* which coexists in the environment and was previously believed to be a biotype of *B. pseudomallei*. Comparisons between these two "biotypes" determined that whilst *B. thailandensis* was able to assimilate L-arabinose and demonstrated a median lethal dose (LD<sub>50</sub>) of 10<sup>6</sup>-10<sup>7</sup> CFUs in a Syrian hamster model of infection, *B. pseudomallei* was unable to and demonstrated an LD<sub>50</sub> of 2-10 CFUs [346, 347]. Differences between these two biotypes became more apparent after 16S rDNA phylogenetic analysis and a new species was proposed, with the less virulent biotype being designated as *B. thailandensis*. [348].

#### 4.1.2 Glanders and melioidosis

Glanders, sometimes referred to as farcy, is one of the oldest known infectious diseases, having first being described in 350 BC by Aristotle [349]. However, it was not until 1882 that the causative agent, *B. mallei*, was first isolated from an infected horse liver [350]. Throughout history there have been several incidents where *B. mallei* has been used as a biological weapon to infect livestock and contaminate animal feed, including during World War I and II and later by the Soviet Union for use in Afghanistan [351, 352]. Since *B. mallei* is unable to survive in the environment infected equines serve as the reservoir for the bacterium. The disease will then typically manifest into either an acute infection in mules or donkeys, leading to mortality within a few days, or a chronic infection in horses, where infection can linger for a few months or even years but will still most often result in fatality [353-357]. Clinical signs of glanders infection vary but are often characterised by nodules on the extremities of infected animals. These can ulcerate and result in an infectious discharge

allowing the transmission to other healthy animals or humans. Symptoms in humans are much the same as they are in equines with the thickening of lymph vessels and nodule formation producing a suppurative exudate [358, 359]. Mortality rates vary significantly depending on the route of transmission but range from 95% if untreated down to approximately 40% with an intensive course of antibiotics [360, 361].

*B. pseudomallei* is most commonly found in wet soil and surface water in areas such as southeast Asia and northern Australia where transmission occurs mostly through subcutaneous inoculation or inhalation [362-364]. The biggest incidence of melioidosis is in northern Thailand where it accounts for 20% of all community-acquired septicaemia and 40% of all sepsis-related mortality [365-367]. Clinical manifestations are protean and can mimic symptoms of other diseases such as tuberculosis, leading to misdiagnosis and disease progression [368-370]. The disease can be described as being either acute septicaemia or a chronic localised infection [367]. Whilst there is usually no evidence of infected wounds or trauma, the disease is characterised by abscess formation in the liver and/or spleen as well as pneumonia, which is present in over 50 % of cases [371-375]. Recurring infections and latency are also a problem for patients with melioidosis.

There is currently no vaccine against either glanders or melioidosis and they are both naturally resistant to several classes of antibiotics [376, 377]. Due to their associated high mortality rates and potential to be transmitted by aerosols, both pathogens are classed as Tier 1 select agents by the Centers for Disease Control and Prevention and are considered to be potential candidates for weaponisation and bioterrorism. Subsequently, there has been renewed scientific investigation into these bacteria in recent years.

#### 4.1.3 Virulence factors

Virulence in *B. mallei* and *B. pseudomallei* is multifactorial and a number of virulence mechanisms have been identified, some of which are listed in appendix table A. One of the virulence factors which distinguish *B. mallei* from *B. pseudomallei* is flagellin, encoded by *fliC*. FliC is known to be involved in motility of *B. pseudomallei*, while *B. mallei* lacks *fliC* and is non-motile [378]. *B. thailandensis* is similar to *B. pseudomallei* in that it is motile and encodes a *fliC* gene, but the *B. thailandensis fliC* gene is significantly shorter than *B.*

*pseudomallei fliC* and can be used to discriminate between the two otherwise highly homologous genomes [349, 361, 379].

The role of flagellum-mediated motility in virulence has largely been attributed to its ability to enhance the invasion of host epithelial cells [359, 377, 380, 381]. Whilst *B. pseudomallei* flagellin mutants remain virulent in mice and hamsters when delivered intraperitoneally, they are attenuated when deposited intranasally suggesting the flagellin-based motility and its role in virulence is dependent on the route of infection [377, 380]. Antibodies raised against *B. pseudomallei* FliC have been shown to reduce bacterial motility as well as providing passive protection against *B. pseudomallei* infection in a diabetic rat model [382]. Additionally, FliC has been recognised as a TLR5 agonist in other motile bacteria, stimulating pro-inflammatory cytokines such as TNF- $\alpha$  which are involved in activation of the innate immune [383].

*B. mallei* and *B. pseudomallei* also encode type VI secretion systems (T6SS) and have four and six gene clusters in their respective genomes [384, 385]. Whilst the functionality for the majority of these gene clusters is currently unknown, there is one homologous T6SS gene cluster shared in both *B. mallei* (T6SS-1; BMAA0744-0730) and *B. pseudomallei* (*tss-5*; BPSS1496-1511) that has been demonstrated to play an essential role in virulence role in animals [384, 386]. There is also some evidence that T6SS also plays a role in multinucleated giant cell formation since these were absent when mammalian cells were infected with *B. pseudomallei* T6SS mutants [351, 387]. Activation of T6SS-1 has been closely linked to both the VirAG-regulated two-component system and BMAA1517, an AraC-type regulator, whereby overexpression of either system results in a 30- or 12- fold increase in T6SS-1 transcription, respectively [384]. Upon activation of T6SS-1, some of the key effectors are a family of haemolysin-coregulatory proteins (Hcp) that share homology to *Vibrio cholerae* Hcp [388]. This family of proteins have been identified as interacting with valine-glycine repeat protein G (VgrG) to assemble into a structure which resembles the cell-penetrating needle of a bacteriophage tail [389-391]. However, as well as being a component of the T6SS, Hcp proteins are also secreted *in vivo* as sera from mice, horses and humans react with Hcp1 [357]. As an effector, Hcp1 (BMAA0742) forms a hexameric ring structure which may form a channel in the target cell membrane to allow other macromolecules to be transported [384]. The T6SS-1 protein Hcp1 has also been shown to provide

significant protection against a lethal inhaled *B. mallei* and *B. pseudomallei* challenge in a murine model of infection [251].

*B. mallei* and *B. pseudomallei* both produce an extracellular capsular polysaccharide, previously characterised as type I O-polysaccharide (O-PS), composed of -3)-2-O-acetyl-6-deoxy- $\beta$ -D-manno-heptopyranose-(1- [392, 393]. The role of capsular polysaccharide in virulence has been demonstrated in animal models of infection whereby *B. pseudomallei* capsular mutants are highly attenuated in both mice and hamsters and *B. mallei* capsular mutants are avirulent [394-396]. The explanation for this phenotype is believed to be the role capsule plays in evading host defence, specifically the complement system, by reducing C3b-mediated opsonisation and phagocytosis [397]. The capsule is also believed to be required for survival and replication in macrophages by protecting the bacterium from reactive nitrogen and oxygen intermediates [398]. The absence of the gene cluster expressing this polysaccharide from *B. thailandensis* has been suggested as one of the factors contributing to its relative avirulence [357, 394, 397]. However, two strains of *B. thailandensis*, E555 and CDC3015869, were recently discovered to have acquired the gene cluster necessary for capsular polysaccharide and have been shown to express neither exhibited enhanced levels of virulence compared with wild-type *B. thailandensis* strains in mice or hamsters [399, 400]. The authors suggest that the major ecological driving force behind this acquisition may have been down to environmental pressures rather than a requirement to infect mammals [399].

Another extracellular polysaccharide produced by *B. pseudomallei* and *B. mallei* is lipopolysaccharide (LPS). As a major component of Gram-negative cell envelopes, the LPS is composed of three covalently linked domains [401]. The first is a hydrophobic domain known as lipid A which anchors LPS into the bacterial outer membrane. This component is believed to be responsible for the endotoxic activity associated with LPS by activating TLR4 and triggering inflammatory responses such as TNF- $\alpha$  and IL-6 [402]. Next are a core of non-repeating oligosaccharides commonly consisting of 3-deoxy-D-mannooctulosonic acid (KDO), which acts as an intermediate linker between lipid A and the distal polysaccharide. The polysaccharide is referred to as the O-antigen and its variability defines the serological specificity in an organism. For *B. mallei*, *B. pseudomallei* and *B. thailandensis* the O-antigen is a repeating D-

glucose and L-talose with a general structure of  $\beta$ -D-glucopyranose-(1-3)-6-deoxy- $\alpha$ -L-talopyranose-(1- in which 33% of the L-talose residues contain 2-O-methyl and 67% contain 2-O-acetyl substitutions. *B. pseudomallei* and *B. thailandensis* also have an O-acetyl substitution at the 4' position on L-talose whilst *B. mallei* has an additional substitution of 3-O-methyl substitution on L-talose [264, 357, 403]. The lack of acetylation at the 4' position on L-talose in *B. mallei* has been attributed to the absence of the *oacA* gene which encodes O-antigen acetylase A in *B. thailandensis* and its homolog BPSL1936 in *B. pseudomallei* K96243 [404, 405]. Despite these minor differences in structure, the biosynthesis cluster responsible for the O-antigen moiety of LPS described is the same in *B. mallei* and *B. pseudomallei*. Strains which produce this genotype are described as typical (LPS genotype A) and include all strains of *B. mallei* and *B. thailandensis* that have so far been tested [406]. There is however some diversity amongst *B. pseudomallei* strains where LPS genotype A accounts for 97.7% of Asian strains and 85.3% of Australian strains [406]. Atypical strains are either genotype B or B2, depending on the biosynthetic gene cluster responsible for generating the O-antigen, and are so-called because they are both serotype B reactive. Of the two atypical gene clusters, B is the most common accounting for 2.3% of Asian strains and 13.8% of Australian strains. So far, only 7 strains of *B. pseudomallei* have been identified as producing LPS genotype B2 [406]. In strains where the LPS O-antigen biosynthesis cluster is missing or defective, LPS is described as "rough". These three separate serotypes of *B. pseudomallei* LPS (A, B and rough) are antigenically distinct by immunoblotting [407].

The primary role of the O-antigen is to protect the bacterium against host defences. This has been demonstrated by constructing mutants of the gene cluster in *B. pseudomallei* required for O-antigen synthesis and showing they are more susceptible to macrophage killing by RAW 246.7 cells and serum killing by the complement system [403, 408]. Since LPS is a major component of the bacterial outer membrane, the specificity of the O-antigen is an important antigen for triggering host recognition. Passive protection studies of mAb's raised against *B. mallei* or *B. pseudomallei* LPS O-antigen were protective against a lethal challenge of glanders or melioidosis in a mouse model of infection [409-412].

In addition to LPS O-antigen, two other polysaccharide loci have been identified in *B. pseudomallei* termed type III O-PS and type IV O-PS which encode genes with predicted functions relating to polysaccharide biosynthesis and transport [344, 413]. Mutants lacking either type III or type IV O-PS show an increased time to death in a mouse model of *B. pseudomallei* compared with wild-type [413]. However, neither cluster is present in *B. mallei* [343].

#### 4.1.4 Objectives

Previous immunisation studies using LPS purified from *B. pseudomallei* and *B. thailandensis* have shown this to provide partial protection against murine melioidosis [413, 414]. However, since LPS is a T-independent antigen, protection is short-lived and animals eventually succumb to disease after approximately 20 days. In order to convert the immune response to one that is T-dependent, polysaccharides can be conjugated to a protein carrier for presentation on MHC I/II molecules. This has been shown with the *Haemophilus influenzae* type b (Hib) and meningococcal type C vaccine [258, 415]. The aim of the work reported in this chapter is to improve the protection afforded by *B. thailandensis* LPS by conjugating it to a protein carrier in the hope of inducing a T-dependant immune response. The protein carriers were initially *Y. pestis* capsular F1 antigen, which was shown in the previous chapter to be highly immunogenic on AuNPs, and tetanus toxoid Hc fragment (TetHc), which is the current choice of protein carrier for several licensed glycoconjugate vaccines [416-418]. The efficacy of using *Burkholderia* specific proteins FliC and Hcp1 was also explored due their reported ability to provide some degree of protection [251, 419].

The use of gold nanoparticles in this vaccine construct should not only improve the immunogenicity of the vaccine but also act as a surface onto which the coupling chemistry can proceed. It is hoped that this will improve the conjugation efficiency.

## 4.2 Materials and Methods

### 4.2.1 LPS purification

LPS was extracted from *B. thailandensis* E264 using a modified hot-phenol extraction method [253]. Cultures were grown as either an overnight culture in LB containing 50 µg/mL kanamycin or as a lawn on LA bioassay dishes containing 50 µg/mL kanamycin for 18-20 hours before colonies were suspended in ice cold 50 mM Na<sub>3</sub>PO<sub>4</sub> with 5 mM EDTA pH 7.4. The cultures were lysed for 16 hours at 4 °C with 15,000 units of lysozyme per mg of bacteria, before adding 20 µg/mL DNase and RNase in MgCl<sub>2</sub> and leaving to digest for a further 16 hours at room temperature. Proteinase K (50 µg/mL) was added and incubated at room temperature for 6 hours. A 90% (w/v) phenol solution heated to 70 °C was added in equal volume to the digested culture with continuous mixing for 20 minutes at 70 °C. The solution was dialysed against de-ionised water for approximately 3 days, changing the buffer daily. The dialysed solution was lyophilised and dissolved in 10 mM Tris with 1 mM CaCl<sub>2</sub> and 1 mM MgCl<sub>2</sub> to a concentration of 30 mg/mL. DNase and RNase were added at 20 µg/mL for 2 hours at 37 °C before adding proteinase k at 50 µg/mL for 4 hours at 37 °C and then ultracentrifuging at 10<sup>5</sup> x g for 3 hours. The resulting pellet was solubilised in de-ionised water before dialysing against de-ionised water for 16 hours. The solution was lyophilised once more before it was dissolved in de-ionised water or 50 mM MES buffer pH 5.5, aliquoted and stored at -80 °C. The purity of LPS was checked by running on a NuPAGE 4-12% Bis-Tris gel with silver staining, and Western blotting using a monoclonal antibody (mAb) specific for *B. pseudomallei* LPS O-antigen (CC6).

### 4.2.2 Coupling chemistry for LPS onto gold nanoparticles

A reductive amination approach was initially taken to couple LPS onto protein carriers [254]. This was done by partially oxidising LPS by incubating 16 mg LPS with 4 µM sodium *meta*-periodate in the dark at 23 °C for either 30, 60 or 90 minutes. Ethylene glycol was then added to quench any residual periodate. The oxidised LPS was dialysed in ultrapure water overnight at 4 °C and lyophilised. AuNPs coupled with either TetHc or an aminated MHDA linker were prepared as previously described before being centrifuged and resuspended in 1 mg/mL oxidised LPS in 0.5 M sodium cyanoborohydride (in 0.1 M sodium

bicarbonate), pH 8.1. The mixture was allowed to incubate at room temperature for 7 days with gentle agitation. Aliquots were taken at various time points to measure the absorption spectra for a spectral shift in  $\lambda_{\max}$  as an indicator of conjugation, however no shift was recorded. A second approach following a modification of protocols based on oxime coupling was also employed [255-257]. AuNP coupled proteins were centrifuged at 13,000 x g for 10 minutes before they were resuspended in a solution containing 0.6 mM EDC, 0.15 mM NHS and 0.1 mM O-(carboxymethyl)hydroxylamine hydrochloride in 50 mM MES buffer pH 5.5. LPS (100  $\mu\text{g}/\text{mL}$ ) was added to aminooxylated proteins and allowed to incubate at room temperature for 18 hours.

A third approach using a modified thiol maleimide chemistry was then applied [258]. To make a 1 mL solution of LPS coupled to AuNPs, 4.3  $\mu\text{L}$  40 mM EDC and 17.3  $\mu\text{L}$  10 mM NHS was added to 0.26 mg LPS in 50 mM MES buffer pH 5.5 and incubated at room temperature for 15 minutes. Following this, 10.9  $\mu\text{L}$  800  $\mu\text{M}$  6-maleimidocaproic acid hydrazide, trifluoroacetic acid salt (EMCH; >90%, Pierce) was added to the LPS solution and incubated at room temperature for a further 15 minutes. The pH of the LPS solution was adjusted to 7.0 using sodium hydroxide and left to incubate for an hour. Meanwhile, AuNPs coupled with a protein carrier of choice was suspended in 874.6  $\mu\text{L}$  potassium phosphate buffer pH 7.5 before adding 25.4  $\mu\text{L}$  250 mM S-acetylthioglycolic acid *N*-hydroxysuccinimide ester (SATA; >95%) and incubating at room temperature for 60 minutes. Hydroxylamine and EDTA were then added to the AuNP solution to quench the reaction with SATA. LPS was centrifuged in a Vivaspin® 6 centrifugal concentrator (Sartorius) for 15 minutes at 3220 x g and desalted into 5 mM EDTA in PBS pH 7. The AuNP solution was also centrifuged, at 13366 x g for 10 minutes before resuspending into the LPS solution and incubating at room temperature for 4 hours. The conjugation reaction was quenched with 5 mM *N*-ethylmaleimide; the nano-glycoconjugates were centrifuged and resuspended in PBS with or without 260  $\mu\text{L}$  13 mg/mL alhydrogel.

LPS was also conjugated onto MHDA functionalised AuNPs without any protein. To MHDA AuNPs, 4.5  $\mu\text{M}$  hydrazine dihydrochloride (>99.9%) and 0.9  $\mu\text{M}$  EDC was added to aminate the terminal carboxyl regions before coupling with LPS, using the thiol maleimide approach as described above.

### 4.3 Results

#### 4.3.1 LPS extraction

LPS was extracted from *B. thailandensis* E264 using a modified hot-phenol extraction method [253]. Cultures of *B. thailandensis* were grown either in LB broth or on LA bioassay dishes before LPS was extracted. The quantity and quality of LPS purified from bacteria grown in these two ways was compared by running through an SDS-PAGE gel and either silver staining or blotting with a monoclonal antibody against the O-antigen. Both methods gave a yield of approximately 8% LPS from the total dry cell weight, which is in general agreement with literature values on Gram-negative bacteria composition [420-422]. There are, however, clear differences between the two forms of purified LPS with the plate-cultured LPS producing a strong band between 35-75 kDa on a silver stained protein gel with some additional low molecular weight bands, Figure 4.1 A. The broth-cultured LPS also has a strong band of around 50 kDa on a silver stained protein gel but is a smaller band than the plate cultured LPS and has an additional ladder banding pattern below 35 kDa which was not seen from the plate cultured LPS, Figure 4.1 B. This suggests that the purity of LPS is higher when purified from plates compared with broth culture. The gels were then transferred onto a nitrocellulose membrane which was probed with a mAb raised against the O-antigen of *B. pseudomallei* LPS (CC6). This showed the O-antigen to be present in the 40-80 kDa region which correlates with the strong band from the silver stain. There is a stronger band seen from plate cultured LPS rather than from broth suggesting a higher content of O-antigen present. For this reason, *B. thailandensis* LPS purified from bioassay plates was used for subsequent studies.

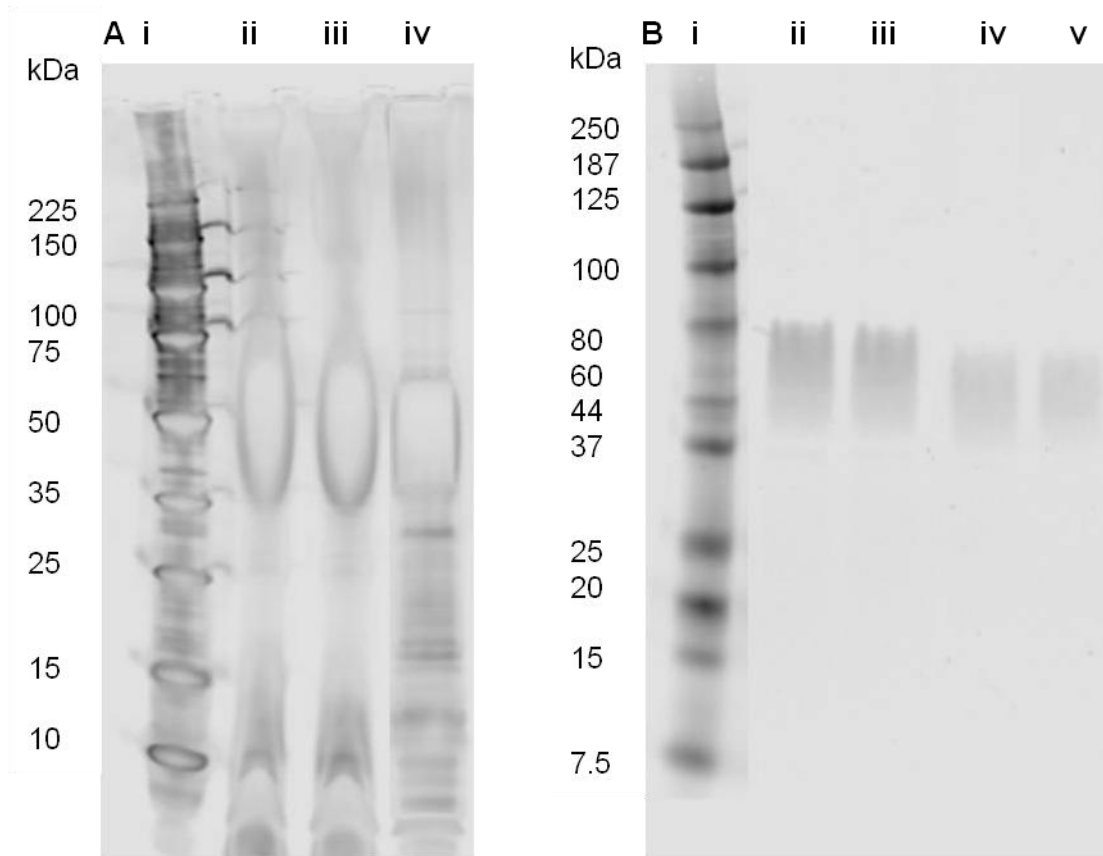


**Figure 4.1.** Silver stained NuPAGE 4-12% Bis-Tris gel of 3  $\mu$ g LPS purified from *B. thailandensis* (A); Perfect Protein™ marker (i), LPS purified from plates (ii and iii), LPS purified from broth (iv). Western blot of *B. thailandensis* LPS separated using a NuPAGE 4-12% Bis-Tris gel and stained using a mouse monoclonal antibody, CC6 (B); IRDye® (680/800) protein marker (i), LPS purified from plates (ii and iii), LPS purified from broth (iv and v).

### 4.3.2 Nano-glycoconjugate synthesis

Several methods of bioconjugation were attempted for conjugating LPS onto protein coupled AuNPs. The first of which was reductive amination, which is currently one of the most popular methods for coupling glycoconjugate vaccines and involves the nucleophilic addition of an amine group to a carbonyl. The carbonyl in this case was an aldehyde formed by mild periodate oxidation of the vicinal diols in the LPS core region. The resulting Schiff base rapidly hydrolyses in aqueous solution and must therefore undergo borohydride reduction to a more stable alkylamine. Based on literature values, a range of conditions were tested for coupling via reductive amination however, none of these were successful and measurements from UV/Vis spectra showed no change to  $\lambda_{max}$ , Figure 4.2 A [423-425]. Another chemistry that was attempted was oxime coupling which is also a nucleophilic addition reaction. Oxidation of LPS was again required to generate aldehydes in the core region which react with aminoxy groups to form an oxime [256, 257]. Analysis of nano-glycoconjugates using UV/Vis spectroscopy indicated that some degree of surface modification had taken place and a phenol-sulphuric acid assay confirmed the presence of LPS, however this was small, Figure 4.2 B. Further attempts to optimise this method were unsuccessful.

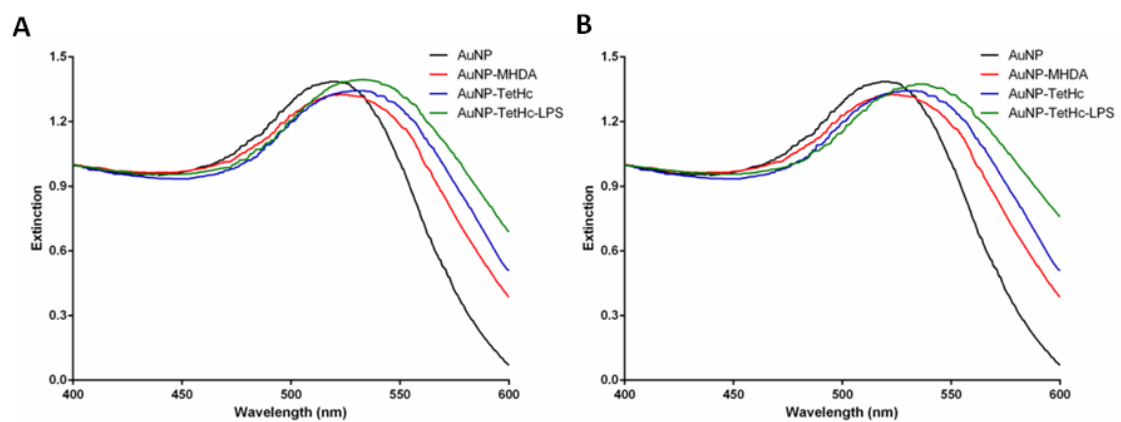


**Figure 4.2.** UV-visible absorption spectra showing the efficiency of conjugation chemistry using either reductive amination (A) or oxime coupling (B). Displayed are AuNPs (black), AuNPs functionalised with MHDA (red), AuNPs functionalised with MHDA coupled with TetHc (blue) and AuNPs coupled with TetHc and *B. thailandensis* LPS (green).

Conjugation of LPS onto protein coupled AuNPs was most successful using thiol-maleimide chemistry, Figure 4.3. Firstly, nucleophilic carbon atoms in carboxyl groups of the LPS core region were activated using EDC and NHS to give amine reactive NHS esters. The addition of EMCH to LPS formed a peptide bond between the hydrazide group and sites of EDC/NHS activation, whilst projecting a sulpho-reactive maleimide group. Free maleimide groups from EMCH in solution were quenched by desalting into a buffer containing EDTA. The carrier protein, (TetHc, F1, Hcp1 or FliC) onto which LPS was conjugated, had additional thiol groups incorporated using SATA. These were to act as sacrificial thiol groups so as to protect the native disulphide groups and hence preserve the 3D configuration and activity of the protein. Hydroxylamine was added to deacetylate the newly introduced, protected sulphydryl groups. The sulphonated protein-AuNPs were then purified using centrifugation and resuspended into the maleimide-containing LPS where a stable thioether linkage is formed between LPS and the protein. The reaction was quenched with the addition of ethylmaleimide and EDTA was added to chelate any divalent metals present that would otherwise promote oxidation of sulphydryl groups. The skeletal structure of *B. thailandensis* LPS, showing the sites of conjugation, is shown in Figure 4.4.

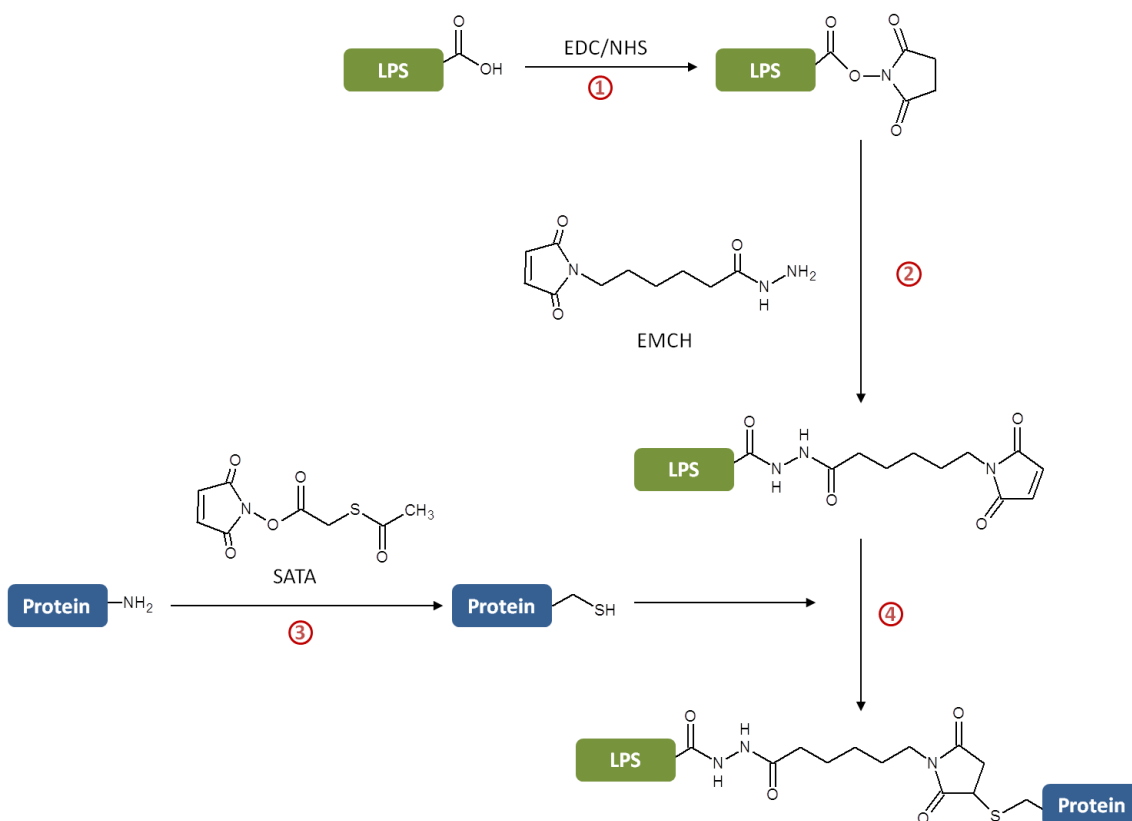


**Figure 4.3.** Reaction scheme of the thiol-maleimide coupling between LPS and a chosen protein carrier; (1) NHS activation of carboxyl groups in LPS core, (2) EMCH linker addition onto LPS, (3) Introduction of terminal thiol groups onto AuNP coupled carrier protein using SATA, (4) Reaction between maleimide LPS and thiolated protein leads to thioether bond formation.

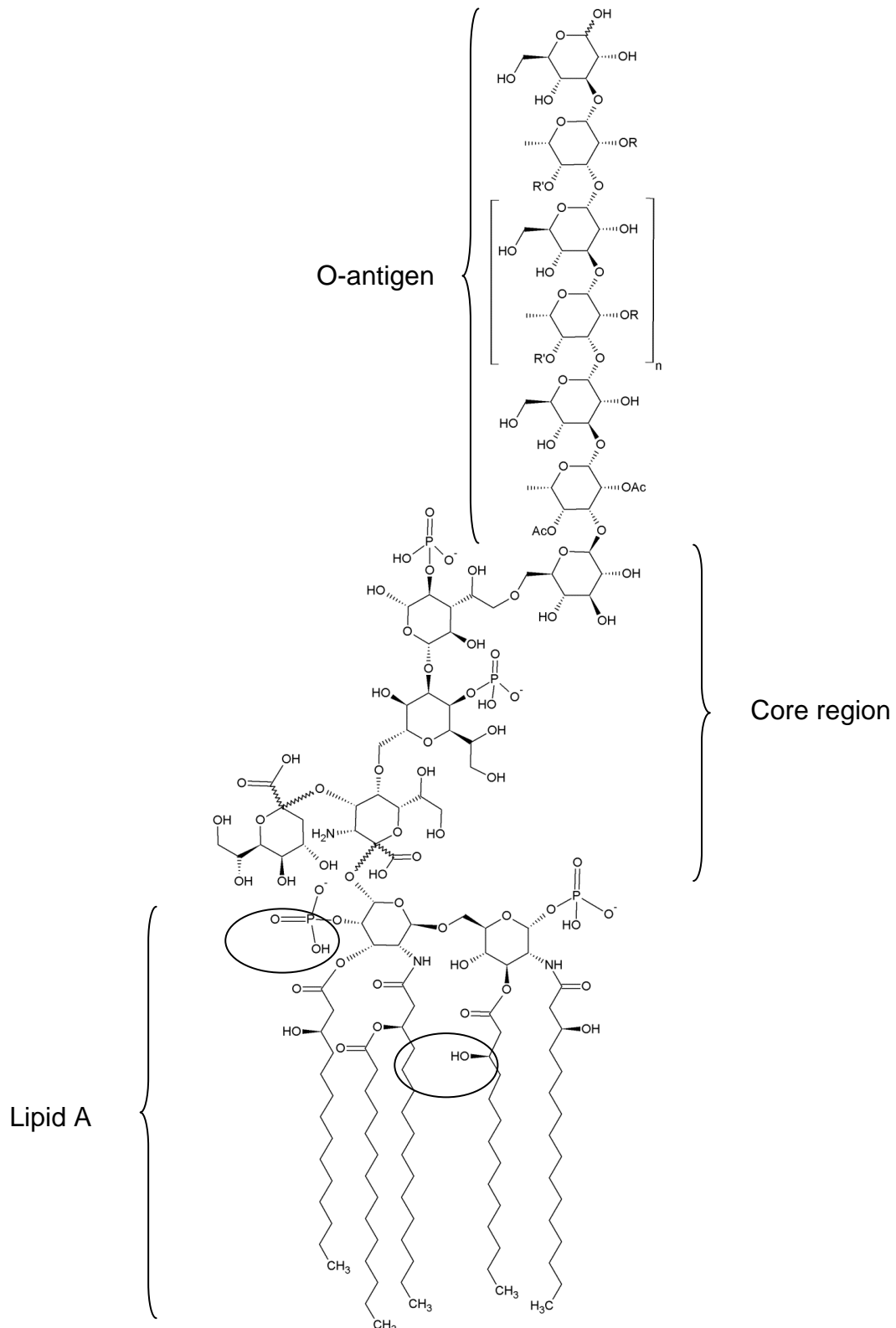


**Figure 4.4.** Skeletal structure of *B. thailandensis* LPS where R = OMe, R' = OAc (33 % of all 6dLTal residues); R = OAc, R' = H (67 % of all 6dLTal residues). O-antigen repeating unit has been highlighted and carboxyl sites for conjugating protein carriers are circled. Lipid A region adapted from Brett *et al.* [426].

Confirmation of nano-glycoconjugate formation was performed by measuring the absorbance spectra of AuNPs, Figure 4.5. An increase in the penetration depth of the AuNP plasmon, as indicated by red-shift in  $\lambda_{\max}$  of 9 nm from 532 nm for AuNP-TetHc to 541 nm, indicates an increase in the mean diameter of AuNP conjugates as a result of LPS conjugation. The extinction peak is also much broader for AuNP-TetHc-LPS which suggest the size distribution of particles is much larger. This is likely to be due to variable lengths of the repeating O-antigen disaccharide on the particles. A two-colour Western blot was used to confirm co-conjugation of TetHc and LPS on AuNPs, Figure 4.6.

After displacing the glycoconjugate from AuNPs using 11-mercapto-1-undecanol the conjugate was separated using SDS-PAGE and transferred onto a nitrocellulose membrane which was incubated with a rabbit pAb specific to TetHc and a mouse mAb specific to LPS. Secondary antibodies against rabbit and mouse with an IR tag of 680 nm and 800 nm, respectively, were then added before the blot was visualised. This revealed the presence of both TetHc and LPS, however the LPS coupled onto TetHc appears to be of a lower molecular weight to the native LPS; this could be due to one of two reasons. Firstly, the thiol-maleimide chemistry between LPS and the protein could favour LPS of a smaller molecular weight, suggesting the larger molecular weight LPS is lost during purification and not seen on the gel. Alternatively, the attachment of TetHc to LPS could cause it to move atypically through the gel due to changes to the overall surface charge of the molecule.

A phenol-sulphuric acid assay was used to determine the concentration of LPS present in nano-glycoconjugates. Using concentrated sulphuric acid, LPS was hydrolysed and dehydrated into monomeric furfural molecules which then formed a chromagen upon addition of phenol [427]. This method allows for a reliable and sensitive determination of polysaccharides down to 1 nmol, with a linear relationship between absorbance and concentration up to 150 nmol [263]. A typical calibration curve for this assay is shown in Figure 4.7. Using this assay, the amount of LPS measured on nano-glycoconjugates was determined to be  $8.4 \pm 0.5 \mu\text{g/mL}$ .

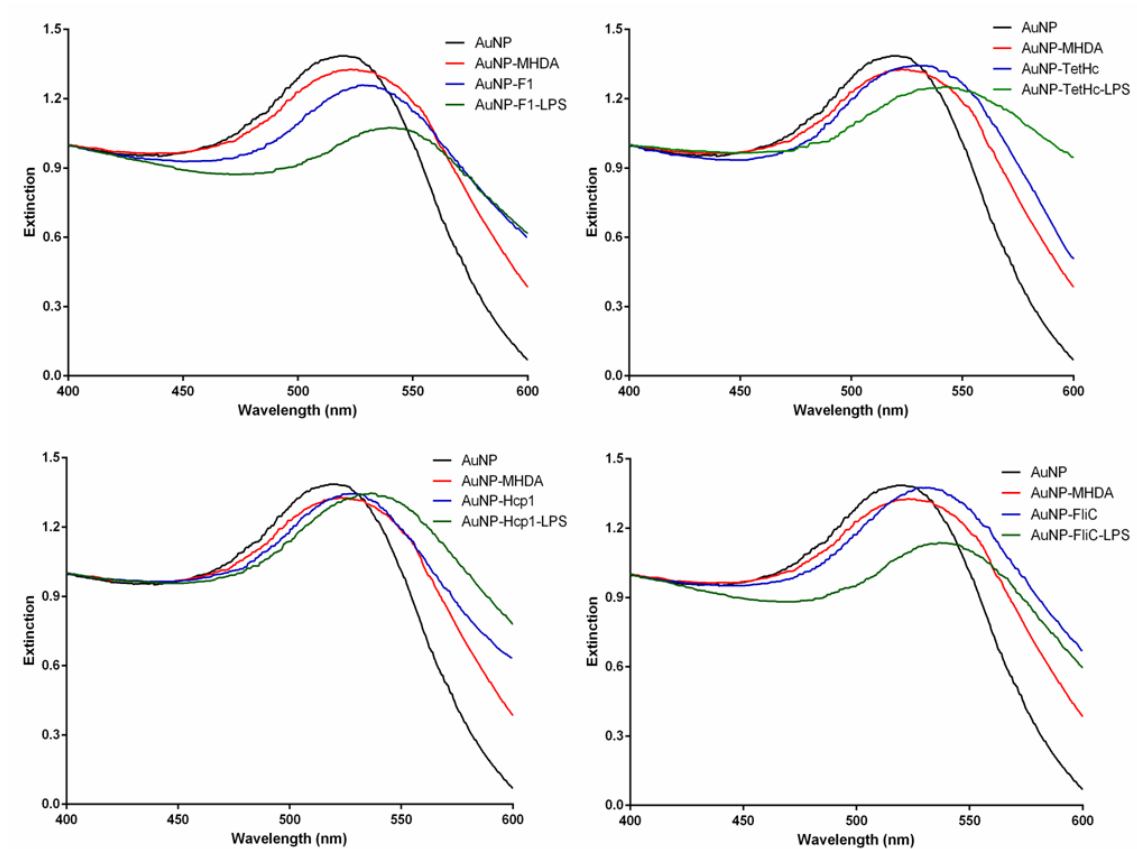


**Figure 4.5** UV-visible absorption spectra for glycoconjugates using thiol maleimide coupling chemistry. Displayed are AuNPs (black), AuNPs functionalised with MHDA (red), AuNPs functionalised with MHDA coupled with TetHc (blue) and AuNPs coupled with TetHc and *B. thailandensis* LPS (green).

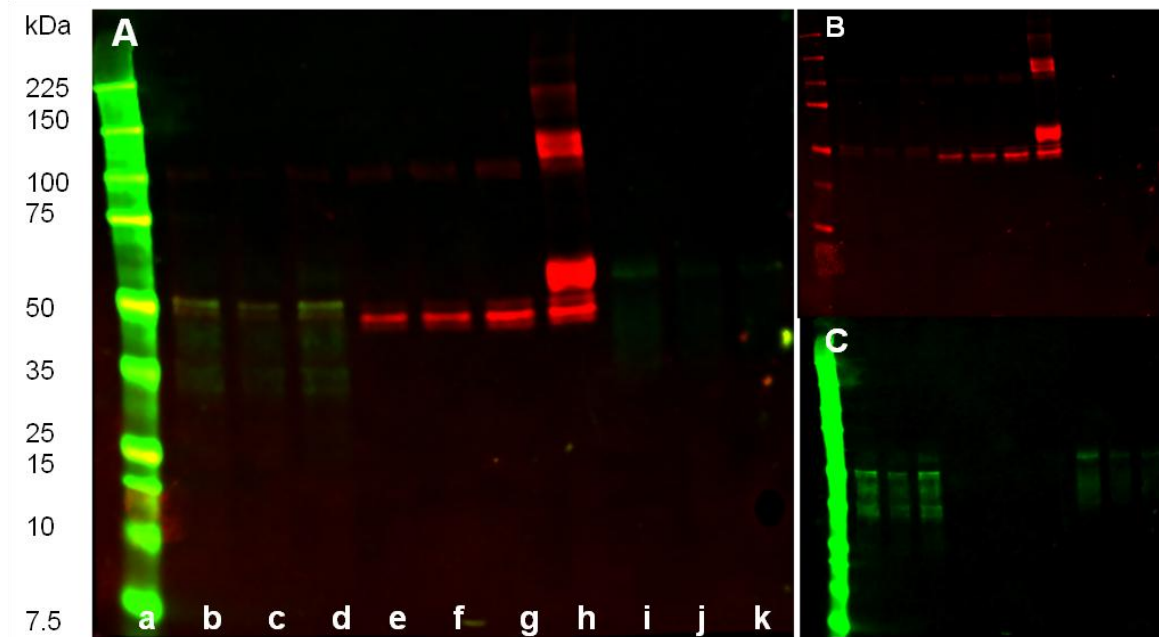


**Figure 4.6.** Two-colour western blot of AuNP-TetHc-LPS separated using a NuPAGE 4-12% Bis-Tris gel (A); IRDye® (680/800) protein marker (a), AuNP-TetHc-LPS treated with 11-mercapto-1-undecanol (b-d), TetHc (e-h), LPS (i-k). Individual IR channels shown for 680 nm (red) (B) and 800 nm (green) (C). A rabbit pAb against Hc and a mouse mAb against LPS were used to bind TetHc and LPS, respectively. Goat anti-rabbit IRDye® 680 and anti-mouse IRDye® 800 secondary antibodies were used to detect primary antibody binding.

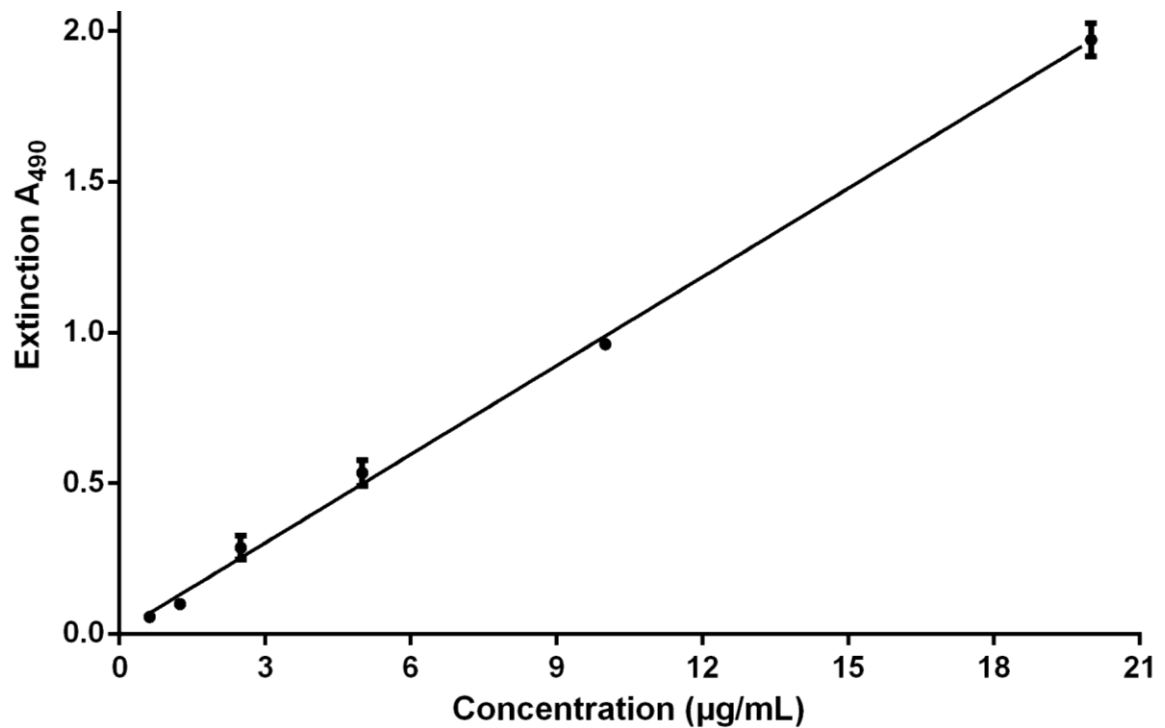


**Figure 4.7.** Typical calibration curve for phenol-sulphuric acid assay showing the relationship between absorption values and LPS concentrations. This was used to determine the concentration of LPS conjugated to protein coupled AuNPs. Each point represents the mean of three values and error bars represent the standard error of the mean.  $R^2=0.9984$ .

### 4.3.3 Serum antibody responses 1

An immunisation and protection study was designed in collaboration with colleagues at UTMB to test the protection of nano-glycoconjugate vaccines against a *B. mallei* inhalation challenge. Immunisations were carried out at UTMB in BALB/c mice with a priming dose followed by two booster immunisations of LPS coupled to a protein carrier on AuNPs with an aluminium hydroxide adjuvant (alhydrogel). Five weeks post immunisation 100  $\mu$ L of blood was taken from the tail vein of each mouse and shipped to Exeter where antibody isotypes and IgG specific subclasses were measured using an ELISA. A typical calibration curve used to calculate the antibody concentrations is shown in Figure 4.8. In this initial study the nano-glycoconjugates we were interested in were LPS conjugated to either F1 or TetHc coupled AuNPs (AuNP-F1-LPS and AuNP-TetHc-LPS, respectively). Total IgG concentrations showed that animals immunised with AuNP-F1-LPS or AuNP-TetHc-LPS generated the highest response compared to all other groups and were both significantly higher than those immunised with LPS alone ( $p < 0.001$ , Figure 4.9). Mice immunised with AuNP-TetHc-LPS developed a significantly higher IgG response compared with those immunised with AuNP-F1-LPS ( $p < 0.05$ ), but not significantly different to those immunised with AuNP-LPS. Interestingly, the total IgG response seen in animals immunised with LPS was comparable to those given AuNP-F1.

LPS-specific IgG concentrations were also measured and showed a similar pattern to total IgG in the degree of response generated, Figure 4.10. The greatest LPS-specific IgG response was seen in animals immunised with AuNP-TetHc-LPS, which was significantly higher than those immunised with AuNP-LPS and LPS alone ( $p < 0.001$ ) as well as AuNP-F1-LPS ( $p < 0.005$ ). The second highest anti-LPS IgG was generated in mice immunised with AuNP-F1-LPS which was significantly higher than mice immunised with AuNP-LPS or LPS alone ( $p < 0.05$  and  $0.01$  respectively). In order to understand the type of immune response generated better, IgG subclasses IgG1 and IgG2a were also measured, Figure 4.11. The first observation is that the amount of IgG1 present relative to IgG2a is significantly higher for both AuNP-F1 and AuNP-LPS groups ( $p < 0.001$ ). In all other groups, the observed concentrations of IgG1 and IgG2a are comparably similar with the exception of AuNP-TetHc-LPS where IgG2a is significantly higher than IgG1 ( $p < 0.001$ ). Moreover, whilst IgG1 and IgG2a

concentrations account for the majority of total IgG measured in all other groups (> 70%), these subclasses account for only 26% of total IgG measured from mice immunised with LPS.

Since LPS is a T-independent antigen, IgM responses were also measured, Figure 4.12. Mice immunised with AuNP-F1-LPS generated the greatest IgM response which was significantly higher than those given AuNP-LPS or LPS ( $p < 0.05$  and  $0.005$  respectively). A similarly high response was also measured in mice immunised with AuNP-TetHc-LPS, significantly higher than LPS ( $p < 0.05$ ). There was also a statistically significant difference in IgM concentration between mice immunised with AuNP-LPS and LPS alone ( $p < 0.01$ ). Immunoglobulin class switching was shown by expressing IgM and IgG titres as a percentage of the overall immune response (IgM + IgG). The data shows a class switch to an IgG dominant response only in mice immunised with AuNP-TetHc-LPS. In all other mice vaccinated with an LPS containing immunogen there was an equal contribution of IgM and IgG to the overall immune response, Table 4.1.

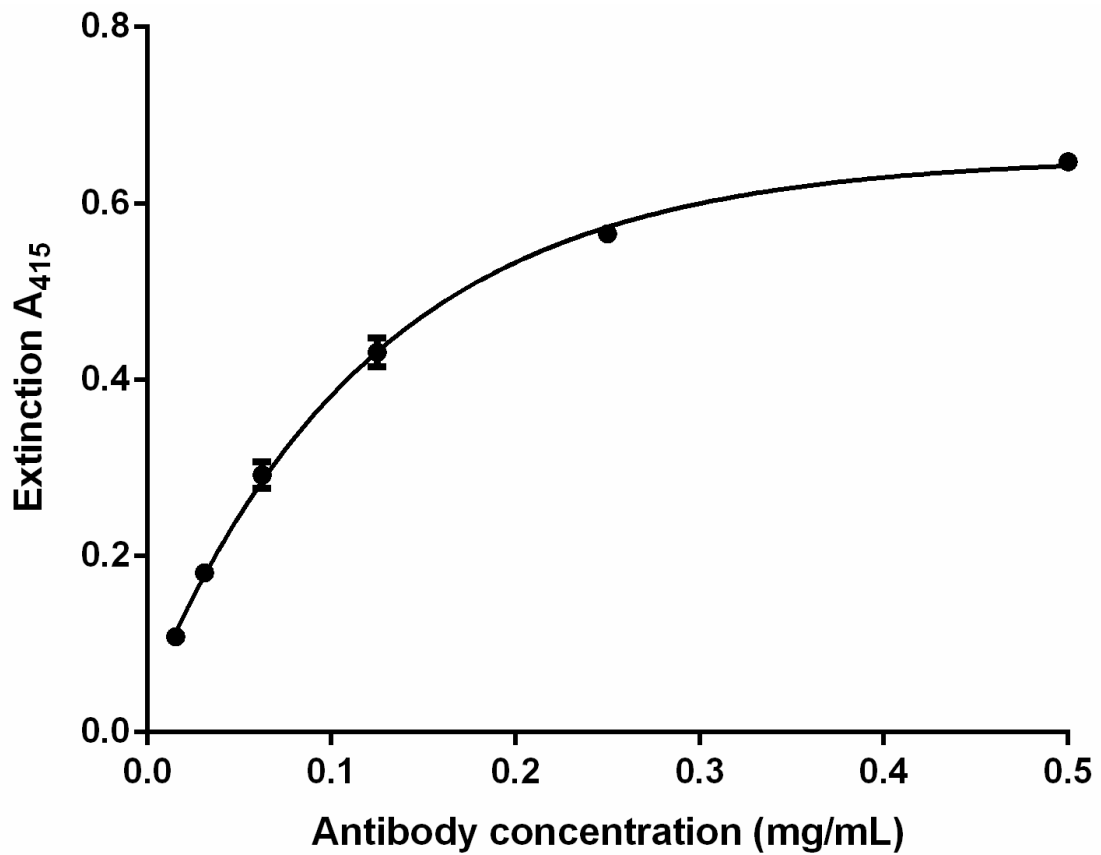


**Figure 4.8.** Typical calibration curve showing the relationship between absorption values and antibody concentrations. This was used to determine the concentration of antibody subclasses in mouse sera. Each point represents the mean of three values and error bars represent the standard error of the mean.  $R^2=0.9973$ .

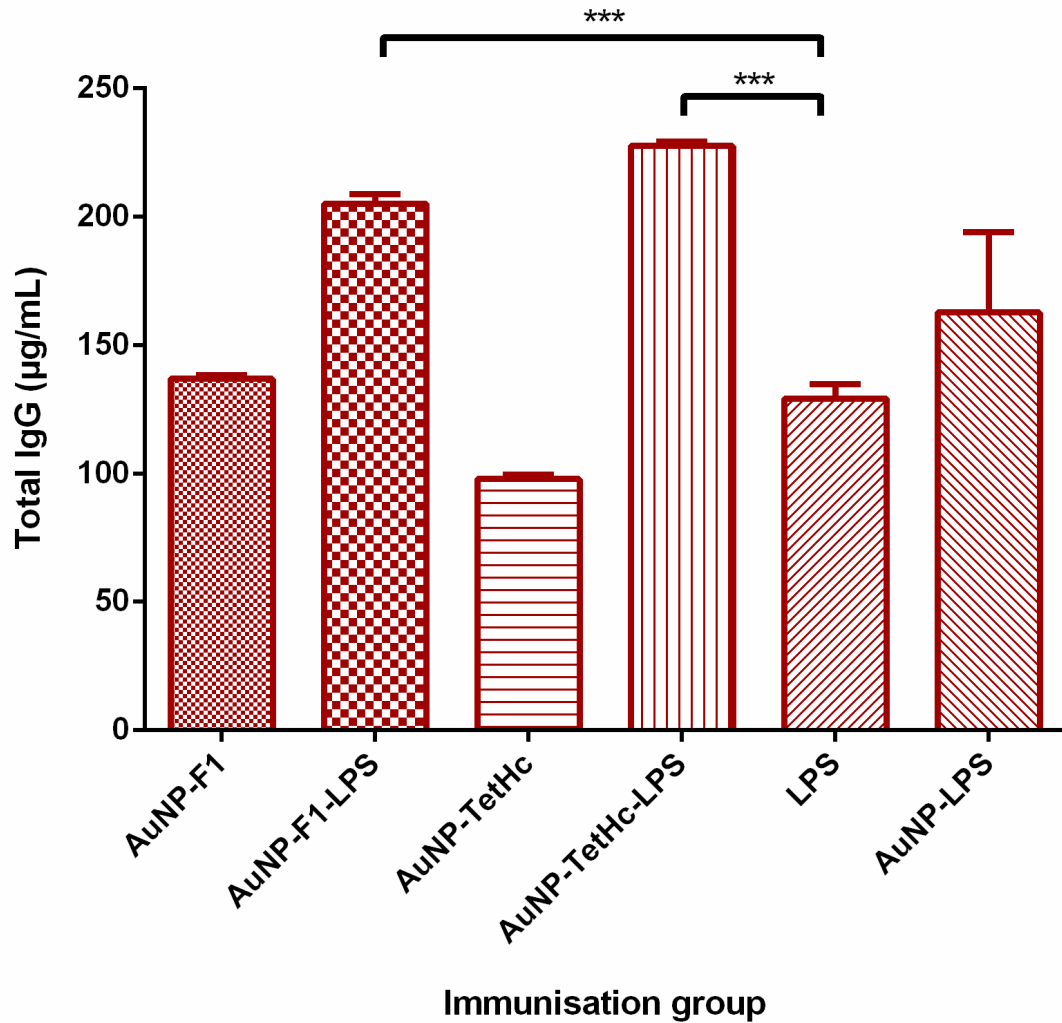


**Figure 4.9.** Total IgG concentration in sera collected from eight mice, five weeks post immunisation with the antigen indicated and determined using quantitative ELISA. Error bars represent the standard error of the mean; asterisks indicate significant differences ( $p < 0.001$ ).

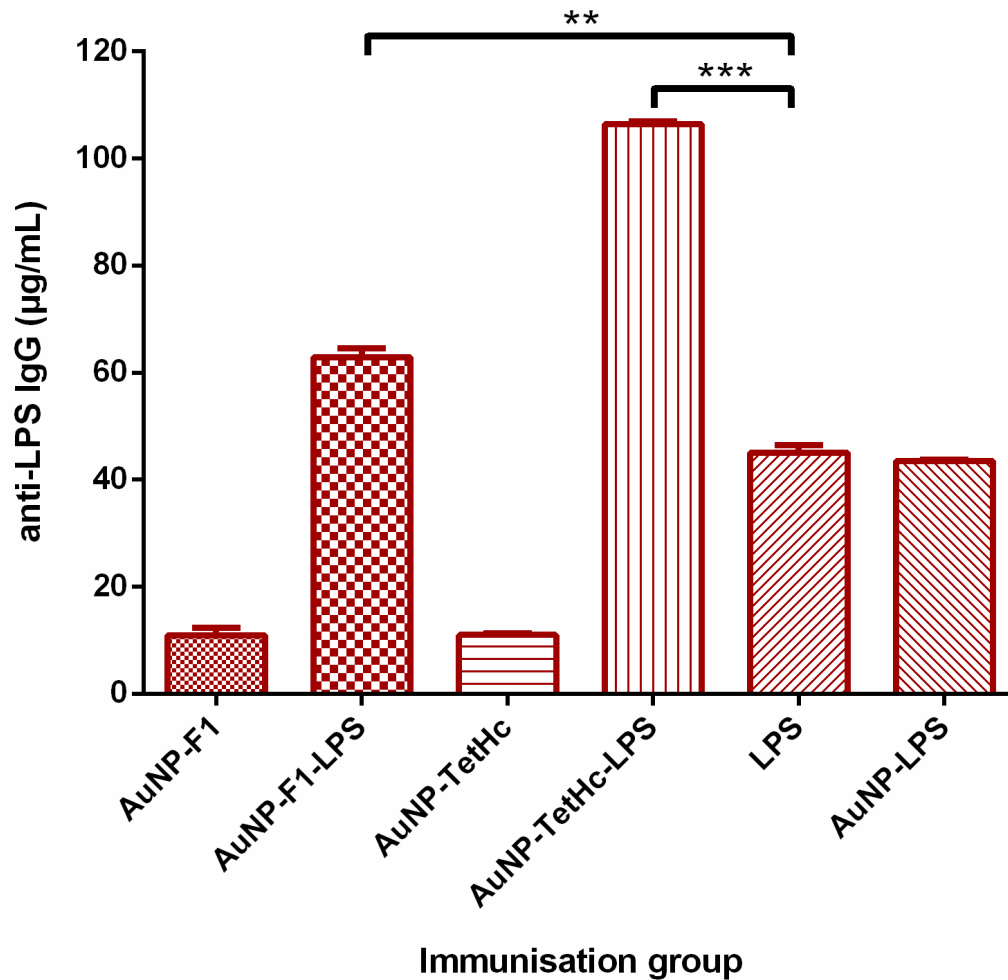


**Figure 4.10.** LPS specific IgG concentration in sera collected from groups of eight mice, five weeks post immunisation with the antigen indicated and determined using quantitative ELISA. Error bars are calculated using the standard error of the mean. \*\*  $p < 0.01$ , \*\*\*  $p < 0.001$ .

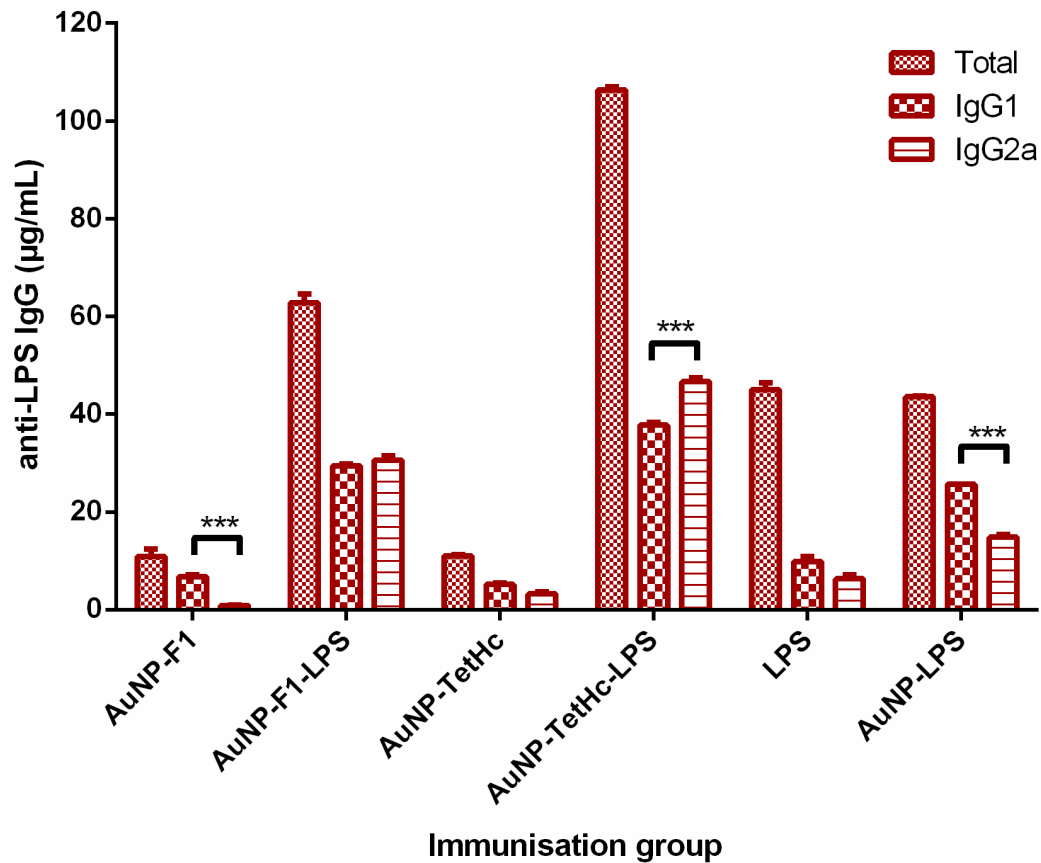


**Figure 4.11.** LPS specific IgG and IgG subclass concentration in sera collected from groups of eight mice, five weeks post immunisation with the antigen indicated and determined using quantitative ELISA. Error bars represent the standard error of the mean; asterisks indicate significant differences ( $p < 0.001$ ).

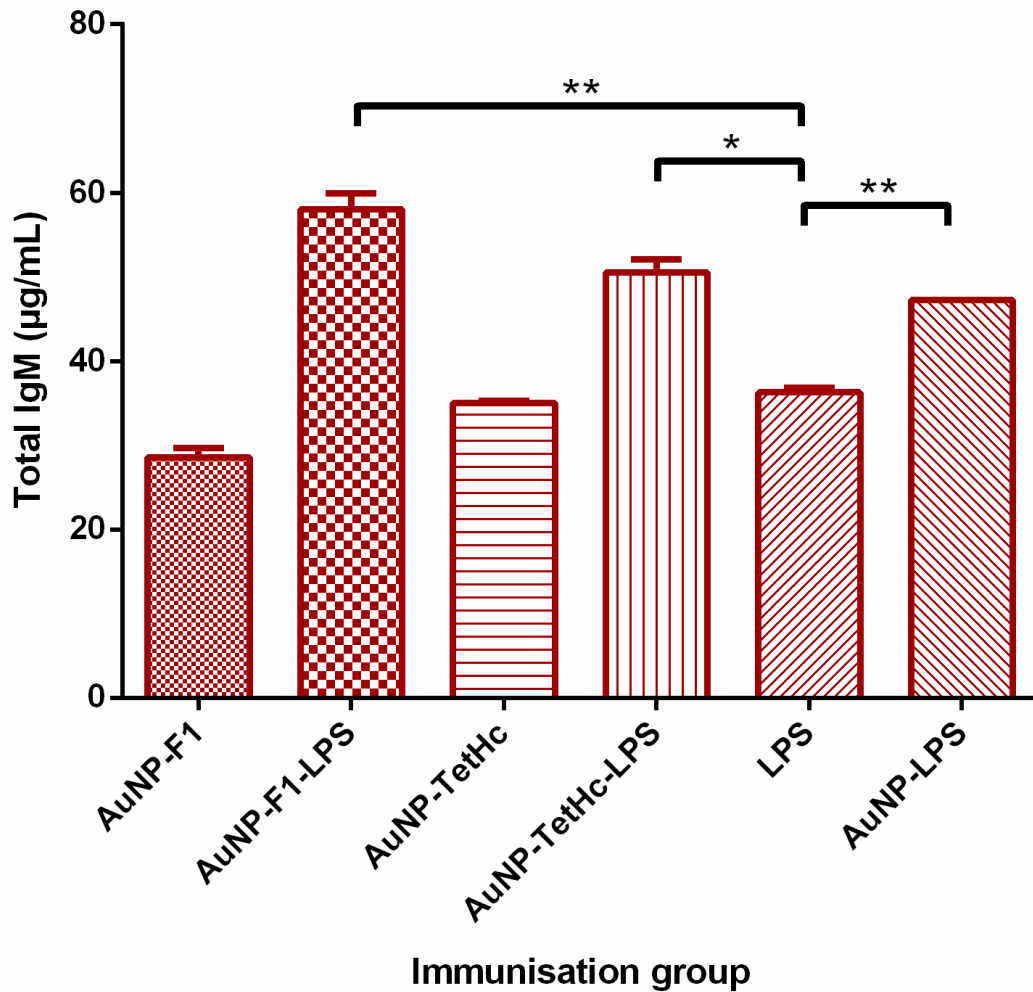


**Figure 4.12.** LPS specific IgM concentration in sera collected from groups of eight mice, five weeks post immunisation with the antigen indicated and determined using quantitative ELISA. Error bars are calculated using the standard error of the mean. \*  $p < 0.05$ , \*\*  $p < 0.01$ .

#### 4.3.4 Protection study

Three weeks after the final immunisation boost of nano-glycoconjugates, BALB/c mice were challenged IN with  $2.27 \times 10^5$  CFU  $50 \mu\text{L}^{-1}$  ( $3 \times \text{LD}_{50}$ ) *B. mallei* China7 strain and their mean time to death was recorded, Figure 3.10. The experiment was terminated at 21 days post challenge, which is within the known range of protection seen from LPS alone [414]. Following termination of the experiment the mice demonstrating the greatest survival were those immunised with LPS and AuNP-F1-LPS with 100% survival, Figure 4.13. Other groups with high levels of survival were those immunised with AuNP-TetHc-LPS and AuNP-LPS, giving an 89% and 78% survival, respectively, although this was not significantly different to groups with 100% survival. Control mice receiving PBS, AuNP-F1 or AuNP-TetHc had a sharp decline in survival after 4 days with only AuNP-F1 and AuNP-TetHc groups making it to the end of the study with 11% and 22% survival, respectively. There was a statistically significant difference between animals immunised with material containing LPS compared to control animals ( $p < 0.001$ ).

Spleens and livers were removed from five surviving mice of each LPS, AuNP-LPS, AuNP-F1-LPS and AuNP-TetHc-LPS immunised groups to determine bacterial load, Figures 4.14 and 4.15. Whilst colony counts of greater than  $1 \times 10^6$  were recovered from all spleens, there were significantly lower counts found in mice immunised with AuNP-TetHc-LPS and AuNP-LPS compared with AuNP-F1-LPS and LPS ( $p < 0.05$ ). Bacterial colonies recovered from the lungs were much lower ( $> 1 \times 10^3$ ) and there was no significant difference between immunisation groups.

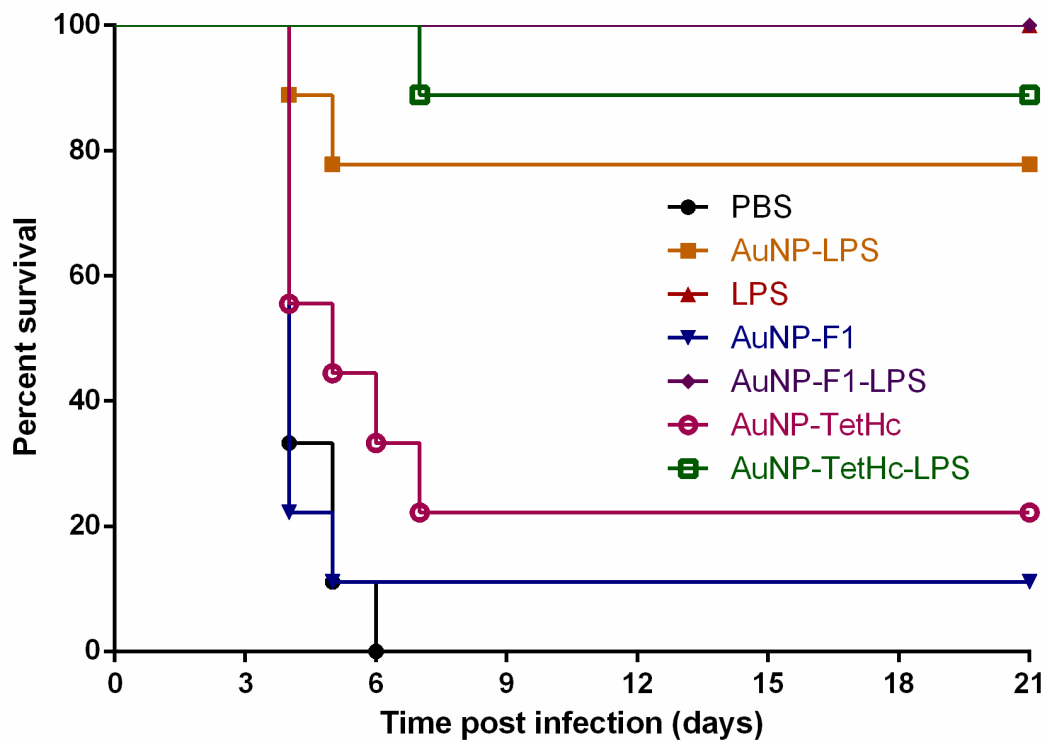


**Figure 4.13.** Survival curve for groups of 10 BALB/c mice challenged IN with 3 x LD<sub>50</sub> *B. mallei* China7, 4 weeks post IP immunisation with 3 x 100 µL doses of AuNP-LPS, LPS, AuNP-F1, AuNP-F1-LPS, AuNP-TetHc or AuNP-TetHc-LPS.

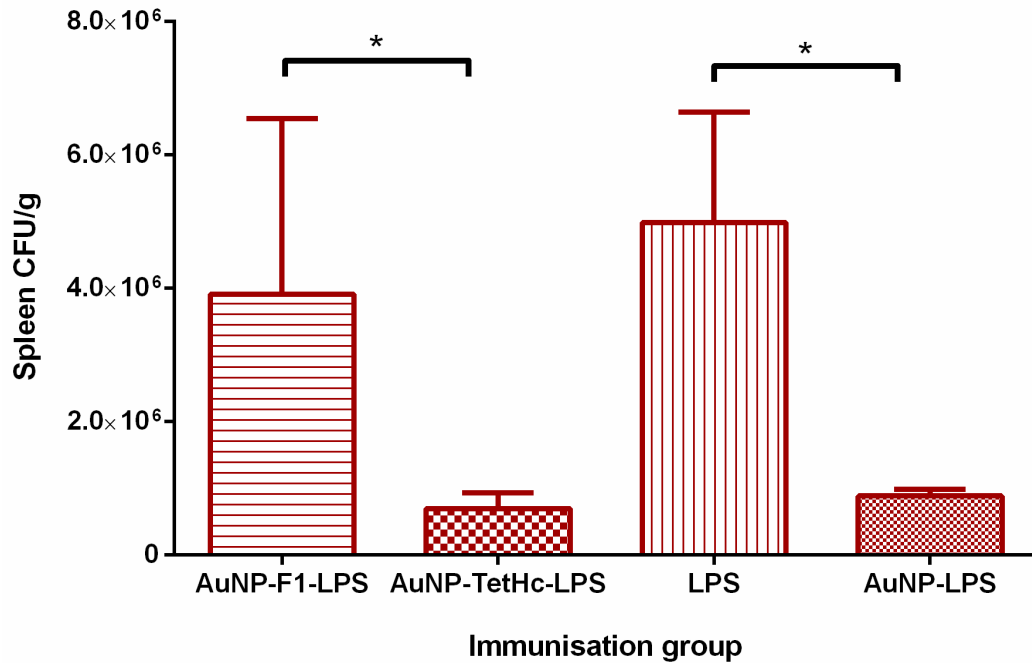


**Figure 4.14.** Colony counts of *B. mallei* taken from homogenised spleens removed three weeks post challenge and plated onto selective Ashdown's medium. Each point is the mean of values from five mice immunised with LPS, AuNP-LPS, AuNP-F1-LPS or AuNP-TetHc-LPS and then challenged with  $3 \times \text{LD}_{50}$  *B. mallei* China 7. Error bars represent the standard error of the mean; asterisks indicate significant differences ( $p < 0.05$ ).

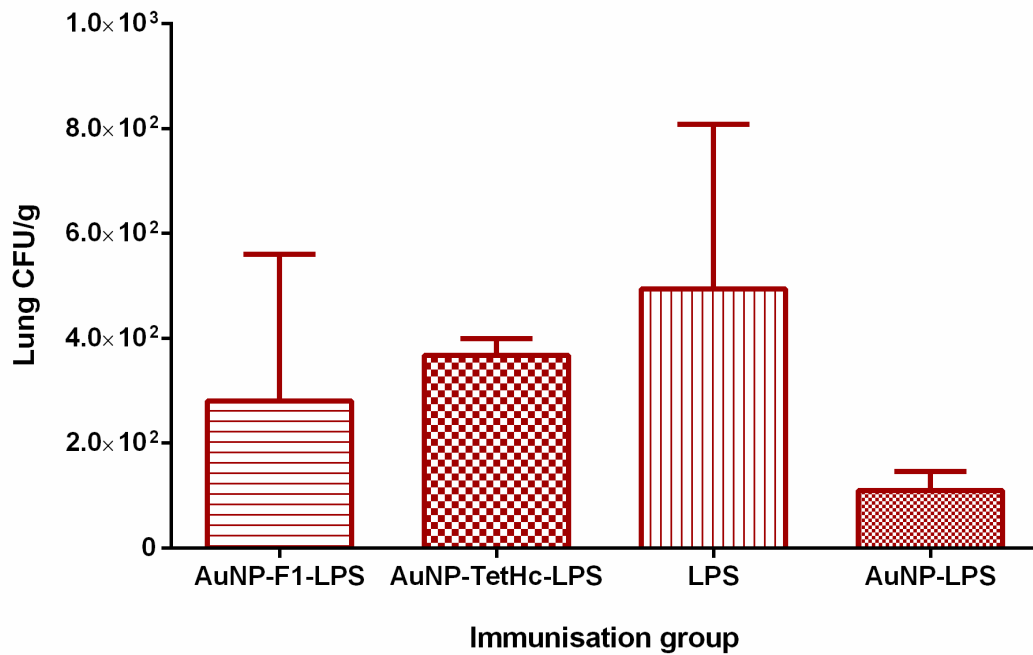


**Figure 4.15.** Colony counts of *B. mallei* taken from homogenised lungs and plated onto selective Ashdown's medium. Each point is the mean of values from five mice immunised with LPS, AuNP-LPS, AuNP-F1-LPS or AuNP-TetHc-LPS and then challenged with  $3 \times \text{LD}_{50}$  *B. mallei* China 7. A lobectomy was performed three weeks post challenge. Error bars are calculated using the standard error of the mean.

**Table 4.1.** Summary of results from “immunisation study 1”. Darkest coloured boxes indicate the highest response induced by the immunogens indicated.

Group	% survival	Total IgG (µg/mL)	IgG2a:1	LPS specific IgG (µg/mL)	Total IgM (µg/mL)	IgG, %	IgM, %
AuNP-F1	11	137 ± 1	0.1	11.0 ± 1.5	29 ± 1	27.7	72.3
AuNP-F1-LPS	100	205 ± 4	1	63 ± 2	58 ± 2	52	48
AuNP-TetHc	22	98 ± 2	0.6	11 ± 0.3	35 ± 0.2	24	76
AuNP-TetHc-LPS	89	228 ± 2	1.1	106.4 ± 0.6	51 ± 2	67.8	32.2
LPS	100	129 ± 6	1.6	45.1 ± 1.5	36 ± 0.5	55.4	44.6
AuNP-LPS	78	163 ± 31	0.6	43 ± 0.2	47 ± 0.1	48	52

#### 4.3.5 Serum antibody responses 2

The previous immunisation study was repeated but on a larger scale to accommodate some additional protein carriers including the *Burkholderia* proteins Hcp1 and FliC. Antibody isotypes and IgG specific subclasses were measured from sera collected from animals 5 weeks post immunisation. Total IgG concentrations show that animals immunised with AuNP-FliC-LPS and AuNP-FliC generated the greatest overall response, Figure 4.16. Whilst the total IgG was significantly higher than all other groups ( $p < 0.01$ ) there was no significant difference between AuNP-FliC-LPS and AuNP-FliC IgG concentrations. Conversely, there was a significant difference between AuNP glycoconjugates and their protein carrier counterparts; AuNP-F1 compared with AuNP-F1-LPS ( $p < 0.005$ ), AuNP-TetHc compared with AuNP-TetHc-LPS ( $p < 0.001$ ) and AuNP-Hcp1 compared with AuNP-Hcp1-LPS ( $p < 0.05$ ). Animals immunised with AuNP-LPS generated a higher IgG concentration than those immunised with LPS alone ( $p < 0.005$ ).

LPS-specific IgG concentrations were also measured and showed a much more definitive picture to the degree of response generated, Figure 4.17. Here, the highest IgG titre came from mice immunised with LPS which is perhaps surprising considering the poor survival rate of these animals. This was closely followed by AuNP-Hcp1-LPS although there was no significant difference between the two groups. The antigen-specific IgG concentrations generated in animals immunised with material containing LPS was significantly higher than their protein carrier counterparts without LPS ( $p < 0.001$ ). There was a statistically higher concentration of LPS-specific IgG raised in mice immunised with LPS compared with AuNP-LPS ( $p < 0.001$ ). IgG subclasses IgG1 and IgG2a were also measured to better understand the type of immune response generated, Figure 4.18. There is a predominant IgG1 immune response in all nano-glycoconjugate groups, with the exception of AuNP-F1-LPS, accounting for >70% of the total LPS-specific IgG concentration. However, in LPS immunised animals, IgG1 accounts for just 22% of LPS-specific IgG and the combined total of IgG1 and IgG2a makes up just less than half of the total LPS-specific IgG. This result was also apparent in the first immunisation study so an ELISA measuring the remaining IgG isotypes was set up, Figure 4.19. The shows that just over a third of the total LPS-specific IgG titre from LPS immunised mice is comprised of IgG3 in both immunisation studies.

Total IgM concentrations were also measured to determine its role in protection against *B. mallei*, Figure 4.20. As with the IgG concentration data, a significantly higher concentration of IgM was raised in animals immunised with material containing LPS compared to their protein carrier alone counterparts ( $p < 0.001$ ). The highest titres were raised in animals given AuNP-LPS which were only marginally higher than those with LPS alone ( $p < 0.05$ ). Whilst high IgM concentrations were measured from mice given AuNP-F1-LPS and AuNP-TetHc-LPS, relatively low IgM concentrations were measured in AuNP-Hcp1-LPS and AuNP-FliC-LPS immunised mice, when compared with the other groups. Immunoglobulin class switching was shown by expressing IgM and IgG titres as a percentage of the overall immune response (IgM + IgG). In contrast with the previous study, the data shows a class switch to an IgG dominant response only in mice immunised with AuNP-Hcp1-LPS. There was an equal contribution of IgM and IgG to the overall immune response in mice immunised with AuNP-FliC-LPS. None of the other immunisation groups were able to class-switch, Table 4.2.

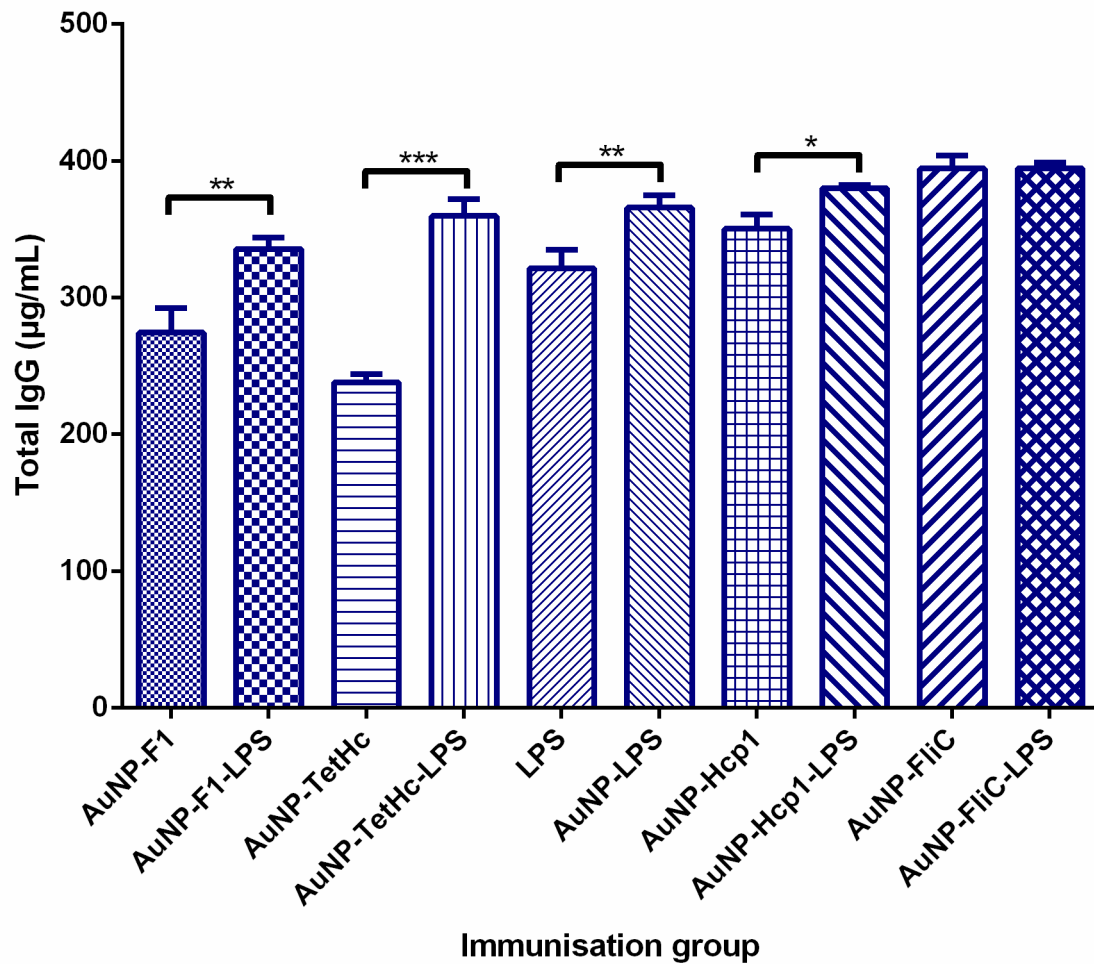


**Figure 4.16.** Total IgG concentration in sera pooled from groups of eight mice, five weeks post immunisation with the antigen indicated and determined using quantitative ELISA. Error bars are calculated using the standard error of the mean. \*  $p < 0.05$ , \*\*  $p < 0.01$ , \*\*\*  $p < 0.001$ .

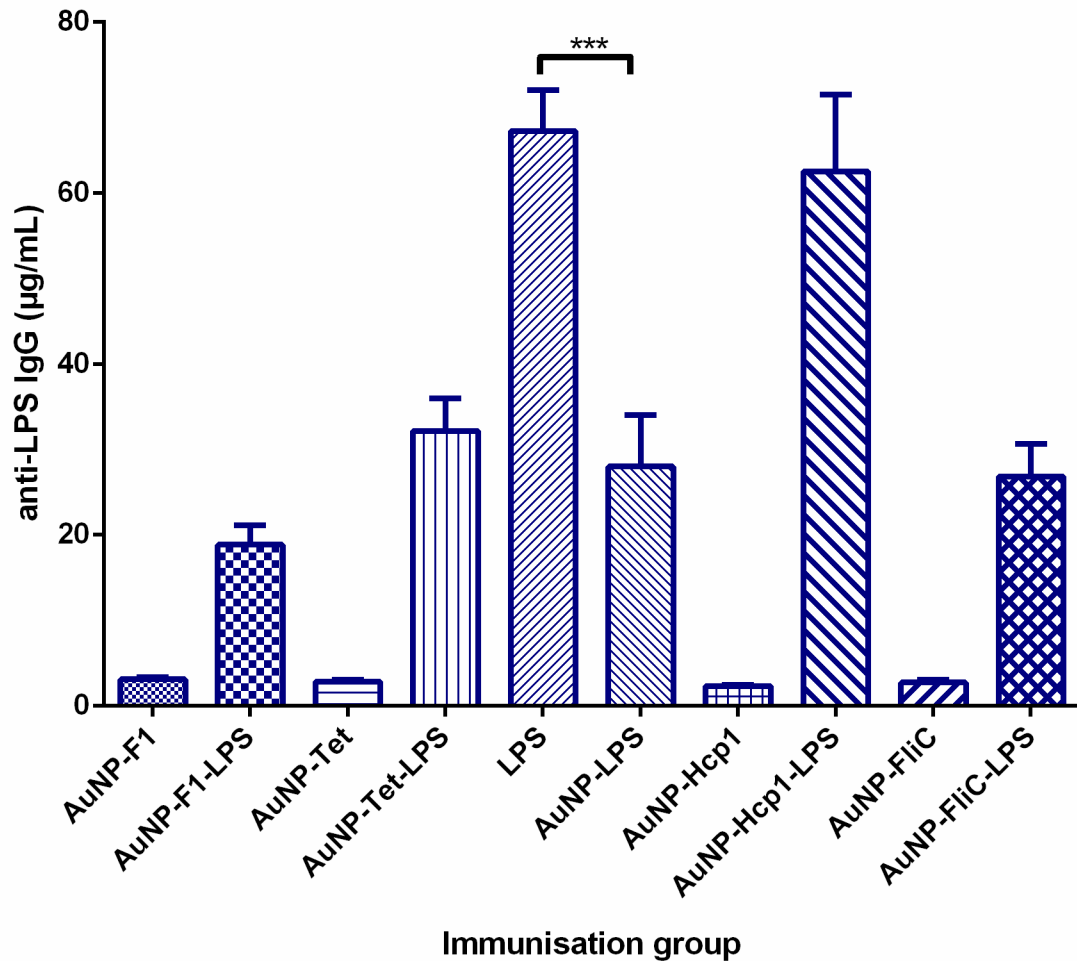


**Figure 4.17.** LPS specific IgG concentration in sera pooled from groups of eight mice, five weeks post immunisation with the antigen indicated and determined using quantitative ELISA. Error bars represent the standard error of the mean; asterisks indicate significant differences ( $p < 0.001$ ).

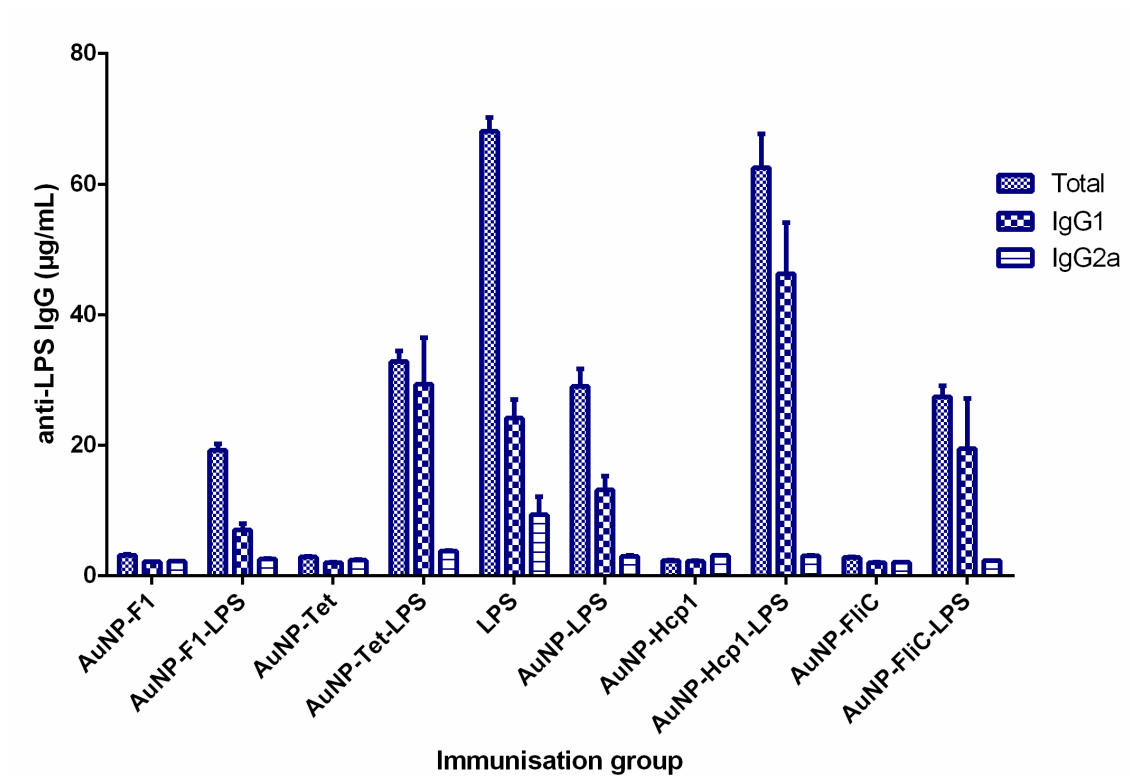


**Figure 4.18.** LPS-specific IgG and IgG subclass concentrations in sera pooled from groups of eight mice, five weeks post immunisation with the antigen indicated and determined using quantitative ELISA. Error bars are calculated using the standard error of the mean.

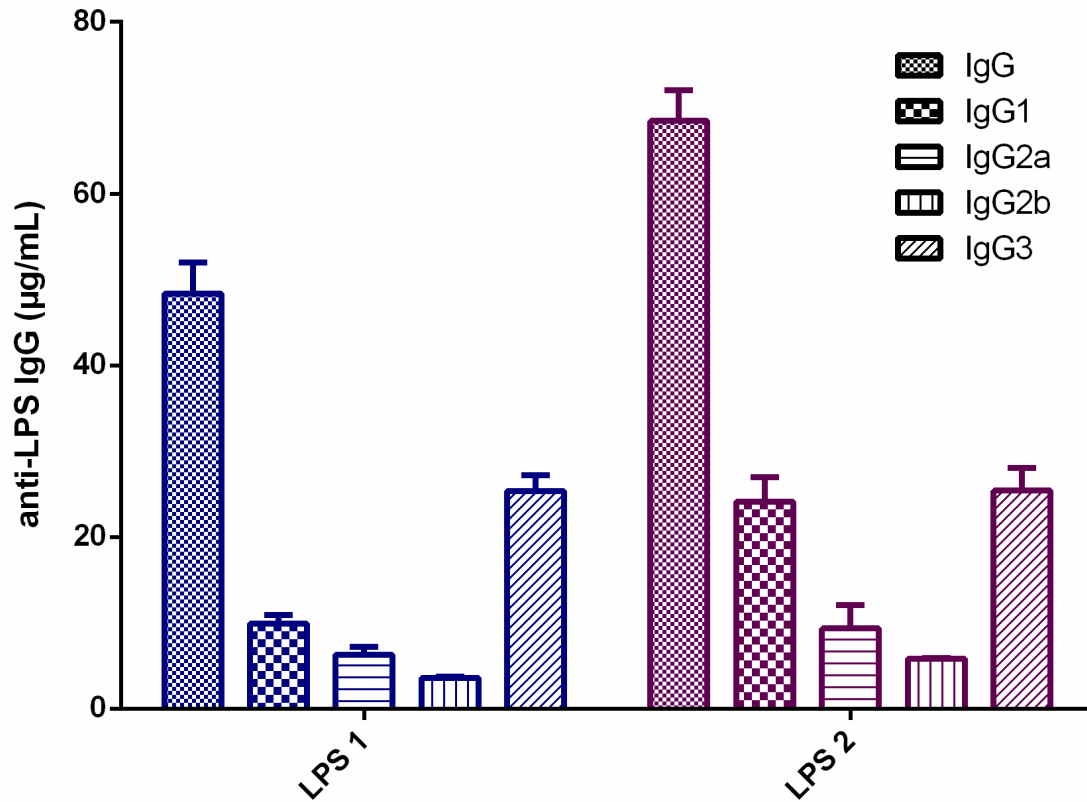


**Figure 4.19.** Side-by-side comparison of LPS-IgG isotypes taken from mice immunised with LPS in “immunisation study 1” (LPS 1) and “immunisation study 2” (LPS 2) Error bars are calculated using the standard error of the mean.

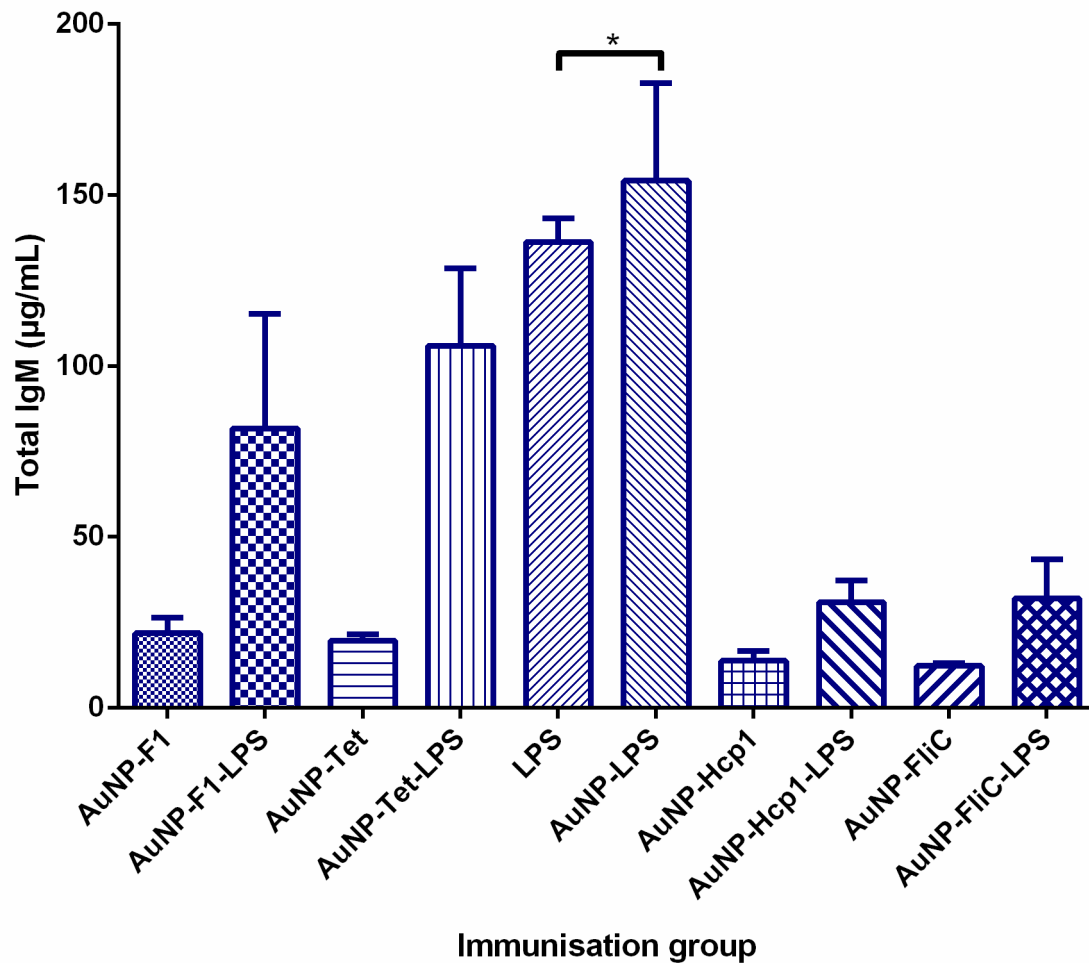


**Figure 4.20.** LPS specific IgM concentration in sera pooled from groups of eight mice, five weeks post immunisation with the antigen indicated and determined using quantitative ELISA. Error bars represent the standard error of the mean; asterisks indicate significant differences ( $p < 0.05$ ).

**Table 4.2.** Summary of results from “immunisation study 2”. Darkest coloured boxes indicate the highest response induced by the immunogens indicated.

Group	Total IgG (µg/mL)	IgG2a:1	LPS specific IgG (µg/mL)	Total IgM (µg/mL)	IgG, %	IgM, %
AuNP-F1	275 ± 18	1	3 ± 0.3	22 ± 5	12.5	87.5
AuNP-F1-LPS	335 ± 8	0.9	19 ± 2	82 ± 34	18.7	81.3
AuNP-TetHc	238 ± 6	1	2.8 ± 0.2	20 ± 2	12.6	87.4
AuNP-TetHc-LPS	360 ± 12	0.7	32 ± 4	106 ± 23	23.3	76.7
LPS	321 ± 13	0.9	67 ± 5	136 ± 7	33.1	66.9
AuNP-LPS	366 ± 9	0.7	28 ± 6	154 ± 29	15.4	84.6
AuNP-Hcp1	350 ± 1	1.2	2 ± 0.1	14 ± 3	14.3	85.7
AuNP-Hcp1-LPS	380 ± 2	0.7	63 ± 9	31 ± 6	67	33
AuNP-FliC	395 ± 10	1	3 ± 0.3	12 ± 0.7	18.1	81.9
AuNP-FliC-LPS	394 ± 4	0.9	27 ± 4	32 ± 11	45.7	54.3

#### 4.4 Discussion

##### *4.4.1 LPS extraction*

*B. thailandensis* was chosen as a source of LPS for the construction of a glycoconjugate vaccine against melioidosis and glanders. Not only does *B. thailandensis* LPS have greater immunological activity in murine macrophages when compared with LPS from *B. pseudomallei* but it has been shown that LPS from *B. thailandensis* displays comparable levels of protection against glanders and melioidosis in a murine model of infection [414, 422, 428] (personal communication). Moreover, there is a material handling consideration; *B. thailandensis* is a biosafety level two (BLS-2) agent so the associated costs and hazards are reduced when compared with *B. pseudomallei* and *B. mallei*, which are both BLS-3 agents.

LPS was purified from *B. thailandensis* strain E264 analysed by SDS-PAGE showed a ladder banding pattern concentrated around 35-75 kDa, similar in appearance to other published reports of LPS, not only from *B. thailandensis* but also from numerous strains of *B. pseudomallei* and *B. mallei* [403, 405, 414, 422, 429]. Additional bands of lower molecular weight were also seen on the silver stained gels, which are likely to consist of O-antigen monomers and protein impurities. The appearance of these impurities are a lot more prevalent in the LPS sample purified from broth culture which suggests that purifying LPS from Petri dishes results in a sample of higher purity. Western blotting using CC6 mAb to compare the O-antigens of LPS purified from bacteria grown in broth to those which were grown on plates showed that the density of the O-antigen was a lot greater in plate purified LPS. Whilst this helped to identify the best method for LPS extraction, it also highlights some potential environmental factors which may influence the biosynthesis of *Burkholderia* LPS. Biofilm formation has previously been associated with LPS biosynthesis in other Gram-negative bacteria, and it is possible the expression of LPS by *B. thailandensis* is upregulated upon biofilm formation [430-433].

##### *4.4.2 LPS coupling*

In this study, LPS was covalently linked to one of four different protein carriers which were immobilised onto AuNPs; F1, TetHc, Hcp1 and FliC. Not only do AuNPs act as an immunostimulant for vaccine delivery but also a catalytic

surface onto which conjugation chemistry can be performed [434]. This is an important feature since many glycoconjugate chemistries suffer from a very poor yield. Whilst a reductive amination approach is traditionally used to couple polysaccharides onto protein carriers, this requires alkaline conditions owing to the high  $pK_a$  of the  $\epsilon$  amino group on the proteins lysine residues. This method of coupling is not only slow and inefficient, typically taking several days, but it forms reversible Schiff bases which require reduction in order to stabilise the linkage formed [257, 435-438]. A borohydride salt is often used as the reducing agent for this chemistry which is not only toxic but can hydrolyze pH sensitive polysaccharides, such as the one from *Neisseria meningitidis* A, and could reduce the ability to provide protective epitopes [257]. As a result, a thiol-maleimide approach was taken to couple LPS onto the chosen protein carriers in this study. Confirmation of conjugation was confirmed by measuring a shift in the  $\lambda_{max}$  of AuNPs from 532 nm for AuNP-TetHc to 541 nm for AuNP-TetHc-LPS; indicating an overall increase in the mean diameter of AuNP conjugates. The extinction peak is also much broader for AuNP-TetHc-LPS suggesting the size distribution of particles is much broader which is likely to be due to variable lengths of the repeating O-antigen disaccharide on the particles.

A two-colour western using a rabbit pAb against TetHc and a mouse mAb raised against LPS O-antigen identified the presence of both antigens after displacing the conjugate from AuNPs and running on an SDS-PAGE. Not only does this confirm the presence of both antigens but also the structural integrity of their respective epitopes after covalent coupling, based on the reactivity with their respective antibodies. Whilst TetHc bands appear to be the same molecular weight as the native protein in the adjacent wells, LPS released from the glycoconjugate is of a lower molecular weight to the native LPS. This observation was also made of a recently characterised *B. pseudomallei* glycoconjugate using a diphtheria toxoid protein carrier [439]. Despite no rationale being provided for this phenomenon, it is possible that the attachment of a protein carrier to LPS could cause it to move atypically through the gel due to changes in the overall surface charge of the molecule.

The quantification of coupled LPS was carried out using a phenol-sulphuric acid assay [262, 263, 440, 441]. Using this fast and reliable method it is possible to accurately determine the carbohydrate content with a detection limit of 1 nmol over the dynamic range 1-150 nmol. This method required a

large amount of optimisation, but was indispensable for maintaining a constant batch of nano-glycoconjugates for immunisation studies thereafter. The concentration of LPS detected on nano-glycoconjugates was determined as 9.6 µg/mL; approximately 20% of the initial LPS used for coupling.

#### 4.4.3 Immunoglobulin G response

Antibody classes and isotypes were measured from sera in an attempt to identify some of the immunological processes that had been triggered by the different vaccines. Over the two immunisation studies, total IgG concentrations were highest amongst mice immunised with AuNP-TetHc-LPS compared with AuNP-F1-LPS. This is likely to be a result of the additional epitopes provided by the carrier protein for recognition by CD4<sup>+</sup> Th cells. An increase in IgG concentrations when TetHc is used as a protein carrier instead of F1 suggests TetHc is a stronger immunogen. This could reflect a higher capacity of TetHc to provide antigenic epitopes for recognition by B cells. In the second experiment, TetHc was shown again to be a stronger immunogen compared to F1 by inducing a higher IgG titre. However, the addition of two nano-glycoconjugates using *Burkholderia* specific proteins (Hcp1 and FliC) to the immunisation study resulted in even higher IgG titres. One explanation for a significantly higher IgG response from nano-glycoconjugated LPS over uncoupled LPS could be its presentation to immune cells. Since the coupling chemistry is selective for nucleophilic carbonyl groups in the LPS core region, this leaves the O-antigen and lipid A regions free. Whilst the O-antigen provides epitopes for the development of antigen-specific antibodies, the lipid A region is a potent agonist for TLR4 and evokes a strong immune response from interaction with B memory cells. Comparisons between the two experiments show that total IgG measured from sera is far greater in the second experiment (2-fold). This could be attributed to environmental factors, such as stress of the animals, or batch variation of nano-vaccines due to the chemical synthesis or even degradation during shipment to UTMB if the samples were handled incorrectly.

Whilst a high immune response from a vaccine is a promising start, the generation of antigen-specific antibodies from memory B cells is key to preventing future infections. Consequently, LPS-specific IgG concentrations were measured and revealed a similar trend to the total IgG measurements; mice immunised with nano-glycoconjugates generated the highest responses.

The LPS-specific IgG concentrations from mice immunised with nano-glycoconjugates was significantly higher than the LPS-IgG from mice immunised with LPS alone. This effect may also be due to the presentation of LPS in its coupled form and the high density of O-antigen epitopes localised on an AuNP surface compared with uncoupled LPS. In the second immunisation study, LPS-IgG titres of mice immunised with nano-glycoconjugates and AuNP-LPS were all similar but significantly lower than the levels measured in the initial study by approximately 66%. The highest LPS-IgG titres were found in mice immunised with LPS alone. With the exception of AuNP-Hcp1-LPS, which generated similarly high levels of IgG, all nano-glycoconjugates generated an LPS-IgG response which was less than half that generated by LPS immunised mice. This contradictory result to the first experiment could be due to oxidation of the O-antigen over time as the conjugates prepared for the second experiment were produced using LPS that had been stored for over a year following the previous experiment. This underscores the potential importance of using high quality LPS for vaccine production, which will be taken into consideration in future experiments. Whilst western blot analysis confirmed the integrity of the epitope to which it is raised, there may be other epitopes on the O-antigen which are no longer available for binding. There may also be unforeseen complications with the coupling chemistry affecting the structural integrity or presenting LPS in an undesirable conformation.

Overall, the data presented here suggests that by co-immunising LPS with a protein carrier, the total IgG immune response is greater than immunising with either a protein or LPS alone. Moreover, the LPS-specific response is also greater when LPS is immunised as a glycoconjugate and even more so when the protein to which it is coupled is a *Burkholderia* antigen. This could be due to the recruitment of T<sub>H</sub> cells, by the protein component of the vaccine, which activate B-cells into generating a higher concentration of LPS-IgG.

#### 4.4.4 Immunoglobulin class switching

Evidence of an immunoglobulin class switching event was determined by measuring IgM titres and comparing with IgG to identify whether the immune response induced in vaccinated mice was in a T-dependent manner. This follows the rationale that if CD4<sup>+</sup> Th cells are present and encounter activated B cells they may skew a class switch recombination event from producing IgM to

IgG. Across the two immunisation studies class switch recombination was only present in mice immunised with nano-glycoconjugate vaccines. However, the dominance of IgG from the TetHc and Hcp1 containing nano-glycoconjugate immunised mice suggests that these are the most potent activators of T cells.

Differentiation of CD4<sup>+</sup> T cells into either Th1 or Th2 were then interpreted by measuring IgG subclass concentrations since IFN- $\gamma$ , produced by Th1 cells, promotes an IgG switch towards IgG2a whereas T<sub>H</sub>2 cells support the generation of IgG1. IgG subclasses from the first study showed that only those immunised with AuNP-TetHc-LPS induced a skewed Th1 response, demonstrated by a dominant IgG2a titre. Mice immunised with AuNP-F1-LPS displayed a balanced IgG1/2a, and therefore a Th/Th2, immune response. These data suggest that mice immunised with either nano-glycoconjugate vaccine in the first study would have been able to develop memory T cells for protection against subsequent challenges in the future. None of the mice in the second experiment were able to generate an IgG subclass switch, meaning the Immunoglobulin class switch seen in AuNP-Hcp1-LPS immunised mice was probably due to CD4<sup>+</sup> Th2 cells. This could be explained by unforeseen complications with the coupling chemistry.

In both experiments, the proportion of IgG1 and 2a as a percentage of the IgG were much lower in mice immunised with LPS alone than for other immunisation groups. Other LPS-specific IgG subclasses including IgG2b and 3 were measured from sera of LPS immunised mice and revealed that IgG3 constituted a significant proportion of the converted IgG from IgM. This is due to the interaction of LPS with TLR4 and the resulting signalling molecules, in particular IL-10, which results in the generation of IgG3 [391, 442]. The reason for the apparent absence of IgG3 from sera other LPS containing immunogens could be explained by the production of IFN- $\gamma$ , predominantly by T cells, which inhibits LPS-mediated switching to IgG3 and IgG2b [389]. Whilst the data suggests that a T<sub>H</sub>1 skewed immune response was only induced in two of the vaccine candidates tested, the generation of CD4<sup>+</sup> T cell mediated immunity has been shown to be important for protection against *B. pseudomallei* infection [443].

#### 4.4.5 Survival and tissue colonisation

It has previously been established that *B. thailandensis* LPS is able to protect against a lethal challenge of glanders and melioidosis so it was not surprising to find that mice immunised with LPS alone should retain 100% survival throughout the study. This level of protection was also seen in mice immunised with AuNP-F1-LPS and similarly with AuNP-TetHc-LPS and AuNP-LPS. However, the scope of the first study (21 days) was not sufficient to determine whether a long-term memory response that would provide protection beyond the timescale within which LPS alone is protective was generated by the nano-glycoconjugates. Future studies will be necessary to determine if the conjugates are able to successfully extend protection from challenge with wild-type bacteria beyond this point.

Whilst sterile immunity was not achieved in any of the groups, a significantly lower bacterial count was recovered from the spleens of mice immunised with AuNP-TetHc-LPS and AuNP-LPS compared with the spleens from mice immunised with AuNP-F1-LPS or LPS ( $p < 0.05$ ). When colony counts were taken from lung tissue, there were no significant differences between the groups of immunised mice to the bacterial burden in the lungs. However, the fewest bacterial counts were also taken from mice immunised with AuNP-LPS. Perhaps if the mice were immunised via a different route, i.e. IN, this may have a bigger influence on the colonisation of the lungs by *B. mallei*.

A comparison between IgM titres and bacterial colony counts from the spleen suggests there may be a negative correlation between the two. This is not entirely unexpected, since the spleen is a major site for IgM antibody production and LPS is a T-independent antigen associated with inducing a strong IgM antibody response [422, 444, 445]. However, the significant increase in IgM titres of mice immunised with AuNP-LPS over LPS alone, in both experiments, suggests that AuNPs themselves play a significant role in generating IgM antibodies. Usually triggered by oligodeoxynucleotides with CpG motifs, TLR 9 activation is known to mediate IgM production of CD27<sup>+</sup> memory B cells [446-448]. The elevated production of IgM in mice immunised with AuNPs suggests this may serve as an additional agonist to TLR 9. IgM plays a key role in pathogen opsonisation by activating the Complement system, specifically the Classical Pathway, to induce the binding of C3b onto antigens

[449]. It is therefore possible that the high levels of IgM concentrations seen in mice given AuNP-F1-LPS, AuNP-TetHc-LPS and AuNP-LPS relative to those induced by LPS are the reason for a reduced bacterial burden in these groups of mice due to improved clearance of bacteria and infected cells. The significant decrease in bacterial colony counts taken from spleen tissue are promising sign of moving closer to a vaccine which not only protects, but is able to provide sterile immunity. The correlation seen here between elevated IgM titres and reduced bacterial numbers suggest that IgM may play a key role in providing sterile immunity.

#### 4.4.6 Conclusions

Growing *B. thailandensis* on LA plates produces LPS with a much higher O-antigen density than when grown in LB broth and with fewer impurities.

Covalent coupling of LPS onto AuNP conjugated proteins was successfully achieved using thiol-maleimide chemistry and quantified using a phenol-sulphuric acid assay.

The choice of protein carrier used in glycoconjugate vaccine has an effect on immunoglobulin titres, with the highest being afforded by antigens able to provide a higher capacity of antigenic epitopes for recognition by B cells

Coupling LPS onto protein carriers resulted in a balanced Th1/ Th2 immune response.

A high concentration of IgM results in fewer bacterial colonies of infected tissues.

Future studies will be required to determine if the nano-glycoconjugates are capable of providing long term protection based on the T-dependent immune response that is induced.

## Chapter 5: A Glycoconjugate Vaccine against Pneumococcus

---

### 5.1 Introduction

#### 5.1.1 *Pneumococcus*

*Streptococcus pneumoniae* (pneumococcus) is a facultatively anaerobic, Gram-positive,  $\alpha$ -haemolytic bacterium. As with all bacteria belonging to the genus *Streptococcus*, *S. pneumoniae* is a commensal bacterium that colonises the throat and upper respiratory tract (nasopharynx) of humans [450]. *S. pneumoniae* is also responsible for a range of invasive and non-invasive pneumococcal diseases including pneumonia, meningitis and septicaemia [451]. Invasive pneumococcal disease constitutes a major global health concern in both developed and developing countries. However, those most at risk are children under the age of two years old. Pneumococcal pneumonia is the leading cause of childhood mortality and accounts for 9% of all deaths in the developing world [452].

Like many invasive bacteria, *S. pneumoniae* is surrounded by a capsular polysaccharide (CPS) which serves as a key virulence determinant. CPS is crucial during colonisation of the nasopharynx and prevents mechanical clearance by mucous secretion [453]. The electronegativity of CPS also prevents uptake by APC's and serves as a barrier to reduce exposure to antibiotics [454, 455]. The presence of immunochemically distinct CPS with very little cross-reactivity between *S. pneumoniae* strains has led to the identification of over 40 different serogroups and 90 different serotypes [456]. The CPS associated with these serotypes varies significantly in their structural composition. However, only a fraction of those identified are commonly associated with causing invasive pneumococcal disease with 12 serogroups attributing to over 80% of clinical isolates, Figure 5.1 [457]. The prevalence of these disease associated serotypes varies significantly with age, sex and geography. For example, serotypes 14, 6B, 19F and 18C are statistically more

prevalent among children whereas serotypes 3, 4 and 9V are more common in adults [9].

Benzyloenicillin is currently the drug of choice for treatment of pneumococcal infections. However, recent years has seen a dramatic increase in the number of multi-drug resistant strains; in some areas as many as 35% of pneumococcal isolates are penicillin resistant [458-460]. With invasive pneumococcal infections a global health burden and the reduced efficacy of antibiotic treatment there is an urgent need to develop a safe and effective pneumococcal vaccine capable of providing protection against every *S. pneumonia* serotype.

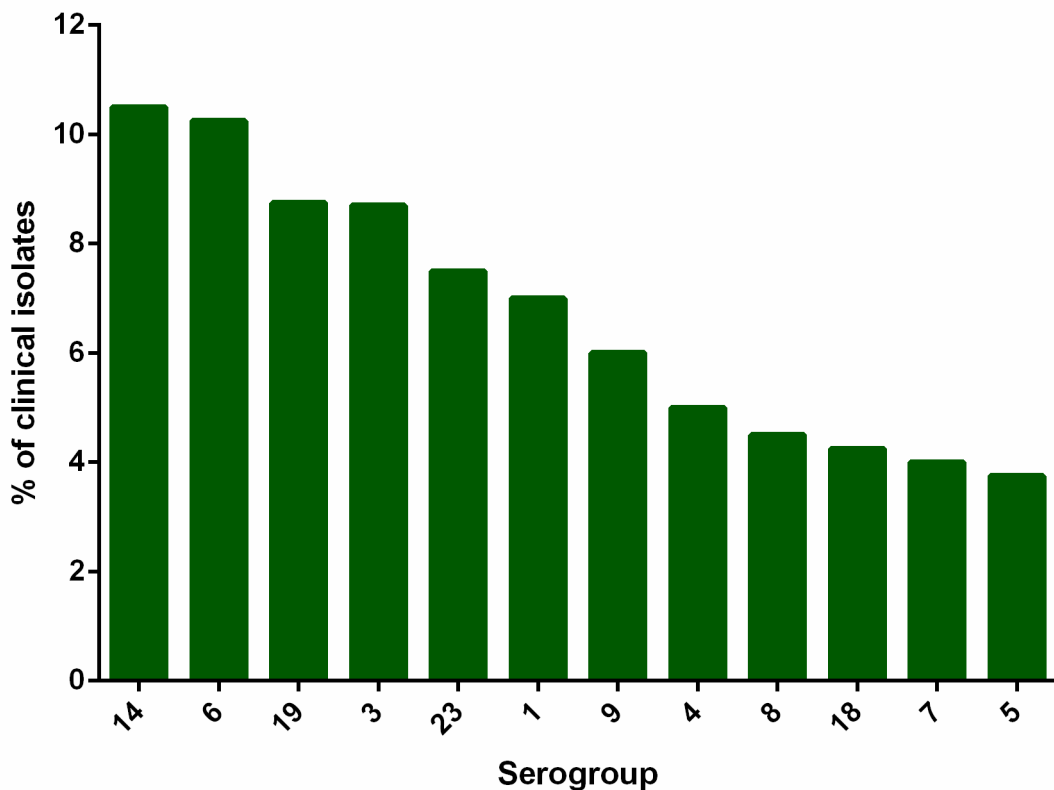


**Figure 5.1.** Serogroups most commonly associated with causing invasive pneumococcal disease. Figure adapted from Scott *et al.* [457].

**Table 5.1.** Structural diversity of *S. pneumoniae* capsular polysaccharide serotypes commonly associated with disease.

<b><i>S. pneumoniae</i></b> <b>serotype</b>	<b>Structure</b>	<b>Reference</b>
Type 1	→4)-α-GalA -(1→3)-α- GalA-(1→3)-α-6dGalNAc4N -(1→	[461]
Type 2	→4)-β-D-Glcp(1→3)-[α-D-GlcpA-(1→6)-α-D-Glcp-(1→2)]-α-L-Rhap-(1→3)-α-L-Rhap-(1→3)β-L-Rhap-(1→	[462]
Type 3	→3)-β-D-GlcA-(1→4)-β-D-Glcp(1→	[463]
Type 4	→3)-β-D-ManpNAc-(1→3)-α-L-FucpNAc-(1→3)-α-D-GalpNAc-(1→4)-α-D-Galp2,3(S)Py-(1→	[464]
Type 5	→4)-β-D-Glcp(1→4)-[α-L-PnepNAc-(1→2)-β-D-GlcpA-(1→3)]-α-L-FucpNAc-(1→3)-β-D-Sugp-(1→	[465]
Type 6B	→2)-α-D-Galp(1→3)-α-D-Glcp(1→3)-α-L-Rhap-(1→4)-D-Rib-ol-(5→P→	[466]
Type 9N	→4)-α-D-GlcpA-(1→3)-α-D-Glcp(1→3)-β-D-ManpNAc-(1→4)-β-D-Glcp(1→4)-α-D-GlcpNAc-(1→	[467]
Type 9V	→4)-α-D-GlcpA(2/3OAc)-(1→3)-α-D-Galp(1→3)-β-D-ManpNAc(4/6OAc)-(1→4)-β-D-Glcp(1→4)-α-D-Glcp(1→	[468]
Type 14	→4)-β-D-Glcp(1→6)-[β-D-Galp(1→4)]-β-D-GlcpNAc-(1→3)-β-D-Galp(1→	[469]
Type 18C	→4)-β-D-Glcp(1→4)-[α-D-Glcp(6OAc)(1→2)][Gro-(1→P→3)]-β-D-Galp(1→4)-α-D-Glcp(1→3)-β-L-Rhap(1→	[470]
Type 19F	→4)-β-D-ManpNAc-(1→4)-α-D-Glcp(1→2)-α-L-Rhap(1→P→	[471]
Type 23F	→4)-β-D-Glcp(1→4)-[α-L-Rhap(1→2)]-[Gro(2→P→3)]-β-D-Galp(1→4)-β-L-Rhap(1→	[472]

### 5.1.2 *Pneumococcal Vaccines*

A polysaccharide vaccine against pneumococcal infection has been available since 1983 which contains CPS from 23 different serotypes (PPV23; serotypes 1, 2, 3, 4, 5, 6B, 7F, 8, 9N, 9V, 10A, 11A, 12F, 14, 15B, 17F, 18C, 19F, 19A, 20, 22F, 23F and 33F) [451]. The serotypes chosen for this vaccine represent 85-90% of those that cause invasive pneumococcal infections [452]. The PPV23 vaccine modulates immunity by stimulating B cells in a T-independent manner, which in turn generates high titres of IgM [473]. The high avidity associated with IgM enhances opsonisation, phagocytosis and killing of *S. pneumoniae*. However, because the immune response is T-independent there is no immunological memory generated and serotype specific antibody levels decline substantially after 5-10 years [452]. Moreover, PPV23 is not effective in children under the age of two among whom 80% of invasive pneumococcal disease occurs [474]. The efficacy of PPV in adults over the age of 65 years also remains uncertain [475].

These shortcomings led to efforts to design a new and improved pneumococcal vaccine based on the strategy employed by the glycoconjugated Hib vaccine, which resulted in a reduction of infection rates by >90% after it was licensed in 1987 [476, 477]. To create a glycoconjugate vaccine against *S. pneumoniae*, diphtheria toxoid cross-reactive material 197 (CRM<sub>197</sub>) was used as a protein carrier to which CPS from thirteen different serotypes was coupled (serotypes 1, 3, 4, 6A, 6B, 7F, 9V, 14, 18C, 19A, 19F, 23F) [478]. Unlike some toxoid antigens which are heat inactivated, CRM<sub>197</sub> is a non-toxic mutant of the original diphtheria exotoxin having a single amino acid substitution from glycine to glutamate in position 52 [97]. This mutation renders the protein non-toxin but remains immunogenic. Conjugation of CPS onto CRM<sub>197</sub> results in T cell activation as APCs display peptides on either MHC I or MHC II molecules. By inducing a T-dependent immune response, B cells are able to undergo isotype switching and develop memory B and T cells. This tridecavalent glycoconjugate vaccine is currently manufactured by Pfizer under the brand name Prevnar 13® and is included in the UK childhood vaccination programme for all children under the age of two.

Since the introduction of pneumococcal vaccines, there has been a dramatic reduction in the global incidence of invasive pneumococcal disease [4, 5]. However, these vaccines have limitations and do not protect against all

pneumococcal serotypes. The inclusion of only a select number of CPS serotypes into vaccines has also had a profound effect on pneumococcal epidemiology. Whilst the incidence of invasive pneumococcal disease caused by vaccine serotypes has declined, the incidence of disease from non-vaccine serotypes is increasing [6, 10, 479]. This is likely to be a result of horizontal gene transfer which enables serotype shifts [6, 8]. There is also some evidence to suggest that the vaccines available do not confer good protection in individuals at the extremes of age (< 2 and > 60 years old), the immunocompromised or pregnant women [261, 480].

### 5.1.3 Objectives

The aim of this chapter is to investigate whether AuNPs could serve as delivery system for a glycoconjugate vaccine against pneumococcus to improve protection over current alternatives. Current pneumococcal vaccines contain several CPS serotypes to protect against those most associated with causing disease however this study will focus on just one, serotype 3. CPS serotype 3 is one of the most commonly associated with disease and was subsequently chosen to be included in both PPV23 and Prevnar 13 vaccines. It is also the simplest CPS serotype of those currently identified from *S. pneumoniae*, consisting of a repeating tetrasaccharide. CPS serotype 3 repeating unit is present in several other *S. pneumoniae* CPS serotypes and is cross-reactive with serotype 8 which is also associated with causing disease [481-483]. If successful with conjugating CPS serotype 3 onto AuNPs then it may be possible to apply this method to coupling other CPS serotypes for a polyvalent vaccine.

Several methods will be employed to aid the coupling of CPS onto protein carrier loaded AuNPs and characterised to ensure antigenicity is retained. The CPS glycoconjugate will then be tested in a mouse model to determine its protective efficacy against a lethal challenge of *S. pneumoniae* as well as measuring immunoglobulin responses to identify the immune responses evoked.

## 5.2 Materials and Methods

### *5.2.1 Coupling chemistry for CPS onto gold nanoparticles*

Thiol maleimide coupling was initially used to couple pneumococcal serotype 3 capsular polysaccharide (CPS; ATCC®) onto protein conjugated AuNPs using a similar approach to one previously mentioned. However, despite varying reagent conditions and increasing concentrations of EDC/NHS and EMCH this method was unsuccessfully for coupling CPS. A second approach using a cyanogen bromide derivative, 1-cyano-4-dimethylaminopyridine tetrafluoroborate (CDAP), was also used in an attempt to couple CPS onto AuNP conjugated proteins [11, 259]. CPS was solubilised in PBS at 10 mg/mL before adding 2.3 M CDAP in 0.1 M acetonitrile. After 30 seconds, 0.2 M triethylamine followed by amine coupled AuNPs. The reaction was left to incubate overnight at 4 °C before adding ethanolamine to quench the reaction. Conjugation with CDAP was unfavourable to AuNPs, often resulting in AuNP aggregation shown by a colour change to the reaction mixture and a skewed plasmon spectrum.

A reductive amination approach was also used to conjugate CPS onto AuNPs [254, 260, 261]. This was done by solubilising 1.6 mg CPS in 990  $\mu$ L PBS and adding 10  $\mu$ L 2 M NaBH<sub>4</sub> (in 0.1 M sodium bicarbonate) for 1 hour at room temperature before dialysing in ultrapure water overnight at 4 °C and lyophilising. The lyophilised product was dissolved at 2 mg/mL in PBS containing 4  $\mu$ M sodium *meta*-periodate in the dark at 23 °C for 90 minutes. Oxidation of the CPS was quenched by adding 100  $\mu$ L ethylene glycol solution. The oxidised CPS was dialysed in ultrapure water overnight at 4 °C and lyophilised. Oxidised CPS was solubilised to 1 mg/mL in 0.5 M sodium cyanoborohydride (in 0.1 M sodium bicarbonate), pH 8.1. AuNPs coupled with either TetHc or an aminated MHDA linker, prepared as previously described, were centrifuged at 1366 x g for 10 minutes and resuspended into the CPS, cyanoborohydride solution. The mixture was allowed to incubate at room temperature for 7 days with gentle agitation. Progress of conjugation was monitored by removing aliquots at various times points and measuring the absorption spectra for a spectral shift in  $\lambda_{\text{max}}$ . Once conjugation was complete, 50  $\mu$ L 2 M sodium borohydride (in 0.1 M sodium bicarbonate) was added for 1

hour at room temperature. The newly formed glycoconjugates were centrifuged and resuspended in PBS with 260  $\mu$ L 13 mg/mL alhydrogel.

As well as confirming conjugation using optical absorption, a western blot using a rabbit polyclonal antibody raised against TetHc and sera against CPS (Statens Serum Institut) was performed. Protein concentration was measured using a BCA assay whilst CPS concentration was content was measured by the previously described phenol-sulphuric acid assay, using the native CPS as a standard.

### 5.3 Results

#### *5.3.1 CPS conjugation*

Several methods were employed in an attempt to conjugate pneumococcal serotype 3 capsular polysaccharide (CPS) onto protein conjugated AuNPs. The first was using thiol maleimide coupling, as described in the previous chapter. However, despite varying reagent conditions and increasing concentrations of EDC/NHS and EMCH to generate a maleimide derivatised CPS, this method proved unsuccessful. Measurements of AuNP plasmon spectra after thiol maleimide coupling showed no change to the extinction and western blots were negative for CPS conjugation. A second method using a cyanogen bromide derivative, 1-cyano-4-dimethylaminopyridine tetrafluoroborate (CDAP), was also employed for conjugating CPS. Treatment of polysaccharides with CDAP results in random activation of hydroxyl groups to which a bifunctional linker can be attached [259]. The simplicity of this three-step reaction was appealing but is limited in its application for AuNP conjugation, resulting in aggregation of AuNPs as shown by a change in solution colour and the plasmon spectra, Figure 5.2. Reductive amination was another technique used, adapted from the methods of Laferrière *et al.* and Jennings [260, 261]. This involved generating an anomeric aldehyde at the reducing termini of CPS by reducing carboxyl groups to alditols prior to limited treatment with periodate, Figure 5.3. Using mild conditions, the degree of oxidation was limited to approximately 25% of carboxyl residues to avoid altering the conformation or antigenicity of the polysaccharide [12]. Protein coupled AuNPs were added to the newly formed aldehyde derivatives which underwent alkylimino-de-oxo-bisubstitution to form a reactive iminium cation. Sodium cyanoborohydride ( $\text{NaBH}_3\text{CN}$ ) was chosen to reduce the imine, which took approximately 7 days. Once conjugation was complete, sodium borohydride was added to reduce any remaining aldehyde groups and the conjugate purified using centrifugation and resuspended into PBS with 0.26% (w/v) alhydrogel. The mechanistic approach for reductive amination coupling is outlined in Figure 5.4.

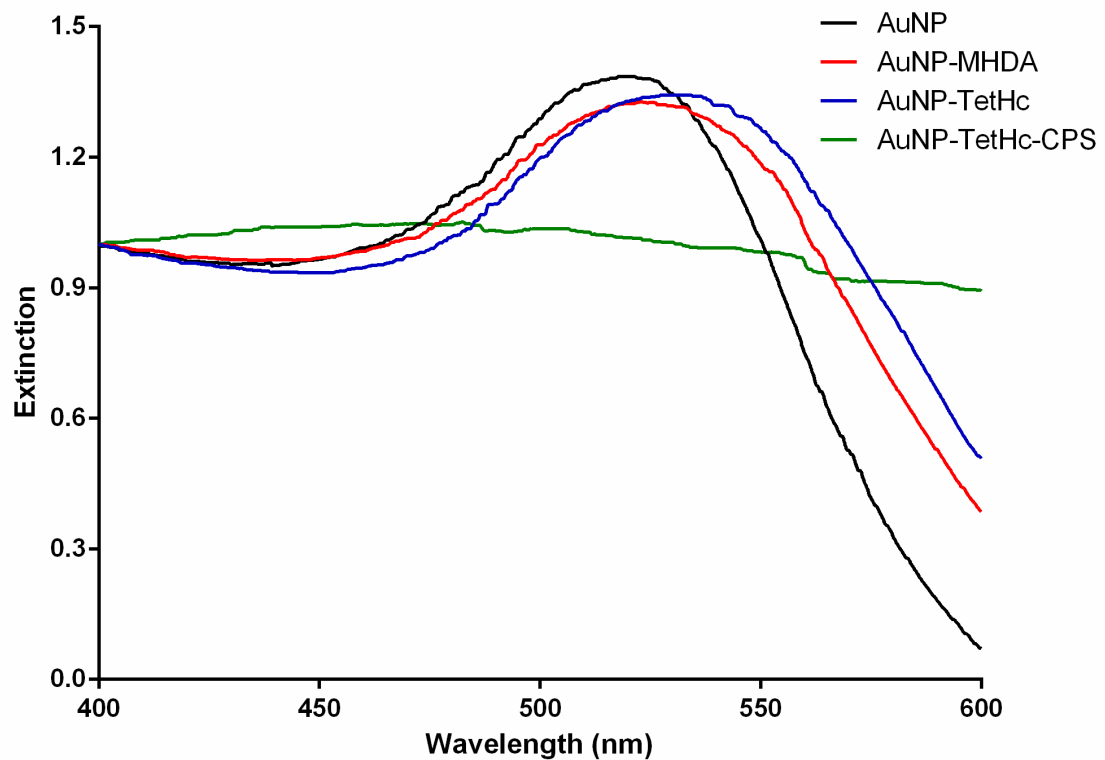


**Figure 5.2.** UV-visible absorption spectra for glycoconjugates using CDAP coupling chemistry. Displayed are AuNPs (black), AuNPs functionalised with MHDA (red), AuNPs functionalised with MHDA coupled with TetHc (blue) and AuNPs coupled with TetHc and *S. pneumoniae* serotype 3 CPS (green).

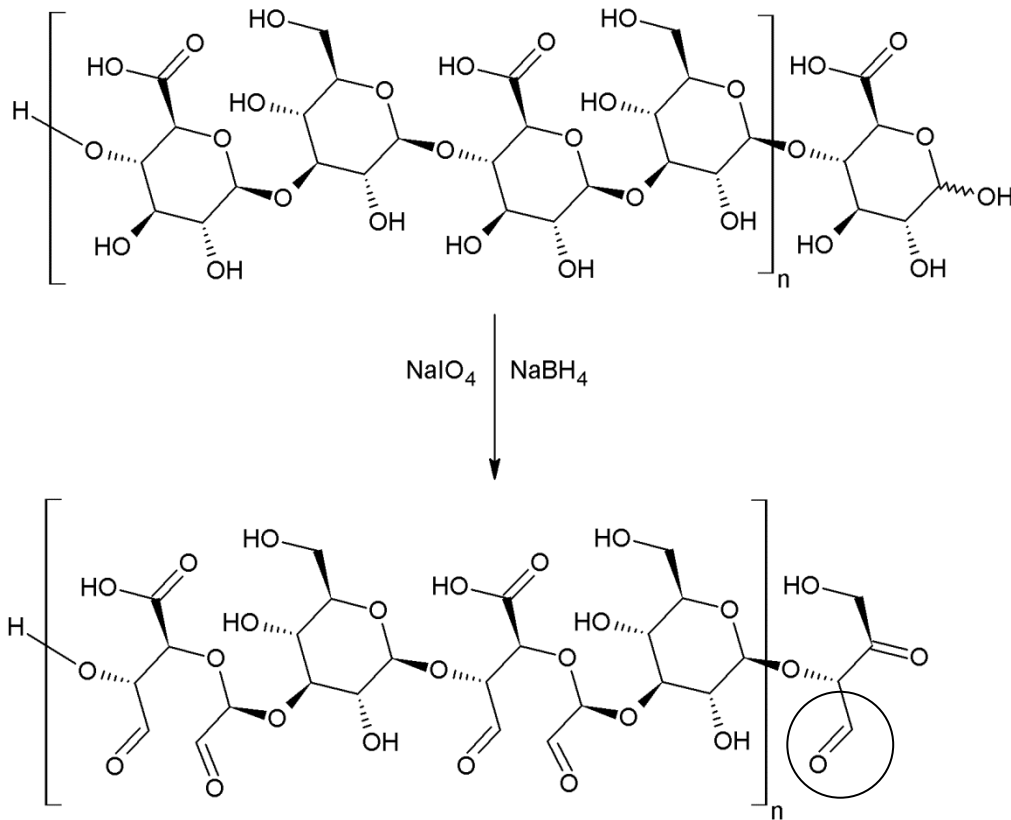


**Figure 5.3.** Skeletal structure of *S. pneumoniae* serotype 3 CPS illustrating the repeating glucuronic acid and glucose tetrasaccharide [ $\rightarrow 4$ ]- $\beta$ -D-GlcUA-(1 $\rightarrow$ 3)- $\beta$ -D-Glc-(1 $\rightarrow$ ]. The anomeric aldehyde for reacting with amines is circled

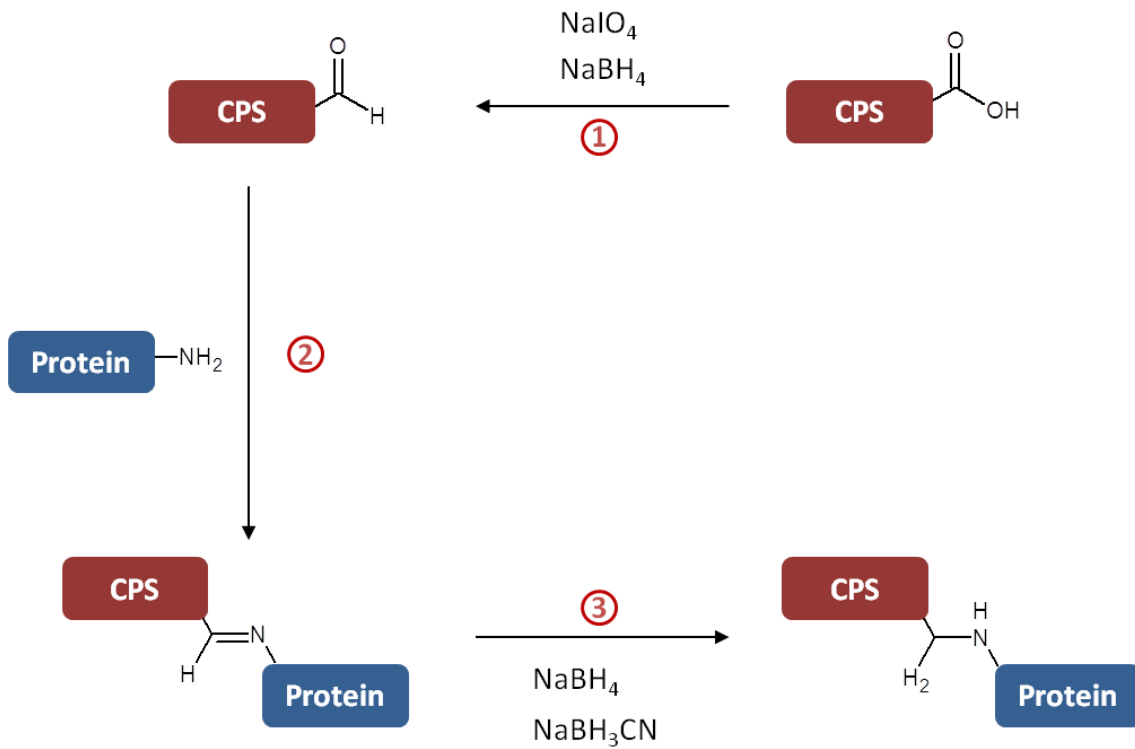


**Figure 5.4.** Reaction scheme of reductive amination between CPS and protein coupled AuNPs; (1) mild oxidation of carboxyl groups at the reducing end of CPS to aldehydes, (2) addition of AuNP-protein to form an iminium cation (secondary aldimine), (3) reduction of imine using cyanoborohydride to form a secondary amine.

### 5.3.2 Glycoconjugate characterisation

The progression of CPS coupling onto AuNPs was monitored by removing aliquots and measuring the optical extinction of AuNPs for a shift in  $\lambda_{\max}$ . Measurements were taken every other day until there was a plateau of readings for  $\lambda_{\max}$ , Figure 5.5. A red-shift in  $\lambda_{\max}$  of 20 nm from 532 nm for AuNP-TetHc to 552 nm indicates an overall increase in the mean diameter of AuNP conjugates as a result of CPS conjugation. This large shift in  $\lambda_{\max}$  is indicative of a large molecular weight molecule binding to the gold surface. The extinction peak is also much broader for AuNP-TetHc-CPS which suggests the size distribution of particles is much larger. This is likely to be due to variable lengths of the repeating tetrasaccharide unit on the particles, Figure 5.6.

Following conjugation of the antigens, the samples were examined by western blotting, Figure 5.7. The glycoconjugate was released from AuNPs using 11-mercapto-1-undecanol before it was separated using SDS-PAGE and transferred onto a nitrocellulose membrane. The membrane was incubated with a rabbit pAb specific to TetHc and rabbit antisera raised against *S. pneumoniae* serotype 3 CPS (Statens Serum Institut). Secondary antibodies raised against rabbit with a horseradish peroxidase conjugate were then added before the blot was visualised. Western blotting confirmed that the structural integrity/antigenicity of the CPS moieties remained intact following chemical activation and linkage to the protein carrier based upon their reactivity with the pAb. The gel also indicates CPS coupling to the TetHc protein carrier from the extended banding region of the conjugated CPS relative to the unconjugated control.

A phenol-sulphuric acid assay was used to determine the concentration of CPS present in glycoconjugates. Using concentrated sulphuric acid, CPS was hydrolysed and dehydrated into monomeric furfural molecules which then formed a chromagen upon addition of phenol [427]. This method allows for a reliable and sensitive determination of polysaccharides down to 1 nmol, with a linear relationship between absorbance and concentration up to 150 nmol [263]. Using this assay, the amount of CPS measured was determined to be 100  $\mu\text{g}/\text{mL}$ .

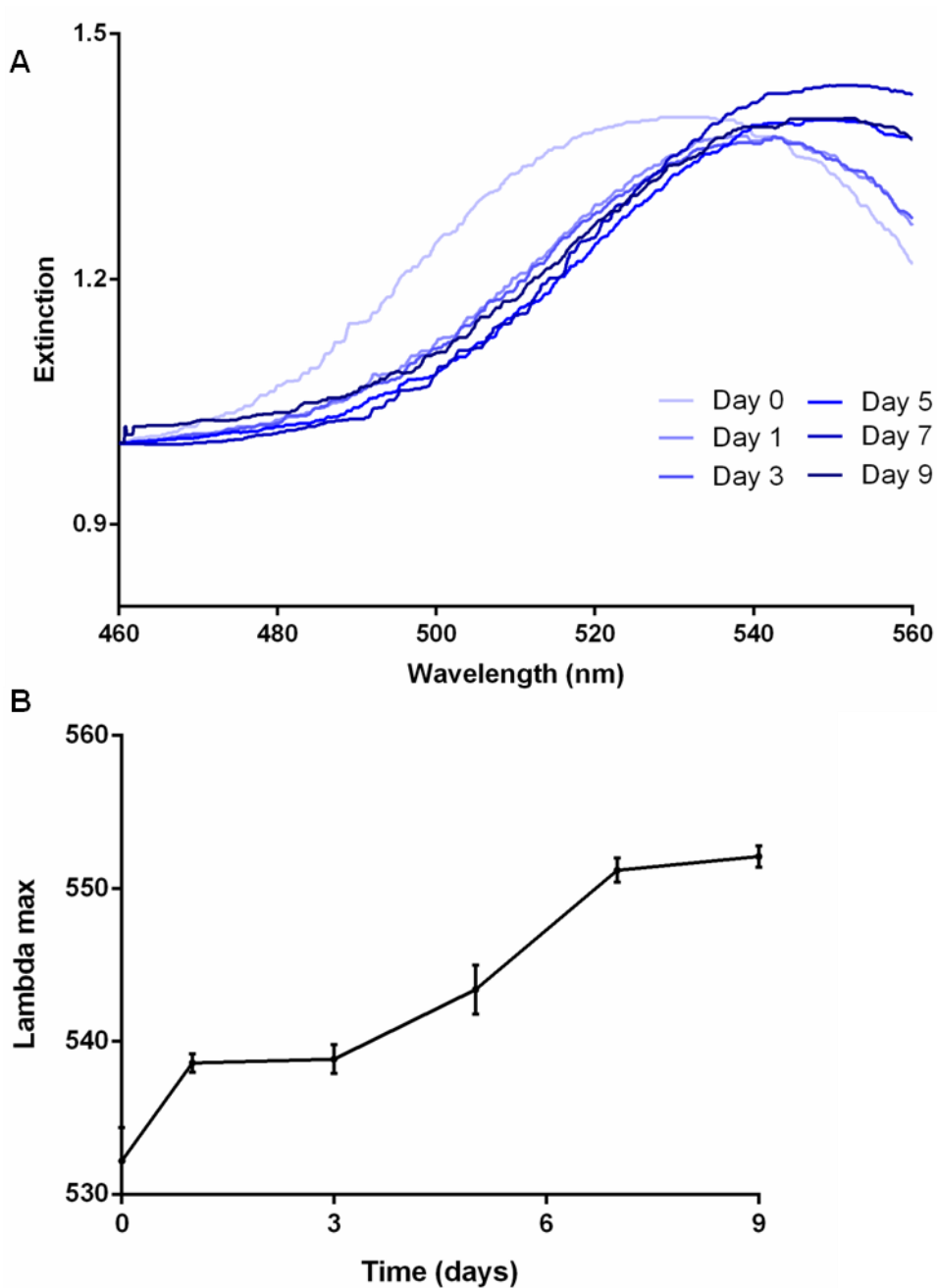


**Figure 5.5.** Progressive UV-visible absorption spectra for CPS coupling to AuNP-TetHc over 9 days; Plasmon spectra of aliquots undergoing reductive amination at days 1, 3, 5, 7 and 10 (A), maximum extinction ( $\lambda_{max}$ ) from spectra measured during the time course (B).

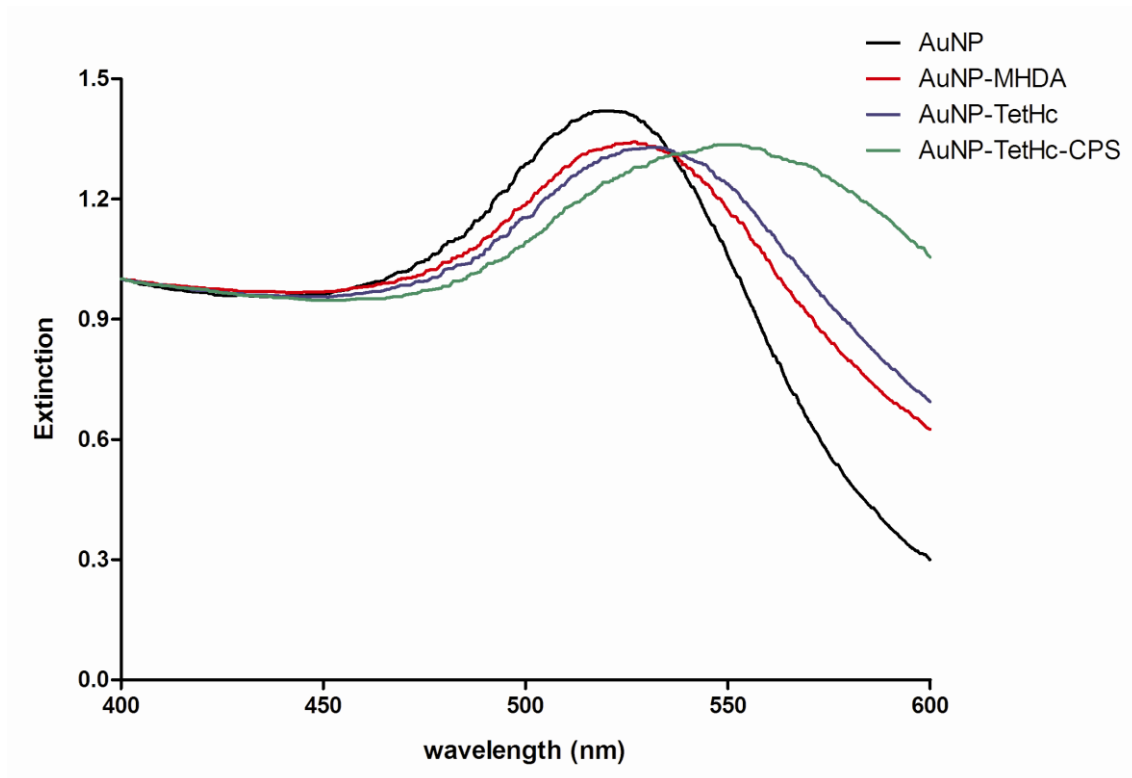


**Figure 5.6.** UV-visible absorption spectra for glycoconjugates using reductive amination coupling chemistry. Displayed are AuNPs (black), AuNPs functionalised with MHDA (red), AuNPs functionalised with MHDA coupled with TetHc (blue) and AuNPs coupled with TetHc and *S. pneumoniae* serotype 3 CPS (green).

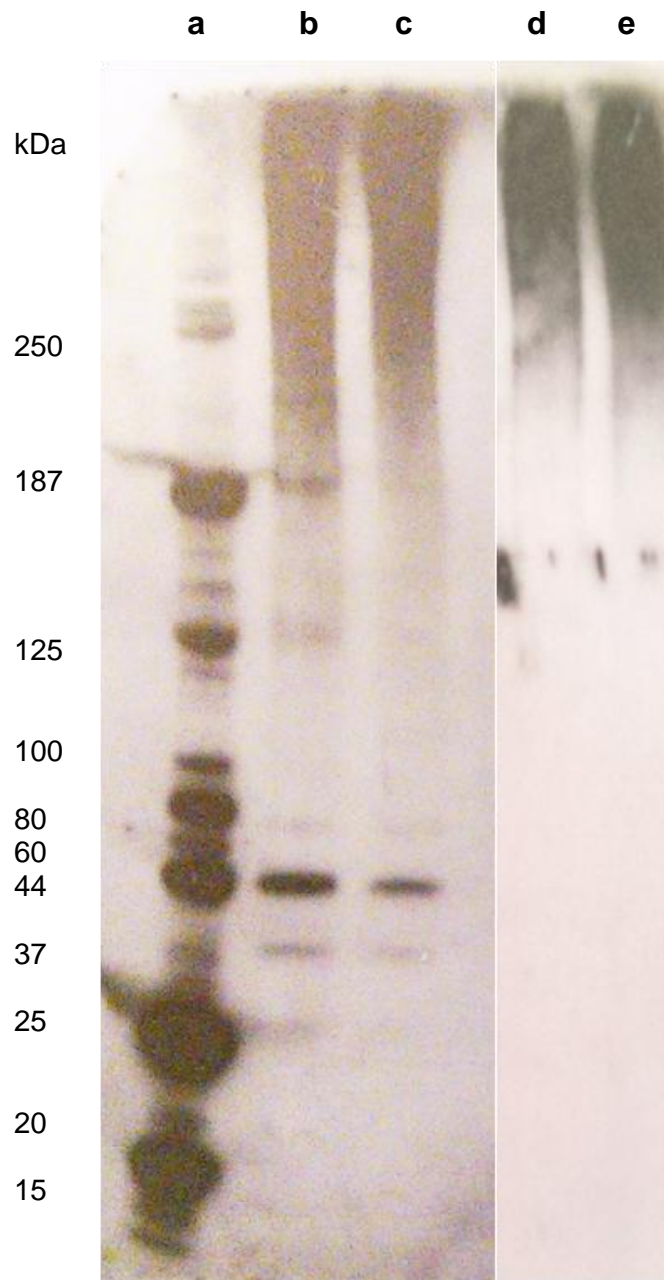


**Figure 5.7.** Western blot of AuNP-TetHc-CPS separated using a NuPAGE 4-12% Bis-Tris gel; LiCor protein marker (a), AuNP-TetHc-CPS treated with 11-mercapto-1-undecanol (b and c), 1 µg CPS (d and e). A rabbit pAb against Hc and rabbit antisera against CPS serotype 3 were used to bind TetHc and CPS, respectively. Goat anti-rabbit HRP conjugated secondary antibodies were used to detect primary antibody binding.

### 5.3.3 Immunoglobulin response

An immunisation and protection study was designed alongside colleagues at Glasgow University to test the protection of nano-glycoconjugate vaccines against a *S. pneumoniae* inhalation challenge. Immunisations were carried out at Glasgow University in MF1 mice with a 100  $\mu$ L priming dose followed by two booster immunisations at the same volume using Pevnar13, AuNP-TetHc, AuNP-CPS or AuNP-TetHc-CPS with an aluminium hydroxide adjuvant (alhydrogel). In a 100  $\mu$ L dose, Pevnar 13 contains 0.44  $\mu$ g of each CPS serotype (except serotype 6B which is 0.88  $\mu$ g) [480]. Therefore a similar dose of 0.5  $\mu$ g serotype 3 CPS was used for the nano-glycoconjugate immunised mice. Five weeks post immunisation 100  $\mu$ L of blood was taken from the tail vein of each mouse and shipped to Exeter where antibody isotypes and IgG specific subclasses were measured using an ELISA.

Total IgG concentrations showed that average IgG titres were higher in mice immunised with either AuNP-TetHc-CPS or Pevnar 13 and lowest for AuNP-CPS immunised mice. However, there was no statistically significant difference in IgG concentration between any of the immunised groups. An IgG concentration of approximately 200  $\mu$ g/mL was measured from sera taken from each group, Figure 5.8. CPS-specific IgG concentrations were also measured and indicated that mice immunised with AuNP-TetHc-CPS exhibited significantly higher anti-CPS IgG titres than those immunised without a protein carrier (AuNP-CPS;  $p < 0.05$ ). Moreover, despite the mice being immunised with the same concentration of CPS serotype 3 there was a significantly higher concentration of anti-CPS IgG from mice immunised with AuNP-TetHc-CPS rather than Pevnar 13 ( $p < 0.001$ ). The amount of anti-CPS IgG generated from AuNP-CPS was also significantly higher than Pevnar 13 ( $p < 0.001$ ), Figure 5.8.

Since CPS is a T-independent antigen, IgM responses were also measured. The highest IgM concentration generated was found in mice immunised with Pevnar 13, which was significantly higher than AuNP-TetHc-CPS ( $p < 0.01$ ). There was no other significant difference in IgM concentration between any of the other immunisation groups, Figure 5.10.

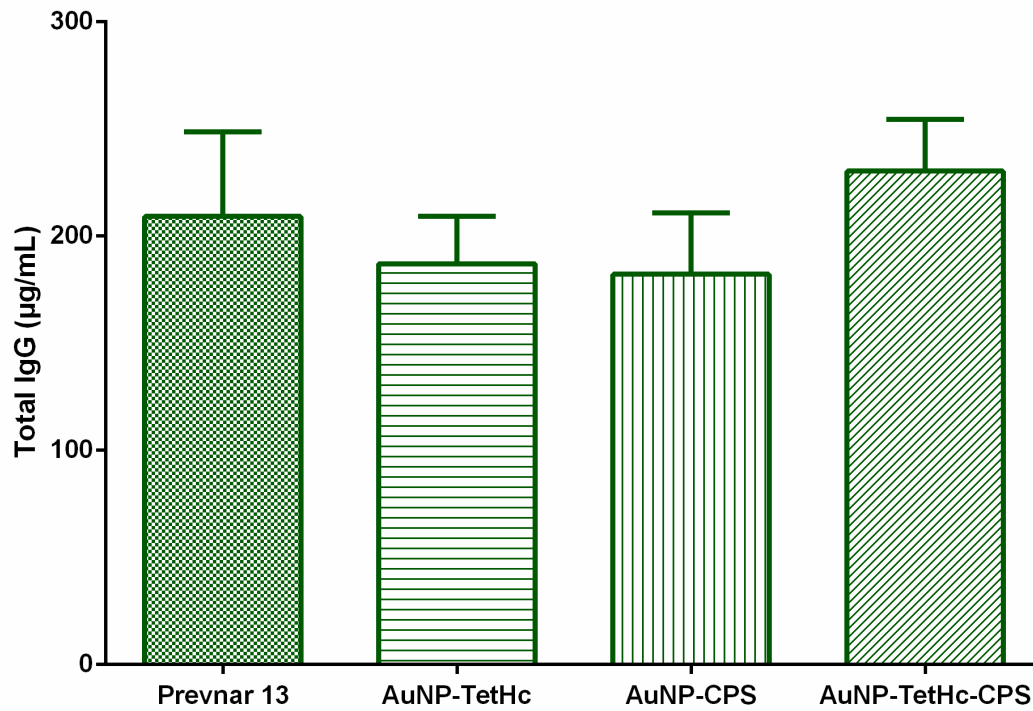


**Figure 5.8.** Total IgG concentration in sera collected from six mice, five weeks post immunisation with the antigen indicated and determined using quantitative ELISA. Error bars are calculated using the standard error of the mean.

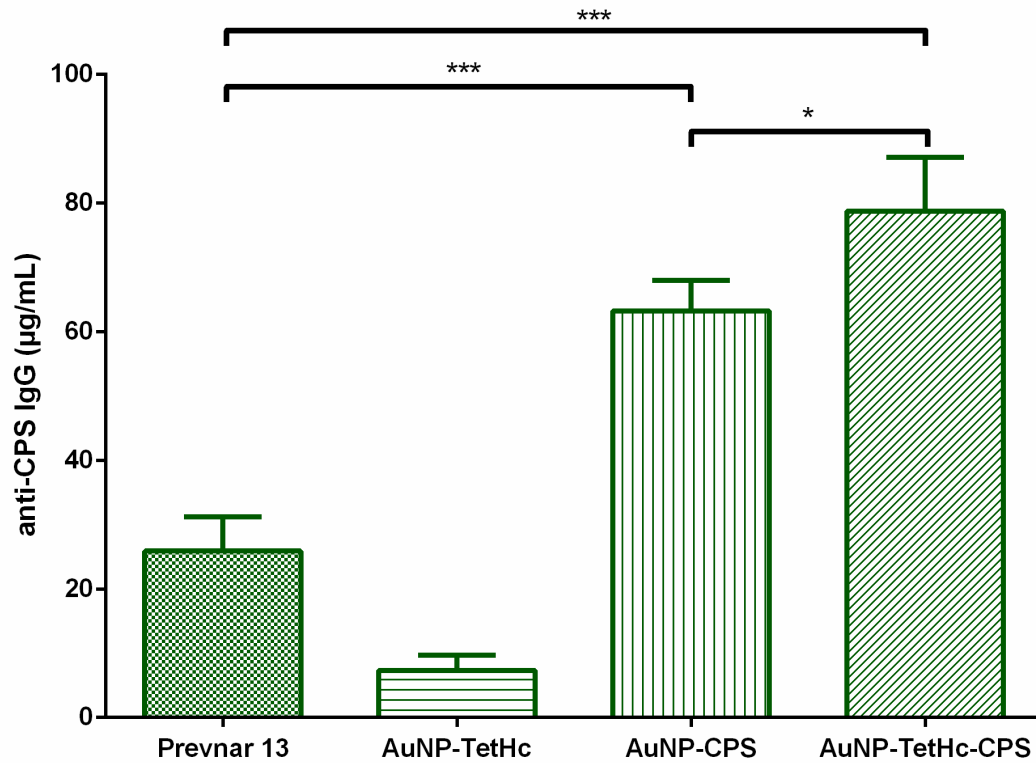


**Figure 5.9.** CPS-specific IgG concentration in sera collected from six mice, five weeks post immunisation with the antigen indicated and determined using quantitative ELISA. Error bars are calculated using the standard error of the mean. \*  $p < 0.05$ , \*\*\*  $p < 0.001$

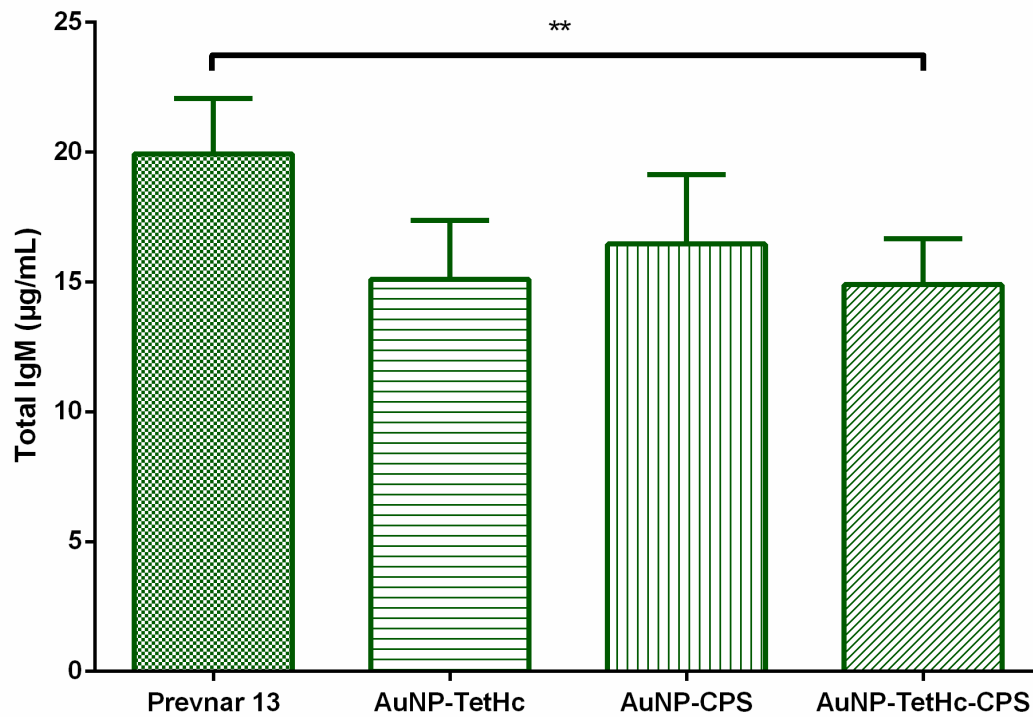


**Figure 5.10.** Total IgM concentration in sera collected from six mice, five weeks post immunisation with the antigen indicated and determined using quantitative ELISA. Error bars represent the standard error of the mean; asterisks indicate significant differences ( $p < 0.01$ )

IgG subclasses IgG1 and IgG2a were measured as an indicator of Th2 or Th1 immune responses, respectively. This identified Prevnar 13 as inducing a predominant IgG1 response, relative to IgG2a, making up a large proportion of total IgG ( $p < 0.01$ ). Mice immunised with AuNP-TetHc-CPS however generated a predominant IgG2a response, with a relatively low IgG1 concentration ( $p < 0.01$ ). The IgG2a concentration generated by AuNP-TetHc-CPS immunised mice was significantly higher than any other group ( $p < 0.01$ ). Subclass switching from IgG1 to IgG2a was also evident in AuNP-CPS immunised mice ( $p < 0.05$ ) whilst those receiving AuNP-TetHc had an equal concentration of IgG1 and IgG2a, Figure 5.11. Further clarification of IgG subclass switching is illustrated in Figure 5.12 which shows a ratio of IgG1 in relation to IgG2a.

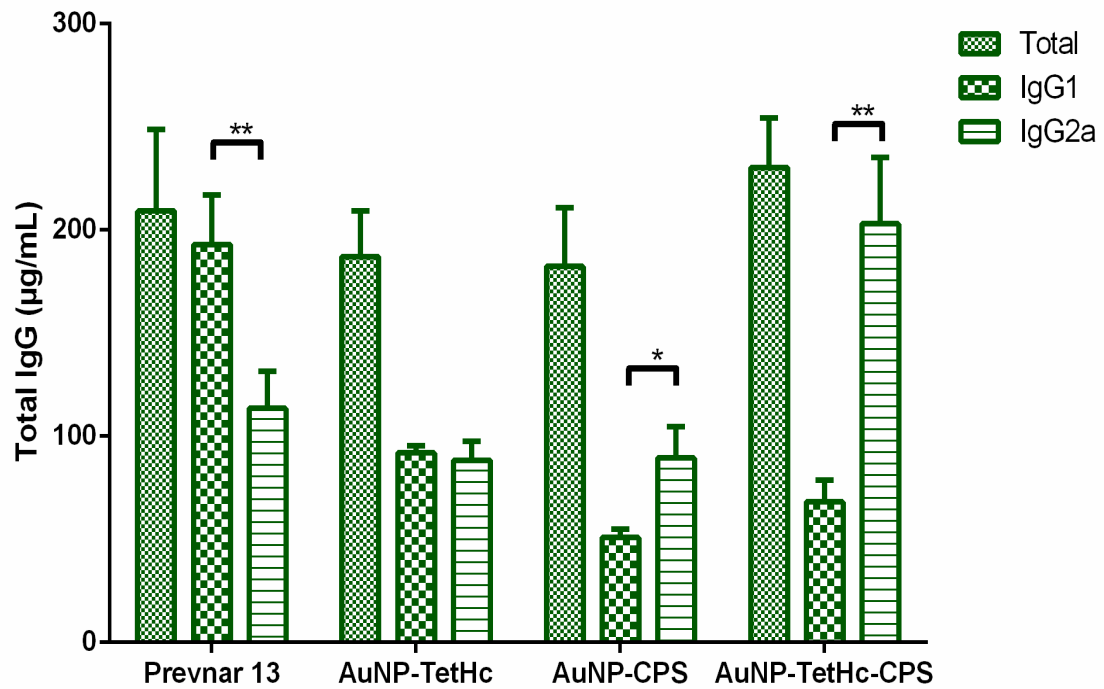


**Figure 5.11.** Total IgG and IgG subclass concentration in sera collected from groups of six mice, five weeks post immunisation with the antigen indicated and determined using quantitative ELISA. Error bars are calculated using the standard error of the mean. \*  $p < 0.05$ , \*\*  $p < 0.01$

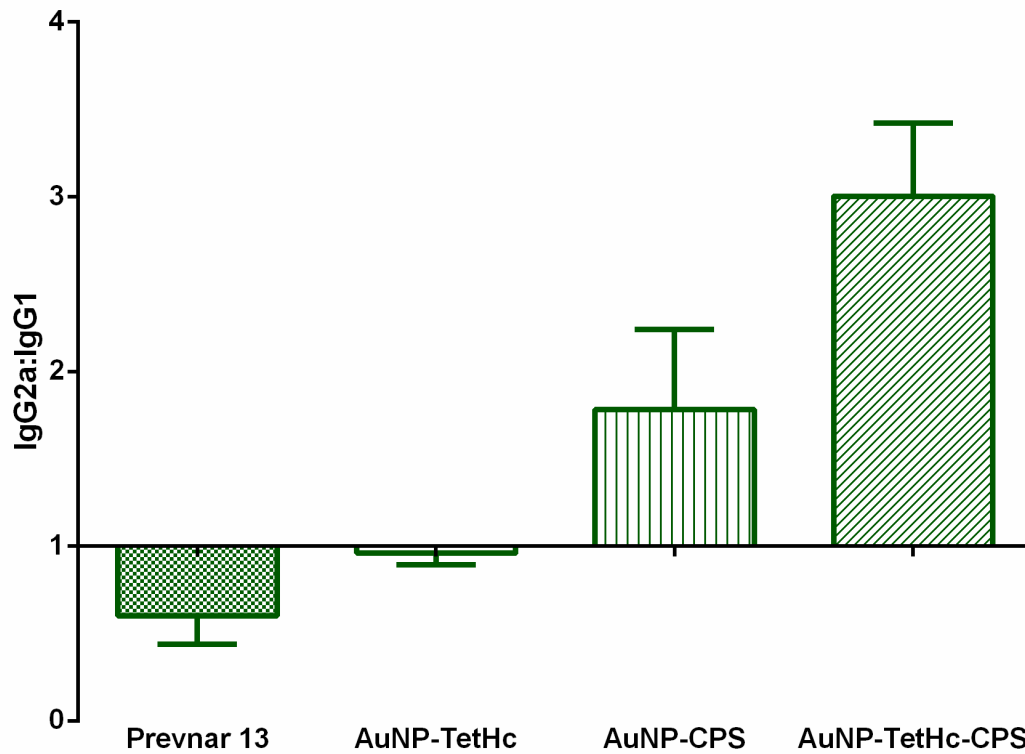


**Figure 5.12.** Relative concentrations of IgG1 and IgG2a in sera from MF1 mice after immunisation with the antigens indicated. Figure presented as a ratio of IgG2a:IgG1. Each point is the mean of values from five mice. Error bars are calculated using the standard error of the mean.

#### 5.3.4 Protection study

Four weeks after the final immunisation boost of nano-glycoconjugates, MF1 mice were challenged IN with  $2.5 \times 10^5$  CFU  $50 \mu\text{L}^{-1}$  *S. pneumoniae* Xen10; a bioluminescent version of the parent strain A66.1 serotype 3. Using this strain enabled unaltered *in vivo* imaging of the disease as it progressed through the mice, Figure 5.10. Mice were imaged every 24 hours and scored according to the degree of luminescence. Within 48 hours post infection (hpi) signs of the disease were evident in PBS mice, with the lungs being the area of greatest colonisation. As the time course continued to 72 hpi, the degree of infection relative to the bioluminescence in PBS mice is greater and the number of animals showing signs is higher. There is also a lung infection in one of the AuNP-TetHc immunised mice. Eight days post infection and colonisation of the nasopharynx is evident in one of the mice immunised with Prevnar 13. Infection was only ever apparent in either the lungs or nasopharynx of the mice. Any mouse which showed signs of colonisation eventually succumb to infection, appendix 3.

The experiment was terminated after 10 days, and the survivability of each immunisation group recorded, Figure 5.11. The only group with 100% survival were those immunised with AuNP-TetHc-CPS. Both AuNP-CPS and Prevnar 13 immunised mice had 83% survival whilst the AuNP-TetHc had 67% survival. There was however no significant difference in mean survival between any of the test groups. A survival rate of 16% was afforded in PBS mice which was a statistically significant difference between these mice and the three test groups ( $p < 0.01$ ).

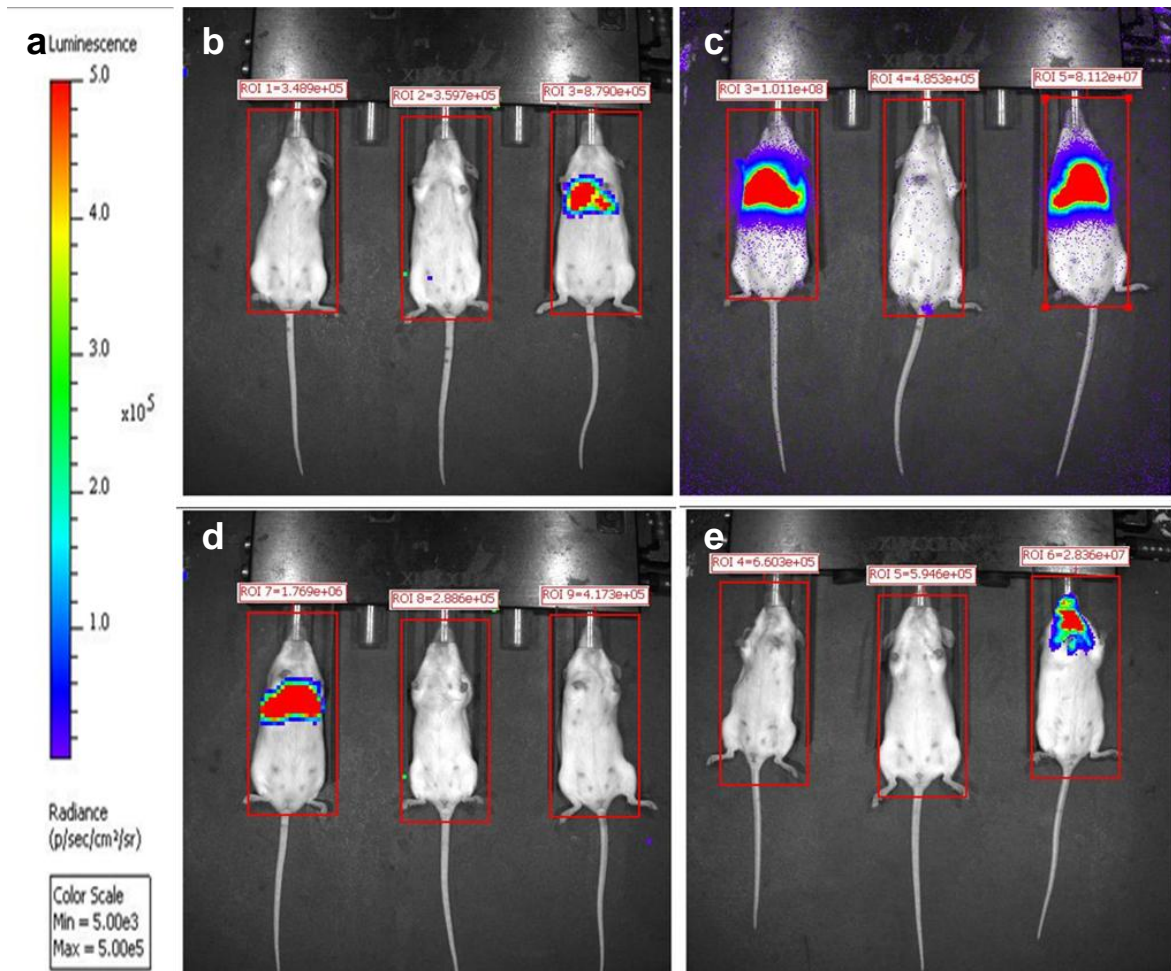


**Figure 5.13.** *In vivo* imaging using FxPro imaging of MF1 mice challenged IN with  $2.5 \times 10^5$  CFU  $50 \mu\text{L}^{-1}$  *S. pneumoniae* Xen10 four weeks post SC immunisation; Luminescence scale in radiance (p/sec/cm<sup>2</sup>/sr) (a), PBS immunised mice 48 hpi (b), PBS immunised mice 72 hpi (c), AuNP-TetHc immunised mice 72 hpi (d), Prevnar 13 immunised mice 8 days pi (e).

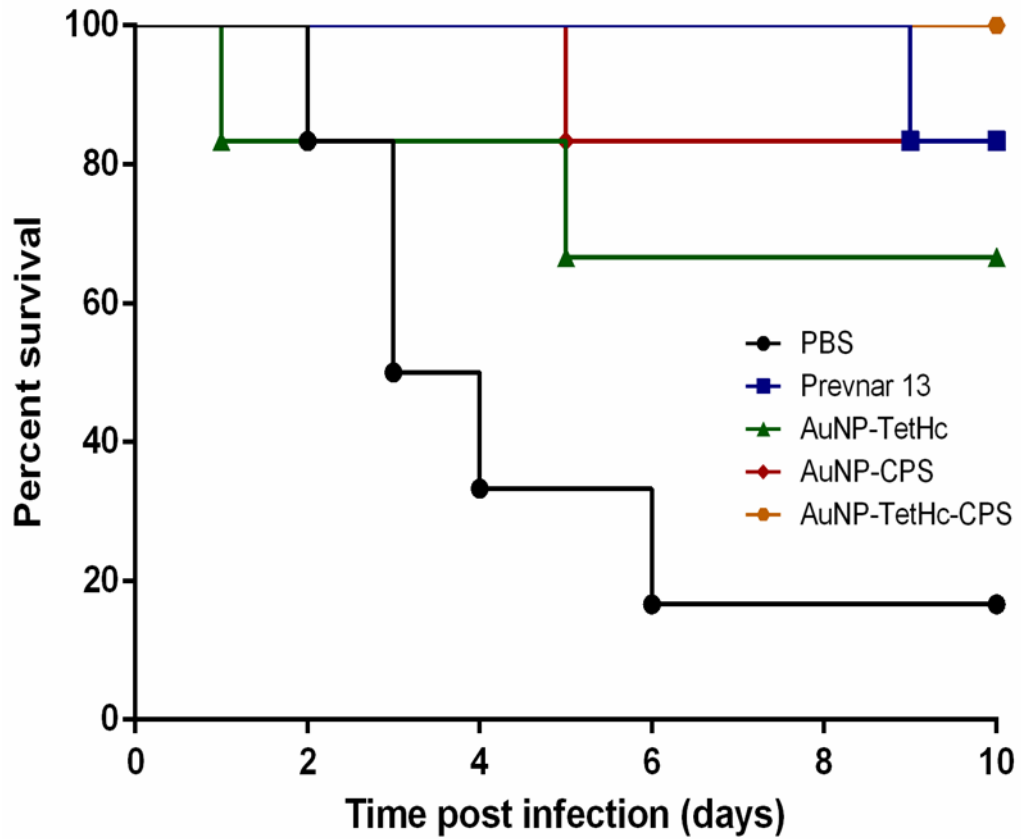


**Figure 5.14.** Survival curve for MF1 mice challenged IN with  $2.5 \times 10^5$  CFU  $50 \mu\text{L}^{-1}$  *S. pneumoniae* Xen10 four weeks post SC immunisation.

## 5.4 Discussion

### *5.4.1 CPS conjugation*

Thiol maleimide, CDAP and reductive amination coupling chemistries were employed for conjugating pneumococcal CPS serotype 3 onto a TetHc protein carrier on AuNPs. Of these methods, reductive amination was the most successful and was chosen for further optimisation. Whilst the conditions required for reductive amination can create a harsh environment for the antigens concerned, steps were taken to avoid this wherever possible. Firstly, the formation of aldehyde groups at the reducing termini of CPS was facilitated by mild periodate oxidation rather than peroxide which can reduce the immunogenicity of antigens [484]. Sodium cyanoborohydride was chosen as the primary reducing agent since, unlike sodium borohydride, it reduces only Schiff bases without modifying other chemical groups in the sample [485]. Finally, the reaction was carried out in sodium bicarbonate rather than sodium hydroxide, which is a weaker nucleophile and results in a slower reaction time but is less likely to create any by-products by reacting with any residues which are sensitive to strong bases [486]. Moreover, reductive amination coupling has several advantages over other coupling techniques used such as the direct formation of neoglycoconjugates rather than using CDAP which creates cross-linked network conjugates [487].

UV/Vis spectroscopy analyses indicated that CPS had covalently linked to TetHc. The extinction peak was also much broader for AuNP-TetHc-CPS suggesting the size distribution of particles is much broader, likely to be due to variable lengths of the repeating tetrasaccharide unit on the particles. SDS-PAGE and western blotting confirmed that not only was the structural integrity of the antigens intact, based on their reactivity with specific antibodies, but also the conjugation of CPS which displayed a lower molecular weight banding pattern to the unconjugated control. This may be the result of selection from the coupling chemistry favouring shorter tetrasaccharide repeats or a result of the highly charged polysaccharide moving atypically through the gel after protein attachment.

#### 5.4.2 Immunoglobulin response

Polysaccharide antigens are weak immunogens unable to elicit T-independent immune response. However, conjugation to a protein carrier recruits Th cells which boost the antigen-specific immune response, stimulate isotype switching and evoke immunological memory [62, 488]. This was demonstrated by immunising MF1 mice with AuNP-TetHc-CPS, AuNP-CPS, AuNP-TetHc or Pevnar 13 and measuring the immunoglobulin responses. Analysis of the resulting serum samples indicated that mice immunised with the glycoconjugate generated a significantly higher concentration of anti-CPS IgG than those immunised with AuNP-CPS. Nano-glycoconjugate immunised mice also exhibited significantly higher IgG2a titres (2-fold) as a result of isotype switching.

The currently licensed glycoconjugate vaccine against pneumococcus, Pevnar 13, was used to evaluate the efficacy of coupling a glycoconjugate onto AuNPs. Despite mice being immunised with the same concentration of CPS serotype 3, mice immunised with AuNP coupled glycoconjugate induced a significantly higher concentration of anti-CPS IgG ( $p < 0.001$ ). Stimulation of isotype switching was also more evident in AuNP-TetHc-CPS immunised mice which generated a lower IgM titre and a dominant IgG2a response. In mice, the production of the IgG2a antibody isotype is widely recognised as characteristic of a Th1 response, which is required for the generation of Tm [389]. Greater stimulation of a Th1 immune response could mean an improved immunological memory over Pevnar 13, resulting in fewer booster shots required for protective immunity, which currently stands at 4 [489]. These results show that the delivery of glycoconjugates by gold nanoparticles can significantly improve the T-dependent immune response generated by the vaccine, suggesting the potential for improved long-term immunity.

#### 5.4.3 Protection study

The efficacy of nano-glycoconjugated vaccines against pneumococcus was tested by challenging mice with a bioluminescent variant of *S. pneumoniae* A66.1 serotype 3, named Xen10 [490]. Once the experiment had been terminated after 10 days, AuNP-TetHc-CPS immunised mice had the highest degree of survival at 100% which, despite being significantly different to AuNP-TetHc immunised mice, showed no difference to any other immunised group.

Moreover, there was a high degree of protection afforded by the negative control, AuNP-TetHc immunised mice, which may be due to the triggering of an innate immune response. To overcome this, the time between final immunisation and challenge should be extended in future studies. In addition, future studies will need to evaluate the ability of gold nanoparticles to improve the protective ability of glycoconjugates based on additional CPS serotypes including but not limited to those covered by the Prevnar 13 vaccine currently on the market to determine if this technology can be more generally applied with similarly positive results.

#### 5.4.4 Conclusions

Covalent coupling of CPS onto AuNP conjugated proteins was successfully achieved using reductive amination chemistry and characterised using measuring plasmon shifts and western blotting.

Coupling CPS onto a TetHc protein carrier resulted in a greater CPS-specific IgG immune response and IgG2a titre.

Coupling a pneumococcal glycoconjugate vaccine onto AuNPs resulted in a dominant Th1 immune response characterised by an IgG2a dominant titre, suggesting an improved T-dependent immune response capable of long term protection.

These results suggest that the gold nanoparticle delivery technique can be applied to improve the glycoconjugate vaccine currently available to protect against *S. pneumoniae* infections.

## Chapter 6: Discussion and Future Work

---

### 6.1 Discussion

The overall goal of this project was to identify a suitable NP composite for use as a vaccine delivery system and explore some of the chemistries available to conjugate antigens onto NPs. Once antigens were successfully coupled onto AuNPs the further aim was to test the efficacy of this newly designed antigen delivery system for use in glycoconjugate vaccines against a number of biologically important human pathogens including *Y. pestis*, *B. mallei* and *S. pneumoniae*.

From the extensive choice of NP materials to choose from non-degradable NPs were selected for surface presentation of antigens. Recent developments in inorganic chemistry have allowed the fabrication of well-dispersed metal NPs of various compositions for exploiting as promising candidates in biomedical applications. Among them are AuNPs, which have been appraised for their excellent biocompatibility and low cytotoxicity [308]. AuNPs have been used in humans since the 1950's, which suggests that future licensing of a NP vaccine might be easier if it were made from gold [491]. In this study, AuNPs were chosen because they can be synthesised to a variety of sizes and shapes which can be manipulated by varying the conditions used to reduce gold (III). Of the methods used to generate AuNPs, citrate reduction was determined to be the optimal method, generating spherical particles which were near monodisperse. The spherical shape afforded by this technique is has been demonstrated as an important feature for increased uptake into dendritic cells, a key component of the adaptive immune response [492, 493]. Moreover, clearance of nanospheres in rodents after immunisation is much greater than for nano-filaments (10-fold) which may be important in reduced toxicity [492]. The monodisperse population of particles generated is thought to be important for consistent antigen loading and epitope density on the NP surface. We believe this consistent antigen delivery will allow us to reproducibly produce homogenous vaccines suitable for reliably determining the protective ability of vaccine candidates.

Another advantage of using AuNPs is the unique optical properties offered by gold due to LSPR. This was manipulated to characterise the surface of AuNPs based on the localised plasmon penetration depth which is limited to 90 nm and is therefore exclusive of the surrounding media [279]. These properties enabled the measurement of substances bound to the nanoparticle surface to characterise surface modifications in a label-free manner, something which is unrealistic for other NP composites. Moreover, the gold composition of NPs used in this study enables surface functionalisation with thiol containing compounds, which have a high affinity for gold (approximately  $200 \text{ kJ mol}^{-1}$ ) [494]. As such, the use of MHDA as a bi-functional linker for antigen coupling readily forms a self-assembled monolayer on the AuNP surface [495].

Having established that AuNPs were a suitable scaffold for vaccine design, we next sought to test the ability of these NPs to be conjugated with protein antigens. Proteins were selected based on their ability to induce a strong immune response (TetHc) or use as subunit vaccine candidates (F1, Hcp1 and FliC) in previous studies. All four proteins were successfully coupled to AuNPs. Of these, F1 coupled AuNPs were chosen for immunising BALB/c mice in preliminary experiments to test the effects of AuNPs on inducing an IgG response because F1 has previously been demonstrated to provide significant protection as a subunit vaccine against a lethal challenge of *Y. pestis* [340]. These immunisation experiments showed that AuNP coupled F1 induced an elevated and prolonged IgG response compared to the protein alone, suggesting that this delivery method has the potential to improve existing vaccine candidates. One explanation for this could be due to the size and shape of the nanoparticles being conducive to repetitive antigen presentation, which is known to lead to an efficient cross-linking of B cell receptors [496, 497]. In turn, B cell cross-linking gives rise to a more sustained production of antibodies; a phenomenon commonly associated with B cell recognition of viral proteins. Alternatively this elevated antibody production could be due to an increased uptake of F1 antigen into dendritic cells.

Protein subunit vaccines have long been investigated for their protective ability, and our data suggests that conjugation to AuNPs could improve their effectiveness. However, these vaccines have had limited success in achieving full protection. In contrast, conjugating a protein antigen to polysaccharides has proved to be a much more successful strategy. For example, Hib,

meningococcal type C and *S. pneumoniae* vaccines. One of the reasons for their success is polysaccharides are known to be one of the most immunogenic bacterial antigens when delivered to mammalian cells but are generally not recognised by T cells and therefore induce a T-independent immune response. One of the biggest problems with glycoconjugate formation is the use of toxic reagents and inefficient yield of resulting glycoconjugates. Thus, the next step in this study was to test whether AuNPs could be used to deliver a glycoconjugate vaccine consisting of previously identified vaccine candidates. The first glycoconjugate designed in this study was against *B. mallei* using LPS coupled to protein antigens previously characterised as binding to AuNPs. One of the reasons for targeting this organism for vaccine development was based on other studies suggesting that a vaccine capable of inducing a T-dependent immune response is likely to be required for protection against glanders and melioidosis [498, 499]. Previously, this was achieved through co-immunising LPS with a covalently linked protein carrier [429, 439, 485]. In doing so, it is believed that the protein carrier elicits T cell help for B cells recognising the O-antigen [500]. Whilst these studies have proven that immunoglobulin isotype switching does occur to a more favourable T-dependent response with glycoconjugate vaccines, there has not yet been any challenge studies to test the protective capabilities of these vaccines. However, Brett and Woods were able to show that immunising rabbits with LPS O-antigen conjugated to flagellin proteins elicited a high IgG titre which was capable of protecting diabetic rats from a *B. pseudomallei* challenge [429]. Glycoconjugation using *B. thailandensis* LPS onto protein carrier-AuNPs was performed using thiol-maleimide coupling. One of the advantages of using this chemistry was the preservation of the O-antigen which remained unaltered by the coupling method. Moreover, the adjuvant lipid A is also presented on the surface which is able to stimulate an innate immune response through its activation of TLR 2 and TLR 4 [501]. Whilst the presence of lipid A might prove useful in these preliminary studies for increasing the immune response, further developments may require cleavage of the lipid A due to its endotoxicity [502]. The promising data gained from this study using *B. thailandensis* LPS glycoconjugate coupled to AuNPs is reflected by its approval to be tested in a macaque model of infection for further investigation.

Some of the most compelling data for NP use in vaccine delivery came from the glycoconjugate vaccine developed against *S. pneumoniae* in this study. Using the same coupling chemistry as the one used to synthesise Prevnar 13, we were able to show elevated antigen-specific IgG titres for CPS conjugated AuNPs in comparison to a currently available pneumococcal vaccine [503]. This was true not only of glycoconjugated CPS on AuNPs but also without a protein carrier to recruit T cell involvement. Glycoconjugated AuNPs were able to generate a significantly higher titre of IgG2a, and ratio to IgG1, compared with Prevnar 13. This suggests a role for AuNPs in inducing immunoglobulin subclass switching which is a key feature of glycoconjugate vaccines and is essential for generating higher avidity antibodies and immunological memory [504].

To determine how AuNPs were able to induce their adjuvant effect, some preliminary studies were performed to look into the mechanisms which regulate their uptake into macrophage cells. Transmission electron microscopy (TEM) was used to identify whether AuNPs were taken up by phagocytic cells and if they could be imaged. After one hour incubation with AuNPs, J774A.1 macrophages were fixed using 4% paraformaldehyde and 1% glutaraldehyde before setting in epon812 polymer resin. 70 nm sections were cut from the resin using a microtome and then imaged using TEM, Figure 6.1. Due to the high electron density of the particles, AuNPs can be clearly seen as distinct black dots. In a second image, Figure 6.2, the AuNP is at the cell's periphery and appears to be surrounded by an invaginated membrane vesicle, suggesting phagocytosis. Due to the 70 nm cross section taken through the cell, we were able to conclude that these particles were inside macrophage cells.

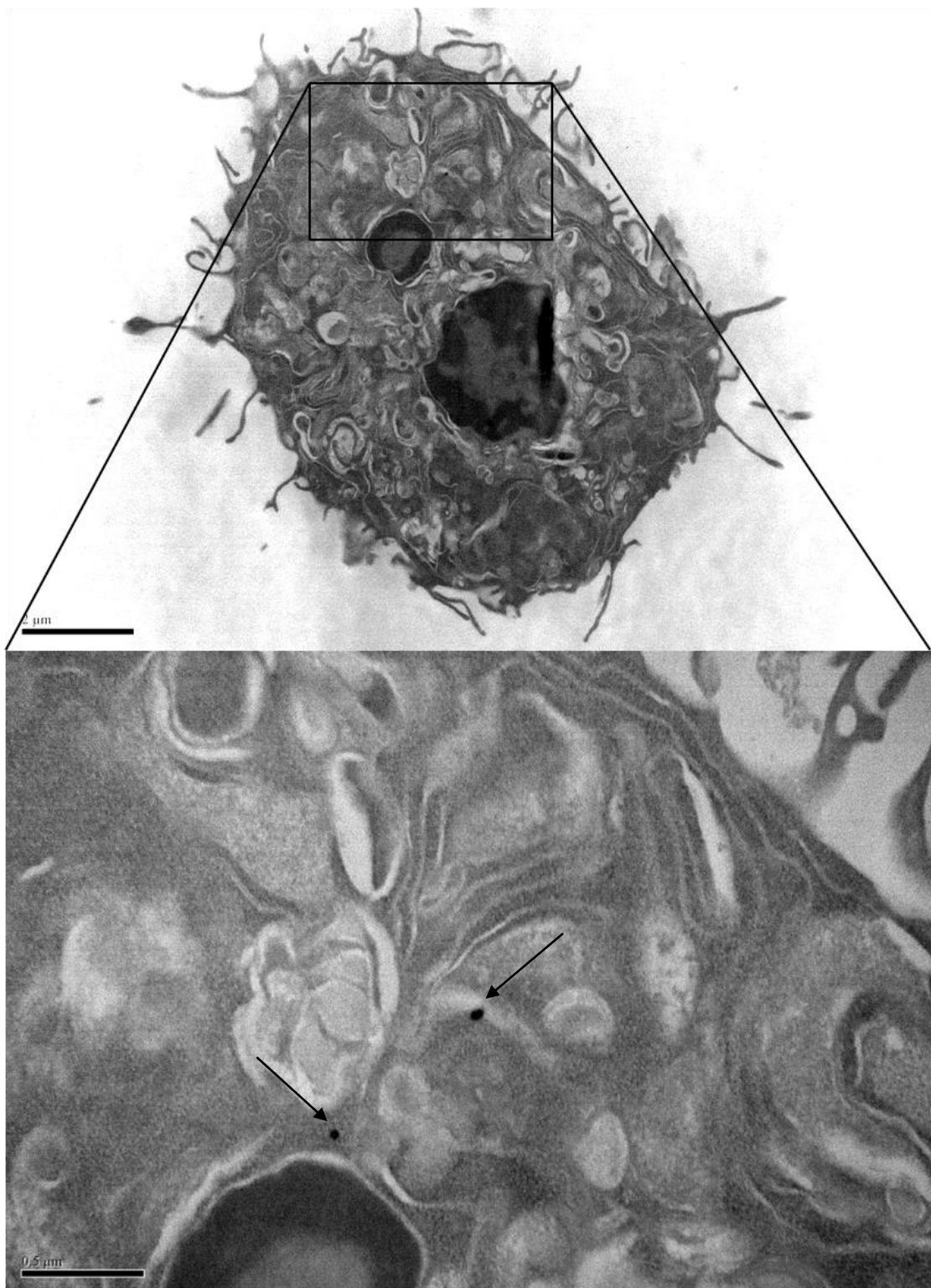


**Figure 6.1** A transmission electron micrograph of a 70 nm slice through a J774A.1 macrophage cell after 1 hour incubation with AuNPs (arrow). Bar is 10 μm.

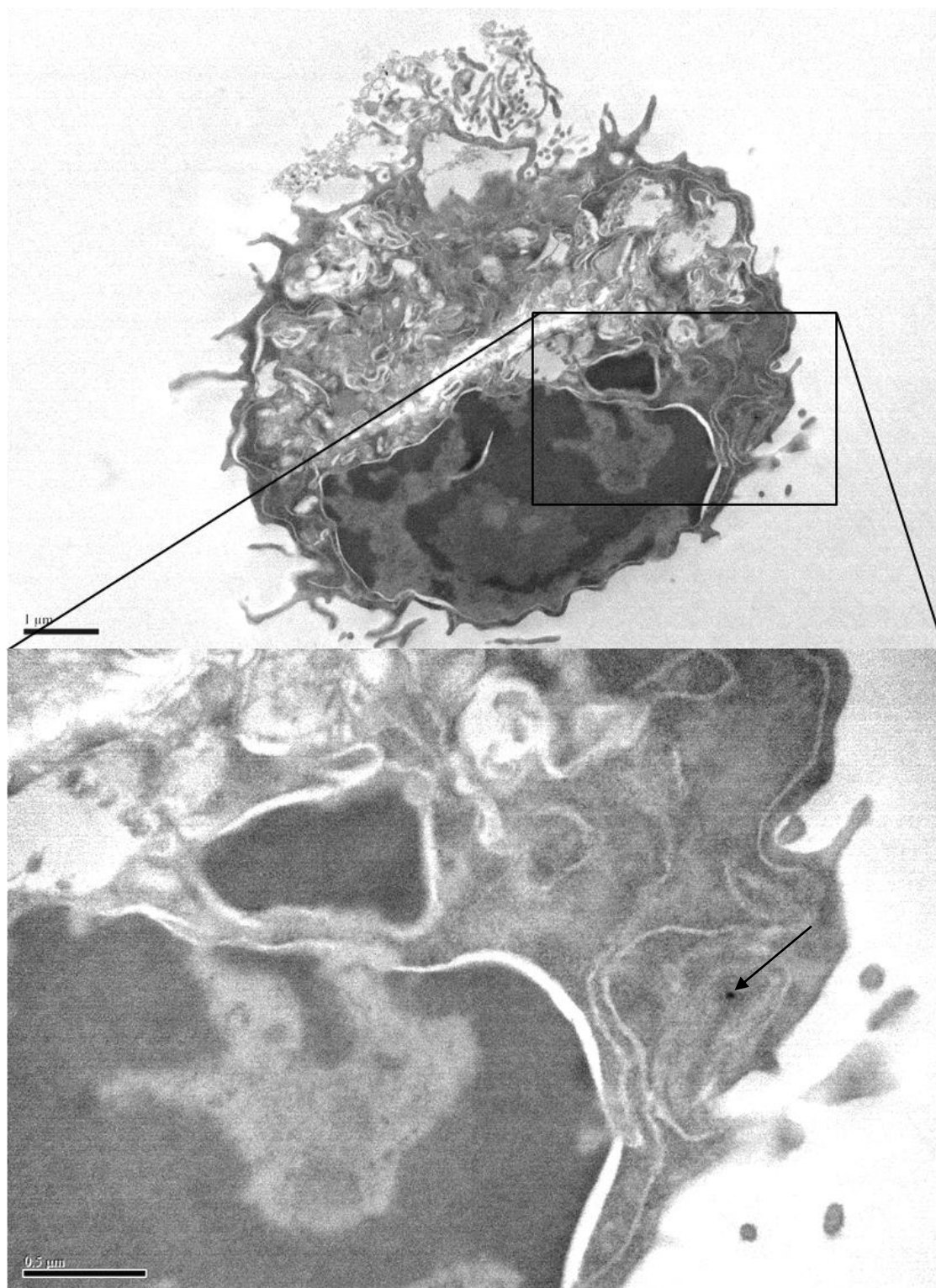


**Figure 6.2** A transmission electron micrograph of a 70 nm slice through a J774A.1 macrophage cell after 1 hour incubation with AuNPs (arrow). Bar is 10 μm.

Once confirmed as being taken up by murine macrophages, it was then the intention to establish some of the mechanisms by which nanoparticles are taken up by cells. This was to be determined by staining for the presence of endosomal compartments in macrophages after incubation with AuNPs. AuNPs were coupled with GFP using carbodiimide chemistry followed by incubation with J774A.1 macrophages for 1 hour. Confocal-laser scanning microscopy was used to image the co-localisation of GFP-fluorescent AuNPs with macrophage cells, Figure 6.3. The image shows a clear association between the cells and GFP conjugated AuNPs. AuNPs also appear to be located in the cytosolic area of macrophage cells with no GFP fluorescence detected in the nucleus of the cell; a result consistent with other studies [193]. The experiment was then repeated to determine whether phagocytic vesicles were formed to internalise AuNPs. A fluorescently tagged antibody against lysosomal-associated membrane protein 1 (LAMP1) was used which identifies markers present in late endosome formation, specifically the fusion event between a phagosome and a lysosomes to form a phagolysosome, Figure 6.5 [505]. A series of optical sections were stacked (Z-stacked) by moving the focal point through the depth of the cell to determine the position of fluorescent indicators within the cell, Figures 6.6 and 6.7. From these images the presence of a LAMP1 within the cell is clear however there is no co-localisation with GFP conjugated AuNPs. One explanation for this could be the Cy5 fluorescence quenching the GFP emission or proteolytic degradation of the amide conjugated GFP in the phagolysosome. Whilst there are several triggers identified for initiating phagocytic uptake by professional phagocytes, size dependency is one of the most important [203]. Phagocytosis is usually triggered in response to larger particles, typically 500 nm [198]. Since the NPs used in this study are only 15 nm in diameter, the association of AuNP uptake and phagocytosis is unusual. Uptake into phagosomes could be due to an aggregation effect of the NPs on the surface of the macrophages. Once aggregation reaches a certain size (> 500 nm) this could trigger a phagocytic response to engulf AuNPs. In addition, there are GFP conjugated AuNPs within the cytosol which are not associated with LAMP1. This could suggest the particles are able to enter macrophage cells through clathrin-independent pathways which typically avoid lysosomal fusion [506]. Alternatively there are some suggestions that NPs are able to enter cells by penetrating through the plasma membrane exclusive of any

macrophage uptake mechanisms [507]. However, the mechanisms involved in NP uptake into mammalian cells remains to be characterised better.

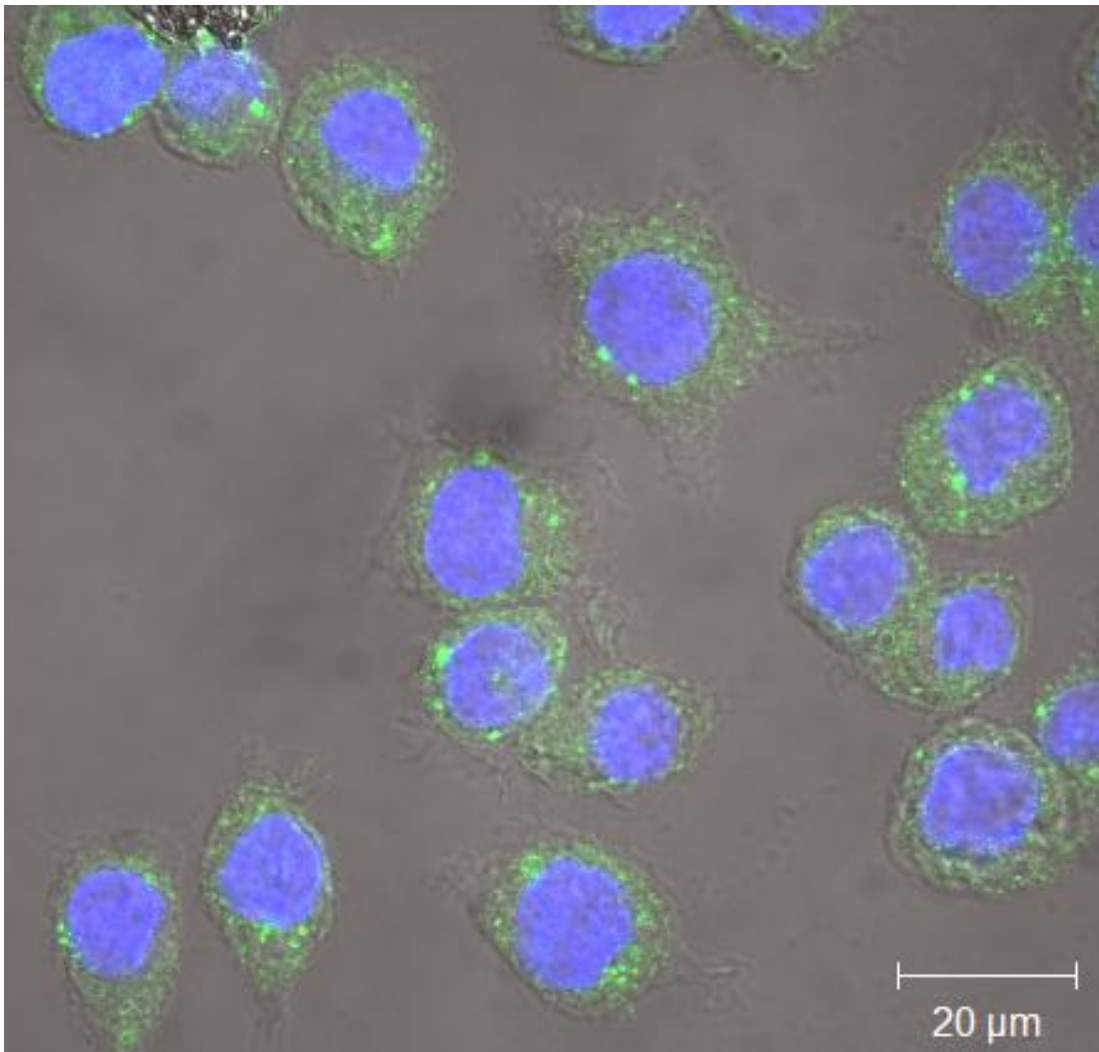


**Figure 6.3** A confocal microscopy image of J774A.1 macrophage cells, stained with DAPI (blue), after 2 hours incubation with GFP conjugated AuNPs (green). Bar is 20 μm.

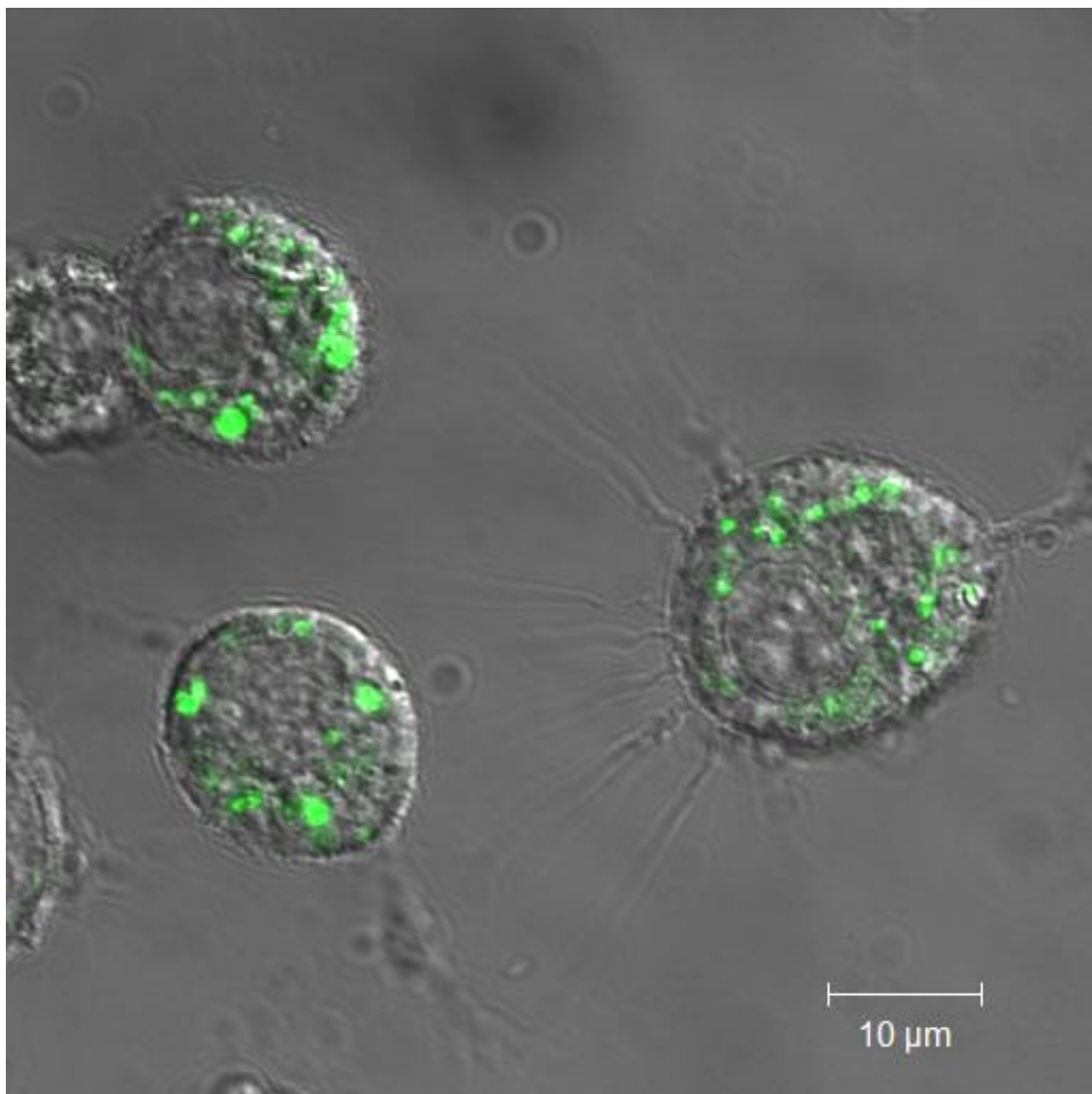


**Figure 6.4** A confocal microscopy image of J774 macrophage cells after 1 hour incubation with GFP conjugated AuNPs (green). Bar is 10  $\mu\text{m}$ .

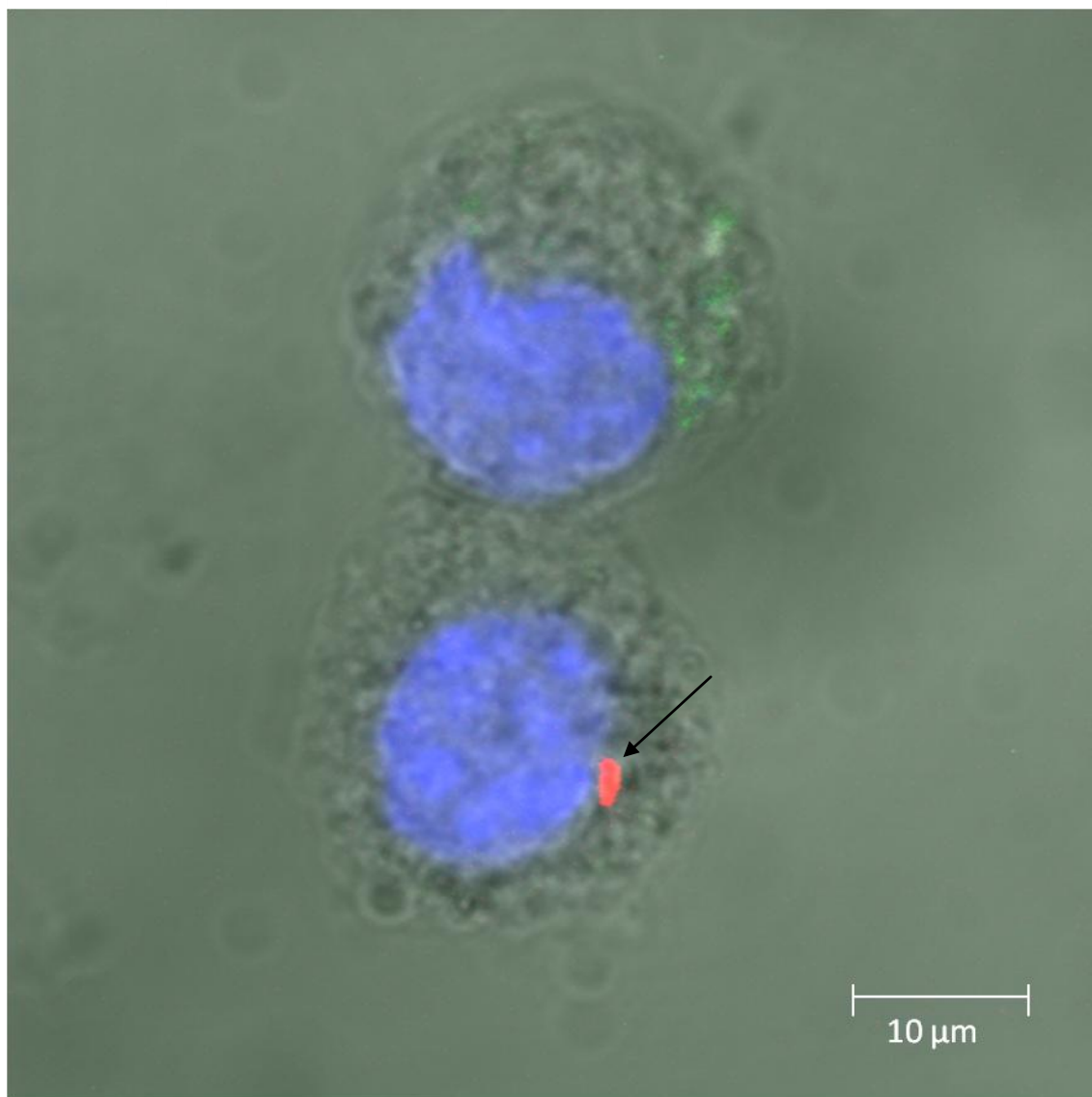


**Figure 6.5** A confocal microscopy image of J774A.1 murine macrophage cells, stained with DAPI (blue), after 2 hours incubation with GFP conjugated AuNPs (green) and probed with LAMP1 endosomal marker (red; arrow). Bar is 10  $\mu\text{m}$ .

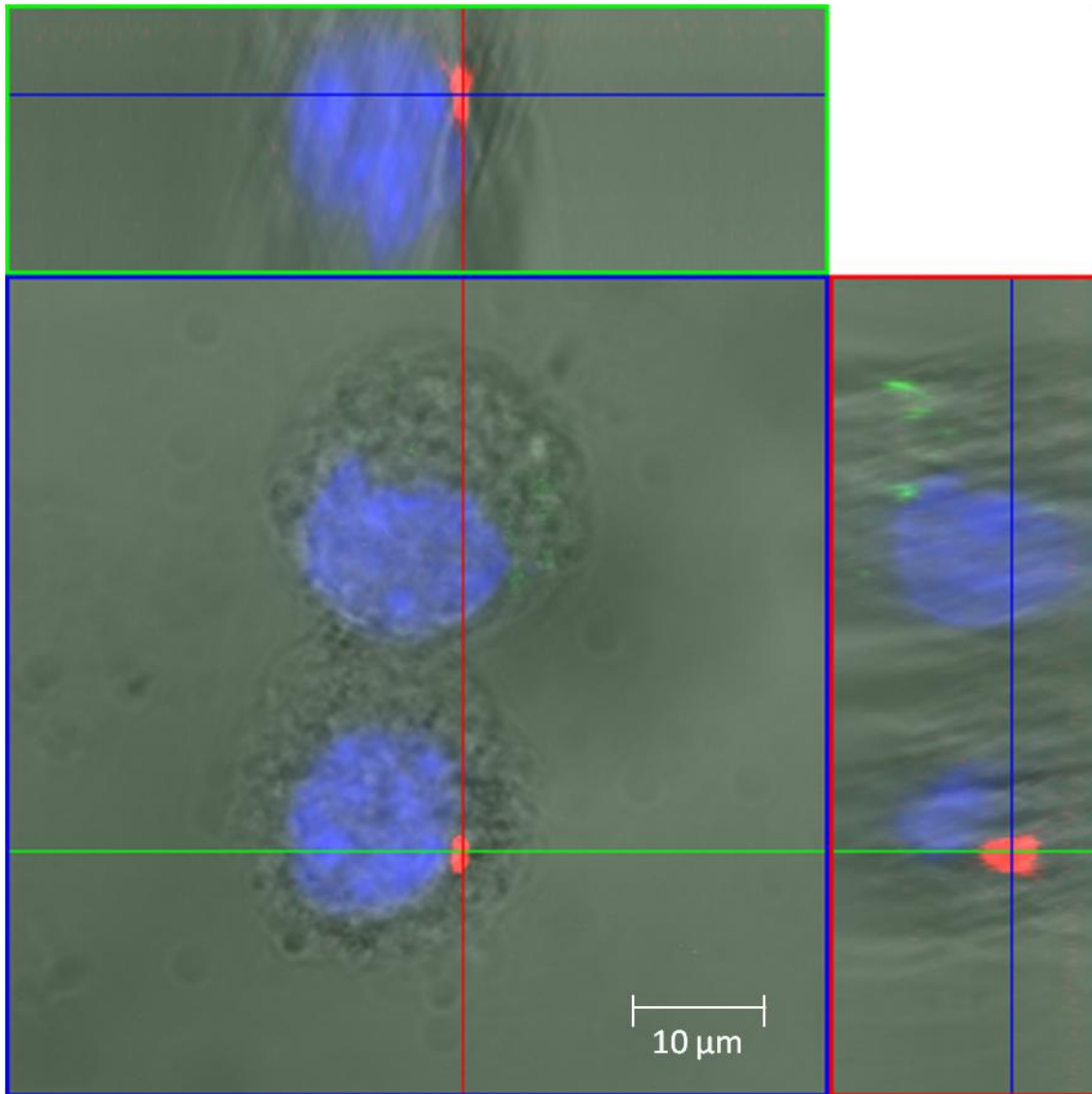


**Figure 6.6** A 4.54  $\mu\text{m}$  z-cross section slice of J774 macrophage cells, stained with DAPI (blue), after 2 hours incubation with GFP conjugated AuNPs (green) and probed with a Cy5 conjugated anti-LAMP1 endosomal marker (red). Bar is 10  $\mu\text{m}$ .

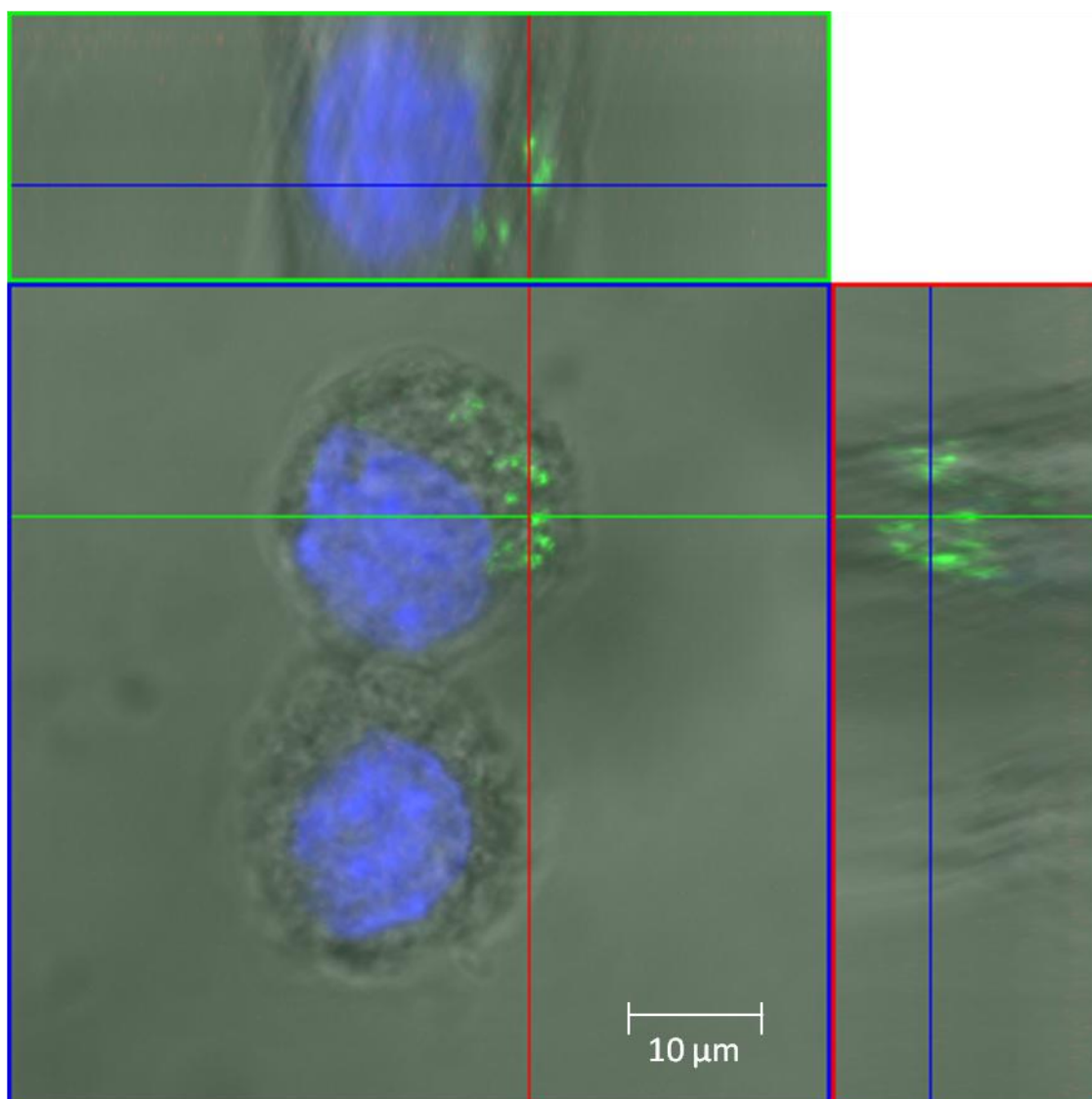


**Figure 6.7** A 9.08  $\mu\text{m}$  z-cross section slice of J774 macrophage cells, stained with DAPI (blue), after 2 hours incubation with GFP conjugated AuNPs (green) and probed with a Cy5 conjugated anti-LAMP1 endosomal marker (red). Bar is 10  $\mu\text{m}$ .

Identifying the mechanisms involved in intracellular uptake of antigens is crucial in understanding how vaccine antigens are processed as part of the immune response they elicit. Endocytic uptake of molecules includes phagocytosis, macropinocytosis, clathrin- and caveolae-mediated endocytosis, which follow the principle components of the endocytic pathway. Once molecules are internalised by an invagination, or “ruffling” of the plasma membrane, the newly formed early endosome and matures into a late endosome [508]. Late endosomes fuses with lysosomes to form endolysosomes which express LAMP1 and degrade the endocytosed cargo [509]. Degraded peptides are then displayed on MHC II receptors for CD4<sup>+</sup> T cell recognition [510]. However, if NPs are able to internalise within cells exclusive of endosomal pathways this could result in protein degradation by the proteasome and a subsequent display of peptides on CD8<sup>+</sup> T cells. This could be particularly beneficially for vaccines against viruses or intracellular pathogens, such as the ones described in this study, since Tc cells play a key role in providing protection against intracellular infections.

### 6.2 Future work

Delivery of both protein and glycoconjugate vaccine candidates using AuNPs has been successfully demonstrated. One of the reasons it is believed that this delivery method is successful at increasing the immune response may be due to the highly repetitive antigen density on the surface of AuNPs. However, it may be possible to couple multiple antigens onto the NP surface for developing a polyvalent vaccine. Polyvalent vaccines are able to provide protection against several pathogens in a single, or fewer number of doses, making it a more favourable immunisation strategy than several doses of multiple vaccines. Polyvalent vaccines have also been shown to be economically favourable due to reduced storage and transport costs.

Organisation of antigens in glycoconjugates on the AuNP surface could be rearranged so that a protein carrier is distal to the NP. This may lead to a faster immune response as protein epitopes are presented to the immune system so the rate at which peptides are processed by B cells and presented on MHC molecules for T cell recruitment is faster. Moreover, other polysaccharides could be tested using the NP delivery system described in this study, such as capsular polysaccharide from *B. pseudomallei* (and certain strains of *B.*

*thailandensis*) and the various other *S. pneumoniae* CPS serotypes. *S. pneumoniae* serotype 1 in particular would be an excellent candidate for AuNP conjugation, which has a repeating trisaccharide of sugars similar to type 3. The similarities between these two sugars means the chemistry may be adaptable for conjugation. *S. pneumoniae* CPS serotype 1 is also biologically relevant and is included in both PPV23 and Prevnar 13 vaccines; it has been identified as an emerging serotype associated with invasive pneumococcal disease in developing countries [511]. Moreover, *S. pneumoniae* CPS 1 is zwitterionic and is therefore recognisable to T cells without the need for a protein carrier [61]. As previously mentioned, future development of a glycoconjugate vaccine consisting of LPS for human use may require cleavage of the lipid A region due to its endotoxicity. Whilst the current method of lipid A cleavage consists of boiling LPS in a harsh acidic environment, it may be possible that more tolerable conditions could be used if LPS is conjugated onto AuNPs due to the semi-solid surface state afforded by NPs. Alternative methods might include the selective cleavage of ketosidic linkages in the LPS core region using ceric ammonium nitrate or enzymatic removal using keto-deoxyoctulosonate hydrolase A, found in the membranes of *H. pylori* and *F. tularensis* [360]. The current inclusion of lipid A in the *B. thailandensis* LPS used in this study is likely to adjuvant the immune response so its removal in future studies may require the addition of exogenous lipid A in the form of MPLA.

The immunology data presented in this study provides an insight into the immune response elicited by the various vaccines devised. However, future studies may benefit from measuring T cell responses directly through T cell proliferation and T cell memory assays. Antibody affinity assays could also be carried out using an array reader to establish whether higher affinity antibodies are generated against antigens conjugated onto AuNPs. Protection assays should be run for longer to determine whether any long-term protection is afforded.

Furthermore, a more detailed understanding of how NP vaccines are able to elicit an improved immune response requires a more detailed approach. One way in which this could be developed further is by analysis of MHC molecules on the surface of professional phagocytes. Using methods such as quantitative polymerase chain reaction (qPCR) one could measure the expression of MHC molecules on the surface of macrophages in response to

NP vaccines. A comparison of MHC expression on macrophages incubated with a NP conjugated antigen compared with an unconjugated antigen could identify whether NPs elicit MHC I presentation of antigens.

## Appendices

**Appendix A.** Virulence factors of *B. pseudomallei* and *B. mallei* and their relevance in an animal model.

Virulence factor	Description	Relevance to animal models
Secreted proteins of the Type II secretion system (T2SS)	Includes protease, lipase and phospholipase C which are all secreted by <i>B. pseudomallei</i> T2SS [512]. <i>B. mallei</i> also exports these proteins but poorly, possibly due to mutations in two T2SS genes [343, 357]	Exoproducts secreted by T2SS play a minor role in <i>B. pseudomallei</i> pathogenesis in a Syrian hamster model of infection [512]
Type III secretion system (T3SS)	Termed the <i>Burkholderia</i> secretion apparatus (Bsa), the T3SS of <i>B. mallei</i> and <i>B. pseudomallei</i> shares homology to the <i>Salmonella inv/spa/prg</i> and <i>Shigella ipa/mxi/spa</i> T3SS's [186, 513, 514]. A needle-like injectisome is used to deliver secreted proteins, known as effectors, directly into the cytosol of host cells [448]. Effectors are then able to manipulate a variety of cellular functions such as host immune responses, intracellular trafficking or inducing apoptosis [446, 447]. Some secreted effectors have also been identified as enabling endocytic vacuole escape and intercellular spreading [345, 387, 513].	<i>B. pseudomallei</i> mutants lacking the Bsa T3SS cluster are unable to escape from endocytic vacuoles and have reduced replication in a murine macrophage cell line [513].
Type IV pili (TFP)	Deletion of a putative pilus structural protein ( <i>pilA</i> ) results in reduced adherence to human epithelial cells [515].	Deletion of a putative pilus structural protein ( <i>pilA</i> ) from <i>B. pseudomallei</i> resulted in reduced virulence in BALB/c mice by the intranasal route [515]. TFP proteins were highly immunogenic in BALB/c mice but failed to protect against a lethal <i>B. mallei</i> aerosol challenge [516]

## Appendices

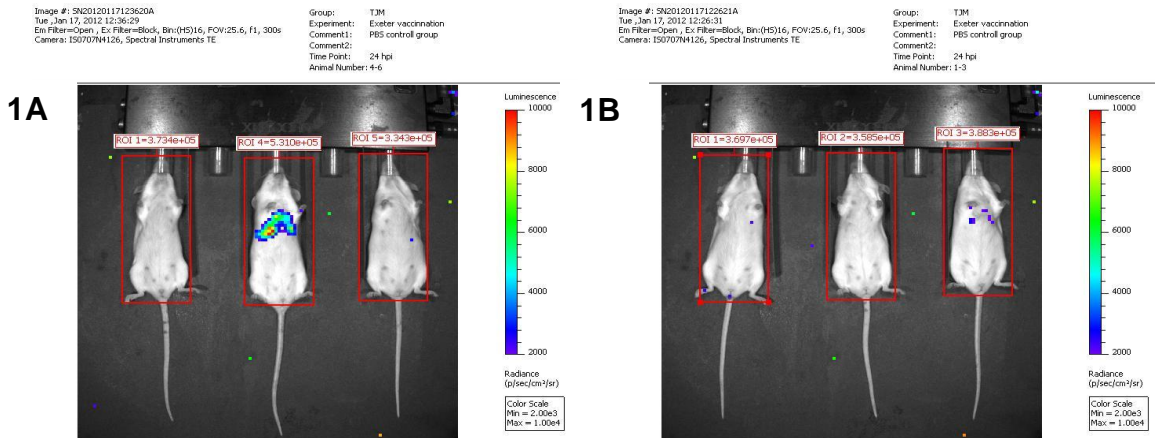
<p>Secreted protein of the Type V secretion system (T5SS)</p>	<p>Important for intracellular motility of <i>B. mallei</i>, <i>B. pseudomallei</i> and <i>B. thailandensis</i>. Designated the <i>Burkholderia</i> intracellular motility (BimA) protein, it is localised at the bacterial surface to bind actin and then promote polymerisation for actin-based motility [500, 517-519]. In <i>B. mallei</i> and <i>B. pseudomallei</i> this promotes cell fusion, leading to the formation of multinucleated giant cells [350].</p>	<p>The virulence of <i>B. mallei</i> <i>bimA</i> mutants was comparable to wild type strain in a Syrian hamster model of infection [384]. Recombinant BimA generated significant protection in BALB/c mice against lethal inhaled challenges of <i>B. mallei</i> and <i>B. pseudomallei</i> [251].</p>
<p>Secreted proteins of the Type VI secretion system (T6SS)</p>	<p>Hcp and VgrG assemble into a cell-penetrating needle to deliver effector proteins into host cells [384, 389-391]. T6SS plays a role in multinucleated giant cell formation since these were absent when RAW264 cells were infected with <i>B. pseudomallei</i> T6SS mutants [351]</p>	<p><i>B. mallei</i> and <i>B. pseudomallei</i> T6SS mutants are highly attenuated in hamsters and mice [384, 385].</p>
<p>Quorum sensing</p>	<p>The <i>B. mallei</i> genome contains two <i>luxI</i> homologs which produce four quorum-sensing molecules that are recognised by four <i>luxR</i> homologs [520, 521]. <i>B. pseudomallei</i> encodes three <i>luxI</i> homologs, producing seven quorum-sensing molecules [522-524]. It has five <i>luxR</i> homologs to detect these signals.</p>	<p>Mutations to <i>luxI</i> and <i>luxR</i> homologs in <i>B. pseudomallei</i> and <i>B. mallei</i> results in reduced virulence in hamster and mouse models of infection [521-523].</p>
<p>Flagellin</p>	<p>Flagellin, encoded by <i>fliC</i>, is involved in <i>B. pseudomallei</i> motility [349, 361]. The role of flagellum-mediated motility in virulence has largely been attributed to its ability to enhance the invasion of host epithelial cells [359, 377, 380, 381].</p>	<p><i>B. pseudomallei</i> flagellin mutants are attenuated in mice when delivered intranasally [377, 380]. Antibodies raised against <i>B. pseudomallei</i> FliC provide passive protection against <i>B. pseudomallei</i> infection in a diabetic rat model [382].</p>

## Appendices

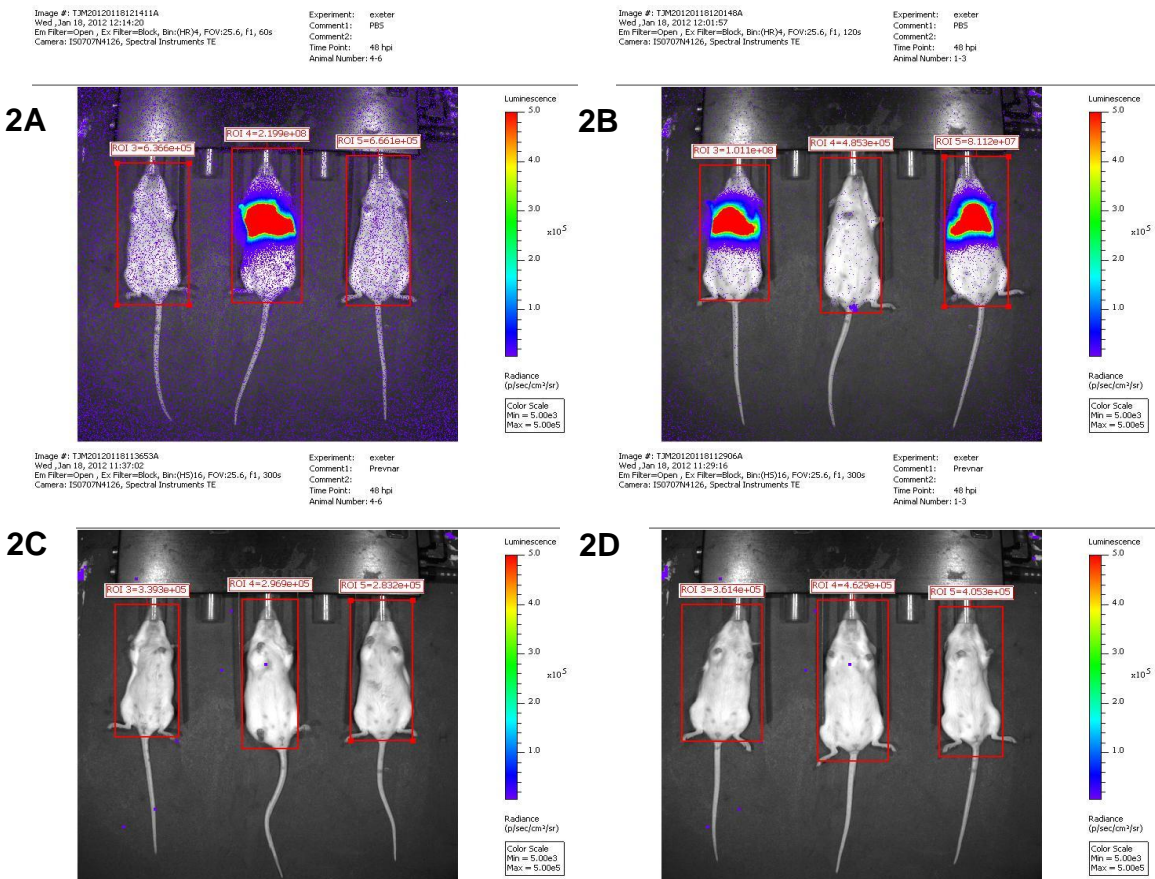
Lipopolysaccharide (LPS)	Consisting of a conserved lipid A and core region for structure and anchoring into the outer membrane. The variable O-antigen region, comprising of a repeating D-glucose and L-talose protects the bacterium against host defences, particularly serum killing [264, 357, 403]. This has been demonstrated by constructing mutants of the gene cluster in <i>B. pseudomallei</i> required for O-antigen synthesis and showing they are more susceptible to macrophage killing by RAW 246.7 cells and serum killing by the complement system [403, 408].	Passive protection studies of mAb's raised against <i>B. mallei</i> or <i>B. pseudomallei</i> LPS O-antigen were protective against a lethal challenge of glanders or melioidosis in a mouse model of infection [409-412]. LPS purified from <i>B. pseudomallei</i> or <i>B. thailandensis</i> is able to provide (short-term) significant protection against an inhalation challenge of <i>B. pseudomallei</i> [414].
Capsular polysaccharide	A 200 kDa group 3 capsular polysaccharide produced by both <i>B. mallei</i> and <i>B. pseudomallei</i> comprising of a homopolymer [392, 393]. The role of capsular polysaccharide in virulence is due to evasion of host defences, specifically the complement system, by reducing C3b-mediated opsonisation and phagocytosis [397]. Capsule is also believed to be required for survival and replication in macrophages by protecting the bacterium from reactive nitrogen and oxygen intermediates [398].	<i>B. pseudomallei</i> capsular mutants are highly attenuated in both mice and hamsters and <i>B. mallei</i> capsular mutants are avirulent [394-396]. Passive immunisation of mice using monoclonal antibodies raised against capsular polysaccharide provided significant protection against an intraperitoneal and intranasal challenge with <i>B. pseudomallei</i> [411, 412].
Type III and type IV O-PS	Functions relating to polysaccharide biosynthesis and transport in <i>B. pseudomallei</i> [344, 413]. Neither cluster is present in <i>B. mallei</i> [343].	Mutants lacking either type III or type IV O-PS show an increased time to death in a mouse model of <i>B. pseudomallei</i> compared with wild-type [413].

## Appendices

**Appendix B.** *In vivo* imaging using FxPro imaging of MF1 mice challenged IN with  $2.5 \times 10^5$  CFU  $50 \mu\text{L}^{-1}$  *S. pneumoniae* Xen10 four weeks post SC immunisation; Luminescence scale in radiance (p/sec/cm<sup>2</sup>/sr)



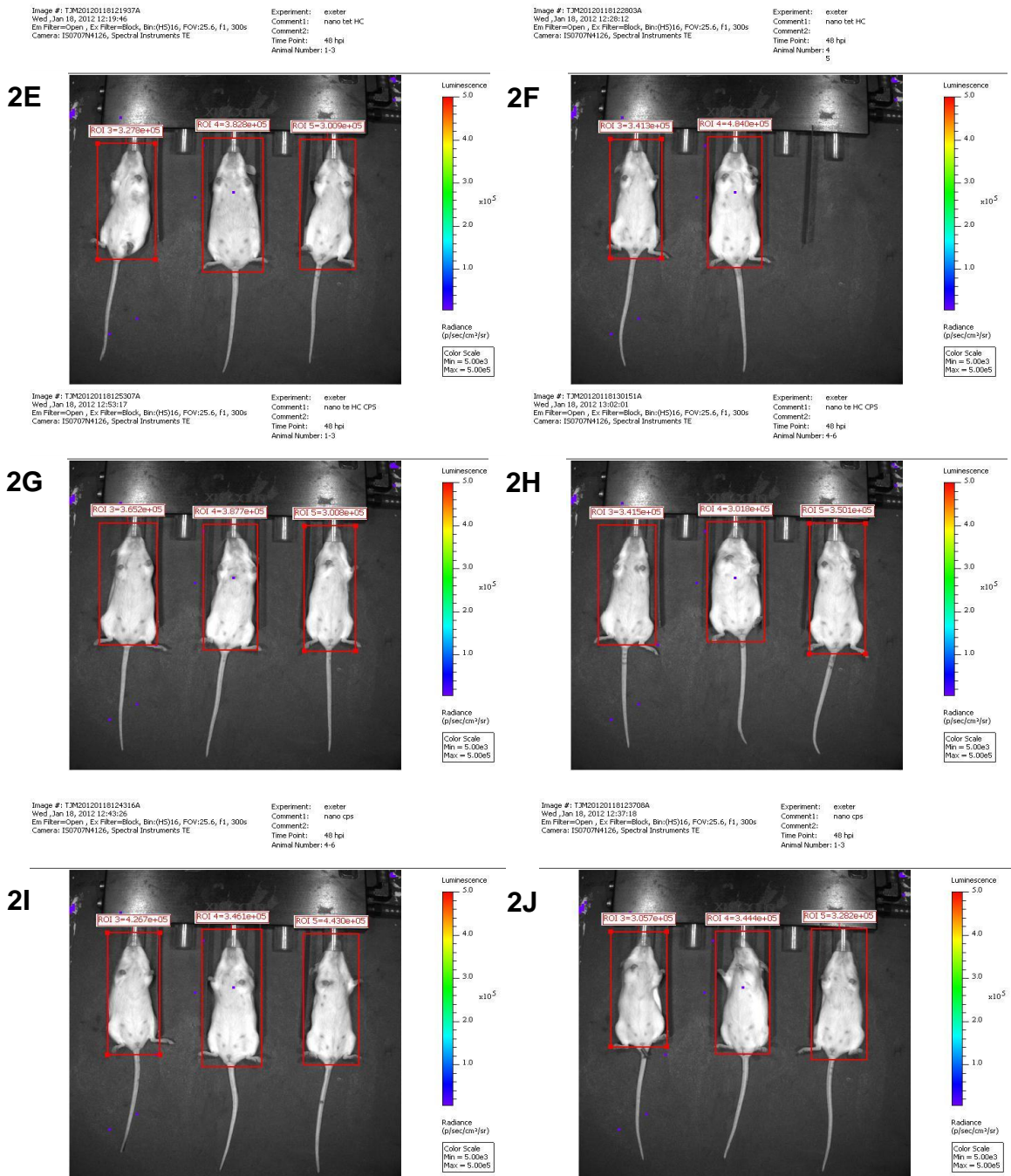
1A and B) PBS immunised 24 hpi



2A and B) PBS immunised 48 hpi

2C and D) Prevnar 13 immunised 48 hpi

# Appendices

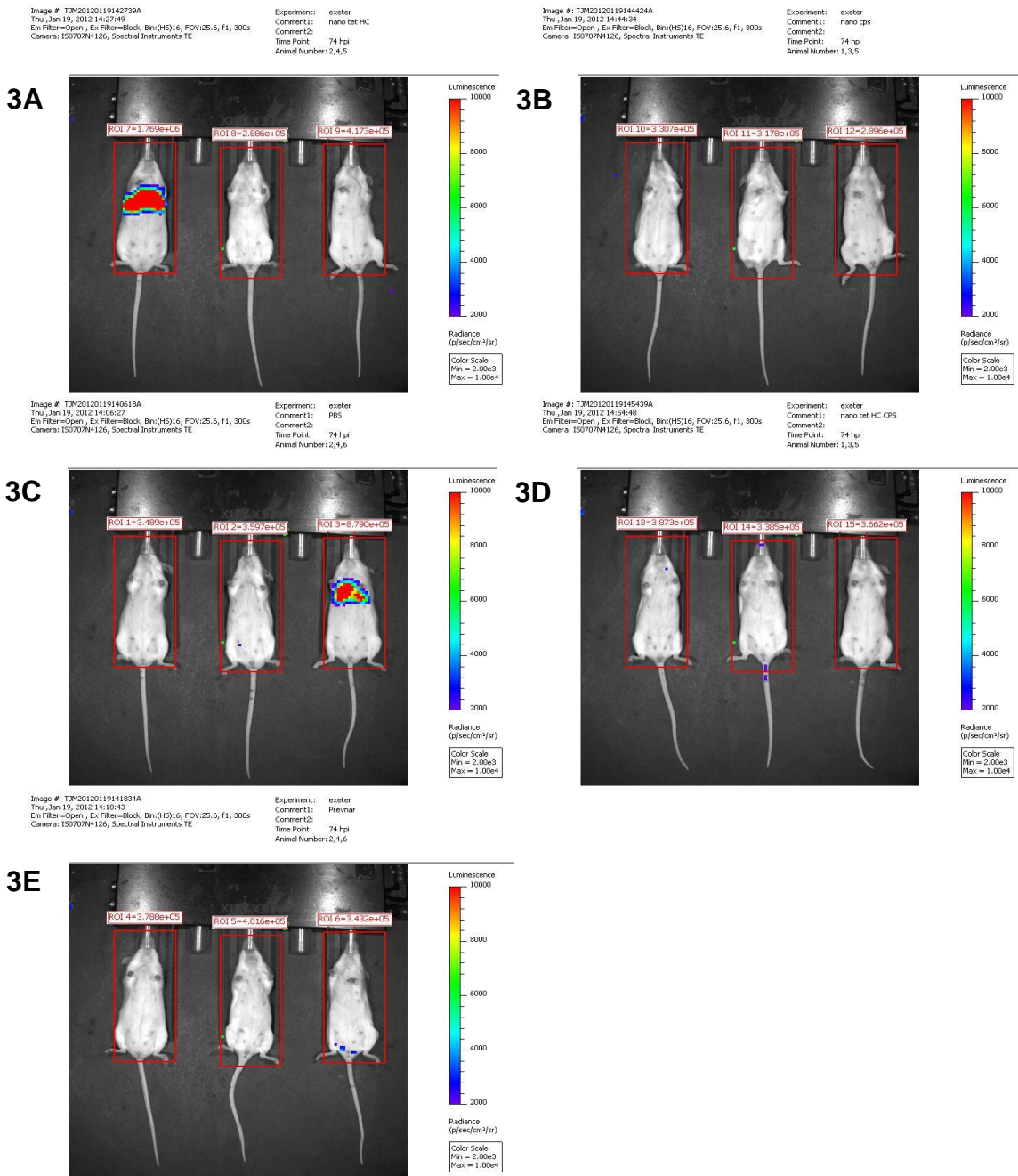


2E and F) AuNP-TetHc immunised 48 hpi

2G and H) AuNP-TetHc-CPS immunised 48 hpi

2I and J) AuNP-CPS immunised 48 hpi

# Appendices



- 3A) PBS immunised 74 hpi
- 3B) Prevnar 13 immunised 74 hpi
- 3C) AuNP-TetHc immunised 74 hpi
- 3D) AuNP-TetHc-CPS immunised 74 hpi
- 3E) AuNP-CPS 74 hpi immunised 74 hpi

# Appendices

Image #: TJM20120125095345A  
Wed Jan 25, 2012 09:53:55  
Em Filter=Open, Ex Filter=Block, Bin:(HS)16, FOV:25.6, f1, 300s  
Camera: IS0707M126, Spectral Instruments TE

Experiment: EXETER  
Comment1: PBS  
Comment2:  
Time Point: 8 DAYS  
Animal Number: 4

4A

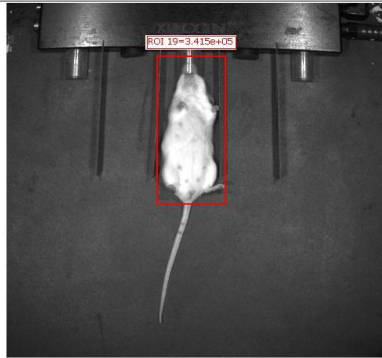
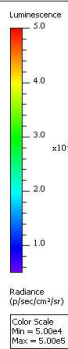


Image #: TJM2012012513621A  
Wed Jan 25, 2012 13:36:20  
Em Filter=Open, Ex Filter=Block, Bin:(HS)16, FOV:25.6, f1, 300s  
Camera: IS0707M126, Spectral Instruments TE

Experiment: EXETER  
Comment1: nano CPS  
Comment2:  
Time Point: 8 DAYS  
Animal Number: 1,2,3



4B

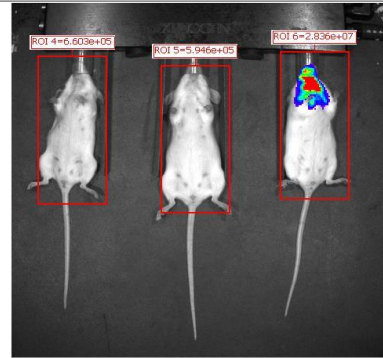
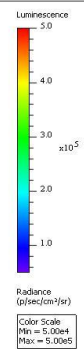


Image #: TJM20120125100427A  
Wed Jan 25, 2012 10:04:36  
Em Filter=Open, Ex Filter=Block, Bin:(HS)16, FOV:25.6, f1, 300s  
Camera: IS0707M126, Spectral Instruments TE

Experiment: EXETER  
Comment1: nano tet HC  
Comment2:  
Time Point: 8 DAYS  
Animal Number: 1,3,4,5



4C

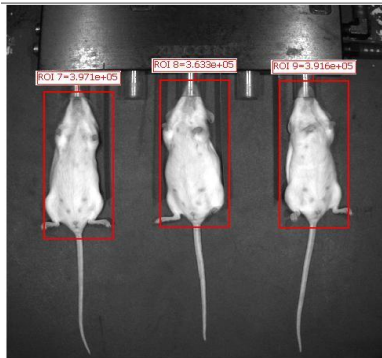
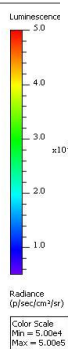


Image #: TJM2012012513455A  
Wed Jan 25, 2012 13:46:02  
Em Filter=Open, Ex Filter=Block, Bin:(HS)16, FOV:25.6, f1, 300s  
Camera: IS0707M126, Spectral Instruments TE

Experiment: EXETER  
Comment1: nano CPS  
Comment2:  
Time Point: 8 DAYS  
Animal Number: 4,5,6



4D

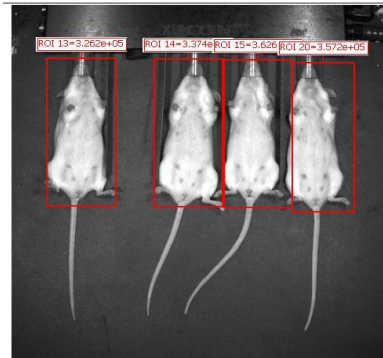
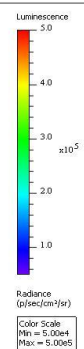


Image #: TJM20120125093035A  
Wed Jan 25, 2012 09:30:45  
Em Filter=Open, Ex Filter=Block, Bin:(HS)16, FOV:25.6, f1, 300s  
Camera: IS0707M126, Spectral Instruments TE

Experiment: EXETER  
Comment1: Pevnar  
Comment2:  
Time Point: 8 DAYS  
Animal Number: 1-3



4E

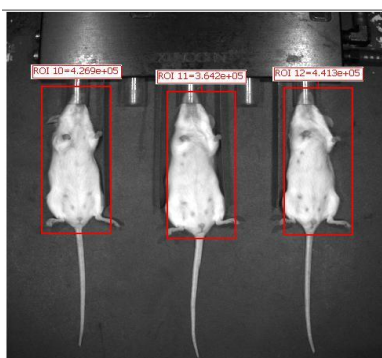
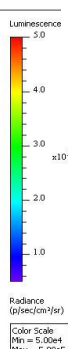


Image #: TJM20120125140011A  
Wed Jan 25, 2012 14:00:20  
Em Filter=Open, Ex Filter=Block, Bin:(HS)16, FOV:25.6, f1, 300s  
Camera: IS0707M126, Spectral Instruments TE

Experiment: EXETER  
Comment1: nano tet HC CPS  
Comment2:  
Time Point: 8 DAYS  
Animal Number: 1,2,4,5,6

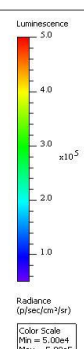


4F



Image #: TJM20120125140011A  
Wed Jan 25, 2012 14:00:20  
Em Filter=Open, Ex Filter=Block, Bin:(HS)16, FOV:25.6, f1, 300s  
Camera: IS0707M126, Spectral Instruments TE

Experiment: EXETER  
Comment1: nano tet HC CPS  
Comment2:  
Time Point: 8 DAYS  
Animal Number: 1,2,4,5,6

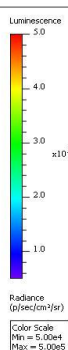


4G



Image #: TJM20120125140011A  
Wed Jan 25, 2012 14:00:20  
Em Filter=Open, Ex Filter=Block, Bin:(HS)16, FOV:25.6, f1, 300s  
Camera: IS0707M126, Spectral Instruments TE

Experiment: EXETER  
Comment1: nano tet HC CPS  
Comment2:  
Time Point: 8 DAYS  
Animal Number: 1,2,4,5,6



4A) PBS, B and C) Pevnar 13, D) AuNP-TetHc, E and F) AuNP-TetHc-CPS, G) AuNP-CPS immunised 8 days post infection.

## **Publications**

Gregory AE, Williamson ED, Prior JL, Butcher WA, Thompson IJ, Shaw AM, Titball RW. Conjugation of *Y. pestis* F1-antigen to gold nanoparticles improves immunogenicity. *Vaccine*. 2012;30:6777-82

Gregory AE, Williamson ED, Titball RW. Vaccine delivery using nanoparticles. *Frontiers in Cellular and Infection Microbiology*. 2013;3

## References

### References

- [1] Jenner E. An Inquiry into the causes and effects of the Variolae Vaccinae, a disease discovered in some of the western counties of England, particularly Gloucestershire and Known by the Name of Cow Pox. London: 1798.
- [2] Impact of vaccines universally recommended for children--United States, 1990-1998. MMWR Morb Mortal Wkly Rep 1999;48(12):243-8.
- [3] Organization WH. Immunizations, Vacines and Biologicals. 2012 [cited November 2013]; Available from:
- [4] Muhammad RD, Oza-Frank R, Zell E, Link-Gelles R, Narayan K MV, Schaffner W, et al. Epidemiology of invasive pneumococcal disease among high-risk adults since the introduction of pneumococcal conjugate vaccine for children. Clinical infectious diseases 2013;56(5):e59-e67.
- [5] Tsigrelis C, Tleyjeh IM, Huskins WC, Lahr BD, Nyre LM, Virk A, et al. Incidence of invasive pneumococcal disease among children after introduction of a 7-valent pneumococcal conjugate vaccine: a population-based study in Olmsted County, Minnesota. Mayo Clinic proceedings Mayo Clinic 2009;84(10):871-5.
- [6] Hanage WP. Serotype-specific problems associated with pneumococcal conjugate vaccination. Future Microbiol 2008;3(1):23-30.
- [7] Jones C. Vaccines based on the cell surface carbohydrates of pathogenic bacteria. An Acad Bras Cienc 2005;77:293-324.
- [8] Nesin M, Ramirez M, Tomasz A. Capsular transformation of a multidrug-resistant *Streptococcus pneumoniae* in vivo. Journal of Infectious Diseases 1998;177(3):707-13.
- [9] Imohl M, Reinert RR, Ocklenburg C, van der Linden M. Association of serotypes of *Streptococcus pneumoniae* with age in invasive pneumococcal disease. J Clin Microbiol 2010;48(4):1291-6.
- [10] Hanage WP, Finkelstein JA, Huang SS, Pelton SI, Stevenson AE, Kleinman K, et al. Evidence that pneumococcal serotype replacement in Massachusetts following conjugate vaccination is now complete. Epidemics 2010;2(2):80-4.
- [11] Lees A, Nelson BL, Mond JJ. Activation of soluble polysaccharides with 1-cyano-4-dimethylaminopyridinium tetrafluoroborate for use in protein-polysaccharide conjugate vaccines and immunological reagents. Vaccine 1996;14(3):190-8.
- [12] Anderson P, Betts R. Human adult immunogenicity of protein-coupled pneumococcal capsular antigens of serotypes prevalent in otitis media. Pediatr Infect Dis J 1989;8(1 Suppl):S50-3.
- [13] Engels EA, Falagas ME, Lau J, Bennish ML. Typhoid fever vaccines: A meta-analysis of studies on efficacy and toxicity. Br Med J 1998;316(7125):110-6.
- [14] Garmory HS, Brown KA, Titball RW. Salmonella vaccines for use in humans: Present and future perspectives. FEMS Microbiol Rev 2002;26(4):339-53.
- [15] McAleer WJ, Buynak EB, Maigetter RZ, Wampler DE, Miller WJ, Hilleman MR. Human hepatitis B vaccine from recombinant yeast. 1984.
- [16] Stevens CE, Taylor PE, Tong MJ, et al. Yeast-recombinant hepatitis b vaccine: Efficacy with hepatitis b immune globulin in prevention of perinatal hepatitis b virus transmission. Jama 1987;257(19):2612-6.
- [17] Harandi AM, Medaglini D, Shattock RJ. Vaccine adjuvants: A priority for vaccine research. Vaccine 2010;28(12):2363-6.
- [18] Guy B. The perfect mix: recent progress in adjuvant research. Nature reviews Microbiology 2007;5(7):505-17.
- [19] Gherardi RK, Coquet M, Cherin P, Belec L, Moretto P, Dreyfus PA, et al. Macrophagic myofasciitis lesions assess long-term persistence of vaccine-derived aluminium hydroxide in muscle. Brain 2001;124(9):1821-31.
- [20] Bachmann MF, Jennings GT. Vaccine delivery: a matter of size, geometry, kinetics and molecular patterns. Nature Reviews Immunology 2010;10(11):787-96.

## References

- [21] Areschoug T, Gordon S. Pattern recognition receptors and their role in innate immunity: focus on microbial protein ligands. *Contrib Microbiol* 2008;15:45-60.
- [22] Gordon S. Pattern Recognition Receptors: Doubling Up for the Innate Immune Response. *Cell* 2002;111(7):927-30.
- [23] Xiang SD, Scholzen A, Minigo G, David C, Apostolopoulos V, Mottram PL, et al. Pathogen recognition and development of particulate vaccines: Does size matter? *Methods* 2006;40:1-9.
- [24] Langenkamp A, Casorati G, Garavaglia C, Dellabona P, Lanzavecchia A, Sallusto F. T cell priming by dendritic cells: thresholds for proliferation, differentiation and death and intracloonal functional diversification. *Eur J Immunol* 2002;32(7):2046-54.
- [25] Siegrist CA. Section 1: general aspects of vaccination; vaccine immunology. *Vaccines* 2008:17-36.
- [26] Lacy P, Stow JL. Cytokine release from innate immune cells: association with diverse membrane trafficking pathways. *Blood* 2011;118(1):9-18.
- [27] Cella M, Sallusto F, Lanzavecchia A. Origin, maturation and antigen presenting function of dendritic cells. *Curr Opin Immunol* 1997;9(1):10-6.
- [28] Hall A, Nobes CD. Rho GTPases: molecular switches that control the organization and dynamics of the actin cytoskeleton. *Philosophical Transactions of the Royal Society of London Series B: Biological Sciences* 2000;355(1399):965-70.
- [29] Conner SD, Schmid SL. Regulated portals of entry into the cell. *Nature* 2003;422(6927):37-44.
- [30] Lambeth JD. NOX enzymes and the biology of reactive oxygen. *Nature reviews Immunology* 2004;4(3):181-9.
- [31] Turley SJ, Inaba K, Garrett WS, Ebersold M, Unternaehrer J, Steinman RM, et al. Transport of Peptide-MHC Class II Complexes in Developing Dendritic Cells. *Science* 2000;288(5465):522-7.
- [32] Scott P. Selective differentiation of CD4+ T helper cell subsets. *Curr Opin Immunol* 1993;5(3):391-7.
- [33] Seder RA, Paul WE, Dvorak AM, Sharkis SJ, Kagey-Sobotka A, Niv Y, et al. Mouse splenic and bone marrow cell populations that express high-affinity Fc epsilon receptors and produce interleukin 4 are highly enriched in basophils. *PNAS* 1991;88(7):2835-9.
- [34] Plaut M, Pierce JH, Watson CJ, Hanley-Hyde J, Nordan RP, Paul WE. Mast cell lines produce lymphokines in response to cross-linkage of Fc epsilon RI or to calcium ionophores. *Nature* 1989;339(6219):64-7.
- [35] Hsieh C, Macatonia S, Tripp C, Wolf S, O'Garra A, Murphy K. Development of TH1 CD4+ T cells through IL-12 produced by Listeria-induced macrophages. *Science* 1993;260(5107):547-9.
- [36] Trinchieri G. Immunobiology of Interleukin-12. *Immunol Res* 1998;17(1-2):269-78.
- [37] Mosmann TR, Cherwinski H, Bond MW, Giedlin MA, Coffman RL. Two types of murine helper T cell clone. I. Definition according to profiles of lymphokine activities and secreted proteins. *The Journal of Immunology* 1986;136(7):2348-57.
- [38] Lighvani AA, Frucht DM, Jankovic D, Yamane H, Aliberti J, Hissong BD, et al. T-bet is rapidly induced by interferon- $\gamma$  in lymphoid and myeloid cells. *PNAS* 2001;98(26):15137-42.
- [39] Ahmed R, Gray D. Immunological memory and protective immunity: understanding their relation. *Science* 1996;272(5258):54-60.
- [40] Le Gros G, Ben-Sasson SZ, Seder R, Finkelman FD, Paul WE. Generation of interleukin 4 (IL-4)-producing cells in vivo and in vitro: IL-2 and IL-4 are required for in vitro generation of IL-4-producing cells. *The Journal of Experimental Medicine* 1990;172(3):921-9.
- [41] Eltholth MM, Marsh VR, Van Winden S, Guitian FJ. Contamination of food products with *Mycobacterium avium* paratuberculosis: a systematic review. *J Appl Microbiol* 2009;107(4):1061-71.
- [42] Swain SL, Weinberg AD, English M, Huston G. IL-4 directs the development of Th2-like helper effectors. *The Journal of Immunology* 1990;145(11):3796-806.

## References

- [43] Parker DC. T Cell-Dependent B Cell Activation. *Annu Rev Immunol* 1993;11(1):331-60.
- [44] Stavnezer J. Immunoglobulin class switching. *Curr Opin Immunol* 1996;8(2):199-205.
- [45] Crotty S. Follicular Helper CD4 T Cells (TFH). *Annu Rev Immunol* 2011;29(1):621-63.
- [46] Vinuesa CG, Tangye SG, Moser B, Mackay CR. Follicular B helper T cells in antibody responses and autoimmunity. *Nature reviews Immunology* 2005;5(11):853-65.
- [47] Chen Y, Kuchroo VK, Inobe J, Hafler DA, Weiner HL. Regulatory T cell clones induced by oral tolerance: suppression of autoimmune encephalomyelitis. *Science* 1994;265(5176):1237-40.
- [48] Dieckmann D, Plottner H, Berchtold S, Berger T, Schuler G. Ex Vivo Isolation and Characterization of Cd4+Cd25+ T Cells with Regulatory Properties from Human Blood. *The Journal of Experimental Medicine* 2001;193(11):1303-10.
- [49] Olivares-Villagómez D, Wensky AK, Wang Y, Lafaille JJ. Repertoire Requirements of CD4+ T Cells That Prevent Spontaneous Autoimmune Encephalomyelitis. *The Journal of Immunology* 2000;164(10):5499-507.
- [50] Levings MK, Roncarolo M-G. T-regulatory 1 cells: A novel subset of CD4+ T cells with immunoregulatory properties. *J Allergy Clin Immunol* 2000;106(1, Part 2):S109-S12.
- [51] Broere F, Apasov S, Sitkovsky M, Eden W. A2 T cell subsets and T cell-mediated immunity. In: Nijkamp FP, Parnham MJ, editors. *Principles of Immunopharmacology*: Birkhäuser Basel, 2011: 15-27.
- [52] Heusel JW, Wesselschmidt RL, Shresta S, Russell JH, Ley TJ. Cytotoxic lymphocytes require granzyme B for the rapid induction of DNA fragmentation and apoptosis in allogeneic target cells. *Cell* 1994;76(6):977-87.
- [53] Shresta S, Pham CTN, Thomas DA, Graubert TA, Ley TJ. How do cytotoxic lymphocytes kill their targets? *Curr Opin Immunol* 1998;10(5):581-7.
- [54] Badovinac VP, Porter BB, Harty JT. Programmed contraction of CD8(+) T cells after infection. *Nature Immunology* 2002;3(7):619-26.
- [55] Kaech SM, Wherry EJ, Ahmed R. Effector and memory T-cell differentiation: implications for vaccine development. *Nature reviews Immunology* 2002;2(4):251-62.
- [56] Rock KL, Shen L. Cross-presentation: underlying mechanisms and role in immune surveillance. *Immunol Rev* 2005;207(1):166-83.
- [57] Guermonprez P, Saveanu L, Kleijmeer M, Davoust J, Van Endert P, Amigorena S. ER-phagosome fusion defines an MHC class I cross-presentation compartment in dendritic cells. *Nature* 2003;425(6956):397-402.
- [58] Pearse MJ, Drane D. ISCOMATRIX® adjuvant for antigen delivery. *Adv Drug Deliv Rev* 2005;57(3):465-74.
- [59] Thiele L, Merkle HP, Walter E. Phagocytosis of synthetic particulate vaccine delivery systems to program dendritic cells. *Expert Rev Vaccines* 2002;1(2):215-26.
- [60] Singh M, Srivastava I. Advances in Vaccine Adjuvants For Infectious Diseases. *Curr HIV Res* 2003;1(3):309-20.
- [61] Kalka-Moll WM, Tzianabos AO, Bryant PW, Niemeyer M, Ploegh HL, Kasper DL. Zwitterionic Polysaccharides Stimulate T Cells by MHC Class II-Dependent Interactions. *The Journal of Immunology* 2002;169(11):6149-53.
- [62] Weintraub A. Immunology of bacterial polysaccharide antigens. *Carbohydrate Research* 2003;338(23):2539-47.
- [63] Lee C-J, Lee L, Lu C-s, Wu A. Bacterial Polysaccharides as Vaccines — Immunity and Chemical Characterization. In: Wu A, editor. *The Molecular Immunology of Complex Carbohydrates —2*: Springer US, 2001: 453-71.
- [64] Lockhart S. Conjugate vaccines. *Expert Rev Vaccines* 2003;2(5):633-48.
- [65] Singh M, O'Hagan D. Advances in vaccine adjuvants. *Nat Biotechnol* 1999;17(11):1075-81.
- [66] Yang RB, Mark MR, Gray A, Huang A, Xie MH, Zhang M, et al. Toll-like receptor-2 mediates lipopolysaccharide-induced cellular signalling. *Nature* 1998;395(6699):284-8.

## References

- [67] Kirschning CJ, Wesche H, Merrill Ayres T, Rothe M. Human Toll-like Receptor 2 Confers Responsiveness to Bacterial Lipopolysaccharide. *The Journal of Experimental Medicine* 1998;188(11):2091-7.
- [68] Rutz M, Metzger J, Gellert T, Luppa P, Lipford GB, Wagner H, et al. Toll-like receptor 9 binds single-stranded CpG-DNA in a sequence- and pH-dependent manner. *Eur J Immunol* 2004;34(9):2541-50.
- [69] Sparwasser T, Koch E-S, Vabulas RM, Heeg K, Lipford GB, Ellwart JW, et al. Bacterial DNA and immunostimulatory CpG oligonucleotides trigger maturation and activation of murine dendritic cells. *Eur J Immunol* 1998;28(6):2045-54.
- [70] Barouch DH, Truitt DM, Letvin NL. Expression kinetics of the interleukin-2/immunoglobulin (IL-2/Ig) plasmid cytokine adjuvant. *Vaccine* 2004;22(23):3092-7.
- [71] Heath A, Playfair J. Cytokines as immunological adjuvants. *Vaccine* 1992;10(7):427-34.
- [72] Harrison WT. Some Observations on the Use of Alum Precipitated Diphtheria Toxoid. *Am J Public Health Nations Health* 1935;25(3):298-300.
- [73] Glenny AT, Buttle AH, Stevens MF. Rate of disappearance of diphtheria toxoid injected into rabbits and guinea pigs: toxoid precipitation with alum. *J Pathol Bacteriol* 1931;34:267-75.
- [74] Holt LB. Developments in diphtheria prophylaxis. London: Heinemann 1950:67-99.
- [75] Weissburg RP, Berman PW, Cleland JL, Eastman D, Farina F, Frie S, et al. Characterization of the MN gp120 HIV-1 vaccine: antigen binding to alum. *Pharm Res* 1995;12(10):1439-46.
- [76] Gupta RK, Chang AC, Griffin P, Rivera R, Siber GR. In vivo distribution of radioactivity in mice after injection of biodegradable polymer microspheres containing <sup>14</sup>C-labelled tetanus toxoid. *Vaccine* 1996;14(15):1412-6.
- [77] Shi Y, HogenEsch H, Regnier FE, Hem SL. Detoxification of endotoxin by aluminum hydroxide adjuvant. *Vaccine* 2001;19(13-14):1747-52.
- [78] Soliakov A, Kelly IF, Lakey JH, Watkinson A. Anthrax sub-unit vaccine: The structural consequences of binding rPA83 to Alhydrogel®. *European Journal of Pharmaceutics and Biopharmaceutics* 2012;80(1):25-32.
- [79] Powell MF, Newman MJ, Burdman JR. Vaccine design: the subunit and adjuvant approach: Plenum Press, 1995.
- [80] Eisenbarth S, Cassel S, Sutterwala F, Flavell R. T.9.5. Aluminum Hydroxide Adjuvants Activate the Immune System Through the Nalp3 Inflammasome. *Clin Immunol* 2009;131, Supplement(0):S49-S50.
- [81] Li H, Willingham SB, Ting JP-Y, Re F. Cutting Edge: Inflammasome Activation by Alum and Alum's Adjuvant Effect Are Mediated by NLRP3. *The Journal of Immunology* 2008;181(1):17-21.
- [82] McKee AS, Munks MW, MacLeod MKL, Fleenor CJ, Van Rooijen N, Kappler JW, et al. Alum Induces Innate Immune Responses through Macrophage and Mast Cell Sensors, But These Sensors Are Not Required for Alum to Act As an Adjuvant for Specific Immunity. *The Journal of Immunology* 2009;183(7):4403-14.
- [83] Li H, Nookala S, Re F. Aluminum Hydroxide Adjuvants Activate Caspase-1 and Induce IL-1 $\beta$  and IL-18 Release. *The Journal of Immunology* 2007;178(8):5271-6.
- [84] Nakae S, Asano M, Horai R, Iwakura Y. Interleukin-1 beta, but not interleukin-1 alpha, is required for T-cell-dependent antibody production. *Immunology* 2001;104(4):402-9.
- [85] Pelka K, Latz E. Getting Closer to the Dirty Little Secret. *Immunity* 2011;34(4):455-8.
- [86] HogenEsch H. Mechanisms of stimulation of the immune response by aluminum adjuvants. *Vaccine* 2002;20, Supplement 3(0):S34-S9.
- [87] Bomford R, Stapleton M, Winsor S, McKnight A, Andronova T. The control of the antibody isotype response to recombinant human immunodeficiency virus gp120 antigen by adjuvants. *AIDS Res Hum Retrovir* 1992;8(10):1765-71.
- [88] Comoy EE, Capron A, Thyphronitis G. In vivo induction of type 1 and 2 immune responses against protein antigens. *Int Immunol* 1997;9(4):523-31.

## References

- [89] Goto N, Kato H, Maeyama J, Eto K, Yoshihara S. Studies on the toxicities of aluminium hydroxide and calcium phosphate as immunological adjuvants for vaccines. *Vaccine* 1993;11(9):914-8.
- [90] Straw BE, MacLachlan NJ, Corbett WT, Carter PB, Schey HM. Comparison of tissue reactions produced by *Haemophilus pleuropneumoniae* vaccines made with six different adjuvants in swine. *Can J Comp Med* 1985;49(2):149-51.
- [91] Campbell A. The potential role of aluminium in Alzheimer's disease. *Nephrol Dial Transplant* 2002;17(suppl 2):17-20.
- [92] ISO/TS 27687:2008 Nanotechnologies -- Terminology and definitions for nano-objects - Nanoparticle, nanofibre and nanoplate. International Organization for Standardization, 2008.
- [93] Demento SL, Cui W, Criscione JM, Stern E, Tulipan J, Kaech SM, et al. Role of sustained antigen release from nanoparticle vaccines in shaping the T cell memory phenotype. *Biomaterials* 2012;33(19):4957-64.
- [94] Musumeci T, Ventura CA, Giannone I, Ruozi B, Montenegro L, Pignatello R, et al. PLA/PLGA nanoparticles for sustained release of docetaxel. *Int J Pharm* 2006;325(1-2):172-9.
- [95] Mahapatro A, Singh DK. Biodegradable nanoparticles are excellent vehicle for site directed in-vivo delivery of drugs and vaccines. *Journal of nanobiotechnology* 2011;9:55.
- [96] Emeny RT, Wheeler CM, Jansen KU, Hunt WC, Fu TM, Smith JF, et al. Priming of human papillomavirus type 11-specific humoral and cellular immune responses in college-aged women with a virus-like particle vaccine. *J Virol* 2002;76(15):7832-42.
- [97] Giannini SL, Hanon E, Moris P, Van Mechelen M, Morel S, Dessy F, et al. Enhanced humoral and memory B cellular immunity using HPV16/18 L1 VLP vaccine formulated with the MPL/aluminium salt combination (AS04) compared to aluminium salt only. *Vaccine* 2006;24(33-34):5937-49.
- [98] Uto T, Akagi T, Hamasaki T, Akashi M, Baba M. Modulation of innate and adaptive immunity by biodegradable nanoparticles. *Immunol Lett* 2009;125(1):46-52.
- [99] Uto T, Wang X, Sato K, Haraguchi M, Akagi T, Akashi M, et al. Targeting of antigen to dendritic cells with poly(gamma-glutamic acid) nanoparticles induces antigen-specific humoral and cellular immunity. *J Immunol* 2007;178(5):2979-86.
- [100] Caputoa A, Castaldello A, Brocca-Cofanoa E, Voltana R, Bortolazzi F, Altavilla G, et al. Induction of humoral and enhanced cellular immune responses by novel core-shell nanosphere- and microsphere-based vaccine formulations following systemic and mucosal administration. *Vaccine* 2009;27:3605-15.
- [101] Kingsman SM, Kingsman AJ. Polyvalent recombinant antigens: a new vaccine strategy. *Vaccine* 1988;6(4):304-6.
- [102] Zeltins A. Construction and characterization of virus-like particles: A review. *Mol Biotechnol* 2012;1-16.
- [103] Roldao A, Mellado MC, Castilho LR, Carrondo MJ, Alves PM. Virus-like particles in vaccine development. *Expert Rev Vaccines* 2010;9(10):1149-76.
- [104] Grgacic EVL, Anderson DA. Virus-like particles: Passport to immune recognition. *Methods* 2006;40(1):60-5.
- [105] Young KR, McBurney SP, Karkhanis LU, Ross TM. Virus-like particles: Designing an effective AIDS vaccine. *Methods* 2006;40(1):98-117.
- [106] Strable E, Finn MG. Chemical modification of viruses and virus-like particles viruses and nanotechnology. In: Manchester M, Steinmetz NF, editors.: Springer Berlin Heidelberg, 2009: 1-21.
- [107] Maurer P, Jennings GT, Willers J, Rohner F, Lindman Y, Roubicek K, et al. A therapeutic vaccine for nicotine dependence: preclinical efficacy, and Phase I safety and immunogenicity. *Eur J Immunol* 2005;35(7):2031-40.
- [108] Patel KG, Swartz JR. Surface functionalization of virus-like particles by direct conjugation using azide-alkyne click chemistry. *Bioconjug Chem* 2011;22(3):376-87.
- [109] Hu YC. Baculovirus as a highly efficient expression vector in insect and mammalian cells. *Acta Pharmacol Sin* 2005;26(4):405-16.

## References

- [110] Palmberger D, Wilson IBH, Berger I, Grabherr R, Rendic D. SweetBac: A New Approach for the Production of Mammalianised Glycoproteins in Insect Cells. *PLoS ONE* 2012;7(4):e34226.
- [111] Hollister JR, Shaper JH, Jarvis DL. Stable expression of mammalian  $\beta$ 1,4-galactosyltransferase extends the N-glycosylation pathway in insect cells. *Glycobiology* 1998;8(5):473-80.
- [112] Aumiller JJ, Hollister JR, Jarvis DL. A transgenic insect cell line engineered to produce CMP-sialic acid and sialylated glycoproteins. *Glycobiology* 2003;13(6):497-507.
- [113] Jarvis DL. Developing baculovirus-insect cell expression systems for humanized recombinant glycoprotein production. *Virology* 2003;310(1):1-7.
- [114] Harrison RL, Jarvis DL, Bryony C, Bonning KMAJS. Protein N-glycosylation in the baculovirus-insect cell expression system and engineering of insect cells to produce "mammalianized" recombinant glycoproteins. *Adv Virus Res: Academic Press*, 2006: 159-91.
- [115] Jarvis DL, Howe D, Aumiller JJ. Novel baculovirus expression vectors that provide sialylation of recombinant glycoproteins in lepidopteran insect cells. *J Virol* 2001;75(13):6223-7.
- [116] Ho Y, Lo HR, Lee TC, Wu CP, Chao YC. Enhancement of correct protein folding in vivo by a non-lytic baculovirus. *The Biochemical journal* 2004;382(Pt 2):695-702.
- [117] Slupetzky K, Gambhira R, Culp TD, Shafti-Keramat S, Schellenbacher C, Christensen ND, et al. A papillomavirus-like particle (VLP) vaccine displaying HPV16 L2 epitopes induces cross-neutralizing antibodies to HPV11. *Vaccine* 2007;25(11):2001-10.
- [118] Villa LL, Costa RLR, Petta CA, Andrade RP, Ault KA, Giuliano AR, et al. Prophylactic quadrivalent human papillomavirus (types 6, 11, 16, and 18) L1 virus-like particle vaccine in young women: a randomised double-blind placebo-controlled multicentre phase II efficacy trial. *Lancet Oncol* 2005;6(5):271-8.
- [119] Villa LL, Ault KA, Giuliano AR, Costa RLR, Petta CA, Andrade RP, et al. Immunologic responses following administration of a vaccine targeting human papillomavirus Types 6, 11, 16, and 18. *Vaccine* 2006;24(27-28):5571-83.
- [120] Olsson S-E, Villa LL, Costa RLR, Petta CA, Andrade RP, Malm C, et al. Induction of immune memory following administration of a prophylactic quadrivalent human papillomavirus (HPV) types 6/11/16/18 L1 virus-like particle (VLP) vaccine. *Vaccine* 2007;25(26):4931-9.
- [121] Sailaja G, Skountzou I, Quan FS, Compans RW, Kang SM. Human immunodeficiency virus-like particles activate multiple types of immune cells. *Virology* 2007;362(2):331-41.
- [122] Kang CY, Luo L, Wainberg MA, Li Y. Development of HIV/AIDS vaccine using chimeric gag-env virus-like particles. *Biological chemistry* 1999;380(3):353-64.
- [123] Takamura S, Niikura M, Li TC, Takeda N, Kusagawa S, Takebe Y, et al. DNA vaccine-encapsulated virus-like particles derived from an orally transmissible virus stimulate mucosal and systemic immune responses by oral administration. *Gene Ther* 2004;11(7):628-35.
- [124] Quan FS, Huang C, Compans RW, Kang SM. Virus-like particle vaccine induces protective immunity against homologous and heterologous strains of influenza virus. *J Virol* 2007;81(7):3514-24.
- [125] Fries LF G, D. M., Richards, R. L., Egan, J. E., Hollingdale, M. R., Gross, M., Silverman, C., Alving, C. R. Liposomal malaria vaccine in humans: a safe and potent adjuvant strategy. 1992(0027-8424 (Print)).
- [126] Alving CR, Richards RL, Moss J, Alving LI, Clements JD, Shiba T, et al. Effectiveness of liposomes as potential carriers of vaccines: applications to cholera toxin and human malaria sporozoite antigen. *Vaccine* 1986;4(3):166-72.
- [127] Karkada M, Weir GM, Quinton T, Fuentes-Ortega A, Mansour M. A liposome-based platform, VacciMax, and its modified water-free platform DepoVax enhance efficacy of in vivo nucleic acid delivery. *Vaccine* 2011;28(38):6176-82.

## References

- [128] Zhao W, Wu W, Xu X. Oral vaccination with liposome-encapsulated recombinant fusion peptide of urease B epitope and cholera toxin B subunit affords prophylactic and therapeutic effects against *H. pylori* infection in BALB/c mice. *Vaccine* 2007;25(44):7664-73.
- [129] Baca-Estrada ME, Foldvari M, Snider M, Harding K, Kournikakis B, Babiuk LA, et al. Intranasal immunization with liposome-formulated *Yersinia pestis* vaccine enhances mucosal immune responses. *Vaccine* 2000;18(21):2203-11.
- [130] Fynan EF, Webster RG, Fuller DH, Haynes JR, Santoro JC, Robinson HL. DNA vaccines: protective immunizations by parenteral, mucosal, and gene-gun inoculations. *Proc Natl Acad Sci U S A* 1993;90(24):11478-82.
- [131] Bharali DJ, Pradhan V, Elkin G, Qi W, Hutson A, Mousa SA, et al. Novel nanoparticles for the delivery of recombinant hepatitis B vaccine. *Nanomedicine: Nanotechnology, Biology, and Medicine* 2008;4:311-7.
- [132] Bhumkar DR, Joshi HM, Sastry M, Pokharkar VB. Chitosan reduced gold nanoparticles as novel carriers for transmucosal delivery of insulin. *Pharmaceutical Research* 2007;24(8):1415 - 26.
- [133] Chen YS, Hung YC, Lin WH, Huang GS. Assessment of gold nanoparticles as a size-dependent vaccine carrier for enhancing the antibody response against synthetic foot-and-mouth disease virus peptide. *Nanotechnology* 2010;21(19):195101.
- [134] Wang T, Zou M, Jiang H, Ji Z, Gao P, Cheng G. Synthesis of a novel kind of carbon nanoparticle with large mesopores and macropores and its application as an oral vaccine adjuvant. *Eur J Pharm Sci* 2011;44(5):653-9.
- [135] Dhar S, Daniel WL, Giljohann DA, Mirkin CA, Lippard SJ. Polyvalent oligonucleotide gold nanoparticle conjugates as delivery vehicles for platinum(IV) warheads. *J Am Chem Soc* 2009;131:14652-3.
- [136] Henriksen-Lacey M, Korsholm KS, Andersen P, Perrie Y, Christensen D. Liposomal vaccine delivery systems. *Expert Opinion on Drug Delivery* 2011;8(4):505-19.
- [137] Heurtault B, Frisch B, Pons F. Liposomes as delivery systems for nasal vaccination: strategies and outcomes. *Expert Opinion on Drug Delivery* 2010;7(7):829-44.
- [138] Riaz M. Liposomes preparation methods. *Pakistan Journal of Pharmaceutical Sciences* 1996;19(1):65-77.
- [139] Sharma S. Liposomes: a review, 2009.
- [140] Samad A, Sultana Y, Aqil M. Liposomal drug delivery systems: an update review. *Curr Drug Delivery* 2007;4(4):297-305.
- [141] Zhu J, Yan F, Guo Z, Marchant RE. Surface modification of liposomes by saccharides: Vesicle size and stability of lactosyl liposomes studied by photon correlation spectroscopy. *Journal of Colloid and Interface Science* 2005;289(2):542-50.
- [142] Kersten GF, Crommelin DJ. Liposomes and ISCOMS as vaccine formulations. *Biochimica et biophysica acta* 1995;1241(2):117-38.
- [143] Lee S-C, Lee K-E, Kim J-J, Lim S-H. The Effect of Cholesterol in the Liposome Bilayer on the Stabilization of Incorporated Retinol. *J Liposome Res* 2005;15(3-4):157-66.
- [144] Waterhouse DN, Madden TD, Cullis PR, Bally MB, Mayer LD, Webb MS. Preparation, characterization, and biological analysis of liposomal formulations of vincristine. In: Nejat D, editor. *Methods Enzymol: Academic Press*, 2005: 40-57.
- [145] Haran G, Cohen R, Bar LK, Barenholz Y. Transmembrane ammonium sulfate gradients in liposomes produce efficient and stable entrapment of amphipathic weak bases. *Biochimica et Biophysica Acta (BBA) - Biomembranes* 1993;1151(2):201-15.
- [146] Fries LF, Gordon DM, Richards RL, Egan JE, Hollingdale MR, Gross M, et al. Liposomal malaria vaccine in humans: a safe and potent adjuvant strategy. *Proc Natl Acad Sci U S A* 1992;89(1):358-62.
- [147] Mowat AM, Donachie AM. ISCOMS — a novel strategy for mucosal immunization? *Immunol Today* 1991;12(11):383-5.
- [148] Barr IG, Sjölander A, Cox JC. ISCOMs and other saponin based adjuvants. *Adv Drug Deliv Rev* 1998;32(3):247-71.

## References

- [149] Kersten GF, Teerlink T, Derks HJ, Verkleij AJ, van Wezel TL, Crommelin DJ, et al. Incorporation of the major outer membrane protein of *Neisseria gonorrhoeae* in saponin-lipid complexes (iscoms): chemical analysis, some structural features, and comparison of their immunogenicity with three other antigen delivery systems. *Infect Immun* 1988;56(2):432-8.
- [150] Lovgren K, Morein B. The requirement of lipids for the formation of immunostimulating complexes (iscoms). *Biotechnology and applied biochemistry* 1988;10(2):161-72.
- [151] Morein B, Lövgren K, Rönnerberg B, Sjölander A, Villacrés-Eriksson M. Immunostimulating complexes. Clinical potential in vaccine development. *Clinical Immunotherapeutics* 1995;3:461-75.
- [152] Morein B, Simons K. Subunit vaccines against enveloped viruses: virosomes, micelles and other protein complexes. *Vaccine* 1985;3:83-93.
- [153] Classen I, Osterhaus A. The iscom structure as an immune enhancing moiety: experiences in viral systems. *Res Immunol* 1992;143:531-41.
- [154] Kersten GF, Spiekstra A, Beuvery EC, Crommelin DJ. On the structure of immune-stimulating saponin-lipid complexes (iscoms). *Biochimica et biophysica acta* 1991;1062(2):165-71.
- [155] Özel M, Höglund S, Gelderblom HR, Morein B. Quaternary structure of the immunostimulating complex (Iscom). *Journal of Ultrastructure and Molecular Structure Research* 1989;102(3):240-8.
- [156] Li X, Deng X, Yuan M, Xiong C, Huang Z, Zhang Y, et al. In vitro degradation and release profiles of poly-DL-lactide-poly(ethylene glycol) microspheres with entrapped proteins. *Journal of Applied Polymer Science* 2000;78(1):140-8.
- [157] Sahoo SK, Panyam J, Prabha S, Labhasetwar V. Residual polyvinyl alcohol associated with poly (d,l-lactide-co-glycolide) nanoparticles affects their physical properties and cellular uptake. *Journal of Controlled Release* 2002;82(1):105-14.
- [158] Lu JM, Wang X, Marin-Muller C, Wang H, Lin PH, Yao Q, et al. Current advances in research and clinical applications of PLGA-based nanotechnology. *Expert Rev Mol Diagn* 2009;9(4):325-41.
- [159] O'Donnell PB, McGinity JW. Preparation of microspheres by the solvent evaporation technique. *Adv Drug Deliv Rev* 1997;28(1):25-42.
- [160] Hari Krishnan R, Balasundaram C, Heo MS. Poly d,l-lactide-co-glycolic acid (PLGA)-encapsulated vaccine on immune system in *Epinephelus bruneus* against *Uronema marinum*. *Exp Parasitol* 2012;131(3):325-32.
- [161] Pai Kasturi S, Qin H, Thomson KS, El-Bereir S, Cha S-c, Neelapu S, et al. Prophylactic anti-tumor effects in a B cell lymphoma model with DNA vaccines delivered on polyethylenimine (PEI) functionalized PLGA microparticles. *Journal of Controlled Release* 2006;113(3):261-70.
- [162] Feng L, Qi XR, Zhou XJ, Maitani Y, Cong Wang S, Jiang Y, et al. Pharmaceutical and immunological evaluation of a single-dose hepatitis B vaccine using PLGA microspheres. *Journal of Controlled Release* 2006;112(1):35-42.
- [163] Sales-Junior PA, Guzman F, Vargas MI, Sossai S, Patarroyo VA, Gonzalez CZ, et al. Use of biodegradable PLGA microspheres as a slow release delivery system for the *Boophilus microplus* synthetic vaccine SBm7462. *Vet Immunol Immunopathol* 2005;107(3-4):281-90.
- [164] Florindo HF, Pandit S, Gonçalves LMD, Videira M, Alpar O, Almeida AnJ. Antibody and cytokine-associated immune responses to *S. equi* antigens entrapped in PLA nanospheres. *Biomaterials* 2009;30(28):5161-9.
- [165] Sah H. Stabilization of proteins against methylene chloride/water interface-induced denaturation and aggregation. *Journal of Controlled Release* 1999;58(2):143-51.
- [166] Matsusaki M, Fuchida T, Kaneko T, Akashi M. Self-assembling bionanoparticles of poly(epsilon-lysine) bearing cholesterol as a biomesogen. *Biomacromolecules* 2005;6(4):2374-9.

## References

- [167] Matsusaki M, Hiwatari K, Higashi M, Kaneko T, Akashi M. Stably-dispersed and surface-functional bionanoparticles prepared by self-assembling amphipathic polymers of hydrophilic poly ( $\gamma$ -glutamic acid) bearing hydrophobic amino acids. *Chem Lett* 2004;33(4):398-9.
- [168] Holowka EP, Sun VZ, Kamei DT, Deming TJ. Polyarginine segments in block copolypeptides drive both vesicular assembly and intracellular delivery. *Nat Mater* 2007;6(1):52-7.
- [169] Lee ES, Shin HJ, Na K, Bae YH. Poly(L-histidine)-PEG block copolymer micelles and pH-induced destabilization. *J Control Release* 2003;90(3):363-74.
- [170] Letchford K, Burt H. A review of the formation and classification of amphiphilic block copolymer nanoparticulate structures: micelles, nanospheres, nanocapsules and polymersomes. *European Journal of Pharmaceutics and Biopharmaceutics* 2007;65(3):259-69.
- [171] Oppermann FB, Fickaitz S, Steinbiichel A. Biodegradation of polyamides. *Polym Degrad Stab* 1998;59:337-44.
- [172] Obst M, Steinbuchel A. Microbial degradation of poly(amino acid)s. *Biomacromolecules* 2004;5(4):1166-76.
- [173] Xu Y, Du Y. Effect of molecular structure of chitosan on protein delivery properties of chitosan nanoparticles. *Int J Pharm* 2003;250(1):215-26.
- [174] Varshosaz J, Ahmadi F, Emami J, Tavakoli N, Minaiyan M, Mahzouni P, et al. Microencapsulation of budesonide with dextran by spray drying technique for colon-targeted delivery: an in vitro/in vivo evaluation in induced colitis in rat. *J Microencapsul* 2011;28(1):62-73.
- [175] Mao H-Q, Roy K, Troung-Le VL, Janes KA, Lin KY, Wang Y, et al. Chitosan-DNA nanoparticles as gene carriers: synthesis, characterization and transfection efficiency. *Journal of Controlled Release* 2001;70(3):399-421.
- [176] Sonaje K, Chuang E-Y, Lin K-J, Yen T-C, Su F-Y, Tseng MT, et al. Opening of epithelial tight junctions and enhancement of paracellular permeation by chitosan: microscopic, ultrastructural, and computed-tomographic observations. *Molecular Pharmaceutics* 2012;9(5):1271-9.
- [177] Lee KY, Kwon IC, Kim YH, Jo WH, Jeong SY. Preparation of chitosan self-aggregates as a gene delivery system. *Journal of Controlled Release* 1998;51(2-3):213-20.
- [178] Tokumitsu H, Ichikawa H, Fukumori Y. Chitosan-gadopentetic acid complex nanoparticles for gadolinium neutron-capture therapy of cancer: preparation by novel emulsion-droplet coalescence technique and characterization *Pharmaceutical Research* 1999;16(12):1830-5.
- [179] Fernandez-Urrusuno R, Calvo P, Remunan-Lopez C, Vila-Jato JL, Alonso MJ. Enhancement of nasal absorption of insulin using chitosan nanoparticles. *Pharm Res* 1999;16(10):1576-81.
- [180] Anne Saupé WM, Thomas Rades & Sarah Hook. Immunostimulatory colloidal delivery systems for cancer vaccines. *Expert Opinion on Drug Delivery* 2006;3(3):345-54.
- [181] Lee P-W, Hsu S-H, Tsai J-S, Chen F-R, Huang P-J, Ke C-J, et al. Multifunctional core-shell polymeric nanoparticles for transdermal DNA delivery and epidermal Langerhans cells tracking. *Biomaterials* 2010;31:2425-34.
- [182] Calvo P, Remuñan-López C, Vila-Jato JL, Alonso MJ. Chitosan and chitosan/ethylene oxide-propylene oxide block copolymer nanoparticles as novel carriers for proteins and vaccines. *Pharmaceutical Research* 1997;14(10):1431-6.
- [183] Mukherjee P, Bhattacharya R, Wang P, Wang L, Basu S, Nagy JA, et al. Antiangiogenic properties of gold nanoparticles. *Clin Cancer Res* 2005;11(9):3530-4.
- [184] Connor EE, Mwamuka J, Gole A, Murphy CJ, Wyatt MD. Gold Nanoparticles Are Taken Up by Human Cells but Do Not Cause Acute Cytotoxicity. *Small* 2005;1(3):325-7.
- [185] Male KB, Lachance B, Hrapovic S, Sunahara G, Luong JHT. Assessment of Cytotoxicity of Quantum Dots and Gold Nanoparticles Using Cell-Based Impedance Spectroscopy. *Anal Chem* 2008;80(14):5487-93.

## References

- [186] Cheung JM, Scarsbrook D, Klinkhoff AV. Characterization of patients with arthritis referred for gold therapy in the era of biologics. *The Journal of Rheumatology* 2012;39(4):716-9.
- [187] Frens G. Controlled Nucleation for the Regulation of the Particle Size in Monodisperse Gold Suspensions. *Nature* 1973;241(105):20-2.
- [188] Zhou X, Zhang X, Yu X, Zha X, Fu Q, Liu B, et al. The effect of conjugation to gold nanoparticles on the ability of low molecular weight chitosan to transfer DNA vaccine. *Biomaterials* 2008;29(1):111-7.
- [189] Turkevich J, Stevenson PC, Hillier J. A study of the nucleation and growth processes in the synthesis of colloidal gold. *Discuss Faraday Soc* 1951;11:55-75.
- [190] Bhumkar D, Joshi H, Sastry M, Pokharkar V. Chitosan Reduced Gold Nanoparticles as Novel Carriers for Transmucosal Delivery of Insulin. *Pharmaceutical research* 2007;24(8):1415-26.
- [191] Akagi T, Baba M, Akashi M. Biodegradable nanoparticles as vaccine adjuvants and delivery systems: regulation of immune responses by nanoparticle-based vaccine. In: Kunugi S, Yamaoka T, editors. *Polymers in Nanomedicine: Springer Berlin Heidelberg*, 2011: 31-64.
- [192] Uto T, Akagi T, Toyama M, Nishi Y, Shima F, Akashi M, et al. Comparative activity of biodegradable nanoparticles with aluminum adjuvants: Antigen uptake by dendritic cells and induction of immune response in mice. *Immunol Lett* 2011;140(1-2):36-43.
- [193] Chithrani BD, Ghazani AA, Chan WCW. Determining the size and shape dependence of gold nanoparticle uptake into mammalian cells. *Nano Letters* 2006;6(4):662-8.
- [194] Foged C, Brodin B, Frokjaer S, Sundblad A. Particle size and surface charge affect particle uptake by human dendritic cells in an in vitro model. *Int J Pharm* 2005;298(2):315-22.
- [195] , Kissel T. Prospects for cationic polymers in gene and oligonucleotide therapy against cancer. *Adv Drug Deliv Rev* 2002;54(5):715-58.
- [196] Xia T, Kovochich M, Liong M, Meng H, Kabehie S, George S, et al. Polyethyleneimine coating enhances the cellular uptake of mesoporous silica nanoparticles and allows safe delivery of siRNA and DNA constructs. *ACS Nano* 2009;3(10):3273-86.
- [197] Champion JA, Mitragotri S. Shape induced inhibition of phagocytosis of polymer particles. *Pharm Res* 2009;26(1):244-9.
- [198] Rejman J, Oberle V, Zuhorn IS, Hoekstra D. Size-dependent internalization of particles via the pathways of clathrin- and caveolae-mediated endocytosis. *The Biochemical journal* 2004;377(Pt 1):159-69.
- [199] Yue H, Wei W, Yue Z, Lv P, Wang L, Ma G, et al. Particle size affects the cellular response in macrophages. *Eur J Pharm Sci* 2010;41(5):650-7.
- [200] Lai SK, Hida K, Man ST, Chen C, Machamer C, Schroer TA, et al. Privileged delivery of polymer nanoparticles to the perinuclear region of live cells via a non-clathrin, non-degradative pathway. *Biomaterials* 2007;28(18):2876-84.
- [201] Champion JA, Mitragotri S. Role of target geometry in phagocytosis. *Proc Natl Acad Sci U S A* 2006;103(13):4930-4.
- [202] Ivanov A. Pharmacological Inhibition of Endocytic Pathways: Is It Specific Enough to Be Useful? In: Ivanov A, editor. *Exocytosis and Endocytosis: Humana Press*, 2008: 15-33.
- [203] Iversen T-G, Skotland T, Sandvig K. Endocytosis and intracellular transport of nanoparticles: Present knowledge and need for future studies. *Nano Today* 2011;6(2):176-85.
- [204] Taylor U, Klein S, Petersen S, Kues W, Barcikowski S, Rath D. Nonendosomal cellular uptake of ligand-free, positively charged gold nanoparticles. *Cytometry Part A : the journal of the International Society for Analytical Cytology* 2010;77(5):439-46.
- [205] dos Santos T, Varela J, Lynch I, Salvati A, Dawson KA. Effects of transport inhibitors on the cellular uptake of carboxylated polystyrene nanoparticles in different cell lines. *PLoS ONE* 2011;6(9):e24438.
- [206] Sharma G, Valenta DT, Altman Y, Harvey S, Xie H, Mitragotri S, et al. Polymer particle shape independently influences binding and internalization by macrophages. *J Control Release* 2010;47(3):408-12.

## References

- [207] Vercauteren D, Vandenbroucke RE, Jones AT, Rejman J, Demeester J, De Smedt SC, et al. The use of inhibitors to study endocytic pathways of gene carriers: optimization and pitfalls. *Molecular therapy : the journal of the American Society of Gene Therapy* 2010;18(3):561-9.
- [208] Mohr E, Cunningham AF, Toellner K-M, Bobat S, Coughlan RE, Bird RA, et al. IFN- $\gamma$  produced by CD8 T cells induces T-bet-dependent and -independent class switching in B cells in responses to alum-precipitated protein vaccine. *PNAS* 2010;107(40):17292-7.
- [209] Gutierrez I, Hernández RM, Igartua M, Gascón AR, Pedraz JL. Size dependent immune response after subcutaneous, oral and intranasal administration of BSA loaded nanospheres. *Vaccine* 2002;21(1-2):67-77.
- [210] Lutsiak ME, Robinson DR, Coester C, Kwon GS, Samuel J. Analysis of poly(D,L-lactic-co-glycolic acid) nanosphere uptake by human dendritic cells and macrophages in vitro. *Pharm Res* 2002;19(10):1480-7.
- [211] Elamanchili P, Diwan M, Cao M, Samuel J. Characterization of poly(d,l-lactic-co-glycolic acid) based nanoparticulate system for enhanced delivery of antigens to dendritic cells. *Vaccine* 2004;22(19):2406-12.
- [212] Copland MJ, Baird MA, Rades T, McKenzie JL, Becker B, Reck F, et al. Liposomal delivery of antigen to human dendritic cells. *Vaccine* 2003;21(9-10):883-90.
- [213] Koutsky LA, Ault KA, Wheeler CM, Brown DR, Barr E, Alvarez FB, et al. A controlled trial of a human papillomavirus type 16 vaccine. *The New England journal of medicine* 2002;347(21):1645-51.
- [214] Breitburd F, Kirnbauer R, Hubbert NL, Nonnenmacher B, Trindinhdesmarquet C, Orth G, et al. Immunization with viruslike particles from cottontail rabbit papillomavirus (CRPV) can protect against experimental CRPV infection. *J Virol* 1995;69(6):3959-63.
- [215] Kirnbauer R, Oneil B, Grindlay J, Armstrong A, Lowy D, Schiller J, et al. Immunization with virus-like particles prevents bovine papillomavirus type 4 mucosal infection of calves. *J Invest Dermatol* 1996;106(4):234-.
- [216] Harper DM, Franco EL, Wheeler C, Ferris DG, Jenkins D, Schuid A, et al. Efficacy of a bivalent L1 virus-like particle vaccine in prevention of infection with human papillomavirus types 16 and 18 in young women: a randomised controlled trial. *Lancet* 2004;364(9447):1757-65.
- [217] Kemp TJ, Hildesheim A, Safaeian M, Dauner JG, Pan Y, Porras C, et al. HPV16/18 L1 VLP vaccine induces cross-neutralizing antibodies that may mediate cross-protection. *Vaccine* 2011;29(11):2011-4.
- [218] Pushko P, Pearce MB, Ahmad A, Tretyakova I, Smith G, Belser JA, et al. Influenza virus-like particle can accommodate multiple subtypes of hemagglutinin and protect from multiple influenza types and subtypes. *Vaccine* 2011;29(35):5911-8.
- [219] Pinto LA, Edwards J, Castle PE, Harro CD, Lowy DR, Schiller JT, et al. Cellular immune responses to human papillomavirus (HPV)-16 L1 in healthy volunteers immunized with recombinant HPV-16 L1 virus-like particles. *J Infect Dis* 2003;188(2):327-38.
- [220] Evans TG, Bonnez W, Rose RC, Koenig S, Demeter L, Suzich JA, et al. A phase 1 study of a recombinant virus-like particle vaccine against human papillomavirus type 11 in healthy adult volunteers. *Journal of Infectious Diseases* 2001;183(10):1485-93.
- [221] Hans ML, Lowman AM. Biodegradable nanoparticles for drug delivery and targeting. *Current Opinion in Solid State and Materials Science* 2002;6(4):319-27.
- [222] Soppimath KS, Aminabhavi TM, Kulkarni AR, Rudzinski WE. Biodegradable polymeric nanoparticles as drug delivery devices. *Journal of Controlled Release* 2001;70(1-2):1-20.
- [223] Filipovic-grcic J, Skalko-Basnet N, Jalsienjak I. Mucoadhesive chitosan-coated liposomes: characteristics and stability. *Journal of Microencapsulation* 2001;18(1):3-12.
- [224] Goren D, Horowitz AT, Tzemach D, Tarshish M, Zalipsky S, Gabizon A. Nuclear delivery of doxorubicin via folate-targeted liposomes with bypass of multidrug-resistance efflux pump. *Clinical Cancer Research* 2000;6(5):1949-57.

## References

- [225] Baras B, Benoit MA, Gillard J. Influence of various technological parameters on the preparation of spray-dried poly(epsilon-caprolactone) microparticles containing a model antigen. *J Microencapsul* 2000;17(4):485-98.
- [226] Valle EMMD, Galan MA. Supercritical fluid technique for particle engineering: Drug delivery applications. *Rev Chem Eng*, 2005: 33.
- [227] Vemavarapu C, Mollan MJ, Lodaya M, Needham TE. Design and process aspects of laboratory scale SCF particle formation systems. *Int J Pharm* 2005;292(1-2):1-16.
- [228] NIOSH. Approaches to safe nanotechnology. In: Department of health and human services CfDCaP, National Institute for Occupational Safety and Health, editor. <http://www.cdc.gov/niosh/docs/2009-125/pdfs/2009-125.pdf>, 2006.
- [229] Oberdorster G, Ferin J, Lehnert BE. Correlation between particle size, in vivo particle persistence, and lung injury. *Environmental health perspectives* 1994;102 Suppl 5:173-9.
- [230] Ophus EM, Rode L, Gylseth B, Nicholson DG, Saeed K. Analysis of titanium pigments in human lung tissue. *Scand J Work Environ Health* 1979;5(3):290-6.
- [231] Tsoli M, Kuhn H, Brandau W, Esche H, Schmid G. Cellular uptake and toxicity of Au55 clusters. *Small* 2005;1(8-9):841-4.
- [232] Pan Y, Neuss S, Leifert A, Fischler M, Wen F, Simon U, et al. Size-Dependent Cytotoxicity of Gold Nanoparticles. *Small* 2007;3(11):1941-9.
- [233] Shukla R, Bansal V, Chaudhary M, Basu A, Bhonde RR, Sastry M. Biocompatibility of Gold Nanoparticles and Their Endocytotic Fate Inside the Cellular Compartment: A Microscopic Overview. *Langmuir* 2005;21(23):10644-54.
- [234] Villiers C, Freitas H, Couderc R, Villiers M-B, Marche P. Analysis of the toxicity of gold nano particles on the immune system: effect on dendritic cell functions. *J Nanopart Res* 2010;12(1):55-60.
- [235] Fitzpatrick JA, Andreko SK, Ernst LA, Waggoner AS, Ballou B, Bruchez MP. Long-term persistence and spectral blue shifting of quantum dots in vivo. *Nano Lett* 2009;9(7):2736-41.
- [236] Wünsch K. Fortschritte der Chemie organischer Naturstoffe / Progress in the Chemistry of Organic Natural Products. *Starch - Stärke* 1994;46(4):161-2.
- [237] Pyle SW, Morein B, Bess JW, Jr., Akerblom L, Nara PL, Nigida SM, Jr., et al. Immune response to immunostimulatory complexes (ISCOMs) prepared from human immunodeficiency virus type 1 (HIV-1) or the HIV-1 external envelope glycoprotein (gp120). *Vaccine* 1989;7(5):465-73.
- [238] Stieneker F, Kersten G, van Bloois L, Crommelin DJ, Hem SL, Lower J, et al. Comparison of 24 different adjuvants for inactivated HIV-2 split whole virus as antigen in mice. Induction of titres of binding antibodies and toxicity of the formulations. *Vaccine* 1995;13(1):45-53.
- [239] Sundquist BG, Czifra G, Stipkovits L. Protective immunity induced in chicken by a single immunization with *Mycoplasma gallisepticum* immunostimulating complexes (ISCOMS). *Vaccine* 1996;14(9):892-7.
- [240] Ma J, Bulger PA, Dante S, Davis DvR, Perilli-Palmer B, Coughlin RT. Characterization of canine humoral immune responses to outer surface protein subunit vaccines and to natural infection by Lyme disease spirochetes. *Journal of Infectious Diseases* 1995;171(4):909-15.
- [241] de Vries P, Heeney JL, Boes J, Dings MEM, Hulskotte EGJ, Dubbes R, et al. Protection of rhesus macaques from SIV infection by immunization with different experimental SIV vaccines. *Vaccine* 1994;12(15):1443-52.
- [242] Vanselow BA, Abetz I, Trenfield K. A bovine ephemeral fever vaccine incorporating adjuvant Quil A: a comparative study using adjuvants Quil A, aluminium hydroxide gel and dextran sulphate. *The Veterinary record* 1985;117(2):37-43.
- [243] Kimling J, Maier M, Okenve B, Kotaidis V, Ballot H, Plech A. Turkevich Method for Gold Nanoparticle Synthesis Revisited. *The Journal of Physical Chemistry B* 2006;110(32):15700-7.
- [244] Fisk JD, Rooth M, Shaw AM. Gold Nanoparticle Adsorption and Aggregation Kinetics at the Silica-Water Interface. *J Phys Chem C* 2006;111:2588-94.
- [245] DiScipio RG. Preparation of Colloidal Gold Particles of Various Sizes Using Sodium Borohydride and Sodium Cyanoborohydride. *Anal Biochem* 1996;236(1):168-70.

## References

- [246] Jana NR, Gearheart L, Murphy CJ. Wet Chemical Synthesis of High Aspect Ratio Cylindrical Gold Nanorods. *The Journal of Physical Chemistry B* 2001;105(19):4065-7.
- [247] Jana NR, Gearheart L, Murphy CJ. Seeding Growth for Size Control of 5–40 nm Diameter Gold Nanoparticles. *Langmuir* 2001;17(22):6782-6.
- [248] Titball RW, Howells AM, Oyston PC, Williamson ED. Expression of the *Yersinia pestis* capsular antigen (F1 antigen) on the surface of an *aroA* mutant of *Salmonella typhimurium* induces high levels of protection against plague. *Infect Immun* 1997;65(5):1926-30.
- [249] Williamson ED, Eley SM, Griffin KF, Green M, Russell P, Leary SE, et al. A new improved sub-unit vaccine for plague: the basis of protection. *FEMS Immunol Med Microbiol* 1995;12(3-4):223-30.
- [250] Sinha K, Box M, Lalli G, Schiavo G, Schneider H, Groves M, et al. Analysis of mutants of tetanus toxin HC fragment: ganglioside binding, cell binding and retrograde axonal transport properties. *Molecular Microbiology* 2000;37(5):1041-51.
- [251] Whitlock GC, Deeraksa A, Qazi O, Judy BM, Taylor K, Propst KL, et al. Protective response to subunit vaccination against intranasal *Burkholderia mallei* and *B. pseudomallei* challenge. *Procedia in Vaccinology* 2010;2(1):73-7.
- [252] Soomi J, Woon-Seok Y. Quantification of proteins on gold nanoparticles by combining MALDI-TOF MS and proteolysis. *Nanotechnology* 2012;23(13):135701.
- [253] Chart H. *Methods in practical laboratory bacteriology*: CRC Press, 1994.
- [254] Wessels MR, Paoletti LC, Guttormsen HK, Michon F, D'Ambra AJ, Kasper DL. Structural properties of group B streptococcal type III polysaccharide conjugate vaccines that influence immunogenicity and efficacy. *Infect Immun* 1998;66(5):2186-92.
- [255] Kubler-Kielb J. Conjugation of LPS-Derived Oligosaccharides to Proteins Using Oxime Chemistry. In: Mark SS, editor. *Bioconjugation Protocols*: Humana Press, 2011: 317-27.
- [256] Kubler-Kielb J, Pozsgay V. A new method for conjugation of carbohydrates to proteins using an aminoxy-thiol heterobifunctional linker. *J Org Chem* 2005;70(17):6987-90.
- [257] Lees A, Sen G, LopezAcosta A. Versatile and efficient synthesis of protein-polysaccharide conjugate vaccines using aminoxy reagents and oxime chemistry. *Vaccine* 2006;24(6):716-29.
- [258] Kandil AA, Chan N, Klein M, Chong P. Chemical synthesis of *Haemophilus influenzae* glycopeptide conjugates. *Glycoconjugate Journal* 1997;14:13-7.
- [259] Shafer DE, Toll B, Schuman RF, Nelson BL, Mond JJ, Lees A. Activation of soluble polysaccharides with 1-cyano-4-dimethylaminopyridinium tetrafluoroborate (CDAP) for use in protein-polysaccharide conjugate vaccines and immunological reagents. II. Selective crosslinking of proteins to CDAP-activated polysaccharides. *Vaccine* 2000;18(13):1273-81.
- [260] Laferrrière CA, Sood RK, de Muys J-M, Michon F, Jennings HJ. The synthesis of *Streptococcus pneumoniae* polysaccharide-tetanus toxoid conjugates and the effect of chain length on immunogenicity. *Vaccine* 1997;15(2):179-86.
- [261] Jennings HJ, Lugowski C. Immunochemistry of groups A, B, and C meningococcal polysaccharide-tetanus toxoid conjugates. *The Journal of Immunology* 1981;127(3):1011-8.
- [262] DuBois M, Gilles KA, Hamilton JK, Rebers PA, Smith F. Colorimetric Method for Determination of Sugars and Related Substances. *Anal Chem* 1956;28(3):350-6.
- [263] Masuko T, Minami A, Iwasaki N, Majima T, Nishimura S-I, Lee YC. Carbohydrate analysis by a phenol-sulfuric acid method in microplate format. *Anal Biochem* 2005;339(1):69-72.
- [264] Heiss C, Burtnick MN, Black I, Azadi P, Brett PJ. Detailed structural analysis of the O-polysaccharide expressed by *Burkholderia thailandensis* E264. *Carbohydrate Research* 2012;363(0):23-8.
- [265] Williamson DE, Sharp GJE, Eley SM, Vesey PM, Pepper TC, Titball RW, et al. Local and systemic immune response a microencapsulated sub-unit vaccine to for plague. *Vaccine* 1996;14:1613-9.

## References

- [266] Williamson ED, Flick-Smith HC, LeButt C, Rowland CA, Jones SM, Waters EL, et al. Human Immune Response to a Plague Vaccine Comprising Recombinant F1 and V Antigens. *Infect Immun* 2005;73:3598–608.
- [267] Di Paola S, Micaroni M, Di Tullio G, Buccione R, Di Girolamo M. PARP16/ARTD15 Is a Novel Endoplasmic-Reticulum-Associated Mono-ADP-Ribosyltransferase That Interacts with, and Modifies Karyopherin- $\beta$ 1. *PLoS ONE* 2012;7(6):e37352.
- [268] Micaroni M, Stanley AC, Khromykh T, Venturato J, Wong CXF, Lim JP, et al. Rab6a/a' are important golgi regulators of pro-inflammatory TNF secretion in macrophages. *PLoS ONE* 2013;8(2):e57034.
- [269] Storrie B, Micaroni M, Morgan Garry P, Jones N, Kamykowski Jeffrey A, Wilkins N, et al. Electron Tomography Reveals Rab6 Is Essential to the Trafficking of trans-Golgi Clathrin and COPI-Coated Vesicles and the Maintenance of Golgi Cisternal Number. *Traffic* 2012;13(5):727-44.
- [270] Connor EE, Mwamuka J, Gole A, Murphy CJ, Wyatt MD. Gold nanoparticles are taken up by human cells but do not cause acute cytotoxicity. *Small* 2005;1:325-7.
- [271] Bhattacharya R, Mukherjee P. Biological properties of “naked” metal nanoparticles. *Adv Drug Deliv Rev* 2008;60(11):1289-306.
- [272] Li T, Guo L, Wang Z. Gold nanoparticle-based surface enhanced raman scattering spectroscopic assay for the detection of protein–protein interactions. *Analytical Sciences* 2008;24:907-10.
- [273] Bergen JM, von Recum HA, Goodman TT, Massey AP, Pun SH. Gold Nanoparticles as a Versatile Platform for Optimizing Physicochemical Parameters for Targeted Drug Delivery. *Macromol Biosci* 2006;6:506-16.
- [274] Pissuwan D, Cortie CH, Valenzuela SM, Cortie MB. Gold Nanosphere-Antibody Conjugates for Hyperthermal Therapeutic Applications. *Gold Bulletin* 2007;40:121-9.
- [275] Schmid G. Large clusters and colloids. Metals in the embryonic state. *Chem Rev* 1992;92(8):1709-27.
- [276] Link S, El-Sayed MA. Size and temperature dependence of the plasmon absorption of colloidal gold nanoparticles. *The Journal of Physical Chemistry B* 1999;103(21):4212-7.
- [277] Link S, El-Sayed MA. Spectral properties and relaxation dynamics of surface plasmon electronic oscillations in gold and silver nanodots and nanorods. *The Journal of Physical Chemistry B* 1999;103(40):8410-26.
- [278] Su KH, Wei QH, Zhang X, Mock JJ, Smith DR, Schultz S. interparticle coupling effects on plasmon resonances of nanogold particles. *Nano Letters* 2003;3(8):1087-90.
- [279] Read T, Olkhov RV, Shaw AM. Measurement of the localised plasmon penetration depth for gold nanoparticles using a non-invasive bio-stacking method. *Physical Chemistry Chemical Physics* 2013;15(16):6122-7.
- [280] Aslan K, R. LJ, Geddes CD. Nanogold-plasmon-resonance-based glucose sensing. *Anal Biochem* 2004;330:144-55.
- [281] Haiss W, Thanh NTK, Aveyard J, Fernig DG. Determination of Size and Concentration of Gold Nanoparticles from UV-Vis Spectra. *Anal Chem* 2007;79:4215-21.
- [282] Willets KA, Van Duyne RP. Localized Surface Plasmon Resonance Spectroscopy and Sensing. *Annu Rev Phys Chem* 2007;58(1):267-97.
- [283] He L, Musick MD, Nicewarner SR, Salinas FG, Benkovic SJ, Natan MJ, et al. Colloidal Au-Enhanced Surface Plasmon Resonance for Ultrasensitive Detection of DNA Hybridization. *Journal of the American Chemical Society* 2000;122(38):9071-7.
- [284] Russel WB, Saville DA, Schowalter WR. *Colloidal Dispersions*: Cambridge University Press, 1992.
- [285] Behrens SH, Christl DI, Emmerzael R, Schurtenberger P, Borkovec M. Charging and aggregation properties of carboxyl latex particles: Experiments versus DLVO theory. *Langmuir* 2000;16(6):2566-75.
- [286] Sattler KD. *Handbook of Nanophysics: Nanoparticles and Quantum Dots*: Taylor & Francis, 2010.

## References

- [287] Lu X, Rycenga M, Skrabalak SE, Wiley B, Xia Y. Chemical Synthesis of Novel Plasmonic Nanoparticles. *Annu Rev Phys Chem* 2009;60(1):167-92.
- [288] Liz-Marzán LM. Tailoring surface plasmons through the morphology and assembly of metal nanoparticles. *Langmuir* 2005;22(1):32-41.
- [289] Hong Y, Huh Y-M, Yoon DS, Yang J. Nanobiosensors Based on Localized Surface Plasmon Resonance for Biomarker Detection. *Journal of Nanomaterials* 2012;2012:13.
- [290] Hilleman MR. Newer Directions in Vaccine Development and Utilization. *The Journal of Infectious Diseases* 1985;151(3):407-19.
- [291] Szmunes W, Stevens CE, Harley EJ, Zang EA, Oleszko WR, William DC, et al. Hepatitis B Vaccine. *N Engl J Med* 1980;303(15):833-41.
- [292] Pablo V, Angelica M, William JR, Gustav A, Benjamin DH. Synthesis and assembly of hepatitis B virus surface antigen particles in yeast. *Nature* 1982;298(5872):347-50.
- [293] Keam S, Harper D. Human Papillomavirus Types 16 and 18 Vaccine (Recombinant, AS04 Adjuvanted Adsorbed) [Cervarix™]. *Drugs* 2008;68(3):359-72.
- [294] McLemore MR. Gardasil: Introducing the new human papillomavirus vaccine. *Clin J Oncol Nurs* 2006;10(5):559-60.
- [295] Reece JC, Geysen HM, Rodda SJ. Mapping the major human T helper epitopes of tetanus toxin. The emerging picture. *The Journal of Immunology* 1993;151(11):6175-84.
- [296] Valmori D, Pessi A, Bianchi E, Corradin G. Use of human universally antigenic tetanus toxin T cell epitopes as carriers for human vaccination. *The Journal of Immunology* 1992;149(2):717-21.
- [297] Petrovsky N, Aguilar JC. Vaccine adjuvants: current state and future trends. *Immunol Cell Biol* 2004;82(5):488-96.
- [298] Cellerai C, Harari A, Vallelian F, Boyman O, Pantaleo G. Functional and phenotypic characterization of tetanus toxoid-specific human CD4+ T cells following re-immunization. *Eur J Immunol* 2007;37(4):1129-38.
- [299] Vitiello A, Ishioka G, Grey HM, Rose R, Farness P, LaFond R, et al. Development of a lipopeptide-based therapeutic vaccine to treat chronic HBV infection. I. Induction of a primary cytotoxic T lymphocyte response in humans. *The Journal of clinical investigation* 1995;95(1):341-9.
- [300] Ben-Yedidia T, Tarrab-Hazdai R, Schechtman D, Arnon R. Intranasal administration of synthetic recombinant peptide-based vaccine protects mice from infection by schistosoma mansoni. *Infect Immun* 1999;67(9):4360-6.
- [301] Honko AN, Sriranganathan N, Lees CJ, Mizel SB. Flagellin Is an Effective Adjuvant for Immunization against Lethal Respiratory Challenge with *Yersinia pestis*. *Infect Immun* 2006;74(2):1113-20.
- [302] Lee LH, Burg E, Baqar S, Bourgeois AL, Burr DH, Ewing CP, et al. Evaluation of a Truncated Recombinant Flagellin Subunit Vaccine against *Campylobacter jejuni*. *Infect Immun* 1999;67(11):5799-805.
- [303] Song L, Zhang Y, Yun NE, Poussard AL, Smith JN, Smith JK, et al. Superior efficacy of a recombinant flagellin:H5N1 HA globular head vaccine is determined by the placement of the globular head within flagellin. *Vaccine* 2009;27(42):5875-84.
- [304] Smith KD, Andersen-Nissen E, Hayashi F, Strobe K, Bergman MA, Barrett SL, et al. Toll-like receptor 5 recognizes a conserved site on flagellin required for protofilament formation and bacterial motility. *Nature immunology* 2003;4(12):1247-53.
- [305] McDermott PF, Ciacci-Woolwine F, Snipes JA, Mizel SB. High-affinity interaction between Gram-negative flagellin and a cell surface polypeptide results in human monocyte activation. *Infect Immun* 2000;68(10):5525-9.
- [306] Bates JT, Honko AN, Graff AH, Kock ND, Mizel SB. Mucosal adjuvant activity of flagellin in aged mice. *Mech Ageing Dev* 2008;129(5):271-81.
- [307] Gewirtz AT, Navas TA, Lyons S, Godowski PJ, Madara JL. Cutting edge: bacterial flagellin activates basolaterally expressed TLR5 to induce epithelial proinflammatory gene expression. *Journal of immunology (Baltimore, Md : 1950)* 2001;167(4):1882-5.

## References

- [308] Cho EC, Glaus C, Chen J, Welch MJ, Xia Y. Inorganic nanoparticle-based contrast agents for molecular imaging. *Trends Mol Med* 2010;16(12):561-73.
- [309] Fang C, Bhattarai N, Sun C, Zhang M. Functionalized Nanoparticles with Long-Term Stability in Biological Media. *Small* 2009;5(14):1637-41.
- [310] Mohammed B, Jamie RL. Nanoparticle dispersity in toxicology. *Nat Nanotechnol* 2013;8(5):308-9.
- [311] Williamson ED, Packer PJ, Waters EL, Simpson AJ, Dyer D, Hartings J, et al. Recombinant (F1+V) vaccine protects cynomolgus macaques against pneumonic plague. *Vaccine* 2011;29(29-30):4771-7.
- [312] Haug R. *Advances in Solid State Physics 46*: Springer Berlin Heidelberg, 2010.
- [313] Kreibig U, Vollmer M. *Optical properties of metal clusters*: Springer, 1995.
- [314] Brewer SH, Glomm WR, Johnson MC, Knag MK, Franzen S. Probing BSA Binding to Citrate-Coated Gold Nanoparticles and Surfaces. *Langmuir* 2005;21:9303-7.
- [315] Gebauer JS, Malissek M, Simon S, Knauer SK, Maskos M, Stauber RH, et al. Impact of the Nanoparticle-Protein Corona on Colloidal Stability and Protein Structure. *Langmuir* 2012;28(25):9673-9.
- [316] Tenzer S, Docter D, Rosfa S, Wlodarski A, Kuharev J, Rekić A, et al. Nanoparticle Size Is a Critical Physicochemical Determinant of the Human Blood Plasma Corona: A Comprehensive Quantitative Proteomic Analysis. *ACS Nano* 2011;5(9):7155-67.
- [317] Cedervall T, Lynch I, Lindman S, Berggård T, Thulin E, Nilsson H, et al. Understanding the nanoparticle-protein corona using methods to quantify exchange rates and affinities of proteins for nanoparticles. *PNAS* 2007;104:2050-5.
- [318] Kah JCY, Chen J, Zubieta A, Hamad-Schifferli K. Exploiting the Protein Corona around Gold Nanorods for Loading and Triggered Release. *ACS Nano* 2012;6(8):6730-40.
- [319] Lundqvist M, Stigler J, Elia G, Lynch I, Cedervall T, Dawson KA. Nanoparticle size and surface properties determine the protein corona with possible implications for biological impacts. *PNAS* 2008;105(38):14265-70.
- [320] Pan H, Qin M, Meng W, Cao Y, Wang W. How Do Proteins Unfold upon Adsorption on Nanoparticle Surfaces? *Langmuir* 2012;28(35):12779-87.
- [321] Chen Y-H, Tsai C-Y, Huang P-Y, Chang M-Y, Cheng P-C, Chou C-H, et al. Methotrexate Conjugated to Gold Nanoparticles Inhibits Tumor Growth in a Syngeneic Lung Tumor Model. *Molecular Pharmaceutics* 2007;4(5):713-22.
- [322] Thomas M, Klibanov AM. Conjugation to gold nanoparticles enhances polyethylenimine's transfer of plasmid DNA into mammalian cells. *PNAS* 2003;100(16):9138-43.
- [323] Gibson JD, Khanal BP, Zubarev ER. Paclitaxel-Functionalized Gold Nanoparticles. *Journal of the American Chemical Society* 2007;129(37):11653-61.
- [324] Patel N, Davies MC, Hartshorne M, Heaton RJ, Roberts CJ, Tendler SJB, et al. Immobilization of Protein Molecules onto Homogeneous and Mixed Carboxylate-Terminated Self-Assembled Monolayers. *Langmuir* 1997;13(24):6485-90.
- [325] Chirra HD, Sexton T, Biswal D, Hersh LB, Hilt JZ. Catalase-coupled gold nanoparticles: Comparison between the carbodiimide and biotin-streptavidin methods. *Acta Biomater* 2011;7(7):2865-72.
- [326] Jahanshahi M, Zhang Z, Lyddiatt A. Subtractive chromatography for purification and recovery of nano-bioproducts. *IEE Proc Nanobiotechnol* 2005;152(3):121-6.
- [327] Limayem I, Charcosset C, Fessi H. Purification of nanoparticle suspensions by a concentration/diafiltration process. *Sep Purif Technol* 2004;38(1):1-9.
- [328] Simpson WJ, Thomas RE, Schwan TG. Recombinant capsular antigen (fraction 1) from *Yersinia pestis* induces a protective antibody response in BALB/c mice. *Am J Trop Med Hyg* 1990;43(4):389-96.
- [329] Andrews GP, Heath DG, Anderson GW, Jr., Welkos SL, Friedlander AM. Fraction 1 capsular antigen (F1) purification from *Yersinia pestis* CO92 and from an *Escherichia coli*

## References

- recombinant strain and efficacy against lethal plague challenge. *Infect Immun* 1996;64(6):2180-7.
- [330] Quenee LE, Ciletti NA, Elli D, Hermanas TM, Schneewind O. Prevention of pneumonic plague in mice, rats, guinea pigs and non-human primates with clinical grade rV10, rV10-2 or F1-V vaccines. *Vaccine* 2011;29(38):6572-83.
- [331] Alonso MJ, Gupta RK, Min C, Siber GR, Langer R. Biodegradable microspheres as controlled-release tetanus toxoid delivery systems. *Vaccine* 1994;12(4):299-306.
- [332] Alonso MJ, Cohen S, Park TG, Gupta RK, Siber GR, Langer R. Determinants of Release Rate of Tetanus Vaccine from Polyester Microspheres. *Pharmaceutical Research* 1993;10(7).
- [333] O'Hagan DT, Jeffery H, Roberts MJJ, McGee JP, Davis SS. Controlled release microparticles for vaccine development. *Vaccine* 1991;9(10):768-71.
- [334] Ozaki A, Fukata K, Fukushima A, Yasuoka M, Yoshida O, Ueno H. Suppression or exacerbation of experimental autoimmune uveoretinitis in Lewis rats by pretreatment with or without an autoantigenic peptide in aluminum hydroxide. *Jpn J Ophthalmol* 2003;47(1):102-6.
- [335] Kool M, Soullié T, van Nimwegen M, Willart MAM, Muskens F, Jung S, et al. Alum adjuvant boosts adaptive immunity by inducing uric acid and activating inflammatory dendritic cells. *The Journal of Experimental Medicine* 2008;205(4):869-82.
- [336] Parween S, Gupta PK, Chauhan VS. Induction of humoral immune response against PfMSP-1(19) and PvMSP-1(19) using gold nanoparticles along with alum. *Vaccine* 2011;29(13):2451-60.
- [337] Wang Y-T, Lu X-M, Zhu F, Huang P, Yu Y, Zeng L, et al. The use of a gold nanoparticle-based adjuvant to improve the therapeutic efficacy of hNgR-Fc protein immunization in spinal cord-injured rats. *Biomaterials* 2011;32(31):7988-98.
- [338] Williamson ED, Flick-Smith HC, Waters E, Miller J, Hodgson I, Le Butt CS, et al. Immunogenicity of the rF1+rV vaccine for plague with identification of potential immune correlates. *Microbial Pathogenesis* 2007;42(1):11-21.
- [339] Williamson ED, Eley SM, Stagg AJ, Green M, Russell P, Titball RW. A sub-unit vaccine elicits IgG in serum, spleen cell cultures and bronchial washings and protects immunized animals against pneumonic plague. *Vaccine* 1997;15(10):1079-84.
- [340] Williamson ED, Vesey PM, Gillhespy KJ, Eley SM, Green M, Titball RW. An IgG1 titre to the F1 and V antigens correlates with protection against plague in the mouse model. *Clin Exp Immunol* 1999;116(1):107-14.
- [341] Wiersinga WJ, Currie BJ, Peacock SJ. Melioidosis. *N Engl J Med* 2012;367(11):1035-44.
- [342] Yabuuchi E, Kosako Y, Oyaizu H, Yano I, Hotta H, Hashimoto Y, et al. Proposal of *Burkholderia* gen. nov. and transfer of seven species of the genus *Pseudomonas* homology group II to the new genus, with the type species *Burkholderia cepacia* (Palleroni and Holmes 1981) comb. nov. *Microbiol Immunol* 1992;36(12):1251-75.
- [343] Nierman WC, DeShazer D, Kim HS, Tettelin H, Nelson KE, Feldblyum T, et al. Structural flexibility in the *Burkholderia mallei* genome. *Proc Natl Acad Sci U S A* 2004;101(39):14246-51.
- [344] Holden MT, Titball RW, Peacock SJ, Cerdeño-Tárraga AM, Atkins T, Crossman LC, et al. Genomic plasticity of the causative agent of melioidosis, *Burkholderia pseudomallei*. *PNAS* 2004;101:14240 - 5.
- [345] Wiersinga WJ, van der Poll T, White NJ, Day NP, Peacock SJ. Melioidosis: insights into the pathogenicity of *Burkholderia pseudomallei*. *Nature reviews* 2006;4:272-82.
- [346] Brett PJ, Deshazer D, Woods DE. Characterization of *Burkholderia pseudomallei* and *Burkholderia pseudomallei*-like strains. *Epidemiol Infect* 1997;118(2):137-48.
- [347] Wuthiekanun V, Smith MD, Dance DAB, Walsh AL, Pitt TL, White NJ. Biochemical characteristics of clinical and environmental isolates of *Burkholderia pseudomallei*. *Journal of Medical Microbiology* 1996;45(6):408-12.
- [348] Brett PJ, DeShazer D, Woods DE. *Burkholderia thailandensis* sp. nov., a *Burkholderia pseudomallei*-like species. *Int J Syst Bacteriol* 1998;48 Pt 1:317-20.

## References

- [349] Wajanarogana S, Sonthayanon P, Wuthiekanun V, Panyim S, Simpson AJ, Tungpradabkul S. Stable marker on flagellin gene sequences related to arabinose non-assimilating pathogenic *Burkholderia pseudomallei*. *Microbiol Immunol* 1999;43(11):995-1001.
- [350] Kespichayawattana W, Rattanachetkul S, Wanun T, Utaisincharoen P, Sirisinha S. *Burkholderia pseudomallei* Induces Cell Fusion and Actin-Associated Membrane Protrusion: a Possible Mechanism for Cell-to-Cell Spreading. *Infect Immun* 2000;68(9):5377-84.
- [351] Burtnick MN, Brett PJ, Harding SV, Ngugi SA, Ribot WJ, Chantratita N, et al. The Cluster 1 Type VI Secretion System Is a Major Virulence Determinant in *Burkholderia pseudomallei*. *Infect Immun* 2011;79(4):1512-25.
- [352] Sun GW, Lu J, Pervaiz S, Cao WP, Gan Y-H. Caspase-1 dependent macrophage death induced by *Burkholderia pseudomallei*. *Cell Microbiol* 2005;7(10):1447-58.
- [353] Whitlock GC, Mark Estes D, Torres AG. Glanders: off to the races with *Burkholderia mallei*. *FEMS Microbiol Lett* 2007;277(2):115-22.
- [354] Patel N, Conejero L, De Reynal M, Easton A, Bancroft GJ, Titball RW. Development of vaccines against *Burkholderia pseudomallei*. *Frontiers in microbiology* 2011;2:198.
- [355] Silva EB, Dow SW. Development of *Burkholderia mallei* and *pseudomallei* vaccines. *Front Cell Infect Microbiol* 2013;3:10.
- [356] Khan I, Wieler LH, Melzer F, Elschner MC, Muhammad G, Ali S, et al. Glanders in animals: a review on epidemiology, clinical presentation, diagnosis and countermeasures. *Transbound Emerg Dis* 2013;60(3):204-21.
- [357] Galyov EE, Brett PJ, DeShazer D. Molecular insights into *Burkholderia pseudomallei* and *Burkholderia mallei* pathogenesis. *Annu Rev Microbiol* 2010;64:495-517.
- [358] Manzo E, Molinaro A, Bedini E, De Castro C, Parrilli M. A very efficient method to cleave Lipid A and saccharide components in bacterial lipopolysaccharides. *Carbohydrate Research* 2001;333(4):339-42.
- [359] Chuaygud T, Tungpradabkul S, Sirisinha S, Chua KL, Utaisincharoen P. A role of *Burkholderia pseudomallei* flagella as a virulent factor. *Transactions of the Royal Society of Tropical Medicine and Hygiene* 2008;102(Supplement 1):S140-S4.
- [360] Chalabaev S, Kim TH, Ross R, Derian A, Kasper DL. 3-Deoxy-D-manno-octulosonic acid (Kdo) hydrolase identified in *Francisella tularensis*, *Helicobacter pylori*, and *Legionella pneumophila*. *J Biol Chem* 2010;285(45):34330-6.
- [361] Winstanley C, Hales BA, Corkill JE, Gallagher MJ, Hart CA. Flagellin gene variation between clinical and environmental isolates of *Burkholderia pseudomallei* contrasts with the invariance among clinical isolates. *Journal of Medical Microbiology* 1998;47(8):689-94.
- [362] Wiersinga WJ, van der Poll T. *Burkholderia pseudomallei* Tropism and the Melioidosis Road Map. *Journal of Infectious Diseases* 2009;199(12):1720-2.
- [363] Inglis TJ, Garrow SC, Adams C, Henderson M, Mayo M, Currie BJ. Acute melioidosis outbreak in Western Australia. *Epidemiol Infect* 1999;123(3):437-43.
- [364] Currie BJ, Mayo M, Anstey NM, Donohoe P, Haase A, Kemp DJ. A cluster of melioidosis cases from an endemic region is clonal and is linked to the water supply using molecular typing of *Burkholderia pseudomallei* isolates. *Am J Trop Med Hyg* 2001;65(3):177-9.
- [365] Dance DA. Melioidosis: the tip of the iceberg? *Clinical Microbiology Reviews* 1991;4(1):52-60.
- [366] Chaowagul W, White NJ, Dance DAB, Wattanagoon Y, Naigowit P, Davis TME, et al. Melioidosis: A Major Cause of Community-Acquired Septicemia in Northeastern Thailand. *The Journal of Infectious Diseases* 1989;159(5):890-9.
- [367] White NJ. Melioidosis. *The Lancet* 2003;361(9370):1715-22.
- [368] Chetchotisakd P, Anunnatsiri S, Kiatchoosakun S, Kularbkaew C. Melioidosis Pericarditis Mimicking Tuberculous Pericarditis. *Clinical infectious diseases* 2010;51(5):e46-e9.
- [369] Vidyalakshmi K, Chakrapani M, Shrikala B, Damodar S, Lipika S, Vishal S. Tuberculosis mimicked by melioidosis. *The international journal of tuberculosis and lung disease : the official journal of the International Union against Tuberculosis and Lung Disease* 2008;12(10):1209-15.

## References

- [370] Saravu K, Mukhopadhyay C, Eshwara V, Shastry B, Ramamoorthy K, Krishna S, et al. Melioidosis presenting with mediastinal lymphadenopathy masquerading as malignancy: a case report. *J Med Case Reports* 2012;6(1):28.
- [371] Wong K, Puthuchearu S, Vadivelu J. The histopathology of human melioidosis. *Histopathology* 1995;26:51 - 5.
- [372] Vatcharapreechasakul T, Suputtamongkol Y, Dance DAB, Chaowagul W, White NJ. *Pseudomonas pseudomallei* Liver Abscesses: A Clinical, Laboratory, and Ultrasonographic Study. *Clinical infectious diseases* 1992;14(2):412-7.
- [373] Rode JW, Webling DD. Melioidosis in the Northern Territory of Australia. *Med J Aust* 1981;1(4):181-4.
- [374] Currie BJ, Jacups SP. Intensity of rainfall and severity of melioidosis, Australia. *Emerg Infect Dis* 2003;9(12):1538-42.
- [375] Mukhopadhyay A, Lee KH, Tambyah PA. Bacteraemic melioidosis pneumonia: impact on outcome, clinical and radiological features. *J Infect* 2004;48(4):334-8.
- [376] Warawa J, Woods DE. Melioidosis vaccines. *Expert Rev Vaccines* 2002;1(4):477-82.
- [377] DeShazer D, Brett PJ, Carlyon R, Woods DE. Mutagenesis of *Burkholderia pseudomallei* with Tn5-OT182: isolation of motility mutants and molecular characterization of the flagellin structural gene. *J Bacteriol* 1997;179(7):2116-25.
- [378] Thibault FM, Valade E, Vidal DR. Identification and Discrimination of *Burkholderia pseudomallei*, *B. mallei*, and *B. thailandensis* by Real-Time PCR Targeting Type III Secretion System Genes. *Journal of Clinical Microbiology* 2004;42:5871-4.
- [379] Sprague LD, Zysk G, Hagen RM, Meyer H, Ellis J, Anuntagool N, et al. A possible pitfall in the identification of *Burkholderia mallei* using molecular identification systems based on the sequence of the flagellin *fliC* gene. *FEMS Immunology and Medical Microbiology* 2002;34(3):231-6.
- [380] Chua KL, Chan YY, Gan YH. Flagella Are Virulence Determinants of *Burkholderia pseudomallei*. *Infect Immun* 2003;71:1622-9.
- [381] Tomich M, Herfst CA, Golden JW, Mohr CD. Role of flagella in host cell invasion by *Burkholderia cepacia*. *Infect Immun* 2002;70(4):1799-806.
- [382] Brett PJ, Mah DC, Woods DE. Isolation and characterization of *Pseudomonas pseudomallei* flagellin proteins. *Infect Immun* 1994;62:1914 - 9.
- [383] Hayashi F, Smith KD, Ozinsky A, Hawn TR, Yi EC, Goodlett DR, et al. The innate immune response to bacterial flagellin is mediated by Toll-like receptor 5. *Nature* 2001;410(6832):1099-103.
- [384] Schell MA, Ulrich RL, Ribot WJ, Brueggemann EE, Hines HB, Chen D, et al. Type VI secretion is a major virulence determinant in *Burkholderia mallei*. *Molecular Microbiology* 2007;64:1466-85.
- [385] Shalom G, Shaw JG, Thomas MS. In vivo expression technology identifies a type VI secretion system locus in *Burkholderia pseudomallei* that is induced upon invasion of macrophages. *Microbiology* 2007;153(8):2689-99.
- [386] Panatto D, Amicizia D, Lai PL, Gasparini R. *Neisseria meningitidis* B vaccines. *Expert Rev Vaccines* 2011;10(9):1337-51.
- [387] French CT, Toesca IJ, Wu T-H, Teslaa T, Beaty SM, Wong W, et al. Dissection of the *Burkholderia* intracellular life cycle using a photothermal nanoblade. *PNAS* 2011;108(29):12095-100.
- [388] Williams SG, Varcoe LT, Attridge SR, Manning PA. *Vibrio cholerae* Hcp, a secreted protein coregulated with HlyA. *Infect Immun* 1996;64(1):283-9.
- [389] Snapper C, Paul W. Interferon-gamma and B cell stimulatory factor-1 reciprocally regulate Ig isotype production. *Science* 1987;236(4804):944-7.
- [390] Pukatzki S, Ma AT, Revel AT, Sturtevant D, Mekalanos JJ. Type VI secretion system translocates a phage tail spike-like protein into target cells where it cross-links actin. *Proc Natl Acad Sci U S A* 2007;104(39):15508-13.

## References

- [391] Quintana FJ, Solomon A, Cohen IR, Nussbaum G. Induction of IgG3 to LPS via Toll-Like Receptor 4 Co-Stimulation. *PLoS ONE* 2008;3(10):e3509.
- [392] Steinmetz I, Rohde M, Brenneke B. Purification and characterization of an exopolysaccharide of *Burkholderia (Pseudomonas) pseudomallei*. *Infect Immun* 1995;63:3959 - 65.
- [393] Isshiki Y, Matsuura M, Dejsirilert S, Ezaki T, Kawahara K. Separation of 6-deoxy-heptan [correction of 6-deoxy-heptane] from a smooth-type lipopolysaccharide preparation of *Burkholderia pseudomallei*. *FEMS microbiology letters* 2001;199(1):21-5.
- [394] Atkins T, Prior R, Mack K, Russell P, Nelson M, Prior J, et al. Characterisation of an acapsular mutant of *Burkholderia pseudomallei* identified by signature tagged mutagenesis. *Journal of Medical Microbiology* 2002;51(7):539-53.
- [395] Cuccui J, Easton A, Chu KK, Bancroft GJ, Oyston PC, Titball RW, et al. Development of signature-tagged mutagenesis in *Burkholderia pseudomallei* to identify genes important in survival and pathogenesis. *Infect Immun* 2007;75(3):1186-95.
- [396] Lopez J, Cops J, Wilhelmsen C, Moore R, Kubay J, St-Jacques M, et al. Characterization of experimental equine glanders. *Microbes Infect* 2003;5(12):1125-31.
- [397] Reckseidler-Zenteno SL, DeVinney R, Woods DE. The capsular polysaccharide of *Burkholderia pseudomallei* contributes to survival in serum by reducing complement factor C3b deposition. *Infect Immun* 2005;73(2):1106-15.
- [398] Wikraiphath C, Charoensap J, Utaisincharoen P, Wongratanacheewin S, Taweechaisupapong S, Woods DE, et al. Comparative in vivo and in vitro analyses of putative virulence factors of *Burkholderia pseudomallei* using lipopolysaccharide, capsule and flagellin mutants. *FEMS Immunol Med Microbiol* 2009;56(3):253-9.
- [399] Sim BM, Chantratita N, Ooi WF, Nandi T, Tewhey R, Wuthiekanun V, et al. Genomic acquisition of a capsular polysaccharide virulence cluster by non-pathogenic *Burkholderia* isolates. *Genome Biol* 2010;11(8):R89.
- [400] DeShazer D. Virulence of clinical and environmental isolates of *Burkholderia oklahomensis* and *Burkholderia thailandensis* in hamsters and mice. *FEMS Microbiol Lett* 2007;277(1):64-9.
- [401] Raetz CRH, Whitfield C. Lipopolysaccharide exotoxins. *Annu Rev Biochem* 2002;71(1):635-700.
- [402] Yamamoto M, Akira S. Lipid A Receptor TLR4-Mediated Signaling Pathways. In: Jeannin J-F, editor. *Lipid A in Cancer Therapy*: Springer New York, 2010: 59-68.
- [403] DeShazer D, Brett PJ, Woods DE. The type II O-antigenic polysaccharide moiety of *Burkholderia pseudomallei* lipopolysaccharide is required for serum resistance and virulence. *Molecular Microbiology* 1998;30(5):1081-100.
- [404] Brett PJ, Burtnick MN, Heiss C, Azadi P, DeShazer D, Woods DE, et al. *Burkholderia thailandensis* oacA Mutants Facilitate the Expression of *Burkholderia mallei*-Like O Polysaccharides. *Infect Immun* 2011;79(2):961-9.
- [405] Burtnick MN, Brett PJ, Woods DE. Molecular and physical characterization of *Burkholderia mallei* O antigens. *J Bacteriol* 2002;184(3):849-52.
- [406] Tuanyok A, Stone JK, Mayo M, Kaestli M, Gruendike J, Georgia S, et al. The Genetic and Molecular Basis of O-Antigenic Diversity in *Burkholderia pseudomallei* Lipopolysaccharide. *PLoS Negl Trop Dis* 2012;6(1):e1453.
- [407] Anuntagool N, Wuthiekanun V, White NJ, Currie BJ, Sermswan RW, Wongratanacheewin S, et al. Lipopolysaccharide heterogeneity among *Burkholderia pseudomallei* from different geographic and clinical origins. *The American Journal of Tropical Medicine and Hygiene* 2006;74(3):348-52.
- [408] Arjcharoen S, Wikraiphath C, Pudla M, Limposuwan K, Woods DE, Sirisinha S, et al. Fate of a *Burkholderia pseudomallei* lipopolysaccharide mutant in the mouse macrophage cell line RAW 264.7: possible role for the O-antigenic polysaccharide moiety of lipopolysaccharide in internalization and intracellular survival. *Infect Immun* 2007;75(9):4298-304.

## References

- [409] Bryan LE, Wong S, Woods DE, Dance DA, Chaowagul W. Passive protection of diabetic rats with antisera specific for the polysaccharide portion of the lipopolysaccharide isolated from *Pseudomonas pseudomallei*. The Canadian journal of infectious diseases = Journal canadien des maladies infectieuses 1994;5(4):170-8.
- [410] Treviño SR, Permenter AR, England MJ, Parthasarathy N, Gibbs PH, Waag DM, et al. Monoclonal Antibodies Passively Protect BALB/c Mice against *Burkholderia mallei* Aerosol Challenge. Infect Immun 2006;74(3):1958-61.
- [411] Jones SM, Ellis JF, Russell P, Griffin KF, Oyston PCF. Passive protection against *Burkholderia pseudomallei* infection in mice by monoclonal antibodies against capsular polysaccharide, lipopolysaccharide or proteins. Journal of Medical Microbiology 2002;51:1055 - 62.
- [412] AuCoin DP, Reed DE, Marlenee NL, Bowen RA, Thorkildson P, Judy BM, et al. Polysaccharide Specific Monoclonal Antibodies Provide Passive Protection against Intranasal Challenge with *Burkholderia pseudomallei*. PLoS ONE 2012;7(4):e35386.
- [413] Sarkar-Tyson M, Thwaite JE, Harding SV, Smither SJ, Oyston PCF, Atkins TP, et al. Polysaccharides and virulence of *Burkholderia pseudomallei*. Journal of Medical Microbiology 2007;56:1005-10.
- [414] Ngugi SA, Ventura VV, Qazi O, Harding SV, Kitto GB, Estes DM, et al. Lipopolysaccharide from *Burkholderia thailandensis* E264 provides protection in a murine model of melioidosis. Vaccine 2010;28(47):7551-5.
- [415] Makela PH. Conjugate vaccines--a breakthrough in vaccine development. Southeast Asian J Trop Med Public Health 2003;34(2):249-53.
- [416] Kaplan SL, Lauer BA, Ward MA, Wiedermann BL, Boyer KM, Dukes CM, et al. Immunogenicity and safety of *Haemophilus influenzae* type b-tetanus protein conjugate vaccine alone or mixed with diphtheria-tetanus-pertussis vaccine in infants. J Pediatr 1994;124(2):323-7.
- [417] Robbins JB, Schneerson R. Polysaccharide-Protein Conjugates: A New Generation of Vaccines. Journal of Infectious Diseases 1990;161(5):821-32.
- [418] Sigurdardottir ST, Vidarsson G, Gudnason T, Kjartansson S, Kristinsson KG, Jonsson S, et al. Immune responses of infants vaccinated with serotype 6B pneumococcal polysaccharide conjugated with tetanus toxoid. Pediatr Infect Dis J 1997;16(7):667-74.
- [419] Chen Y-S, Hsiao Y-S, Lin H-H, Yen C-M, Chen S-C, Chen Y-L. Immunogenicity and anti-*Burkholderia pseudomallei* activity in Balb/c mice immunized with plasmid DNA encoding flagellin. Vaccine 2006;24(6):750-8.
- [420] Osborn MJ, Rosen SM, Rothfield L, Zeleznick LD, Horecker BL. Lipopolysaccharide of the Gram-Negative Cell Wall: Biosynthesis of a complex heteropolysaccharide occurs by successive addition of specific sugar residues. Science 1964;145(3634):783-9.
- [421] Todar K. Online textbook of bacteriology. Structure and function of bacterial cells, 2009.
- [422] Nelson M, Prior JL, Lever MS, Jones HE, P. AT, Titball RW. Evaluation of lipopolysaccharide and capsular polysaccharide as subunit vaccines against experimental melioidosis. Journal of Medical Microbiology 2004;53:1177-82.
- [423] Bystricky S, Paulovicova E, Machova E. Synthesis and immunogenicity of polysaccharide-protein conjugate composed of galactoglucoylomannan of *Cryptococcus laurentii*. FEMS microbiology letters 2004;235(2):311-4.
- [424] Kaban Ş, Fidaner Z. Synthesis of Schiff bases by condensation of hetarylcarboxaldehydes with<i> &lt;i>phenetidine. Monatshefte für Chemie / Chemical Monthly 1990;121(6):525-8.
- [425] Chegel V, Shirshov Y, Avilov S, Demchenko M, Mustafaev M. A novel aldehyde dextran sulfonate matrix for affinity biosensors. J Biochem Biophys Methods 2002;50(2-3):201-16.
- [426] Brett PJ, Burtnick MN, Snyder DS, Shannon JG, Azadi P, Gherardini FC. *Burkholderia mallei* expresses a unique lipopolysaccharide mixture that is a potent activator of human Toll-like receptor 4 complexes. Molecular Microbiology 2007;63(2):379-90.

## References

- [427] Rao P, Pattabiraman TN. Further studies on the mechanism of phenol-sulfuric acid reaction with furaldehyde derivatives. *Anal Biochem* 1990;189(2):178-81.
- [428] Novem V, Shui G, Wang D, Bendt AK, Sim SH, Liu Y, et al. Structural and biological diversity of lipopolysaccharides from *Burkholderia pseudomallei* and *Burkholderia thailandensis*. *Clin Vaccine Immunol* 2009;16(10):1420-8.
- [429] Brett PJ, Woods DE. Structural and Immunological Characterization of *Burkholderia pseudomallei* O-Polysaccharide-Flagellin Protein Conjugates. *Infect Immun* 1996;64(7):2824-8.
- [430] Balestrino D, Ghigo J-M, Charbonnel N, Haagensen JAJ, Forestier C. The characterization of functions involved in the establishment and maturation of *Klebsiella pneumoniae* in vitro biofilm reveals dual roles for surface exopolysaccharides. *Environ Microbiol* 2008;10(3):685-701.
- [431] De Araujo C, Balestrino D, Roth L, Charbonnel N, Forestier C. Quorum sensing affects biofilm formation through lipopolysaccharide synthesis in *Klebsiella pneumoniae*. *Res Microbiol* 2010;161(7):595-603.
- [432] Huang T-P, Somers EB, Wong ACL. Differential biofilm formation and motility associated with lipopolysaccharide/exopolysaccharide-coupled biosynthetic genes in *Stenotrophomonas maltophilia*. *J Bacteriol* 2006;188(8):3116-20.
- [433] Spears PA, Temple LM, Orndorff PE. A role for lipopolysaccharide in turkey tracheal colonization by *Bordetella avium* as demonstrated in vivo and in vitro. *Molecular Microbiology* 2000;36(6):1425-35.
- [434] Gregory AE, Williamson ED, Prior JL, Butcher WA, Thompson IJ, Shaw AM, et al. Conjugation of *Y. pestis* F1-antigen to gold nanoparticles improves immunogenicity. *Vaccine* 2012;30(48):6777-82.
- [435] Pawlowski A, Källenius G, Svenson SB. Preparation of pneumococcal capsular polysaccharide-protein conjugate vaccines utilizing new fragmentation and conjugation technologies. *Vaccine* 2000;18(18):1873-85.
- [436] Michon F, Fusco PC, Minetti CASA, Laude-Sharp M, Uitz C, Huang C-H, et al. Multivalent pneumococcal capsular polysaccharide conjugate vaccines employing genetically detoxified pneumolysin as a carrier protein. *Vaccine* 1998;16(18):1732-41.
- [437] Costantino P, Viti S, Podda A, Velmonte MA, Nencioni L, Rappuoli R. Development and phase 1 clinical testing of a conjugate vaccine against meningococcus A and C. *Vaccine* 1992;10(10):691-8.
- [438] Gildersleeve JC, Oyelaran O, Simpson JT, Allred B. Improved Procedure for Direct Coupling of Carbohydrates to Proteins via Reductive Amination. *Bioconjugate Chemistry* 2008;19(7):1485-90.
- [439] Burtnick MN, Heiss C, Schuler AM, Azadi P, Brett PJ. Development of novel O-polysaccharide based glycoconjugates for immunization against glanders. *Frontiers in Cellular and Infection Microbiology* 2012;2.
- [440] Dubois M, Gilles K, Hamilton JK, Rebers PA, Smith F. A colorimetric method for the determination of sugars. *Nature* 1951;168(4265):167.
- [441] Lee YC, McKelvy JF, Lang D. Rapid automatic analysis of sugar components of glycoproteins. II. Neutral sugars. *Anal Biochem* 1969;27(3):567-74.
- [442] Snapper CM, Marcu KB, Zelazowski P. The Immunoglobulin Class Switch: Beyond "Accessibility". *Immunity* 1997;6(3):217-23.
- [443] Haque A, Chu K, Easton A, Stevens MP, Galyov EE, Atkins T, et al. A Live Experimental Vaccine against *Burkholderia pseudomallei* Elicits CD4+ T Cell-Mediated Immunity, Priming T Cells Specific for 2 Type III Secretion System Proteins. *The Journal of Infectious Diseases* 2006;194:1241-8.
- [444] Pirofski LA, Casadevall A. Use of licensed vaccines for active immunization of the immunocompromised host. *Clinical Microbiology Reviews* 1998;11(1):1-26.
- [445] Jonsson R, Pitts A, Mestecky J, Koopman W. Local IgA and IgM rheumatoid factor production in autoimmune MRL/lpr mice. *Autoimmunity* 1991;10(1):7-14.

## References

- [446] Giordani L, Sanchez M, Libri I, Quaranta MG, Mattioli B, Viora M. IFN- $\alpha$  amplifies human naïve B cell TLR-9-mediated activation and Ig production. *J Leukocyte Biol* 2009;86(2):261-71.
- [447] Hanten J, Vasilakos J, Riter C, Neys L, Lipson K, Alkan S, et al. Comparison of human B cell activation by TLR7 and TLR9 agonists. *BMC Immunol* 2008;9(1):39.
- [448] Kikuchi K, Lian Z-X, Yang G-X, Ansari AA, Ikehara S, Kaplan M, et al. Bacterial CpG induces hyper-IgM production in CD27+ memory B cells in primary biliary cirrhosis. *Gastroenterology* 2005;128(2):304-12.
- [449] Wellek B, Hahn H, Opferkuch W. Opsonizing activities of IgG, IgM antibodies and the C3b inactivator-cleaved third component of complement in macrophage phagocytosis. *Agents Actions* 1976;6(1-3):260-2.
- [450] Hoskins J, Alborn WE, Arnold J, Blaszczyk LC, Burgett S, DeHoff BS, et al. Genome of the Bacterium *Streptococcus pneumoniae* Strain R6. *J Bacteriol* 2001;183(19):5709-17.
- [451] Pletz MW, Maus U, Krug N, Welte T, Lode H. Pneumococcal vaccines: mechanism of action, impact on epidemiology and adaptation of the species. *Int J Antimicrob Agents* 2008;32(3):199-206.
- [452] Poland GA. The burden of pneumococcal disease: the role of conjugate vaccines. *Vaccine* 1999;17(13-14):1674-9.
- [453] Nelson AL, Roche AM, Gould JM, Chim K, Ratner AJ, Weiser JN. Capsule Enhances Pneumococcal Colonization by Limiting Mucus-Mediated Clearance. *Infect Immun* 2007;75(1):83-90.
- [454] Jonsson S, Musher DM, Chapman A, Goree A, Lawrence EC. Phagocytosis and Killing of Common Bacterial Pathogens of the Lung by Human Alveolar Macrophages. *Journal of Infectious Diseases* 1985;152(1):4-13.
- [455] Hammerschmidt S, Wolff S, Hocke A, Rosseau S, Müller E, Rohde M. Illustration of Pneumococcal Polysaccharide Capsule during Adherence and Invasion of Epithelial Cells. *Infect Immun* 2005;73(8):4653-67.
- [456] Park IH, Pritchard DG, Cartee R, Brandao A, Brandileone MCC, Nahm MH. Discovery of a New Capsular Serotype (6C) within Serogroup 6 of *Streptococcus pneumoniae*. *Journal of Clinical Microbiology* 2007;45(4):1225-33.
- [457] Scott JAG, Hall AJ, Dagan R, Dixon JMS, Eykyn SJ, Fenoll A, et al. Serogroup-Specific Epidemiology of *Streptococcus pneumoniae*: Associations with Age, Sex, and Geography in 7,000 Episodes of Invasive Disease. *Clinical infectious diseases* 1996;22(6):973-81.
- [458] Arnold KE, Leggiadro RJ, Breiman RF, Lipman HB, Schwartz B, Appleton MA, et al. Risk factors for carriage of drug-resistant *Streptococcus pneumoniae* among children in Memphis, Tennessee. *The Journal of Pediatrics* 1996;128(6):757-64.
- [459] Duchin JS, Breiman RF, Diamond A, Lipman HB, Block SL, Hedrick JA, et al. High prevalence of multidrug-resistant *Streptococcus pneumoniae* among children in a rural Kentucky community. *Pediatr Infect Dis J* 1995;14(9):745-50.
- [460] Hofmann J, Cetron MS, Farley MM, Baughman WS, Facklam RR, Elliott JA, et al. The Prevalence of Drug-Resistant *Streptococcus pneumoniae* In Atlanta. *N Engl J Med* 1995;333(8):481-6.
- [461] Stroop CJ, Xu Q, Retzlaff M, Abeygunawardana C, Bush CA. Structural analysis and chemical depolymerization of the capsular polysaccharide of *Streptococcus pneumoniae* type 1. *Carbohydrate Research* 2002;337(4):335-44.
- [462] Jansson P-E, Lindberg B, Andersson M, Lindquist U, Henrichsen J. Structural studies of the capsular polysaccharide from *Streptococcus pneumoniae* type 2, a reinvestigation. *Carbohydrate Research* 1988;182(1):111-7.
- [463] Reeves RE, Goebel WF. Chemoimmunological studies on the soluble specific substance of pneumococcus: v. the structure of the type iii polysaccharide. *Journal of Biological Chemistry* 1941;139(2):511-9.

## References

- [464] Jones C, Currie F, Forster MJ. Nmr and conformational analysis of the capsular polysaccharide from *Streptococcus pneumoniae* type 4. Carbohydrate Research 1991;221(1):95-121.
- [465] Jansson P-E, Lindberg B, Lindquist U. Structural studies of the capsular polysaccharide from *Streptococcus pneumoniae* type 5. Carbohydrate Research 1985;140(1):101-10.
- [466] Kenne L, Lindberg B, Madden JK. Structural studies of the capsular antigen from *Streptococcus pneumoniae* type 26. Carbohydrate Research 1979;73(1):175-82.
- [467] Jones C, Mulloy B, Wilson A, Dell A, Oates JE. Structure of the capsular polysaccharide from *Streptococcus pneumoniae* type 9. J Chem Soc, Perkin Trans 1 1985:1665-73.
- [468] Rutherford TJ, Jones C, Davies DB, Clare Elliott A. Location and quantitation of the sites of O-acetylation on the capsular polysaccharide from *Streptococcus pneumoniae* type 9V by 1-H n.m.r. spectroscopy: comparison with type 9A. Carbohydrate Research 1991;218:175-84.
- [469] Lindberg B, Lonngren J, Powell DA. Structural studies on the specific type-14 pneumococcal polysaccharide. Carbohydrate Research 1977;58(1):177-86.
- [470] Lindberg J. Structural studies of bacterial polysaccharides using N.M.R. spectroscopy and mass spectrometry: Department of Organic Chemistry, University of Stockholm, 1990.
- [471] Jennings HJ, Rosell K-G, Carlo DJ. Structural determination of the capsular polysaccharide of *Streptococcus pneumoniae* type-19 (19F). Can J Chem 1980;58(11):1069-74.
- [472] Richards JC, Perry MB. Structure of the specific capsular polysaccharide of *Streptococcus pneumoniae* type 23F (American type 23). Biochem Cell Biol 1988;66(7):758-71.
- [473] Stein KE. Thymus-Independent and Thymus-Dependent Responses to Polysaccharide Antigens. Journal of Infectious Diseases 1992;165(Supplement 1):S49-S52.
- [474] Eskola J, Anttila M. Pneumococcal conjugate vaccines. Pediatr Infect Dis J 1999;18(6):543-51.
- [475] Rubins JB, Puri AKG, Loch J, Charboneau D, MacDonald R, Opstad N, et al. Magnitude, Duration, Quality, and Function of Pneumococcal Vaccine Responses in Elderly Adults. The Journal of Infectious Diseases 1998;178(2):431-40.
- [476] Adams WG, Deaver KA, Cochi SL, et al. Decline of childhood *Haemophilus influenzae* type b (hib) disease in the hib vaccine era. Jama 1993;269(2):221-6.
- [477] Schneerson R, Barrera O, Sutton A, Robbins JB. Preparation, characterization, and immunogenicity of *Haemophilus influenzae* type b polysaccharide-protein conjugates. The Journal of Experimental Medicine 1980;152(2):361-76.
- [478] Cooper D, Yu X, Sidhu M, Nahm MH, Fernsten P, Jansen KU. The 13-valent pneumococcal conjugate vaccine (PCV13) elicits cross-functional opsonophagocytic killing responses in humans to *Streptococcus pneumoniae* serotypes 6C and 7A. Vaccine 2011;29(41):7207-11.
- [479] Weinberger DM, Malley R, Lipsitch M. Serotype replacement in disease after pneumococcal vaccination. Lancet 2011;378(9807):1962-73.
- [480] Bryant KA, Block SL, Baker SA, Gruber WC, Scott DA, Group ftPIS. Safety and Immunogenicity of a 13-Valent Pneumococcal Conjugate Vaccine. Pediatrics 2010;125(5):866-75.
- [481] Heidelberger M. Precipitating cross-reactions among pneumococcal types. Infect Immun 1983;41(3):1234-44.
- [482] Heidelberger M, Kabat EA, Mayer M. A further study of the cross reaction between the specific polysaccharides of types iii and viii pneumococci in horse antisera. The Journal of Experimental Medicine 1942;75(1):35-47.
- [483] Heidelberger M, Kabat EA, Shrivastava DL. A quantitative study of the cross reaction of types iii and viii pneumococci in horse and rabbit antisera. The Journal of Experimental Medicine 1937;65(4):487-96.
- [484] Maggio ET. Polysorbates, Peroxides, Protein Aggregation, and Immunogenicity: A Growing Concern. J Excip Food Chem 2012;3(2).

## References

- [485] Burtneck MN, Heiss C, Roberts RA, Schweizer HP, Azadi P, Brett PJ. Development of capsular polysaccharide-based glycoconjugates for immunization against melioidosis and glanders. *Frontiers in Cellular and Infection Microbiology* 2012;2.
- [486] Hase S, Ibuki T, Ikenaka T. Reexamination of the pyridylation used for fluorescence labelling of oligosaccharides and its application to glycoproteins. *J Biochem (Tokyo)* 1984;95(1):197-203.
- [487] Jones C. Vaccines based on the cell surface carbohydrates of pathogenic bacteria. *An Acad Bras Cienc* 2005;77(2):293-324.
- [488] Lesinski GB, Westerink J. Vaccines against polysaccharide antigens. *Current Drug Targets-Infectious Disorders* 2001;1(3):325-34.
- [489] Isaacman DJ, Fletcher MA, Fritzell B, Ciuryla V, Schranz J. Indirect effects associated with widespread vaccination of infants with heptavalent pneumococcal conjugate vaccine (PCV7; Prevnar). *Vaccine* 2007;25(13):2420-7.
- [490] Francis KP, Yu J, Bellinger-Kawahara C, Joh D, Hawkinson MJ, Xiao G, et al. Visualizing pneumococcal infections in the lungs of live mice using bioluminescent *Streptococcus pneumoniae* transformed with a novel Gram positive lux transposon. *Infect Immun* 2001;69(5):3350-8.
- [491] Baker WS, Jr. Carcinoma of the uterine cervix. Interstitial radioactive colloidal gold therapy of the lateral pelvic nodes. *Calif Med* 1960;92:25-30.
- [492] Geng Y, Dalhaimer P, Cai S, Tsai R, Tewari M, Minko T, et al. Shape effects of filaments versus spherical particles in flow and drug delivery. *Nat Nano* 2007;2(4):249-55.
- [493] Klippstein R, Pozo D. Nanotechnology-based manipulation of dendritic cells for enhanced immunotherapy strategies. *Nanomedicine* 2010;6(4):523-9.
- [494] Love JC, Estroff LA, Kriebel JK, Nuzzo RG, Whitesides GM. Self-Assembled Monolayers of Thiolates on Metals as a Form of Nanotechnology. *Chem Rev* 2005;105(4):1103-70.
- [495] Sperling RA, Parak WJ. Surface modification, functionalization and bioconjugation of colloidal inorganic nanoparticles. *Philosophical Transactions of the Royal Society A: Mathematical, Physical and Engineering Sciences* 2010;368(1915):1333-83.
- [496] Choi Y, Conferences A. *Osteoimmunology*: Springer, 2007.
- [497] Baschong W, Hasler L, Häner M, Kistler J, Aebi U. Repetitive versus monomeric antigen presentation: direct visualization of antibody affinity and specificity. *J Struct Biol* 2003;143(3):258-62.
- [498] Amemiya K, Bush GV, DeShazer D, Waag DM. Nonviable *Burkholderia mallei* induces a mixed Th1- and Th2-like cytokine response in BALB/c mice. *Infect Immun* 2002;70(5):2319-25.
- [499] Amemiya K, Meyers JL, Trevino SR, Chanh TC, Norris SL, Waag DM. Interleukin-12 induces a Th1-like response to *Burkholderia mallei* and limited protection in BALB/c mice. *Vaccine* 2006;24(9):1413-20.
- [500] Guttormsen H-K, Sharpe AH, Chandraker AK, Brigtsen AK, Sayegh MH, Kasper DL. Cognate Stimulatory B-Cell-T-Cell Interactions Are Critical for T-Cell Help Recruited by Glycoconjugate Vaccines. *Infect Immun* 1999;67(12):6375-84.
- [501] West TE, Ernst R, Jansson-Hutson M, Skerrett S. Activation of Toll-like receptors by *Burkholderia pseudomallei*. *BMC Immunol* 2008;9(1):46.
- [502] Raetz C, Whitfield C. Lipopolysaccharide endotoxins. *Annu Rev Biochem* 2002;71:635 - 700.
- [503] Paradiso PR. Advances in Pneumococcal Disease Prevention: 13-Valent Pneumococcal Conjugate Vaccine for Infants and Children. *Clinical infectious diseases* 2011;52(10):1241-7.
- [504] Lindberg AA. Glycoprotein conjugate vaccines. *Vaccine* 1999;17, Supplement 2(0):S28-S36.
- [505] Pitt A, Mayorga LS, Schwartz AL, Stahl PD. Transport of phagosomal components to an endosomal compartment. *Journal of Biological Chemistry* 1992;267(1):126-32.
- [506] Bareford LM, Swaan PW. Endocytic mechanisms for targeted drug delivery. *Adv Drug Deliv Rev* 2007;59(8):748-58.

## References

- [507] Xia T, Rome L, Nel A. Nanobiology: Particles slip cell security. *Nat Mater* 2008;7(7):519-20.
- [508] Stoorvogel W, Strous GJ, Geuze HJ, Oorschot V, Schwartz AL. Late endosomes derive from early endosomes by maturation. *Cell* 1991;65(3):417-27.
- [509] Huotari J, Helenius A. Endosome maturation. *The EMBO Journal* 2011;30(17):3481-500.
- [510] Buschow SI, Nolte-t Hoen ENM, Van Niel G, Pols MS, Ten Broeke T, Lauwen M, et al. MHC II in Dendritic Cells is Targeted to Lysosomes or T Cell-Induced Exosomes Via Distinct Multivesicular Body Pathways. *Traffic* 2009;10(10):1528-42.
- [511] Bagnoli F, Moschioni M, Donati C, Dimitrovska V, Ferlenghi I, Facciotti C, et al. A Second Pilus Type in *Streptococcus pneumoniae* Is Prevalent in Emerging Serotypes and Mediates Adhesion to Host Cells. *J Bacteriol* 2008;190(15):5480-92.
- [512] DeShazer D, Brett PJ, Burtnick MN, Woods DE. Molecular Characterization of Genetic Loci Required for Secretion of Exoproducts in *Burkholderia pseudomallei*. *J Bacteriol* 1999;181(15):4661-4.
- [513] Stevens MP, Wood MW, Taylor LA, Monaghan P, Hawes P, Jones PW, et al. An Inv/Mxi-Spa-like type III protein secretion system in *Burkholderia pseudomallei* modulates intracellular behaviour of the pathogen. *Mol Microbiol* 2002;46(3):649-59.
- [514] Rainbow L, Hart CA, Winstanley C. Distribution of type III secretion gene clusters in *Burkholderia pseudomallei*, *B. thailandensis* and *B. mallei*. *J Med Microbiol* 2002;51(5):374-84.
- [515] Essex-Lopresti AE, Boddey JA, Thomas R, Smith MP, Hartley MG, Atkins T, et al. A Type IV Pilin, PilA, Contributes to Adherence of *Burkholderia pseudomallei* and Virulence In Vivo. *Infect Immun* 2005;73(2):1260-4.
- [516] Fernandes PJ, Guo Q, Waag DM, Donnenberg MS. The Type IV Pilin of *Burkholderia mallei* Is Highly Immunogenic but Fails To Protect against Lethal Aerosol Challenge in a Murine Model. *Infect Immun* 2007;75(6):3027-32.
- [517] Stevens JM, Galyov EE, Stevens MP. Actin-dependent movement of bacterial pathogens. *Nat Rev Microbiol* 2006;4(2):91-101.
- [518] Oosterhuis-Kafeja F, Beutels P, Van Damme P. Immunogenicity, efficacy, safety and effectiveness of pneumococcal conjugate vaccines (1998–2006). *Vaccine* 2007;25(12):2194-212.
- [519] Stevens MP, Stevens JM, Jeng RL, Taylor LA, Wood MW, Hawes P, et al. Identification of a bacterial factor required for actin-based motility of *Burkholderia pseudomallei*. *Mol Microbiol* 2005;56(1):40-53.
- [520] Duerkop BA, Herman JP, Ulrich RL, Churchill MEA, Greenberg EP. The *Burkholderia mallei* BmaR3-BmaI3 Quorum-Sensing System Produces and Responds to N-3-Hydroxy-Octanoyl Homoserine Lactone. *J Bacteriol* 2008;190(14):5137-41.
- [521] Ulrich RL, DeShazer D, Hines HB, Jeddelloh JA. Quorum Sensing: a Transcriptional regulatory system involved in the pathogenicity of *Burkholderia mallei*. *Infect Immun* 2004;72(11):6589-96.
- [522] Ulrich RL, Deshazer D, Brueggemann EE, Hines HB, Oyston PC, Jeddelloh JA. Role of quorum sensing in the pathogenicity of *Burkholderia pseudomallei*. *J Med Microbiol* 2004;53(Pt 11):1053-64.
- [523] Valade E, Thibault FM, Gauthier YP, Palencia M, Popoff MY, Vidal DR. The PmlI-PmlR Quorum-Sensing System in *Burkholderia pseudomallei* Plays a Key Role in Virulence and Modulates Production of the MprA Protease. *J Bacteriol* 2004;186(8):2288-94.
- [524] Song Y, Xie C, Ong Y-M, Gan Y-H, Chua K-L. The BpsIR Quorum-Sensing System of *Burkholderia pseudomallei*. *J Bacteriol* 2005;187(2):785-90.